# Alternative Designs to Alleviate Freeway Bottlenecks at Merging, Diverging, and Weaving Areas

U.S. Department of Transportation
**Federal Highway Administration**

# FOREWORD

Merging, diverging, and weaving areas are major bottleneck locations on uninterrupted flow facilities and are a significant source of recurring congestion. This report summarizes the development of five alternative designs for application at freeway merging, diverging, and weaving areas: split merge points, managed lanes on the right-hand side, mainline metering, coordinated ramp metering, and speed optimization via traffic calming devices. This report also includes simulations of the innovative treatments to evaluate the benefits of the designs. This report will be of interest to State and local departments of transportation who are interested in exploring innovative methods to more effectively manage their facilities.

<div align="right">
Brian P. Cronin, P.E.
Director, Office of Safety and Operations
Research and Development
</div>

# TECHNICAL REPORT DOCUMENTATION PAGE

| 1. Report No.<br>FHWA-HRT-20-008 | 2. Government Accession No. | 3. Recipient's Catalog No. |
|---|---|---|
| 4. Title and Subtitle<br>Alternative Designs to Alleviate Freeway Bottlenecks at Merging, Diverging, and Weaving Areas | | 5. Report Date<br>May 2020 |
| | | 6. Performing Organization Code: |
| 7. Author(s)<br>David K. Hale (ORCID: 0000-0001-5486-9367), Jiaqi Ma (ORCID: 0000-0002-8184-5157), Amir Ghiasi (ORCID: 0000-0002-0986-9840), Pascal Volet (ORCID: 0000-0002-1753-0935), Burak Cesme (ORCID: 0000-0002-1265-981X), Alexandra Kondyli (ORCID: 0000-0002-3462-0000), Bastian Schroeder (ORCID: 0000-0001-8916-421X), Sonika Sethi (ORCID: 0000-0002-5236-0003), Laura Torres (ORCID: 0000-0001-8250-0436), and Francois Belisle (ORCID: 0000-0003-1592-3986) | | 8. Performing Organization Report No. |
| 9. Performing Organization Name and Address<br>Leidos, Inc.<br>11251 Roger Bacon Drive<br>Reston, VA 20190-5201 | | 10. Work Unit No. |
| | | 11. Contract or Grant No.<br>DFTH6116D00030 |
| 12. Sponsoring Agency Name and Address<br>U.S. Department of Transportation<br>Federal Highway Administration<br>6300 Georgetown Pike<br>McLean, VA 22101-2296 | | 13. Type of Report and Period Covered<br>Final Report; July 2017–September 2018 |
| | | 14. Sponsoring Agency Code<br>HRDO-20 |
| 15. Supplementary Notes<br>The Contracting Officer's Representative was Joe Bared (HRDO-20). | | |

16. Abstract

Alternative intersections and interchanges brought major benefits to the United States during the 2008–2018 time period. Given the positive impacts, it stands to reason that similar breakthroughs might be possible at freeway merge and diverge locations. This report describes the outcomes of a project that examined this possibility. The primary tool of evaluation was sensitivity analysis via microscopic traffic simulation, also known as microsimulation. The split merge design, and the positioning of managed lanes on the right side of the freeway, are two unrelated designs that showed excellent promise (in terms of benefit–cost ratio). Coordinated ramp metering did not show significant additional benefits beyond conventional asservissement linéaire d'entrée autoutière, also known as ALINEA, metering. Speed optimization showed excellent benefits but only during narrow ranges of traffic congestion. Mainline metering also showed reasonably good benefits but could be challenging to implement. It is conceivable that speed optimization and mainline metering could produce more favorable benefit–cost ratios if they could be implemented via connected and automated vehicle (CAV) technologies. However, the split merge and right-side managed lane designs produced excellent benefits without the need for CAV technologies.

| 17. Key Words<br>Split merge, managed lanes, mainline metering, coordinated ramp metering, speed optimization, freeway merge | | 18. Distribution Statement<br>No restrictions. This document is available to the public through the National Technical Information Service, Springfield, VA 22161.<br>http://www.ntis.gov | | |
|---|---|---|---|---|
| 19. Security Classif. (of this report)<br>Unclassified | | 20. Security Classif. (of this page)<br>Unclassified | 21. No. of Pages<br>182 | 22. Price<br>N/A |

**Form DOT F 1700.7 (8-72)**        Reproduction of completed page authorized.

# SI* (MODERN METRIC) CONVERSION FACTORS

## APPROXIMATE CONVERSIONS TO SI UNITS

| Symbol | When You Know | Multiply By | To Find | Symbol |
|---|---|---|---|---|
| **LENGTH** | | | | |
| in | inches | 25.4 | millimeters | mm |
| ft | feet | 0.305 | meters | m |
| yd | yards | 0.914 | meters | m |
| mi | miles | 1.61 | kilometers | km |
| **AREA** | | | | |
| $in^2$ | square inches | 645.2 | square millimeters | $mm^2$ |
| $ft^2$ | square feet | 0.093 | square meters | $m^2$ |
| $yd^2$ | square yard | 0.836 | square meters | $m^2$ |
| ac | acres | 0.405 | hectares | ha |
| $mi^2$ | square miles | 2.59 | square kilometers | $km^2$ |
| **VOLUME** | | | | |
| fl oz | fluid ounces | 29.57 | milliliters | mL |
| gal | gallons | 3.785 | liters | L |
| $ft^3$ | cubic feet | 0.028 | cubic meters | $m^3$ |
| $yd^3$ | cubic yards | 0.765 | cubic meters | $m^3$ |
| NOTE: volumes greater than 1,000 L shall be shown in $m^3$ | | | | |
| **MASS** | | | | |
| oz | ounces | 28.35 | grams | g |
| lb | pounds | 0.454 | kilograms | kg |
| T | short tons (2,000 lb) | 0.907 | megagrams (or "metric ton") | Mg (or "t") |
| **TEMPERATURE (exact degrees)** | | | | |
| °F | Fahrenheit | 5 (F-32)/9 or (F-32)/1.8 | Celsius | °C |
| **ILLUMINATION** | | | | |
| fc | foot-candles | 10.76 | lux | lx |
| fl | foot-Lamberts | 3.426 | candela/$m^2$ | $cd/m^2$ |
| **FORCE and PRESSURE or STRESS** | | | | |
| lbf | poundforce | 4.45 | newtons | N |
| $lbf/in^2$ | poundforce per square inch | 6.89 | kilopascals | kPa |

## APPROXIMATE CONVERSIONS FROM SI UNITS

| Symbol | When You Know | Multiply By | To Find | Symbol |
|---|---|---|---|---|
| **LENGTH** | | | | |
| mm | millimeters | 0.039 | inches | in |
| m | meters | 3.28 | feet | ft |
| m | meters | 1.09 | yards | yd |
| km | kilometers | 0.621 | miles | mi |
| **AREA** | | | | |
| $mm^2$ | square millimeters | 0.0016 | square inches | $in^2$ |
| $m^2$ | square meters | 10.764 | square feet | $ft^2$ |
| $m^2$ | square meters | 1.195 | square yards | $yd^2$ |
| ha | hectares | 2.47 | acres | ac |
| $km^2$ | square kilometers | 0.386 | square miles | $mi^2$ |
| **VOLUME** | | | | |
| mL | milliliters | 0.034 | fluid ounces | fl oz |
| L | liters | 0.264 | gallons | gal |
| $m^3$ | cubic meters | 35.314 | cubic feet | $ft^3$ |
| $m^3$ | cubic meters | 1.307 | cubic yards | $yd^3$ |
| **MASS** | | | | |
| g | grams | 0.035 | ounces | oz |
| kg | kilograms | 2.202 | pounds | lb |
| Mg (or "t") | megagrams (or "metric ton") | 1.103 | short tons (2,000 lb) | T |
| **TEMPERATURE (exact degrees)** | | | | |
| °C | Celsius | 1.8C+32 | Fahrenheit | °F |
| **ILLUMINATION** | | | | |
| lx | lux | 0.0929 | foot-candles | fc |
| $cd/m^2$ | candela/m2 | 0.2919 | foot-Lamberts | fl |
| **FORCE and PRESSURE or STRESS** | | | | |
| N | newtons | 2.225 | poundforce | lbf |
| kPa | kilopascals | 0.145 | poundforce per square inch | $lbf/in^2$ |

*SI is the symbol for International System of Units. Appropriate rounding should be made to comply with Section 4 of ASTM E380.
(Revised March 2003)

# TABLE OF CONTENTS

# LIST OF FIGURES

# LIST OF TABLES

# LIST OF ABBREVIATIONS

AASHTO     American Association of State Highway and Transportation Officials
ADT        average daily traffic
ALINEA     asservissement linéaire d'entrée autoroutière
ANOVA      analysis of variance
API        application programming interface
ATDM       advanced transportation demand management
ATM        active transportation management
Caltrans   California Department of Transportation
CARMA      Continuous Association Rule Mining Algorithm
CAV        connected and automated vehicle
CD         collector-distributor
CPS        congestion pricing system
CRM        coordinated ramp metering
CVSL       cycle-based variable speed limits
DHSR       dynamic hard shoulder running
DMC        dynamic merge control
DOT        department of transportation
FHWA       Federal Highway Administration
FSP        Freeway Service Patrol
GP         general purpose
*HCM*      *Highway Capacity Manual, Sixth Edition: A Guide for Multimodal Mobility Analysis*
HCS        Highway Capacity Software
HERO       heuristic ramp metering coordination
HOT        high-occupancy toll
HOV        high-occupancy vehicle
I2V        infrastructure-to-vehicle
ICM        integrated corridor management
ITE        Institute of Transportation Engineers
ITS        intelligent transportation systems
KDOT       Kansas Department of Transportation
LHD        Latin hypercube sampling design
LOS        level of service
ML         managed lane
MnDOT      Minnesota Department of Transportation
MOE        measure of effectiveness
MOP        measure of performance
NCHRP      National Cooperative Highway Research Program
O-D        origin–destination
PeMS       Caltrans Performance Measurement System
PennDOT    Pennsylvania Department of Transportation
PTSU       part-time shoulder use
RITIS      Regional Integrated Transportation Information System
RMIS       ramp metering information system

| | |
|---|---|
| RTMS | remote traffic microwave sensor |
| SDRMS | San Diego ramp metering system |
| STOL | Saxton Transportation Operations Laboratory |
| SWARM | Systemwide adaptive ramp metering |
| TCRP | Transit Cooperative Research Program |
| V/C | volume-to-capacity |
| VDOT | Virginia Department of Transportation |
| veh/h | vehicles per hour |
| veh/h/l | vehicles per hour per lane |
| VHT | vehicle hours traveled |
| VicRoads | Roads Corporation of Victoria |
| VMT | vehicle miles traveled |
| VSL | variable speed limit |
| WSDOT | Washington State Department of Transportation |

# EXECUTIVE SUMMARY

The so-called "alternative" intersections and interchanges represent one of the biggest success stories for surface transportation mobility in recent years. Indeed, in the 1990s, few would have imagined that a small set of radical changes to the fundamental geometric design of signalized intersections could reduce delays and crashes by nearly one-half in many instances (Bared and Zhang 2016). Nonetheless, currently, real-world implementations of the diverging diamond interchange, restricted crossing U-turn, median U-turn, and displaced left turn now collectively number in the hundreds in the United States, and expectations are that their implementation will increase (Sieminski 2017).

Given the widespread, positive impacts of these alternative designs, it stands to reason that similar breakthroughs might well be possible at freeway merge and diverge locations, which have long been a major source of traffic congestion, delays, and crashes. This report describes the planning and outcomes of a research project that aimed to examine this possibility. The primary tool of evaluation was a sensitivity analysis via microscopic traffic simulation, also known as microsimulation, which is the ideal platform to test hundreds of possible designs safely and efficiently prior to implementation in the field. The objective of this project was to identify alternative freeway designs that achieved significant mobility benefits (e.g., reduced delay, increased throughput) in the virtual simulation environment, such that subsequent human factors studies and/or field testing would be warranted.

Before the simulation sensitivity analyses could begin, an initial phase of brainstorming and literature review was necessary to identify alternative freeway designs as candidates for this study. From this review of literature, the researchers selected five top-candidate designs for further investigation. These alternative designs incorporated control strategies as well as geometric modifications and are listed below:

- Split merge and diverge points.
- Managed lanes (ML) on the right.
- Mainline metering.
- Coordinated ramp metering (CRM).
- Speed optimization via traffic calming devices.

This report details the project's motivation (chapter 1), synthesis of research and findings (chapter 2), research work plan (chapter 3), simulation results (chapter 4), and conclusions (chapter 5). An appendix is also included to describe the approach to data collection and microsimulation calibration. Ultimately, the top two alternative design candidates (i.e., split merge points and MLs on the right-hand side) showed the most promise in the simulation tests. Figure 1 illustrates the split merge design, where vehicles can no longer cause turbulence by merging in the middle of the acceleration lane.

Connecting Spacing
0.25 – 0.5 mi

0.25 mi

← Traffic Flow

1.85 mi    1.25 mi

0.25 mi

**Figure 1. Illustration. Split merge design on an acceleration lane.**

The split merge design is the most analogous to the alternative intersection and interchange designs, which represent low-cost geometric improvements capable of achieving significant mobility benefits. The split merge design achieved delay reductions up to 80 percent in some cases. The best benefits were observed under near capacity levels of traffic congestion. A split diverge design was also tested, but did not consistently achieve significant benefits. The simulations in this report only evaluated one-lane ramps, but the researchers believe two-lane ramps would exhibit similar impacts.

In the United States, open-access MLs are typically not located on the right side of the freeway because it would likely degrade mobility on the ML. However, this project tested the following initial hypotheses:

- Although managed lane mobility would be degraded, it would still provide superior overall level of service when compared to the general purpose (GP) lanes.
- The substantial GP lane benefits would far exceed any mobility losses on the MLs, resulting in significant improvement in overall freeway mobility.

When comparing simulation tests, MLs located on the right showed overall delay reductions up to 30 percent relative to MLs on the left.

The mainline metering strategy is intended to temporarily treat on-ramp merge junctions like conventional signalized intersections once vehicle speeds reach a low enough level. The simulation tests showed delay reductions up to 21 percent under mainline metering algorithms when stopping mainline traffic and on-ramp traffic successively like a two-phase traffic signal. However, the mainline metering strategy would require unprecedented signalization on the mainline, a finely-tuned algorithm, and new safety risks. As such, the cost-effectiveness of such a strategy remains questionable. It is conceivable that enhanced improvements could be possible by deploying the strategy at several locations within a congested corridor.

CRM has already received significant research attention and a few real-world deployments. This study found improvements of only 2 percent over the proven, conventional ramp metering approaches of asservissement linéaire d'entrée autoroutière (ALINEA) metering, literally meaning "linear enslavement of a freeway entrance." Thus, the cost-effectiveness of coordinating the ramp meters is also questionable under the tested scenarios. CRM may provide benefits under other geometric and volume configurations or if combined with mainline metering

in a "managed motorways" approach, as done in Australia. Indeed, the Roads Corporation of Victoria (VicRoads) reports much success with its implementation of city-wide CRM in Melbourne. However, this study did not investigate large-scale deployments like this.

Finally, the researchers considered the possibility of reducing vehicle speeds to prevent bottleneck formation through deployment of traffic calming devices. Although traffic calming devices cannot be modeled explicitly through microsimulation, in some cases, simply lowering posted speed limits (e.g., from 65 to 55 mi/h) resulted in substantial improvements in vehicle speed (e.g., from 9 to 52 mi/h). The caveat was that the benefits were only attainable at certain site-specific congestion levels, implying the need for accurate simulation models and/or historical data to determine the target congestion level for any given site. Moreover, an additional assumption is that installing traffic calming devices on freeways would still be safe but would make high-speed travel uncomfortable. Therefore, the cost-effectiveness of speed optimization via traffic calming devices is questionable.

# CHAPTER 1. INTRODUCTION

Cities face increasing freeway congestion, and few short-term options exist for increasing freeway capacities. Widening roadways or implementing connected and automated vehicles (CAVs) are longer-term solutions that will provide benefits, but there are solutions that show short-term promise. This report evaluates freeway merge and diverge area improvements where increased lane changing results in slowing due to the increased lane changing and accommodation for vehicles entering or exiting the freeway. Freeway merge and diverge areas are a primary source of turbulence, congestion, and traffic breakdown, both at the sites and upstream. In fact, research has shown that the capacity at merge or diverge segments is significantly less than the basic freeway segments reported in the *Highway Capacity Manual, Sixth Edition: A Guide for Multimodal Mobility Analysis* (*HCM*) (Kondyli et al. 2017).

In most cases, traffic breakdowns occur on the right-hand side of the mainline, as incoming and outgoing ramp vehicles produce excessive friction. Figure 2 illustrates the onset of severe congestion and queuing caused by typical freeway weaving maneuvers. Once a breakdown like this begins, the resulting shockwaves and queue spillback can eventually stretch back for miles, causing area-wide travel time reliability problems.
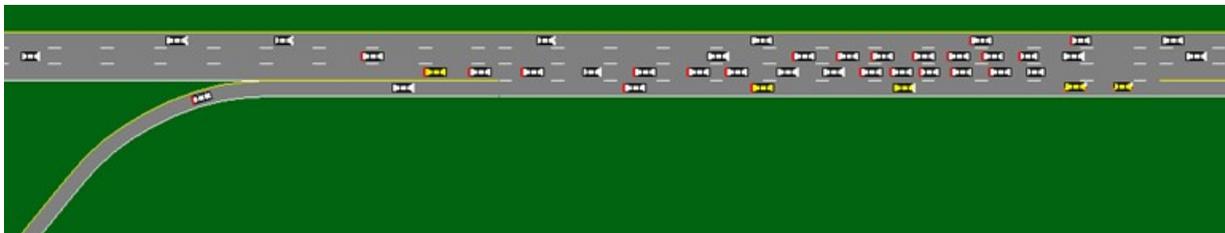


Source: FHWA.

**Figure 2. Screenshot. Simulation of congestion formation at a freeway weaving area.**

Similar breakdowns have originated on the left-hand side of the freeway because of managed high-occupancy vehicle (HOV) lanes. The need for managed lane (ML) vehicles to weave to and from the right-side on-ramps and off-ramps further exacerbates these breakdowns by causing a substantial amount of turbulence and interference within the general purpose (GP) lanes.

Given the prevalence of the freeway merge problem, any low-cost solution to reduce the friction associated with vehicle maneuvers, or facilitate smoother merging/diverging operations, could produce great improvements in traffic flow. This is because a nationwide deployment solution, at dozens if not hundreds of sites, could continuously produce daily time savings for peak-hour commuters throughout the year. The solution could fall within the realm of dynamic message signs, traffic control devices, geometric design modifications, traffic calming devices, new forms of driver information, or new traffic management algorithms. The alternative intersection and interchange designs (e.g., median U-turn) are examples of such solutions for urban arterial streets.

This report describes the development and testing of innovative designs and traffic management systems that may alleviate merging problems on the left- and/or right-hand sides of the freeway. To verify operational effectiveness of the proposed designs, the team conducted comprehensive

sensitivity and scenario analyses in a traffic microsimulation environment. The ultimate goal is to achieve widespread implementation of one or more effective designs.

The primary tool of evaluation is sensitivity analysis via microscopic traffic simulation, also known as microsimulation. Microsimulation reproduces vehicle behavior and interaction during merging, changing lanes, acceleration, and deceleration, and replicates the impact on traffic flow. This helps to predict the impact of changes in traffic patterns resulting from changes to traffic flow or the physical environment. For this study, microsimulation helped evaluate changes in merge lanes, placement of HOV lanes, signaling, and the physical environment, such as the narrowing of lanes or the relocation of junction stop lines.

# CHAPTER 2. SYNTHESIS OF RESEARCH AND FINDINGS

The team conducted a literature search of current practices and designs for mitigating freeway merge and diverge congestion problems on both sides of the freeway, with the left-hand side typically involving MLs. The team further identified several real-world sites that would potentially benefit from further analysis and weaving mitigation, understanding that some findings would be based on reported experiences (i.e., unpublished). The intent was not to conduct site-specific analysis, but rather to expand the use of these sites for generic analyses and recommendations. Site selection considered the following site-specific criteria:

- The side of the freeway (left- or right-hand) responsible for the congestion.
- Spatial and temporal extent of congestion (too short or too long may not be suitable).
- Availability of sufficient, good-quality data.
- Presence of a preexisting mitigation strategy.
- Availability of preexisting microsimulation datasets.
- Interested local representatives who could provide assistance.
- Expense required to develop a brand-new simulation dataset.

Originally, the following categories defined the team's synthesis of research and findings:

- Innovative strategies.
- Relevant literature.
- Relevant individuals, agencies, and sites.
- Known resources (e.g., available data and simulation datasets).

Chapter 2 summarizes the innovative and relevant literature findings.

## INNOVATIVE STRATEGIES

### Alternative Geometric Designs

Chapter 1 stated that the alternative intersection and interchange designs are examples of innovative geometric design solutions for urban arterial streets. The first alternative geometric design conceived within the boundaries of this project is a set of two alternative auxiliary lane designs: one design for the acceleration lanes that follow on-ramps and a second design for the deceleration lanes that precede off-ramps. Figure 3 shows the alternative acceleration lane design intended to reduce merging friction by limiting the exposure of on-ramp vehicles to two specific entry points.



Source: FHWA.

**Figure 3. Illustration. Freeway acceleration lane with split merge points.**

7

Figure 4 shows the alternative deceleration lane design intended to reduce diverging friction by limiting the weaving of off-ramp vehicles to two specific exit points. Presumably, in this design, the two exiting lanes enable merging further downstream on the off-ramp.
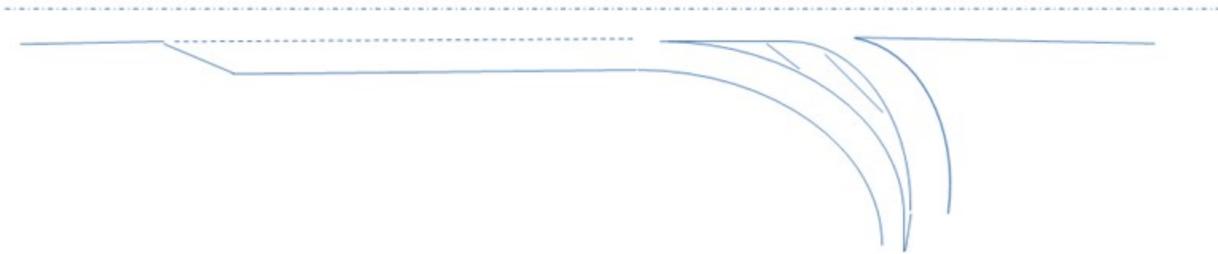


Source: FHWA.

**Figure 4. Illustration. Freeway deceleration lane with split diverge points.**

A third alternative geometric design conceived by the researchers is the placement of MLs on the right-hand side of the freeway. This design is intended to be compatible with unpaid open-access HOV lanes only. Traditionally, MLs were designed to provide a higher level of service than GP lanes. Weaving maneuvers from GP lane vehicles through HOV traffic on a right-side ML could compromise the level of service on the ML, undermining its purpose. For example, why would drivers carpool if the level of service on an ML is comparable or inferior to the GP lanes? However, since there are usually more GP lanes than MLs, it is conceivable that overall traffic flow (accounting for all lanes) could benefit. The team further envisioned microsimulation experiments that would focus on traffic flow operations as opposed to pricing.

A fourth alternative geometric design considered by the researchers is the grade-separated ramp for MLs, also known as a direct access ramp. Atlanta, GA; the Washington, DC area; and San Diego, CA, have deployed grade-separated ML ramps. Following the review of literature and findings, the team would decide whether to examine such ramps further. Even though not necessarily considered innovative, comparison of their performance to the performance of other innovative designs is possible and useful. One stakeholder made the following relevant comment on the Institute of Transportation Engineers (ITE) Community blog (ITE Community 2017):

> A useful, but expensive design feature is to provide direct access connections to and from the HOV/HOT [high-occupancy toll] lanes. The direct exit connections are the most useful because it is very difficult to determine how far in advance of an interchange a driver should exit the HOV/HOT lane to reach their destination. It is this exit maneuver that causes the greatest turbulence to the through lane flow because it has to happen in a given distance. In comparison, an entering HOV can work its way to the diamond lane as conditions permit. The arrangement on I–5 in Orange, Co. to the north at Disneyland is a good example of this. At that location, there are direct exit ramps from the diamond lanes, but entering traffic from Disney must weave from the outside to reach them on their return trip. The traffic flow characteristics at Disneyland work well with this arrangement since traffic leaves Disneyland after the PM peak on the freeway.

The purpose of grade-separated ramps for MLs is to reduce weaving across GP lanes to enter and exit ML facilities. According to the Texas Department of Transportation's *Managed Lanes Handbook*, which presents 5 years of research by the Texas Transportation Institute on MLs, the design of ML facilities should accommodate grade-separated or direct ramps during a later phase if not included in the initial design (Kuhn et al. 2005). Several types of grade-separated ramps for MLs, also called direct access ramps, are in use and include T-ramps/drop ramps and flyover ramps/Y-ramps. T-ramps (figure 5) or drop ramps (figure 6) use a T-shaped ramp design that drops from the ML to the freeway, local street, or other facility. This ramp design works best with a low ramp speed design (less than 35 mi/h), can be suited to low vehicle volumes, and can be spaced frequently (less than 3 mi apart). Construction of T-ramps can also provide direct access between the ML and a park-and-ride lot.

Flyover ramps include Y-ramps (figure 7) where each direction of travel diverges from the inside to opposite sides of the freeway facility and more conventional flyover designs providing access to and from the ML facility. Y-ramps and flyover ramps are suited to high-speed (greater than 35 mi/h) and high-volume (greater than 400 vehicles per hour (veh/h)) conditions (Kuhn et al. 2005).

To Park-and-Ride Lot or
Arterial Street

Connections Designed To Reverse
Direction of Ramp operation

Mountable Curb

A.M.

P.M.

P.M. Exit Taper

P.M. Acceleration
Lane Length

P.M. Deceleration
Lane Length

P.M. Entrance Taper

A.M.→

← P.M.

A.M.

← P.M.

← P.M.   A.M.→

Reversible-Flow Managed HOV Lane

Elevated Structure
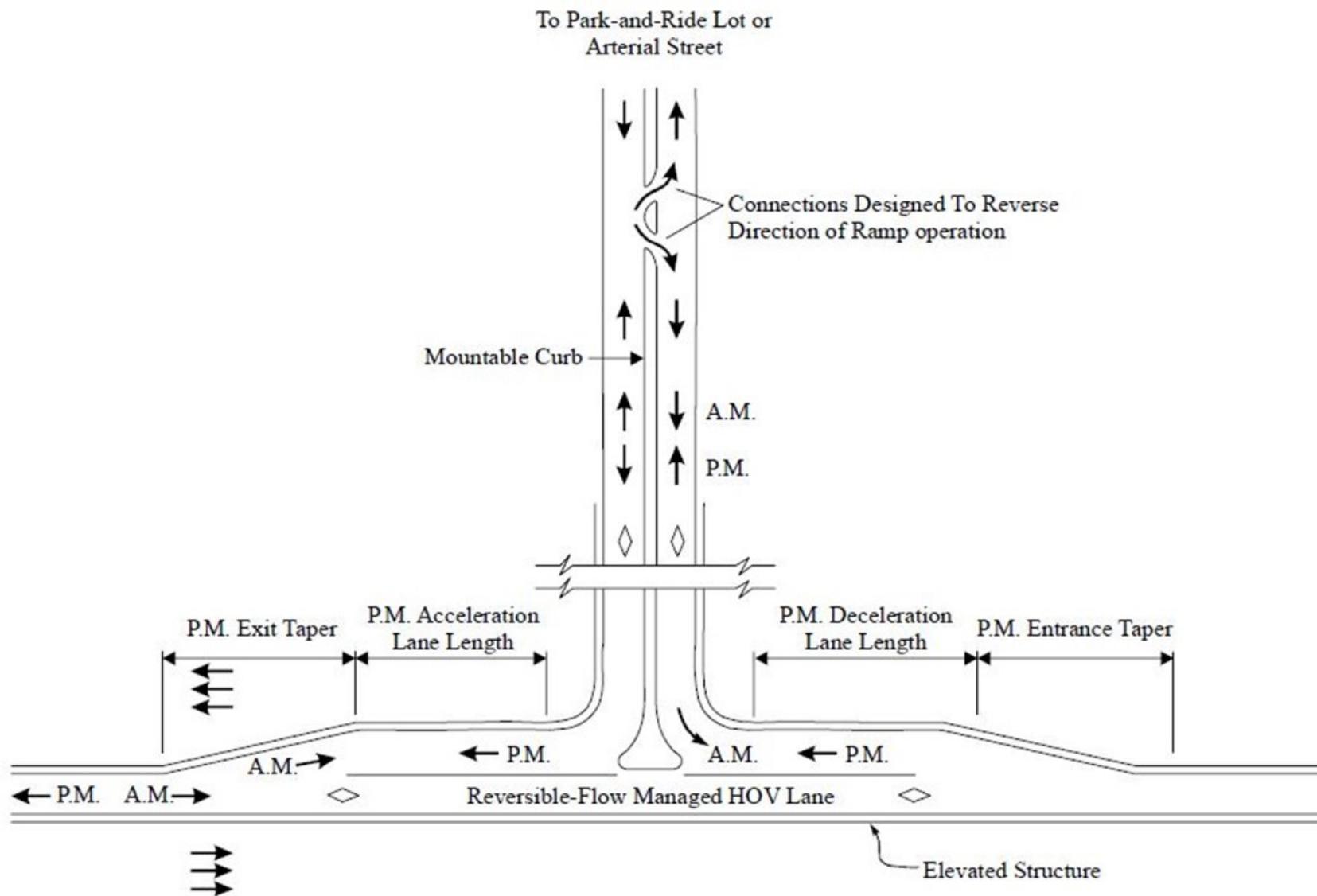
© 2005 Beverly Kuhn.

**Figure 5. Illustration. Typical T-ramp for reversible-flow MLs facility (Kuhn et al. 2005).**

© 2005 Beverly Kuhn.
1 ft = 0.3 m.

**Figure 6. Illustration. Typical drop ramp for reversible-flow MLs facility (Kuhn et al. 2005).**

**Figure 7. Illustration. Typical Y-ramp for two-lane reversible-flow MLs facility (Kuhn et al. 2005).**

Earlier research supported the development of the Texas Department of Transportation's *Managed Lanes Handbook*, focusing specifically on on-ramp design issues (Fitzpatrick, Brewer, and Venglar 2003). Simulation of at-grade ML ramps that varied the ramp spacing, lane volumes, and percent of entering ramp traffic to the ML facility using Vissim, a microscopic traffic simulator, found that in the 30 percent weaving with 1,750 vehicles per hour per lane (veh/h/l), speeds fell below 45 mi/h, and a large percentage of vehicles were not serviced during the simulation run due to congestion (PTV Group 2019). The simulation also investigated when grade-separated ramps should be used. Results supported guidance that a grade-separated ramp should be considered when ramp volume is 400 veh/h. In their abstract and conclusions sections, Fitzpatrick, Brewer, and Venglar (2003) also state that, "if a more conservative approach to preserving freeway performance is desired, then a direct connect ramp should be considered at 275 veh/h" to maintain a minimum speed of 45 mi/h.

## Speed Optimization

Extensive research conducted at the Saxton Transportation Operations Laboratory (STOL) looked at speed harmonization and variable speed limits (VSLs). One team developed a VSL synthesis. Three separate STOL task orders conducted extensive research on infrastructure-to-vehicle (I2V)-based speed harmonization (Hale et al. 2016). The projects produced an extensive bibliography containing dozens of speed harmonization sources. The consensus of this research is that VSL (which optimizes speed limits as opposed to actual speeds) is primarily beneficial for improving safety and suffers from driver compliance rates that are too low to achieve significant operational benefits in most cases. Regarding speed harmonization, the consensus is that the strategy is not highly beneficial without advanced vehicle technologies. However, the STOL projects have shown that CAV penetration rates as low as 10 percent can produce significant operational benefits. These outcomes imply that speed optimization via non-CAV methods are also likely to produce significant operational benefits. The simulation experiments from this project attempt to confirm this.

Regarding speed optimization via non-CAV methods, the team focused on two methods. First, the team looked at quasi-exhaustive sensitivity analysis of freeway merging (and possibly diverging) at "ideal" speeds (i.e., in the 30–35 mi/h range) (figure 8).
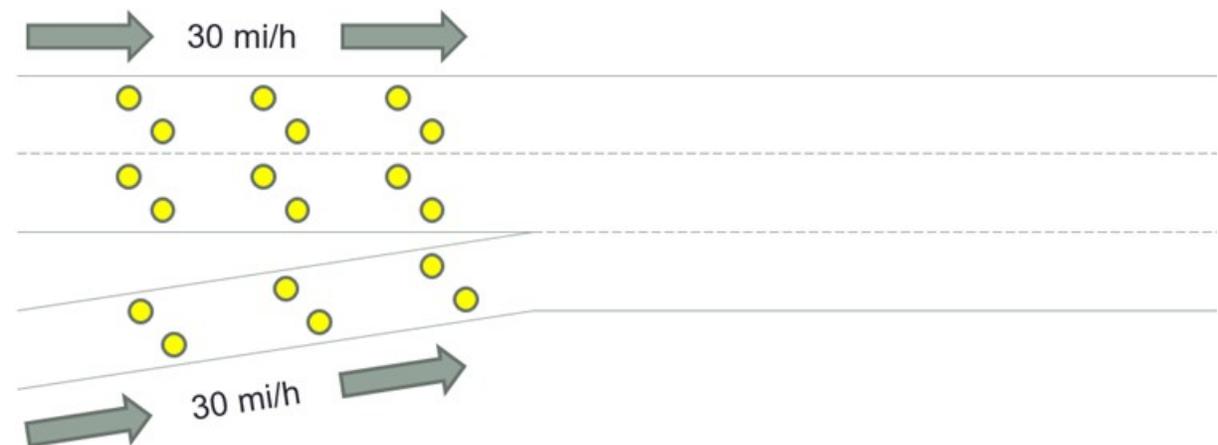


Source: FHWA.

**Figure 8. Illustration. Dynamic traffic calming.**

If optimized speeds were found to improve traffic flow by more than a few percentage points, the team would then recommend future investigation of dynamic traffic calming devices (e.g., rumble strips, circular dots) that could improve driver compliance rates with mid-level speeds without producing unsafe rides or conditions.

Second, the team looked at mainline metering. This would involve dynamic signal control of the mainline and ramp when all speeds drop below a fixed threshold (e.g., 5 mi/h). There is no known literature on this strategy (figure 9), but the team continued searching and inquired with stakeholders. One stakeholder made the following comment on the ITE Community blog (ITE Community 2017):

> I do want to mention the idea of metering the mainline, which I haven't seen implemented anywhere. If density at the bottleneck exceeds max flow density, an upstream meter could be used to limit density and increase flow to the max through the bottleneck, intentionally creating an upstream queue that is shorter than the queue that would result from allowing the bottleneck to jam up. We traditionally think of meters as red and green traffic signals, but some agencies are considering rumble strips as pseudo meters because they slow traffic without requiring a stop.

Indeed, the rumble strips comment is relevant to both envisioned non-CAV methods of speed optimization (i.e., dynamic traffic calming and dynamic mainline metering via signal control).
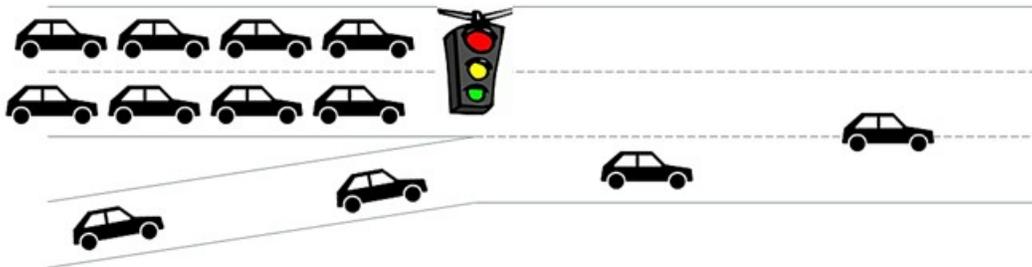


Source: FHWA.

**Figure 9. Illustration. Dynamic signal control for both mainline and ramp.**

**Enforcing Late Merge**

Enforced "zippering" maneuvers could help to achieve better efficiency at merge areas but may be difficult to achieve without CAV technologies. The team considered conducting simulations of late merging to assess the potential benefits (figure 10). Conceivably, signage can encourage late merging. The main concern is that the potential capacity gain could be too small for the strategy to be worthwhile. Therefore, this strategy was ultimately ruled out for detailed investigations.

**Coordinated Ramp Metering (CRM)**

Whereas traditional ramp meters have operated in isolation, CRM provides more of a facility-wide approach, similar to coordinated signalized surface arterials. Although some of the team's ideas listed in this chapter do not have any known literature or associated studies, several studies have investigated CRM. Moreover, a limited number of cities have deployed CRM already. As such, the relevant literature section of this chapter gives a more extensive writeup of CRM.
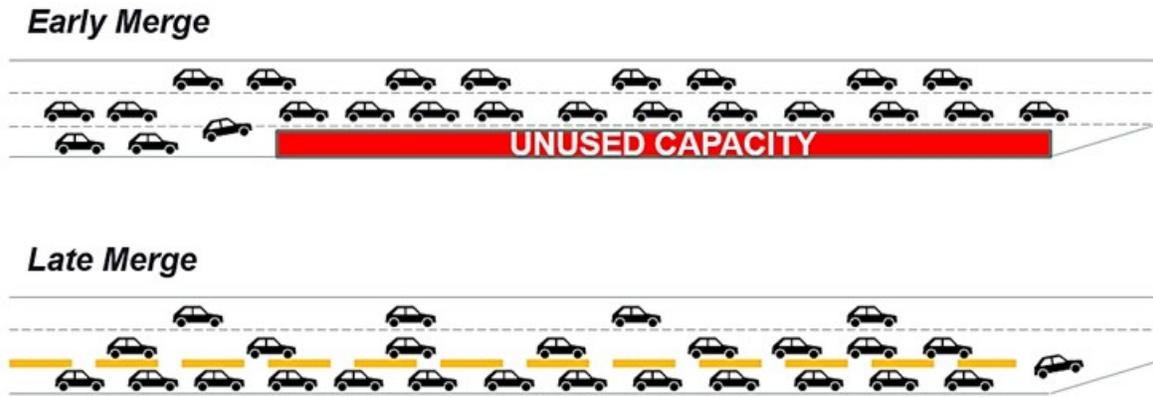


Source: FHWA.

**Figure 10. Illustrations. Improved capacity utilization from late merges.**

**Dynamic Hard Shoulder Running (DHSR)**

Several studies have investigated DHSR deployed in a limited number of cities. As such, the relevant literature section of this chapter gives a more extensive writeup of DHSR.

**ML Access Point Optimization**

Proper design of the distance between managed lane entry/exit points and right-side on/off-ramps can facilitate traffic flow (Zitzow, Parikh, and Hourdos 2018). One stakeholder made the following comment on the ITE Community blog (ITE Community 2017):

> Where barrier striping is used to separate the diamond lane, locating the entrance and exit points requires extensive knowledge of the overall freeway operation in those segments. The research team used extensive traffic simulation to determine those locations during the design of the I–394 HOT lane project west of Minneapolis.

**Other Strategies**

For various reasons, some identified, innovative strategies were ruled out from further consideration during the brainstorming phase of the project. These include:

- Law enforcement: perhaps not suitable for a simulation study.
- Lane change speed advisories: perhaps not viable with CAV technologies.
- Lane change location signs (creating gaps): perhaps not viable with CAV technologies.

- Integrated corridor management (ICM) strategies: the team favored point strategies over ICM-type demand management strategies.
- ML access restriction.
- Dynamic message signs.
- Dynamic lane markings.

## RELEVANT LITERATURE

### Recurring Traffic Bottlenecks: a Primer

The primer says agencies should focus on "chokepoints" for which numerous low-cost solutions are possible (Spiller, Blizzard, and Margiotta 2017). The primer provides three principles for efficient merging: low speeds, large gaps between vehicles, and zippering. This overlaps with two of the strategies previously identified in the innovative strategies section: speed optimization and enforcing late merge. However, the primer does not appear to provide technical insights into the implementation of strategies. Large gaps between vehicles would be helpful, but a method for achieving that without CAV technologies seems elusive. A method to accomplish zippering without CAV technologies also seems elusive.

### Part-Time Shoulder Use (PTSU)

PTSU is the temporary conversion of highway shoulders to travel lanes to relieve congestion. Also known as temporary shoulder use, hard shoulder running, or dynamic shoulder use, this strategy is a low-cost method to increase capacity when most needed, either for general traffic or for transit vehicles only. Recent research projects investigated the planning, design, operations, and safety aspects of PTSU (Jenior et al. 2016; Dowling, Margiotta, and Jacobsen 2011; Dowling et al. 2016; and Martin, Levinson, and Institute 2012). Further, Transit Cooperative Research Program (TCRP) Report 151 provides guidance for implementing shoulder use strategies for bus transit (Martin et al. 2012).

Sixteen States have implemented PTSU, but application tends to be ad hoc with little consistency across cases. Fourteen States use bus-on-shoulder strategies, with most applications on the right-side shoulder. Eight States (Colorado, Georgia, Hawaii, Massachusetts, New Jersey, Virginia, Texas, and Washington) allow general traffic to use freeway shoulders during fixed times of the day. Minneapolis and Virginia have documented use of dynamic PTSU through traffic-responsive dynamic signs, but several states are planning dynamic PTSU. The most complex aspect of implementing successful PTSU is the need for multiagency and multistakeholder coordination. Before and after study data primarily comes from Europe (Netherlands, Germany, United Kingdom, and Ireland) due to the limited number of recent deployments in the United States (Jenior et al. 2016). Static part-time, dynamic shoulder use is not necessarily an "innovative" strategy, but it is a resourceful strategy and, given its lack of widespread but growing implementation, is somewhat innovative.

In general, PTSU increases capacity; however, applications that do not allow shoulder use through interchanges require shoulder traffic to merge back into GP lanes. One strategy to reduce weaving at the end of shoulder-use sections is to add a GP lane in advance of an interchange (Jenior et al. 2016). Dowling et al. (2011) note that it would be useful to measure the weaving

intensity factor for weaving sections with PTSU, but data collection is cost prohibitive. Microsimulation studies showed that dynamic PTSU could be effective at mitigating traffic bottlenecks formed by property-damage-only traffic accidents (Ma et al. 2016).

Jenior et al. (2016) illustrate various types of merge and diverge areas for PTSU and recommend temporarily converting taper ramps to parallel-style ramps with speed change lanes to reduce conflicts between vehicles using the shoulder and crossing traffic. This could potentially increase capacity, as shown in figure 11.
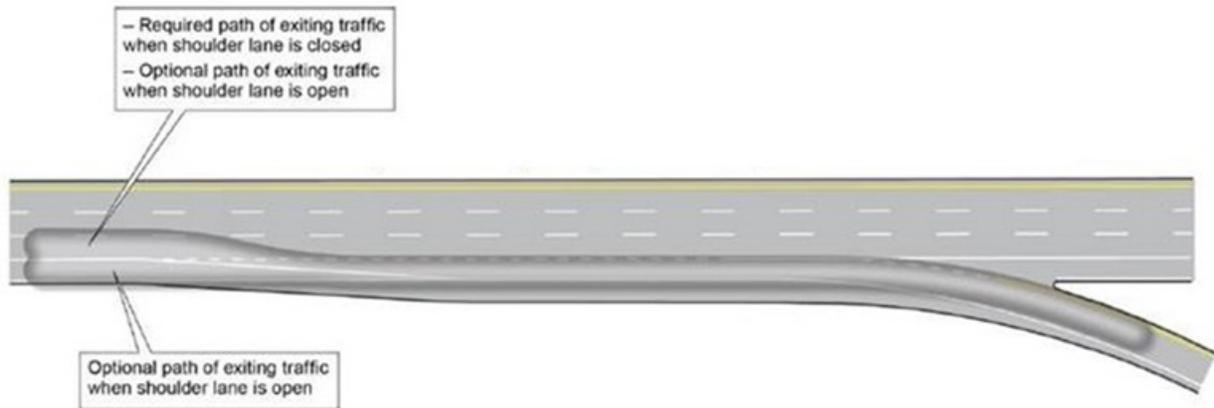
A. Parallel-style off-ramp traffic with PTSU.
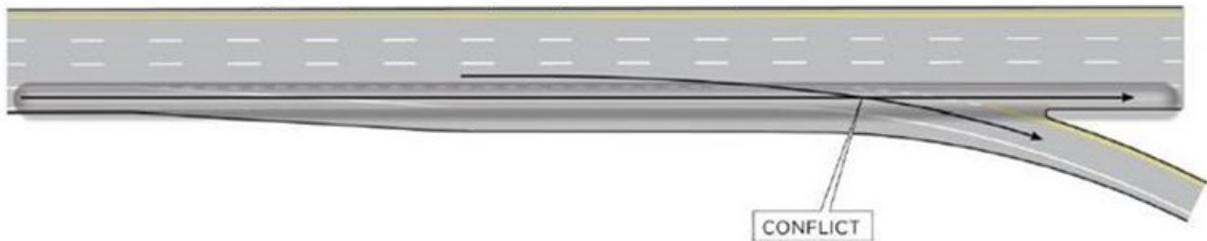
B. Taper-style off-ramp ramp traffic with PTSU.
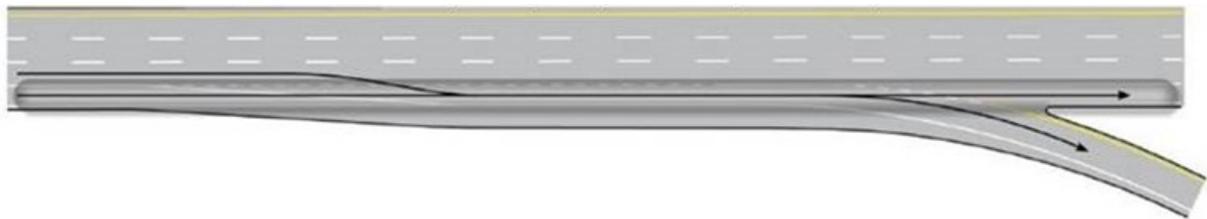
C. Conversion of taper-style to parallel-style off-ramp.

**Figure 11. Illustrations. Parallel-style and taper-style off-ramps with PTSU (Jenior et al. 2016).**

The temporary conversion depicted in figure 11-C can be achieved with pavement markings, but the geometry of the existing ramp (specifically the convergence angle at the gore area) will affect the degree of maneuverability afforded. A larger convergence angle allows for less maneuver area, resulting in greater impacts to capacity. Conversion of two-lane taper ramps may require the addition of another speed change lane downstream of the entry gore or upstream of the exit gore (Jenior et al. 2016).

In addition to design and operational considerations, Kuhn et al. (2013) discuss benefits and drawbacks of advanced transportation demand management (ATDM) strategies that complement PTSU, including VSLs, queue warning, dynamic merge control (DMC), and dynamic traveler information. They note that many of these require intelligent transportation systems (ITS) technologies and interagency coordination and deployment accompanied by performance measures.

## ICM

There is an extensive body of literature related to ICM. According to Zhang et al. (2014), ICM is a proven congestion relief strategy. However, expectations were that this project would focus on facility strategies as opposed to corridor-wide strategies.

## CRM

### *Heuristic Ramp Metering Coordination (HERO)*

Professor Markos Papageorgiou and Dr. Ioannis Papamichail at the Dynamic Systems and Simulation Laboratory of the Technical University of Crete, Greece, developed a traffic responsive feedback control strategy that coordinates local ramp metering actions for freeway networks (Papamichail et al. 2010). HERO, the proposed coordination scheme, has seen extensive testing via simulation and in-field implementations. HERO is modular in structure and includes many interacting and cooperating feedback control loops (such as mainstream occupancy control, ramp queue-length control, and waiting time control) as well as two Kalman filters for estimation of ramp queue length and mainstream critical occupancy (Samad and Annaswamy 2011).

HERO uses an extended version of the ALINEA feedback control algorithm used in the field at a local level (i.e., individual junctions). The HERO control strategy is coordinated, feedback-based, ruled-based, reactive (no real-time modeling needed), and generally applicable to any freeway network. The HERO algorithm employs at its base the local, uncoordinated control algorithm ALINEA, used at 100 on-ramps around the world since its development in the 1980s. HERO introduces coordination to the system on an as-needed basis by setting minimum ramp queue lengths that supersede the ALINEA algorithm. This reallocates congestion from a ramp at the bottleneck to a temporary cluster of upstream ramps until the congestion dissolves and the cluster deactivates. Figure 12 shows a schematic of the HERO software.
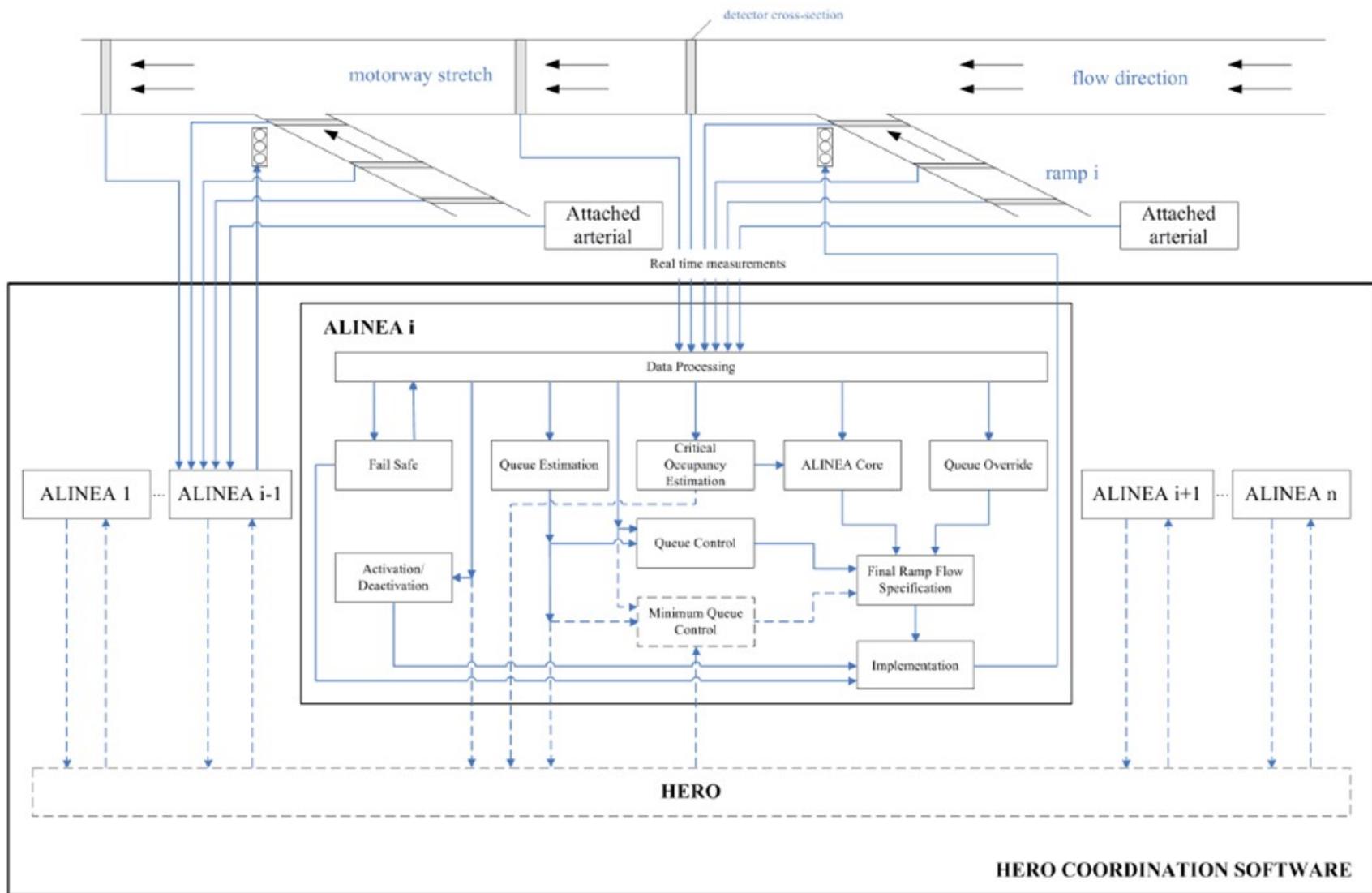
**Figure 12. Diagram. HERO coordination software (Papamichail et al. 2010).**

The HERO traffic-responsive ramp metering system uses upstream ramp storage to postpone freeway congestion. Delft University researchers' Vissim simulation HERO algorithm study showed that HERO-coordinated control outperformed noncoordinated ramp metering (Yuan et al. 2009).

Amini (2015) said that ramp meters affect not only the performance of the motorway, but also the performance of the arterial road network. Use of the available literature directs implementation of the HERO ramp metering system as closely as possible using the Aimsun application programming interface. The implemented algorithm is evaluated using a network-wide approach. In addition, introduction of a set of novel measures facilitates the evaluation of the impacts of a ramp metering system on the entire network.

The conclusion is that HERO provides a maximum mainline speed benefit of approximately 34 percent over various motorway sections (for the specific network and demand profiles examined). However, the arterial speeds were negatively affected in certain cases (thereby establishing the need to examine broader metrics than the mainline motorway). For instance, the network-wide impact (considering both mainline and arterials) on total system travel time is found to range from -1.4 percent to 1.7 percent, further highlighting that the implementation of ramp metering could result in network improvements or deterioration depending on the specific case being examined, calibration "fine-tuning," and the coordination with the arterial street network. In other words, even in some cases where the mainline improved, the overall system could suffer (e.g., if ramp metering is not optimally deployed with a consideration of the network impact). This highlights the need to consider metrics beyond only mainline conditions and stresses overall deployment, planning, and configuration.

A study on a HERO pilot project at six consecutive on-ramps on the Monash Freeway in Melbourne, Australia, showed significant increase in throughput and reduction in travel times compared to the previous ramp metering system (Papamichail et al. 2010). Implementation of the system is now taking place at 63 on-ramps. Similarly, in a before-and-after study of a HERO pilot application, ramp metering with traffic-responsive feedback control strategy (HERO) outperformed fixed rate ramp metering systems and had a benefit–cost ratio of 13.8:1 (Faulkner et al. 2014).

### *Fuzzy Logic*

This is a system-wide ramp metering algorithm in use in Seattle, WA, and Miami, FL. An evaluation of the fuzzy logic ramp metering in 2000 in Seattle showed that compared to local metering and to the bottleneck ramp metering algorithm, the fuzzy algorithm had improved travel times and higher throughput system-wide (Taylor and Meldrum 2000). According to the report:

> The fuzzy logic algorithm metered more restrictively than the local algorithm or bottleneck algorithm when preventing a mainline bottleneck, secondary queue formation, or an excessive queue. In cases where there were no tangible system-wide benefits to metering more restrictively, the metering rates during fuzzy metering were higher than those of the local or bottleneck algorithms in order to increase the throughput.

The fuzzy logic algorithm takes traffic data from sensors and converts them to textual values in a process called "fuzzification." Based on this, the controller determines the control actions which are defuzzified to metering rates (Taylor, Meldrum, and Jacobson 1998).

### *Systemwide Adaptive Ramp Metering (SWARM)*

California Department of Transportation (Caltrans) developed SWARM and implemented it in Orange, Los Angeles, and Ventura counties in the late 1990s; this system was later installed along six corridors in Portland, OR, in 2005. SWARM has two modes: global and local. Metering rates calculated from each mode determine the most restrictive one, which is applied. In the coordinated global mode, the future state of density is estimated from field data using regression and applying a Kalman filter to capture nonlinearity. The excess density (difference between forecast density and predetermined threshold value) is used to calculate the volume reduction at each detector station. The local mode uses real-time local traffic conditions at each ramp. Field experiments by Caltrans revealed that the SWARM algorithm increased mainline speed by 11 percent, decreased travel time by 14 percent, and reduced delay by 17 percent. Also, the queue lengths increased by more than 40 percent at the nine busiest on-ramps. A pilot study in Portland did not show significantly favorable results (Ahn et al. 2007). Total delay is found to have increased with SWARM, probably due to higher metering rates at most on-ramps.

### DMC

It appears that DMC is not gaining much traction in the United States despite some European implementations. Virginia Department of Transportation (VDOT) performed detailed microsimulations of DMC in the Richmond area and found it is not an ideal solution (Schneider Electric and RK&K 2015). Jiang's DMC simulation study found DMC to be hugely beneficial, but these results seem overly optimistic (Jiang et al. 2015). It is possible that congestion is simply moved upstream of the network entry nodes being simulated. DMC should only be beneficial when one can afford to remove a mainline lane without substantial negative consequences (a dubious proposition in most urban areas). In terms of the ramifications for the Alternative Freeway Designs at Merge and Diverge Segments project, deployment of DMC is conceivable in tandem with a strategy like ramp metering that assists the mainline at the expense of the ramp. In other words, one could dynamically switch back and forth between DMC and ramp metering depending on which upstream feeding road flows more favorably. Unfortunately, where both upstream feeding roads are congested, this seems costly and ineffective. In essence, DMC is a lane closure strategy, and it is difficult to envision an effective freeway merge (or diverge) strategy that would be based on lane closure. An ATDM study confirmed little benefit from DMC on its own, but some benefits were shown when combined with other ATDM strategies (Yelchuru et al. 2017).

### VSLs

VSL systems utilize information on traffic speed, occupancy, volume detection, weather, and road surface conditions to determine the appropriate speeds at which drivers should be traveling (Katz et al. 2017). During adverse conditions, such as heavy traffic and adverse weather, the use of VSLs can improve safety by decreasing the risks associated with traveling at speeds that are higher than appropriate and by reducing speed variance in traffic. In addition, VSLs can be used

to dynamically manage speeds during planned (rush hour congestion) and unplanned (incidents) events. Used in conjunction with MLs and other active traffic management strategies, VSLs can respond to downstream congestion to eliminate or delay bottlenecks and mitigate the possibility of crashes. Based on a comprehensive literature review along with agency interviews to gather information on existing, deactivated, and planned VSL systems, this synthesis provides a comprehensive review of current practices on VSL operations, focusing on deployments in the United States. The synthesis identifies successful and best practices from the following perspectives: planning and policy, design, deployment, and standards, operations and maintenance, and outcomes.

## Cycle-based Variable Speed Limits (CVSLs)

Figure 13 shows the CVSL strategy, which dynamically creates gaps in mainline traffic by frequently adjusting speed limits (Zhang et al. 2017). Although this would seemingly require CAV technology to be effective, it could work if implemented via dynamic traffic calming devices. Consideration of different intervals and durations of speed optimization could show that short intervals and durations of speed optimization are successful within the microsimulation experiments. If so, the final project report could recommend further research on dynamic traffic calming devices and CVSLs.
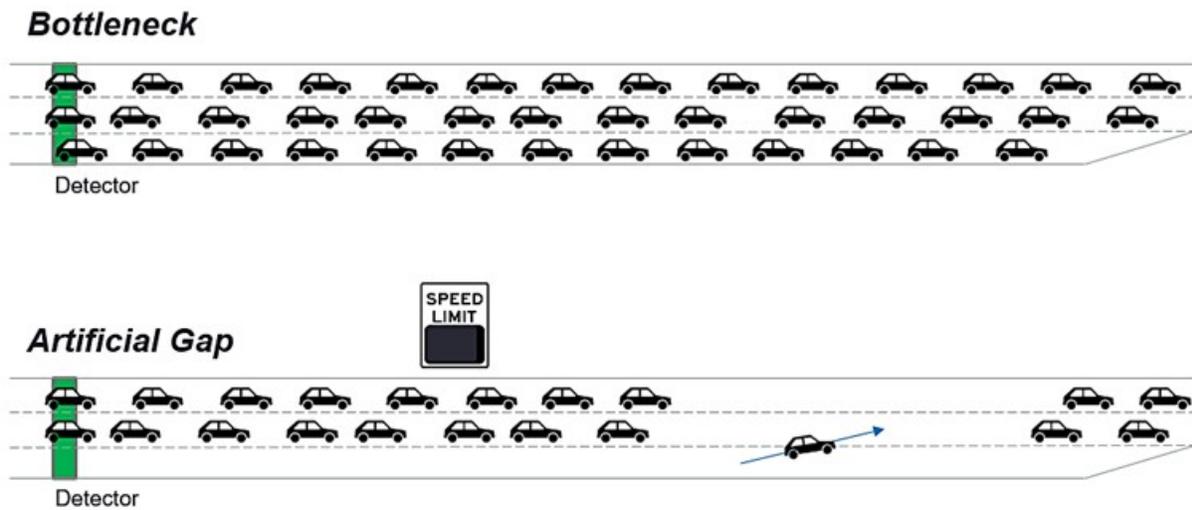


Source: FHWA.

**Figure 13. Illustration. The CVSL concept.**

## Design of MLs

Stanitsas et al. (2014) evaluated shockwaves resulting from two ML access typologies: restricted access (I–394) and several points on continuous access (I–35W). Design of the first dynamically priced high-occupancy toll (HOT) lane used a closed access philosophy, meaning that for the greater length of the roadway, access to the HOT lane is restricted with only specific entry points over short-length sections. Specifically, one location on the southbound direction of I–35W causes the biggest shockwaves on the facility. The study concluded that it is difficult to compare the two design philosophies because they serve the needs of the two distinct roadways. The

researchers stated that it would have been difficult to follow a closed access design on I–35W, and their research results led them to conclude that it would have made little difference in terms of mobility and safety. Comparisons of shockwave characteristics of four access zones show that, although the volumes at each access zone were different, the shockwave lengths observed were comparable, indicating no difference in terms of safety between the two design philosophies. California's most recent designs recommend openings of 2,000 ft in length, including dimensions for lane-change maneuvers to adjacent entrance and exit ramps (California Department of Transportation 2011).

The *HCM* contains a methodology for evaluating the operational performance of MLs (Transportation Research Board 2016). The ML analysis is typically performed as part of a freeway facility analysis, which encompasses a 10–15-mi-long facility and evaluates its operational performance over multiple time periods. Figure 14 distinguishes between five ML segment types.
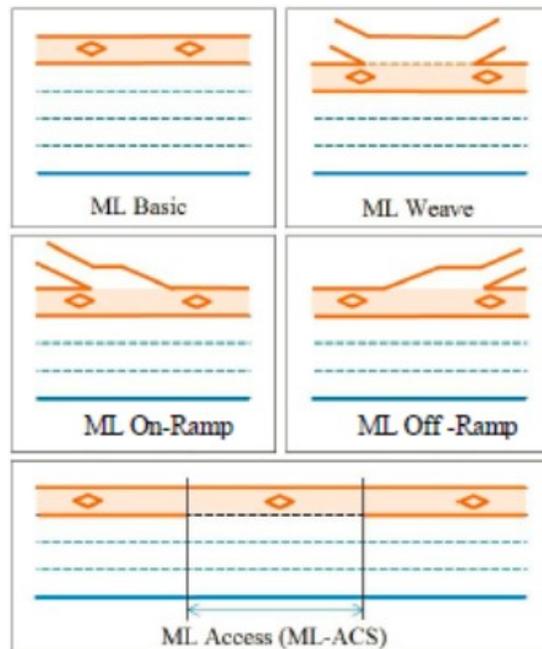
**Figure 14. Illustration. ML segment types in the *HCM* (Wang et al. 2012).**

The *HCM* ML method was initially developed as part of the National Cooperative Highway Research Program (NCHRP) Project 03-96, and is documented in NCHRP web-only document 191 (Wang et al. 2012). The research collected data at ML facilities across the United States and developed speed-flow relationships of various ML segment types. The methodology distinguishes between three separation types, including stripe-only separation, painted buffer separation, and physical barrier separation. Figure 15 illustrates the separation types and shows two-lane options for buffer and barrier separation.
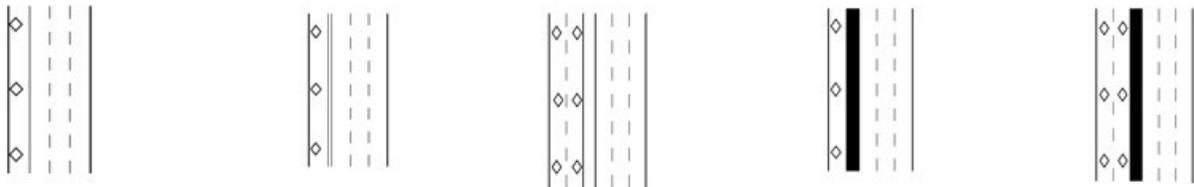
**Figure 15. Illustration. ML separation types in the *HCM***
**(Transportation Research Board 2010).**

The *HCM* discusses separate speed-flow relationships developed for each separation type, as well as for one-lane versus two-lane ML facilities. For facilities with only paint or buffer separation, the *HCM* further defines an "adjacent friction effect," which lowers the speed-flow curves in the MLs when GP lane densities exceed 35 passenger cars per mile per lane. In other words, the performance of the MLs is impacted by congestion in the adjacent GP lanes.

The *HCM* ML method also includes a new type of weaving maneuver, referred to as the "cross-weave effect." The cross-weave effect quantifies the capacity reducing impacts of the two-sided weaving maneuver between a GP on-ramp and an ML access point (or vice versa). Figure 16 illustrates the cross-weave effect. The *HCM* ML method is limited in its ability to evaluate impacts of specific ML terminus configurations, which is beyond the scope of the original project. As a result, no specific guidance is given in the *HCM* about the performance of different access point geometries or ML start or end points.
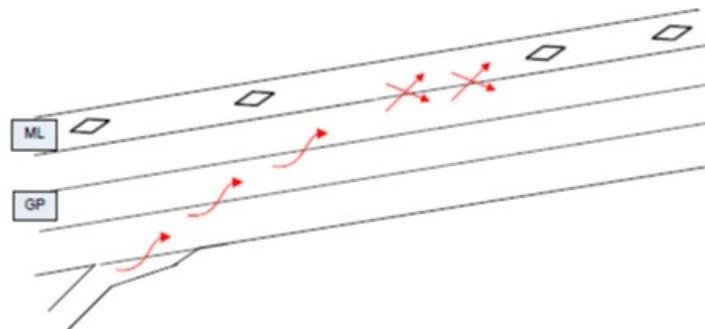
**Figure 16. Illustration. ML cross-weave effect (Wang et al. 2012).**

**Summary**

The brainstorming exercise for conceiving alternative freeway designs produced 12 viable strategies for this research project. In the next stage of the project, the team needed to create a shorter list of alternative strategies for microsimulation-based sensitivity analysis. Categories of the strategies included the following:

- Innovative geometric designs.
- Vehicle speed or speed limit control.
- Dynamic lane closures.
- Advanced or alternative freeway signalization.
- ML design.
- Advanced signage.

A literature review conducted in parallel found few innovative geometric designs but a fair number of sources in the other categories. This literature review helped to expand and finalize the list of viable strategies.

# CHAPTER 3. RESEARCH WORK PLAN

The researchers developed a comprehensive research work plan for data collection and analysis after reviewing viable strategies and the relevant literature. The plan included approaches to modeling the traffic in microsimulation and calibrating the existing conditions for all selected freeway segments. The plan also described a search for and selection of several sites experiencing freeway merge/diverge deficiencies and speed-change areas resulting in capacity reduction. Similarly, for the left-side ML problem, the team identified sites with open-access HOV or HOT lanes that have an ML located on the left-hand side of the freeway cross section. The intent is to expand the use of these sites for generic analyses and recommendations.

The team began with discussion of a shorter list of five top-candidate strategies, listed and described below, that the group identified and down-selected during task 2: synthesis of research and findings. The strategies are:

- Acceleration and deceleration lane designs.
- Speed optimization (e.g., via dynamic traffic calming devices).
- Mainline metering (i.e., dynamic signal control).
- Coordinated adaptive ramp metering system (e.g., HERO).
- Open-access MLs on the right-hand side.

## ACCELERATION AND DECELERATION LANE DESIGNS

Restricting merging drivers to a specific new set of acceleration and deceleration lane locations may help to smooth traffic flow. Regarding acceleration lanes, figure 3 shows how drivers are prohibited from merging at the midsection of acceleration lanes. By eliminating the uncertainty of merge maneuvers for both mainline and ramp drivers, both sets of drivers can prepare for and execute the merging maneuver efficiently. Regarding deceleration lanes, figure 4 shows how drivers merge at a mid-section of the off-ramp. Separating the turbulence associated with diverge maneuvers potentially mitigates mainline congestion.

## SPEED OPTIMIZATION (E.G., VIA DYNAMIC TRAFFIC CALMING DEVICES)

Speed harmonization and VSL studies for optimizing freeway traffic flow imply that medium free-flow speeds (e.g., 30 mi/h) would be more effective than low speeds (e.g., 5 mi/h) or high speeds (e.g., 65 mi/h). Although this project endeavored to focus on strategies not requiring CAV technologies, the team believes that dynamic traffic calming devices (e.g., retractable rumble strips) may someday be capable of coercing drivers to obey medium speeds at higher rates of compliance. Figure 8 illustrates this concept.

## MAINLINE METERING (I.E., DYNAMIC SIGNAL CONTROL)

A form of mainline metering to reduce demand and improve flow uses traffic metering upstream from a bottleneck, thereby regulating the number of vehicles moving through the bottleneck. At locations where capacity expansion is not feasible (i.e., at tunnels and bridges), implementation of this form of mainline metering can help. For example, metering for traffic arriving at the

bridge or tunnel is used at the Bay Bridge in Oakland, CA; the Hampton Roads Bridge-Tunnel connecting Hampton, VA, and Norfolk, VA; and the Baltimore Harbor Tunnel in Baltimore, MD.

In situations where mainline and ramp vehicle speeds are both very low, and fall below a defined threshold, such as 5 or 10 mi/h, traffic signal control applied to both upstream approaches could optimize the operation by eliminating merge friction. Figure 9 illustrates this concept. However, there is no known application of the treatment.

## COORDINATED ADAPTIVE RAMP METERING SYSTEM (E.G., HERO)

Traditional ramp metering measures upstream freeway mainline volume to determine ramp flow, but rarely monitors downstream conditions. Downstream problems only show when congestion reaches the upstream ramp detector. Coordinated adaptive ramp metering uses feedback logic in a closed loop control system. Traffic conditions measured at downstream bottlenecks determine critical occupancy and appropriate levels of traffic entering from upstream. The process assumes a historic or theoretical value of freeway capacity. Downstream flow conditions provide feedback to determine real-time ramp flow and optimal occupancy. When applied on a holistic, coordinated, system-wide basis, all ramps continuously communicate with each other to resolve complex traffic flow situations. One example of such a system is called HERO, but the team identified several similar algorithms and systems during the task 2 effort.

## OPEN-ACCESS MLs ON THE RIGHT-HAND SIDE

Typically in the United States, managed HOV/HOT lanes provide an improved level of service to drivers and are at the far left-hand side, next to the median. Although locating the ML on the right-hand side would reduce its capacity, the overall impact on all lanes could be beneficial. This project compared right-side ML designs to left-side designs (i.e., with continuous access or partial access). Reduction by 300 veh/h in the overall capacity of a four-lane freeway occurs if the right-side ML capacity is reduced from 2,000 to 1,700 veh/h, and the other three lanes remain at 2,000 veh/h. However, left-side MLs can result in a much larger capacity loss since all lanes can experience the 300 veh/h capacity loss due to vehicles weaving from the right to the left. Even if only the middle two lanes were impacted by this weave friction and turbulence, there may be a capacity loss of 300 x 2 = 600 veh/h, or twice that of a right-side ML.

## SITE SELECTION

To test the alternative designs noted above, the team considered the following site selection criteria:

- Exhibits one of the two typical merging problems (i.e., right-side on-ramp, left-side ML) described by the project scope of work.
- Does not currently employ active transportation management (ATM) strategies or already have reconstruction plans.
- Has nearby stakeholders supportive of pursuing innovative treatments.

- Has existing calibrated microsimulation datasets that realistically replicate car following and lane changing operations (or readily available data to support coding of new datasets).
- Well described in project reports and papers in terms of existing conditions, maps, endpoints, and so on.

**Table 1. Site selection matrix of characteristics.**

| Site | Merge | ATM | Support | Datasets | Details |
|------|-------|-----|---------|----------|---------|
| I–270 MD | — | None | Yes | Vissim (calibrated) | Yes |
| I–95 PA | Both (no ML) | None | — | Vissim (uncalibrated) | Yes |
| I–35 KS | Right side | Ramp meters | Yes | Vissim (uncalibrated) | Yes |
| I–66 VA | Both | — | — | Vissim (calibrated) | Yes |
| US 95 NV | — | None | — | Aimsun (uncalibrated) | Yes |
| I–15 CA | Both | None | — | Aimsun (calibrated) | Yes |
| I–35W MN(1) | — | — | Yes | Aimsun (calibrated) | — |
| I–394 MN(1) | Both | — | Yes | Aimsun (calibrated) | — |
| I–94 MN | — | — | Yes | Aimsun (calibrated) | — |
| I–35W MN(2) | Both | None | Yes | TSIS-CORSIM (calibrated) | Yes |
| I–394 MN(2) | — | — | Yes | TSIS-CORSIM (calibrated) | Yes |
| C–470 CO | Right side | — | Yes | (Possibly) | Yes |
| I–5 WA | Right side | None | Yes | Yes | Yes |
| SR 535 FL | Right side | None | Yes | Vissim | — |

—No data.
Note: Numbers in parenthesis indicate particular run of simulation model.

Table 1 reveals some mismatches between sites having local support and sites where usable datasets are currently available. During the 3-mo task 3 effort for data collection and model calibration (i.e., October 12, 2017–January 12, 2018), the team endeavored to find local support for innovative solutions and to find data (or datasets) at sites where local support already exists. The team accepted support offered by Washington State, Colorado, and Maryland. As shown in table 1, the initial datasets provided mostly included calibrated or uncalibrated microsimulation models. For the sites that were selected to test the alternative designs, the team ensured that the simulation models were calibrated properly to site conditions by adjusting car following and/or lane changing behavior. Detailed calibration information along with calibration results are provided in the appendix.

The specific sites selected for potential use in the study were:

- I–270 MD.
- I–95 PA.
- I–35 KS.
- I–66 VA.

- US 95 NV.
- I–15 CA.
- I–35W MN.
- C–470 CO.
- I–5 WA.

**I–270 MD**

This project used a calibrated I–270 MD Vissim dataset developed for the Federal Highway Administration (FHWA) Narrowing Freeway Lanes and Shoulders to Create Additional Travel Lanes project. The dataset was recently exported from Visum (a macroscopic simulation tool, unlike Vissim), which implies that it might not be calibrated. Moreover, because the Narrowing Freeway Lanes and Shoulders to Create Additional Travel Lanes project developed the dataset, it might not satisfy criterion A listed above. Separately, FHWA and the Maryland State Highway Administration provided an I–270 MD Vissim dataset with static demands and an accompanying calibration report[1].

**I–95 PA**

The team identified an I–95 facility exhibiting right-side merge problems and an available Vissim dataset. The team contacted Pennsylvania and Delaware officials to solicit local support. In 2011, Vissim models were developed in Pennsylvania Department of Transportation (PennDOT) District 6 for the a.m., p.m., and weekend peak hours. The study area extends approximately 16 mi along I–95, from the Delaware State line to the Schuykill River. The following interchanges were also included:

- Chichester Avenue interchange (two unsignalized ramp terminals).
- Market Street interchange (one signalized and one unsignalized ramp terminal).
- US 322 Conchester Highway interchange (one signalized and one unsignalized ramp terminal).
- US 322 Barry Bridge approach (system interchange).
- Kerlin Street ramps (ramp terminals not modeled).
- Edgemont Avenue interchange (clustered signal at Edgemont Avenue).
- Chestnut Street interchange (ramp terminal not modeled).
- I–476 interchange (system interchange).
- Stewart Avenue interchange (two signalized ramp terminals).
- Wanamaker Avenue interchange (cloverleaf interchange).
- Airport area (see model for specific details).
- Bartram Avenue interchange (signalized ramp terminal).
- Enterprise Avenue ramps.

---

[1]I–270 Modeling Calibration Methodologies Memorandum.pdf

Figure 17 through figure 19 show that the study corridor consists of several right- and left-side merge and diverge locations; however, it does not include MLs. Traffic volumes for the mainline of I–95 and all ramps were developed by using two sources of data:

- Hourly mainline counts at select locations collected by the Delaware Valley Regional Planning Commission, the region's metropolitan planning organization.
- Origin–destination (O-D) data for each interchange recorded using Bluetooth data. The O-D data consisted entirely of percentages of vehicle routes and not counts. Separate O-D data are provided for each time period (a.m., p.m., and weekend).

The combination of hourly mainline counts with the O-D percent data allowed computing all volumes in the study area, maintaining the O-D route pattern structure. This ensured that the weaving behavior and its effect on capacity were better captured in the simulation, particularly at the merge/diverge locations. Vissim models used static demand data (i.e., not varying within the peak period). The model includes 7,200 s of demand data, where the first 3,600 s comprises the "warm-up" period. The heavy vehicle proportion is 9 percent in both the a.m. and p.m. peaks.



Original photo: © 2017 Microsoft® (see acknowledgements).

**Figure 17. Map. Southern part of the I–95 Vissim study corridor in PennDOT District 6.**

Original photo: © 2017 Microsoft® (see acknowledgements).

**Figure 18. Map. Middle part of the I–95 Vissim study corridor in PennDOT District 6.**



Original photo: © 2017 Microsoft® (see acknowledgements).

**Figure 19. Map. Northern part of the I–95 Vissim study corridor in PennDOT District 6.**

*Field Observations and Bottleneck Locations*

The study corridor experiences both right side and left side merge and diverge issues. For some of the on-ramp locations, relatively short merge on-ramps further exacerbate the weaving problem. As part of the initial modeling project, the team conducted site visits to observe operations from the field. Although the site visits took place in October 2011, the problem locations identified as part of the 2011 study still existed for this project based on 2017 Google® Maps™ traffic information and estimated travel times along the corridor during the peak periods. Google® Maps™ provided the data and detailed information discussed below.

Google® Maps™ traffic information and field visits indicated the bottleneck locations in the a.m. peak. Field observations indicated northbound congestion prior to Exit 3 where traffic speeds drop approximately to 30 mi/h due to the left-side US 322 on-ramp. High traffic volumes and a relatively short merge area are the primary sources of congestion. While the observations are from 2011, 2017 Google® Maps™ traffic prediction showed similar patterns. Figure 20 and figure 21 display both the ramp configuration in Vissim and present year estimated travel time and bottleneck locations from Google® Maps™.

32
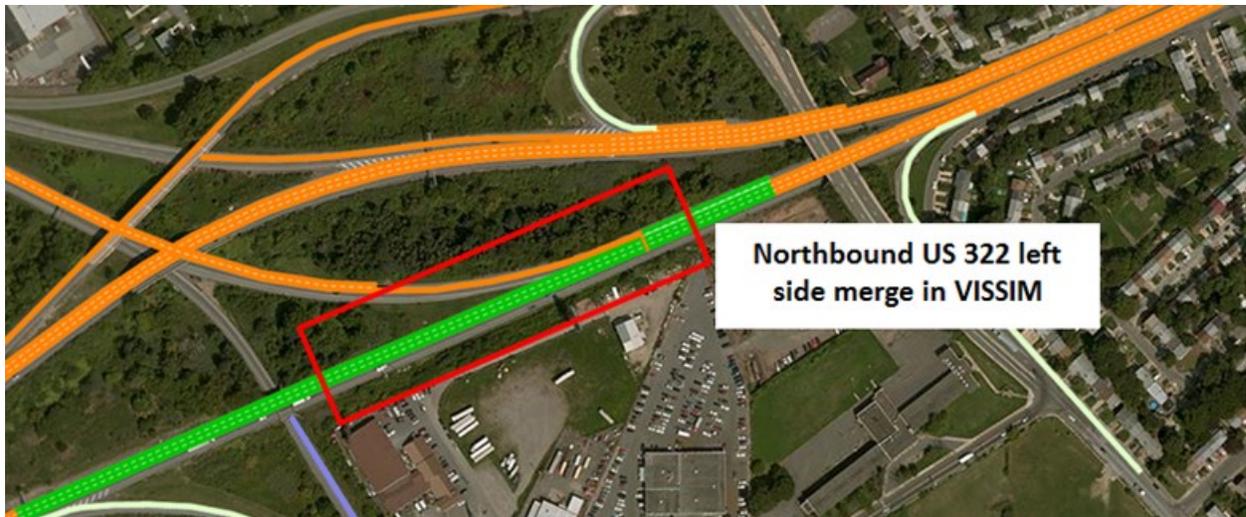
**Figure 20. Map. Northbound US 322 left-side merge in Vissim.**
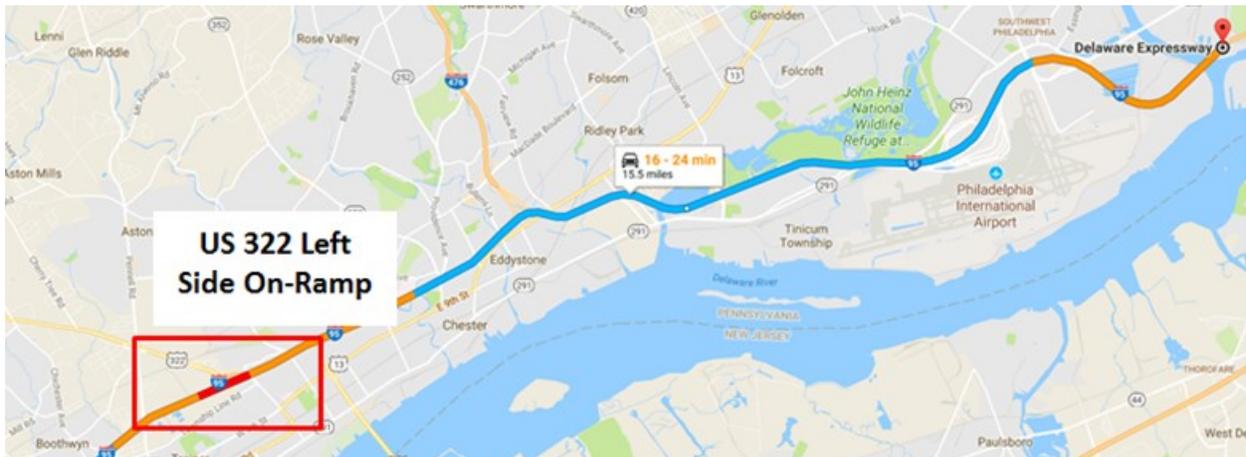
**Figure 21. Map. Estimated travel times in the northbound direction during the a.m. peak: estimated travel time for a typical Wednesday around 8 a.m.**

Field observations from 2011 in conjunction with 2017 Google® Maps™ traffic data indicated that the I–476 interchange is another bottleneck in the corridor in the southbound direction during the a.m. peak. Figure 22 and figure 23 show the ramp configuration in Vissim and the estimated southbound travel time along the corridor on a typical Wednesday around 8 a.m. and highlights bottleneck locations. The congestion resulted from the I–476 on-ramp and the weave between it and the exit 6/Providence Avenue/Edgmont off-ramp.

**Figure 22. Map. Southbound I–476 right-side merge in Vissim.**
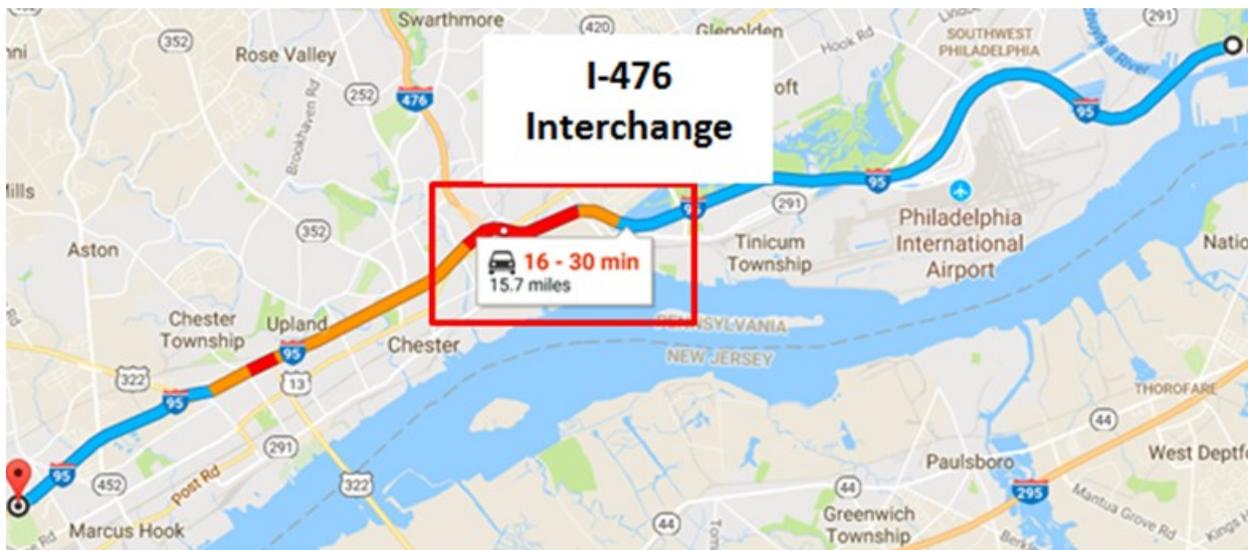
**Figure 23. Map. Estimated travel times in the southbound direction during the a.m. peak: estimated travel time for a typical Wednesday around 8 a.m.**

Google® Maps™ traffic information and field visits indicated the bottleneck locations in the p.m. peak. Similar to the a.m. peak, field observations indicated that the US 322 left-side on-ramp is a source of congestion, resulting in lower speeds and stop-and-go conditions during certain times. The observations from 2011 were also confirmed with the estimated travel time

from Google® Maps™, as illustrated in figure 24, indicating heavy congestion in the northbound direction resulting from the US 322 on-ramp and weaving.
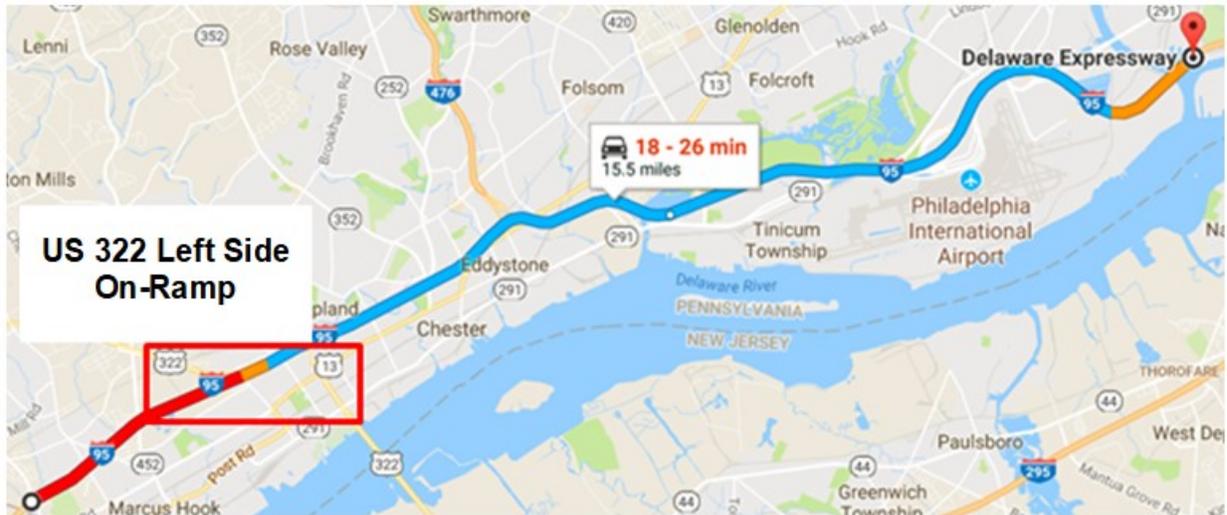


Original photo: © 2017 Google® (see acknowledgements).

**Figure 24. Map. Estimated travel times in the northbound direction during the p.m. peak: estimated travel time for a typical Wednesday around 5 p.m.**

Field results indicated that the I–476 interchange appeared to be the primary source of congestion. According to the 2011 field observations, I–95 traffic flowed around 30–40 mi/h through the interchange. Figure 25 shows similar Google® Maps™ traffic information findings.
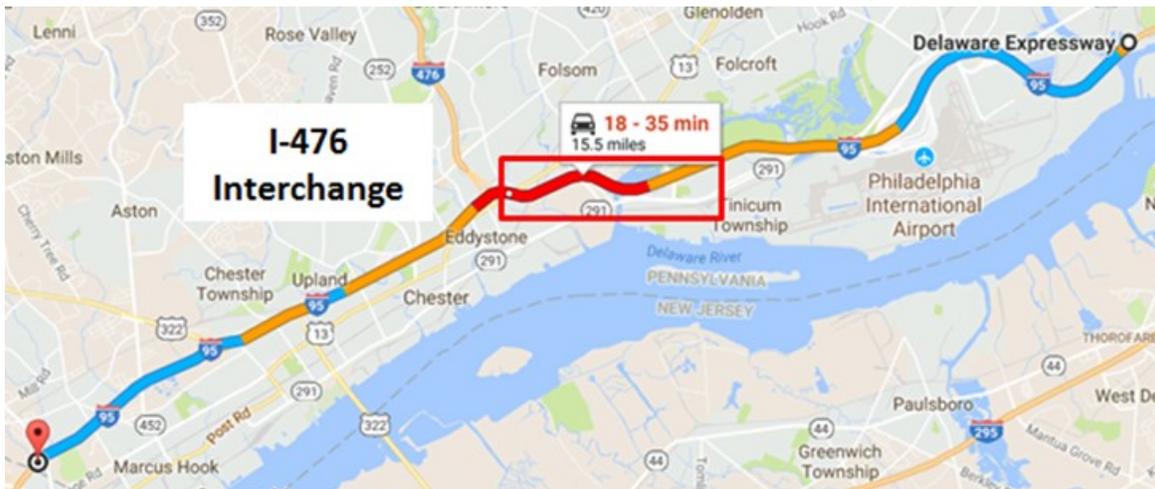


Original photo: © 2017 Google® (see acknowledgements).

**Figure 25. Map. Estimated travel times in the southbound direction during the p.m. peak: estimated travel time for a typical Wednesday around 5 p.m.**

*Data Needs*

Since the 2011 development of the initial Vissim model, including demand data, the data need updating to reflect existing conditions more accurately. Use of Bluetooth provided the O-D data. Conversion of these data within Visum gave both entry volumes and routing decisions within Vissim. Given the extent of the study corridor and the comprehensive data collection efforts as part of the previous effort, the team developed 2017 volumes by applying a "global" growth rate. This allows for maintaining the originally developed O-D demand structure while simulating traffic volumes closer to the field values.

For the development of the global rate, the latest average daily traffic (ADT) data comparison of the 2011 ADT data, combined with local knowledge and engineering judgment, can help estimate a growth rate along the corridor. Where available, the team will also compare a.m. and p.m. peak hour or peak period traffic data to identify whether this is a big discrepancy between the a.m. and p.m. peak growth rates.

The calibration used collected travel time (see below for details). The Regional Integrated Transportation Information System (RITIS) platform was used to obtain travel time results from the corridor.

*Calibration Approach*

As part of the calibration process, the team used the travel time information obtained through probe data. Simulation runs were performed 10 times with a modeling resolution of 10 time steps per second. Performance of each model run gives a total of 7,200 s, with the first 3,600 s being used as the warmup period. For the calibration, the team followed the guidance provided in the FHWA Traffic Analysis Toolbox Volume III: Guidelines for Applying Traffic Microsimulation Modeling Software (Dowling et al. 2004).

In addition to the travel time calibration, the team ensured Vissim yields realistic capacity outputs at the bottleneck locations. For segments where freeway capacity was found to be high (or low), car following and lane changing driving behavior parameters were updated in Vissim to decrease (or increase) freeway capacity. The team also observed driving behavior at merge/diverge locations to capture friction accurately along the freeway. Calibration details, including the results, are discussed in the appendix.

The Vissim model was calibrated for the p.m. peak conditions. The team reviewed existing traffic volumes including directionality and volume profiles as well as bottleneck locations (e.g., speed profiles through probe data) to determine the peak that would be most useful for the testing of innovative strategies. Since there would be additional sensitivity analysis as part of the analysis, the primary objective of the calibration effort was to setup a realistic base model that reflects actual traffic conditions.

## I–35 KS

The team obtained permission from Kansas Department of Transportation (KDOT) to use their I–35 Vissim model. This facility is approximately 10 mi long and it consists of several interchanges. The bottlenecks at the southbound direction are located at Southwest Boulevard

(merge), Shawnee Mission Parkway (weave), and 67th Street (merge). The last two bottlenecks interact with each other and it appears that queue from 67th Street propagates upstream to Shawnee Mission Parkway, and even further upstream (spillback reaches the Metcalf Avenue interchange). At the southbound direction, KDOT is operating ramp metering at 7th Street, Southwest Boulevard, 18th Street, and 67th Street.

Northbound, the facility experiences recurrent congestion at the 87th Street interchange (merge). In that direction, ramp meters operate at the 7th Street on-ramp and at Johnson Drive. Figure 26 shows a map of the facility, the congestion areas, and the locations of the ramp meters. The bottleneck locations had only two of the six ramp meters installed in the summer of 2017. The algorithm currently used is the Continuous Association Rule Mining Algorithm (CARMA) algorithm—a system-wide algorithm based on speeds. KDOT decided to switch to another system-wide algorithm that uses occupancies as thresholds for metering rate determination. The exact specifications of the new algorithm are not known to date. However, given that the metered ramps are not consecutive, it is not possible to leverage the full capabilities of a system-wide ramp metering algorithm.
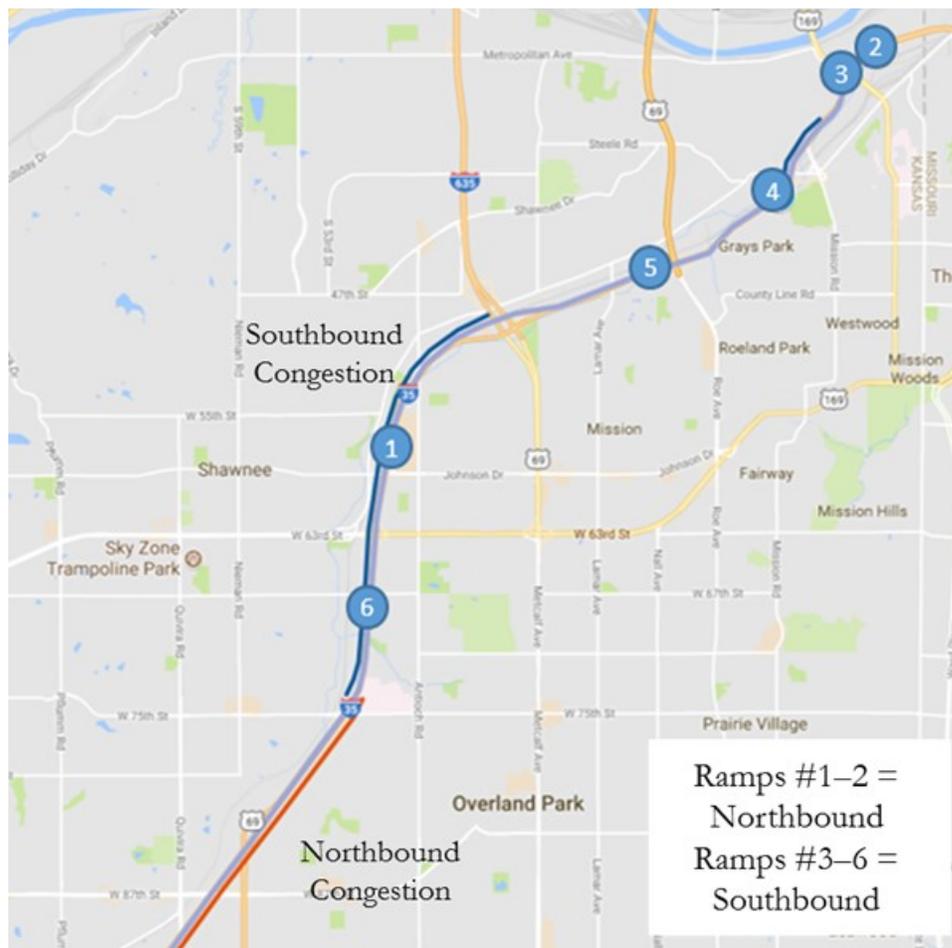


Original photo: © 2017 Google® (see acknowledgements).

**Figure 26. Map. I–35 Kansas City, KS, facility.**

KDOT provided the Vissim simulation network of the I–35 corridor, and the team performed the model calibration task. The facility is equipped with radar sensors. Field data at those sensor locations along the freeway and the on-ramps are available to the researchers through Kansas City Scout (Kansas DOT and Missouri DOT 2018).

**I–66 VA**

Various research projects use the I–66 VA Vissim dataset extensively. VDOT has multiple ATM deployments along the corridor. Currently, VDOT is upgrading I–66 outside I–495 (the Capital Beltway) to include three regular lanes in each direction and two express lanes in each direction from the Capital Beltway to Gainesville, VA. Calibration of the existing Vissim simulation network takes place before the upgrade, but the team still can use the dataset in the sensitivity analysis experiments. The simulation network is a 13-mi stretch of I–66 outside the Capital Beltway. This is a major east-west commuter corridor near Washington, DC, with four lanes in each direction. This stretch of the freeway experiences recurring congestion westbound in the p.m. peak every weekday. Figure 27 illustrates the layout of the road. The existing HOV lane has open access to the adjacent lanes with two HOV-only entrances/exits.
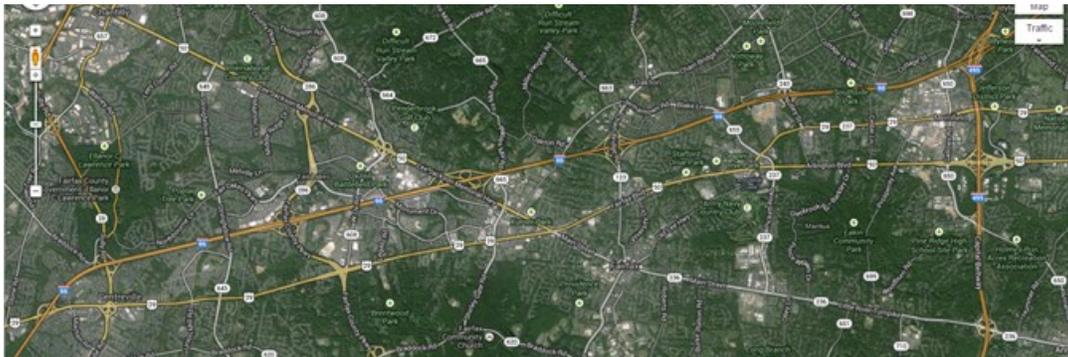


© 2016 Google®.

**Figure 27. Map. Illustration of the I–66 freeway testbed.**

The network further contains the following characteristics:

- Start: mile marker 64 (intersection with I–495).
- End: mile marker 51 (intersection with US 29).
- Length: 13 mi.
- Number of Interchanges: six.
- Average distance between interchanges: 2.3 mi.
- Number of lanes: four lanes/direction.
- Full length lanes: three (in some sections, the rightmost lane turns into a hard shoulder).

The team collected field data to build time-dependent travel demand O-D matrices for Vissim. This included collecting traffic counts and speeds on each individual lane, including HOV lanes, for the mainline, on-ramps, and off-ramps. A combination of remote traffic microwave sensor (RTMS) radar detectors, video cameras, portable action cameras, and manual counts provided speeds, volumes, and occupancies. Figure 28 shows their deployment locations. The QueensOD software, a model for estimating O-D traffic demands, provided estimates of the O-D matrices

(Van Aerde 1993). Results indicate an excellent correlation between field-measured volume and volume estimated from using O-D trips in simulation, as shown in figure 29.
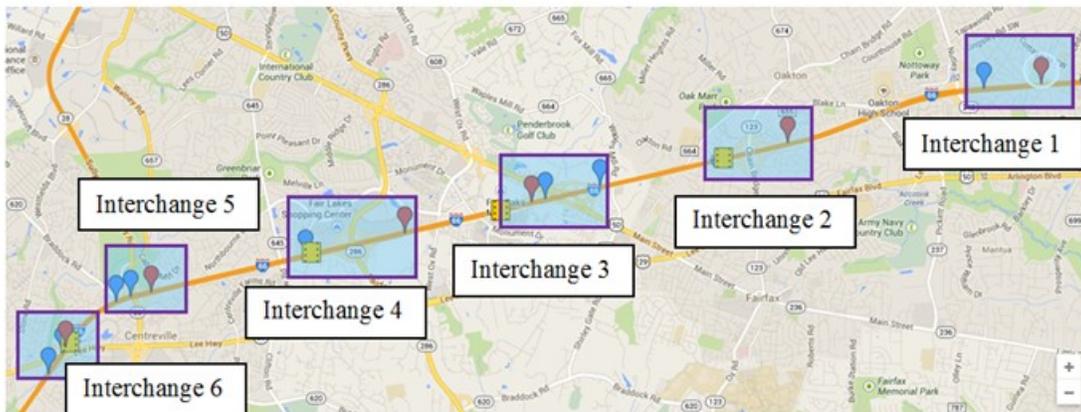


Original photo: © 2017 Google® (see acknowledgements).

**Figure 28. Map. Locations of RTMS trailers and portable action cameras.**
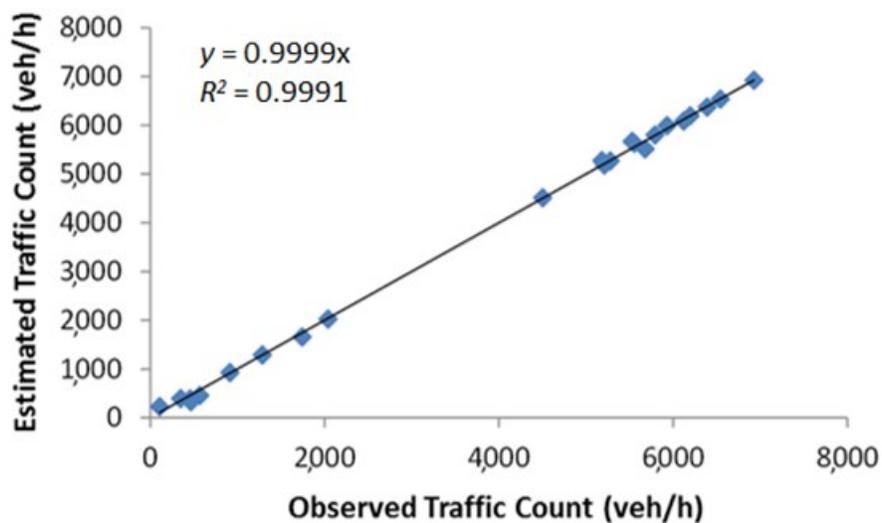


Source: FHWA.

**Figure 29. Chart. Comparison of estimated flow and observed flow from 3:00–3:15 p.m.**

## I–15 CA

The team applied coordinated adaptive ramp metering strategies in complex networks, such as San Diego, CA, and locations around the world. The team will utilize the San Diego, CA, I–15 network for testing ramp metering strategies. This network was modeled using Aimsun (2019).

The placement of ramp meters is ideal for testing adaptive ramp metering algorithms. The other network the team will utilize for this task is the San Diego, CA, ICM network shown in figure 30. This network has been developed and calibrated.
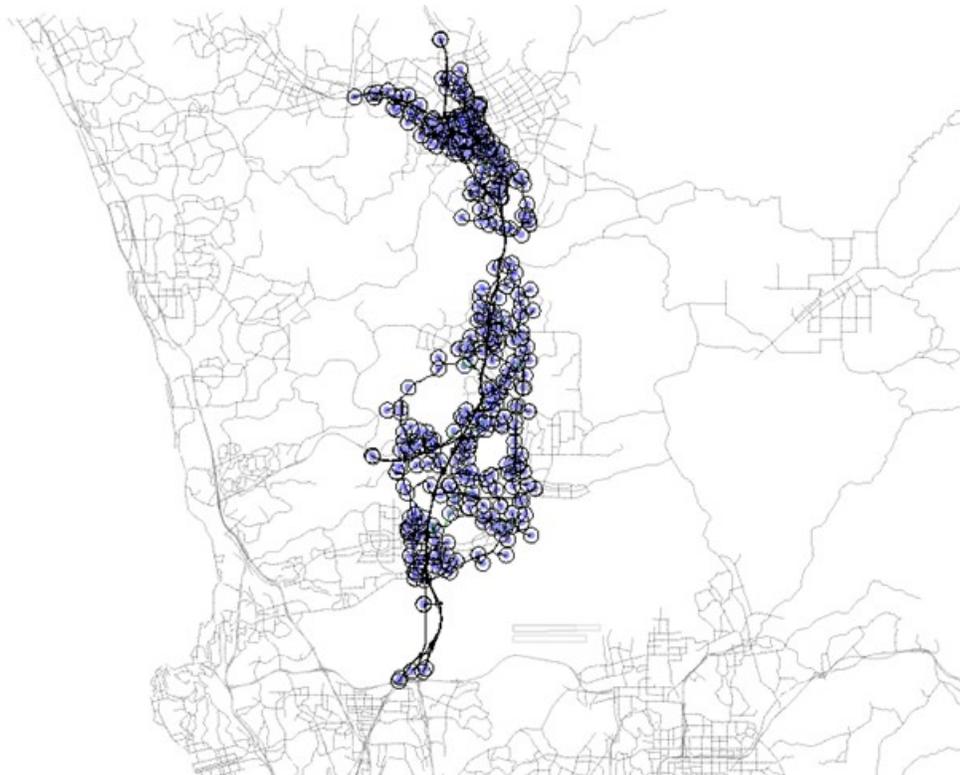
**Figure 30. Map. San Diego, CA, I–15 network.**

**I–35W MN**

The Minnesota Department of Transportation (MnDOT) has 85 percent of their freeway system covered by TSIS-CORSIM simulation models, a freely available microscopic simulation software tool. Calibration of the I–35 dataset is described within Xiao et al. (2015). MnDOT has a public access area for retrieval of their loop detector data. Some of these date back to the early 1990s.

The first link of the MnDOT Traffic Operations website under "How?" goes to the freeway data site (the traffic surveillance line) (Minnesota Department of Transportation 2019). At the top of the next screen, there are three items highlighted in blue:

- The "DataPlot" program allows the user to examine different detector data.
- The "DataExtract" program allows the user to filter and extract the freeway data in a number of ways.
- The "All Detector Report" lists all of the detectors and their locations.

**C–470 CO**

C–470 stretches from Quincy, CO, to Morrison, CO. US 285 falls within these limits (figure 31). There is no ML on this corridor yet since it is a long-range plan. US 285 comes onto C–470 as a lane add, but just north of the lane add is a buttonhook ramp (figure 32) that provided the major

merging conditions needed for this project. FHWA also provided a document to explain their calibration procedure (Cambridge Systematics, Inc. 2017).

**Figure 31. Photo. Aerial view of C–470 at US 285.**

**Figure 32. Photo. Buttonhook ramp near the junction of C–470 and US 285.**

**I–5 WA**

At the I–5/US 101 interchange in Olympia, WA, (figure 33) peak hour I–5 southbound p.m. movement creates congestion that backs up for miles each weekday. Washington State Department of Transportation (WSDOT) has a microsimulation model and a dynamic traffic assignment model available for this area. There are no MLs or ATM strategies through this stretch, but WSDOT is currently working on a study to develop operational/transportation systems management and operations/transportation demand management strategies.
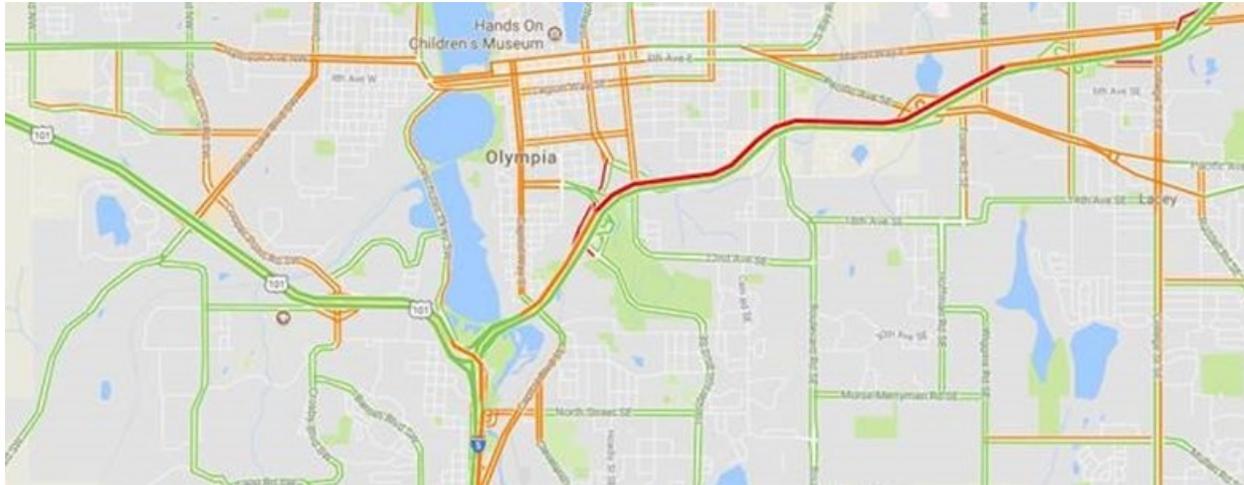


© 2017 Google®.

**Figure 33. Map. Aerial view of I–5 at US 101.**

**EXPERIMENTAL APPROACH**

The task 3 timeframe (October 12, 2017–January 12, 2018) was devoted to calibration of simulation datasets to existing conditions and coordination with interested agencies. To the extent possible, the team calibrated existing simulation datasets and/or acquired calibrated datasets, as opposed to coding new datasets from scratch. The task 4 timeframe (January 12, 2018–July 12, 2018) was devoted to simulating the proposed alternative designs. The goal is to demonstrate effectiveness of the alternative designs at real-world locations, using the task 3 collection of calibrated datasets.

The team also decided to use relatively simple networks as the first step of the simulation evaluation. For example, the evaluation of strategy 1 (acceleration and deceleration lane designs) can benefit by using a simple straight segment with an on-ramp or off-ramp. On one hand, the evaluation avoids potential influence of confounding factors (e.g., roadway curvature) on the results. On the other hand, simulations on simple segments are faster than on large, real-world networks, and the evaluation can benefit by running a large number of scenarios (e.g., factorial design of system parameters, such as demand volume, speed limit, and distance between two access points) to obtain systematic insights of the new, innovative geometric treatment.

Simulation data collected from the large number of simulation runs were then analyzed using advanced statistical methods, such as analysis of variance (ANOVA) and post-hoc tests, to understand the effects of various system parameters. This step can help the team understand how

to optimize the design of the new treatment and under what circumstances (e.g., traffic volume) the treatment can be most effective. After obtaining these insights, applying the new treatment's optimal design to a selected site will provide further evaluation capabilities, dependent on the attributes of the selected site. In the base case, the new treatment will enhance the calibrated simulation network. Based on results from the simulation on simple networks, the team can identify the most relevant design scenarios. The team conducted simulation runs of the selected scenarios to confirm effectiveness of the new treatment when deployed at the selected site. Managerial insights gave the local agency understanding for designing the treatment and its potential effectiveness.

## Input and Output Parameters

The following inputs provided sensitivity analysis during the simulation studies:

- Demand volumes (ramp and mainline).
- Car following/lane changing aggressiveness.
- Heavy vehicle percentage.
- Acceleration/deceleration lane geometries (strategy 1).
- Speed limit (strategy 2).
- Metering rate/timing (strategies 3 and 4).
- Algorithms, detection strategies (strategy 4).
- ML access point locations (strategy 5).
- Random number seeds.

The team progressively determined the exact number of runs and variations after they conducted their preliminary runs.

The team examined the following output performance measures during the simulation studies:

- Network-wide outputs.
- Segment-specific outputs (on both ramps and mainlines).
  - Throughput.
  - Travel times.
  - Speeds (using heat maps sometimes).
  - Delays.
  - Congestion duration.
  - Latent delays and queues.
  - Number of lane changes.

## Prioritization of Strategies

The team ultimately assigned three simulation modelers who completed a thorough analysis of the five top-candidate strategies during the available 6-mo window. This made prioritization of the strategies unnecessary during the sensitivity analysis phase of the project. The sensitivity analysis results ultimately implied that some strategies were more promising in terms of cost-effectiveness, as discussed in the Executive Summary and chapter 5.

# CHAPTER 4. SENSITIVITY ANALYSIS EXPERIMENTS

Following a 3-mo data collection and simulation model calibration process described in the appendix, the team carried out the main 6-mo period of simulation sensitivity analysis experiments. These experiments would determine which alternative design strategies show the most promise for improving traffic flow at freeway merge and diverge locations across the country. The work plan for conducting these experiments is described in chapter 3. This chapter describes the experimental parameters and results that cover:

- Acceleration and deceleration lane designs.
- Speed optimization.
- Mainline metering.
- Coordinated adaptive ramp metering system.
- Open-access MLs on the right-hand side.

## ACCELERATION AND DECELERATION LANE DESIGNS

Restricting merging drivers to a specific new set of acceleration and deceleration lane locations may help to smooth traffic flow. Regarding acceleration lanes, figure 3 shows how drivers are prohibited from merging at the mid-section of acceleration lanes. By eliminating the uncertainty of merge maneuvers for both mainline and ramp drivers, both sets of drivers can prepare for and execute the merging maneuver efficiently. Regarding deceleration lanes, figure 4 shows how drivers merge at a mid-section of the off-ramp. Separating the turbulence associated with diverge maneuvers potentially mitigates mainline congestion.

This study uses microscopic simulation to evaluate the effectiveness of the alternative geometric design of split merging, diverging, and weaving for reducing bottleneck congestion. Making geometric changes to create two merge or diverge points (as well as multiple points for weaving) at off-ramp areas spatially distributes potential conflicts for mainline and ramp traffic. This can potentially decrease the unnecessary interactions between the mainline and ramp vehicles and relieve congestion at these bottleneck areas with limited additional construction. This provides managerial insights for State departments of transportation (DOT) to better design, enhance, and manage their freeway systems in the future.

### Experimental Design

The simulation experiments used two sets of simple, synthetic networks to study the effectiveness of the proposed split design while excluding confounding factors that can exist in real-world segments (e.g., effects of the nearby downstream merge area). The first simulation network set represents one type of geometry, such as merge or diverge. The simulation also uses a calibrated I–66 network by converting selected merge areas with congestion problems to the proposed split merge design. The goal is to test the proposed split design in a complex environment and inform the State DOT concerning the design potential. These simulations only evaluated one-lane ramps, but the researchers believe two-lane ramps would exhibit similar impacts.

Figure 34 provides sketches of the proposed split merge and diverge areas used in the simulation. It shows the approximate length of the synthetic network (mainline) is 3.35 mi for the merge simulation and 3.21 mi for the diverge simulation. The assumed simulation traffic speed is approximately 70 mi/h. The American Association of State Highway and Transportation Officials' (AASHTO) book, *A Policy on Geometric Design of Highways and Streets,* (the *AASHTO Green Book*) recommends 30 mi/h for the lower range on-ramp and off-ramp speeds, 0.25 mi for the length of acceleration lane, and 0.1 mi for the length of the deceleration lane (AASHTO 2018). The team conducted the simulations for merge (on-ramp area) and diverge (off-ramp area) separately to see how different factors would affect operations of the network under the split merge/diverge design.

© 2019 Jiaqi Ma.

A. On-ramp benchmark.

© 2019 Jiaqi Ma.

C. Off-ramp benchmark.

© 2019 Jiaqi Ma.

B. On-ramp alternative design.

© 2019 Jiaqi Ma.

D. Off-ramp alternative design.
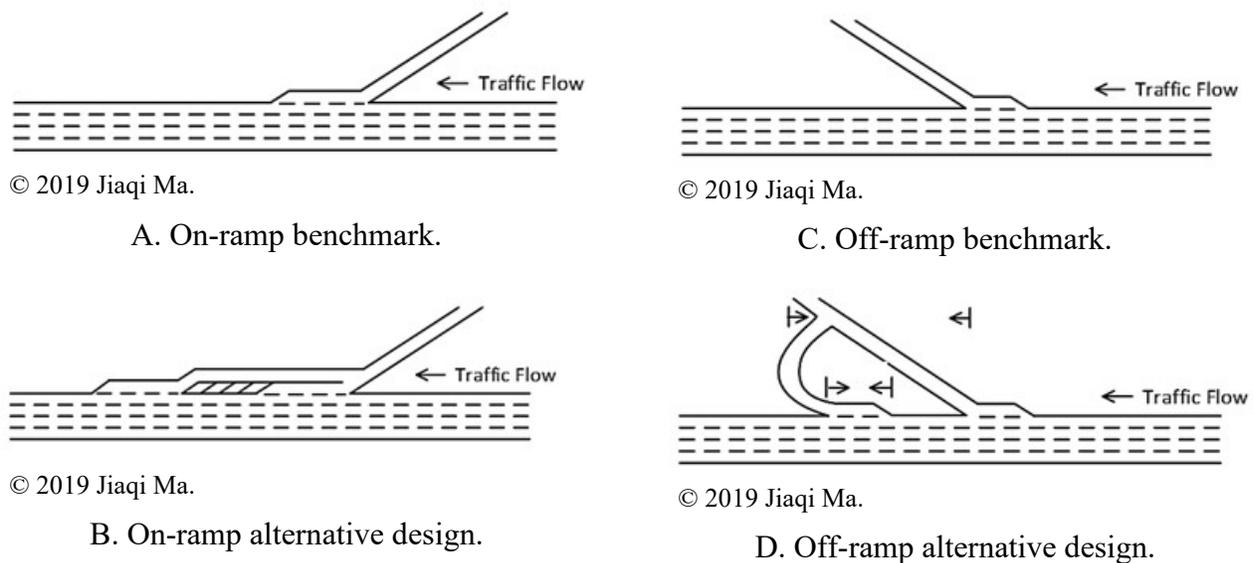
**Figure 34. Illustrations. Split merge and diverge areas on a synthetic simulation network.**

Figure 35 shows a possible geometry for the weaving segment, which is a usual urban case where the distance between the on-ramp and off-ramp is about 1.0 mi. It is the basic design of weaving segment, as defined in the *HCM*, where both on-ramp and off-ramp vehicles need to make at least one lane change to reach their destination. In addition, the length between the ramps is usually less than a maximum length, beyond which the merge and diverge area may not affect each other and the network reduces to the simple combination of the merge and diverge. Figure 35 is essentially a full split weaving design. An alternative geometry is given by the partial split weaving, for which only one of the merge or diverge is converted to the split design. The hypothesis of this study is that it is only necessary to adopt the full split weaving if both split merge and diverge designs are effective in improving the bottleneck performance.
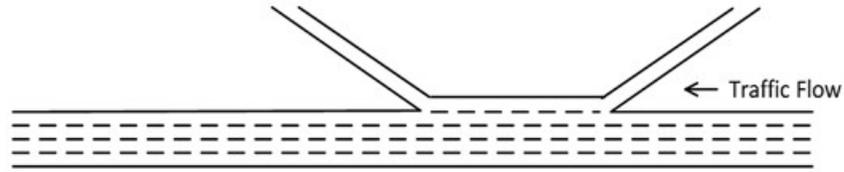
© 2019 Jiaqi Ma.

A. Weave benchmark design.
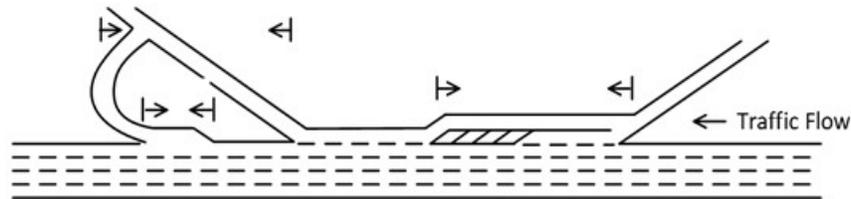


© 2019 Jiaqi Ma.

B. Weave alternative design.

**Figure 35. Illustrations. Two designs for the synthetic simulation network geometry (weaving).**

Studying factors that can influence the effectiveness of the proposed split design include three additional key factors in the simulation-based sensitivity analysis: the mainline congestion (volume-to-capacity ratio (V/C)), ramp traffic volume, and the length between the gores (connection spacing). Table 2 lists different levels of the three factors. For the merge or diverge, there are 81 scenarios in total; for each scenario, the team performed 10 simulation runs.

**Table 2. System parameters considered in this study.**

| Parameters (Units) | Levels | Number of Levels |
|---|---|---|
| Mainline input volume—VolPerLane (veh/h/l) | 1,221 (V/C = 0.6); 1,832 (V/C = 0.9); 2,443 (V/C = 1.2) | Three |
| On-ramp volume—VolMerge (veh/h/l) | 500; 1,000; 1,500 | Three |
| Off-ramp volume—VolDiverge (veh/h/l) | 500; 1,000; 1,500 | Three |
| Connection spacing—ConSpace (mi) | 0.25, 0.375, 0.5 (merge) 0.125, 0.25, 0.5 (diverge) | Three |
| Weaving area length (mi) | 1 | One |

After initial data collection on the synthetic simulation network (with specified driver parameters used in previous studies and networks), the team determined the freeway mainline capacity of the highway in Vissim at 2,036 veh/h/l. Therefore, the team set the three input volumes: 1,221 (V/C = 0.6); 1,832 (V/C = 0.9); and 2,443 (V/C = 1.2) to test the alternative design under different mainline congestion levels. Ramp traffic volume usually affects the number of lane changes directly, which indicates the intensity of disruptions to the original mainline traffic. The

team used different on/off-ramp volumes of 500 veh/h/l; 1,000 veh/h/l; and 1,500 veh/h/l to indicate low, medium, and high levels of ramp traffic.

The length between the gores (connection spacing), can also affect the performance of the split design. Long connection spacing can have two distinct effects: reduce disruption and reduce throughput. It can reduce the disruption of on-ramp vehicles on the mainline traffic by distributing the disruption to two locations. However, the vehicles on the frontage road travel at a lower speed than on the parallel freeway, and this can reduce the throughput. Therefore, the team set three connection spacing values for merge or diverge and conducted sensitivity analysis to understand their effects.

The team used two performance measures: average delay and total throughput. The average delay reported in this study is the average travel delay for individuals, while the total throughput is the sum of mainline and on/off-ramp throughputs under different scenarios. In the final statistical analysis, comparing the performance measures between the benchmark and split design across different scenarios provides understanding of the effectiveness of the proposed split design.

**Synthetic Network Results**

Table 3 presents the simulation results of the synthetic simulation networks for the split merge design. The team reported three values for each scenario: the absolute value, the absolute difference, and the percent difference. The team found that the split merge design solution can generally increase the throughput and reduce the average delay, except when the sum of the mainline and ramp traffic volumes are low (e.g., V/C = 0.6, V/C = 0.9, and ramp volume = 500 veh/h). Under light traffic conditions, there are few conflict points between the mainline and on-ramp traffic and therefore the split merge design, whose effect mostly comes from the spatial distribution of the conflict points, may not be significantly effective. When the traffic volumes are at the medium or high level, the team can see substantial improvements in terms of both throughput and average delay in many cases.

For all of the congested cases, the team found that the best bottleneck performance occurs when the connection space is 0.25 or 0.5 mi; longer connection spacing (e.g., 0.5 mi) deteriorates the performance. The team explained the sensitivity analysis of the lengths of connection spacing as follows:

- When the connection spacing is short, the traffic that arrives at the second conflict point is still less than at the regular merge conflict point and may still be traveling slowly. Therefore, a small disturbance at the second conflict point may not cause problems.
- If the connection spacing is long, the traffic that arrives at the second conflict point may have already resumed full travel speed and the volume that has already resumed their full speed is already relatively high. In this case, the disturbance from the second conflict area may have a relatively significant negative impact on the mainline arriving traffic.

Based on these results, the team recommend short connection spacing to maximize operational benefits. This also helps reduce the construction and right-of-way costs by occupying less land space.

**Table 3. Simulation results for split merge connection spacing.**

| V/C Ratio | Merge Volume | Benchmark Throughput (veh/h) | Benchmark Average Delay(s) | 1,312 ft Throughput (veh/h) | 1,312 ft Average Delay(s) | 1,969 ft Throughput (veh/h) | 1,969 ft Average Delay(s) | 2,625 ft Throughput (veh/h) | 2,625 ft Average Delay(s) |
|---|---|---|---|---|---|---|---|---|---|
| 0.6 | 500 | 4,168 | 12.15 | 4,166 (−2, −0.05%) | 11.90 (−0.25, −2.06%) | 4,165 (−3, −0.07%) | 11.92 (−0.23, −1.89%) | 4,167 (−1, −0.02%) | 12.02 (−0.13, −1.07%) |
| 0.6 | 1,000 | 4,669 | 13.77 | 4,665 (−4, −0.09%) | 13.36 (−0.41, −2.98%) | 4,666 (−3, −0.06%) | 13.37 (−0.4, −2.90%) | 4,668 (−1, −0.02%) | 13.47 (−0.3, −2.18%) |
| 0.6 | 1,500 | 5,175 | 15.98 | 5,169 (−6, −0.12%) | 15.50 (−0.48, −3.00%) | 5,170 (−5, −0.10%) | 15.53 (−0.45, −2.82%) | 5,175 (0, 0.00%) | 15.77 (−0.21, −1.31%) |
| 0.9 | 500 | 6,024 | 19.41 | 6,030 (6, 0.10%) | 19.21 (−0.2, −1.03%) | 6,011 (−13, −0.22%) | 23.32 (3.91, 20.14%) | 6,024 (0, 0.00%) | 19.32 (−0.9, −0.46%) |
| 0.9 | 1,000 | 6,022 | 195.45 | 6,515 (493, 8.19%) | 38.00 (−157.45, −80.56%) | 6,442 (420, 6.97%) | 60.04 (−135.41, −69.28%) | 6,197 (175, 2.91%) | 157.82 (−37.63, −19.25%) |
| 0.9 | 1,500 | 5,954 | 329.95 | 6,520 (566, 9.51%) | 191.67 (−138.28, −41.91%) | 6,396 (442, 7.42%) | 214.96 (−114.99, −34.85%) | 6,293 (339, 5.69%) | 262.90 (−67.05, −20.32%) |
| 1.2 | 500 | 5,965 | 107.77 | 6,094 (129, 2.16%) | 30.32 (−77.45, −71.87%) | 6,090 (125, 2.10%) | 30.27 (−77.5, −71.91%) | 6,082 (117, 1.96%) | 47.04 (−60.73, −56.35%) |
| 1.2 | 1,000 | 5,966 | 254.84 | 6,427 (461, 7.74%) | 82.28 (−172.56, −67.71%) | 6,531 (565, 9.48%) | 52.12 (−202.72, −79.55%) | 6,250 (284, 4.76%) | 174.51 (−80.33, −31.52%) |
| 1.2 | 1,500 | 6,011 | 319.32 | 6,422 (411, 6.85%) | 245.19 (−74.13, −23.21%) | 6,478 (467, 7.77%) | 206.29 (−113.03, −35.40%) | 6,316 (305, 5.07%) | 282.82 (−36.5, −11.43%) |

Note: When three values are reported, this indicates the absolute value, the absolute difference relative to the benchmark case (first value in parentheses), and the percent difference relative to the benchmark case (second value in parentheses).

The researchers conducted the simulation described in table 3 with the assumption of a 50–50 split scenario, meaning that 50 percent of the merge traffic uses the first merge location and 50 percent uses the second merge location. This is a reasonable assumption because if the public can freely choose between the two merge locations, the long-term expected value of volume split is 50–50. However, it is also possible that the traffic managers can control the volume split with advanced traffic control strategies, such as dynamic message signs or in-vehicle information. Therefore, the team conducted sensitivity analyses and compared the bottleneck performance under three different splits: 30–70, 50–50, and 70–30. The team tested medium and high levels of traffic with the 0.25-mi connection spacing. Results from figure 36 clearly demonstrate that the 50–50 split results in the best performance under most scenarios or performs almost as well as the remaining two splits for other scenarios. This result implies that the traffic managers need to let the public know that drivers can freely choose either merge location through road signs or public outreach. If the traffic managers detect that more drivers are using one of the merge locations, there needs to be a method to guide drivers to use the merge locations on a 50–50 basis. Advanced methods with ITS equipment, such as using dynamic message signs, is another consideration.

Table 4 presents the results of the same analyses for the split diverge design, in which the team reported the results under different scenarios of the V/C ratios, diverge volumes, and connection spacing. The percent changes in each scenario, including the scenarios under heavy traffic, are small. Statistical tests show that these minor differences are not statistically significant, indicating that the team find the split diverge design results in enhanced diverge area performance insignificant compared to the regular diverge. The insignificance of the benefits of the split diverge design implies that the spatial distribution strategy is not effective at the diverge area. This may be partly due to the fact that diverge area congestion is less severe than at the merge. Since the split diverge design is not effective even under the most congested scenarios, the team did not evaluate the full split weaving design in figure 35. The team did not evaluate the full split weaving design because the split diverge portion may not experience high traffic volume as in the pure split merge design simulation due to the congestion upstream at the merge portion. The team believes it will not generate any operational benefits with the additional construction at the diverge in figure 35. Therefore, the team recommend the use of the split merge design at congested merge or weaving areas.

**Table 4. Simulation results for split diverge distance between gores.**

| V/C Ratio | Merge Volume (veh/h) | Benchmark Throughput (veh/h) | Benchmark Average Delay(s) | 1,312 ft Throughput (veh/h) | 1,312 ft Average Delay(s) | 1,969 ft Throughput (veh/h) | 1,969 ft Average Delay(s) | 2,625 ft Throughput (veh/h) | 2,625 ft Average Delay(s) |
|---|---|---|---|---|---|---|---|---|---|
| 0.6 | 500 | 3,650 | 8.20 | 3,647 (−3, −0.08%) | 8.43 (0.23, 2.80%) | 3,647 (−3, −0.08%) | 8.57 (0.37, 4.51%) | 3,651 (1, 0.03%) | 8.76 (0.56, 6.83%) |
| 0.6 | 1,000 | 3,658 | 8.32 | 3,649 (−9, −0.25%) | 8.48 (0.16, 1.92%) | 3,652 (−6, −0.16%) | 8.50 (0.18, 2.16%) | 3,653 (−5, −0.14%) | 8.74 (0.42, 5.05%) |
| 0.6 | 1,500 | 3,659 | 9.61 | 3,651 (−8, −0.22%) | 9.65 (0.04, 0.42%) | 3,651 (−8, −0.22%) | 9.53 (−0.08, −0.83%) | 3,653 (−6, −0.16%) | 9.81 (0.20, 2.08%) |
| 0.9 | 500 | 5,489 | 14.45 | 5,485 (−4, −0.07%) | 14.73 (0.28, 1.94%) | 5,482 (−7, −0.13%) | 14.97 (0.52, 3.60%) | 5,486 (−3, −0.05%) | 15.24 (0.79, 5.47%) |
| 0.9 | 1,000 | 5,494 | 13.66 | 5,488 (−6, −0.11%) | 13.91 (0.25, 1.83%) | 5,484 (−10, −0.18%) | 14.06 (0.40, 2.93%) | 5,487 (−7, −0.13%) | 14.41 (0.75, 5.49%) |
| 0.9 | 1,500 | 5,492 | 13.66 | 5,495 (3, 0.05%) | 13.80 (0.14, 1.02%) | 5,491 (−1, −0.02%) | 13.88 (0.22, 1.61%) | 5,494 (2, 0.04%) | 14.14 (0.48, 3.51%) |
| 1.2 | 500 | 7,260 | 23.02 | 7,258 (−2, −0.03%) | 24.42 (1.40, 6.08%) | 7,262 (2, 0.03%) | 24.53 (1.51, 6.56%) | 7,257 (−3, −0.04%) | 24.85 (1.83, 7.95%) |
| 1.2 | 1,000 | 7,260 | 23.02 | 7,260 (0, 0.00%) | 23.80 (0.78, 3.39%) | 7,260 (0, 0.00%) | 23.60 (0.58, 2.52%) | 7,251 (−9, −0.12%) | 24.39 (1.37, 5.95%) |
| 1.2 | 1,500 | 7,261 | 23.01 | 7,266 (5, 0.07%) | 23.74 (0.73, 3.17%) | 7,263 (2, 0.03%) | 23.4 (0.39, 1.69%) | 7,266 (5, 0.07%) | 24.82 (1.81, 7.87%) |

Note: When three values are reported, this indicates the absolute value, the absolute difference relative to the benchmark case (first value in parentheses), and the percent difference relative to the benchmark case (second value in parentheses).
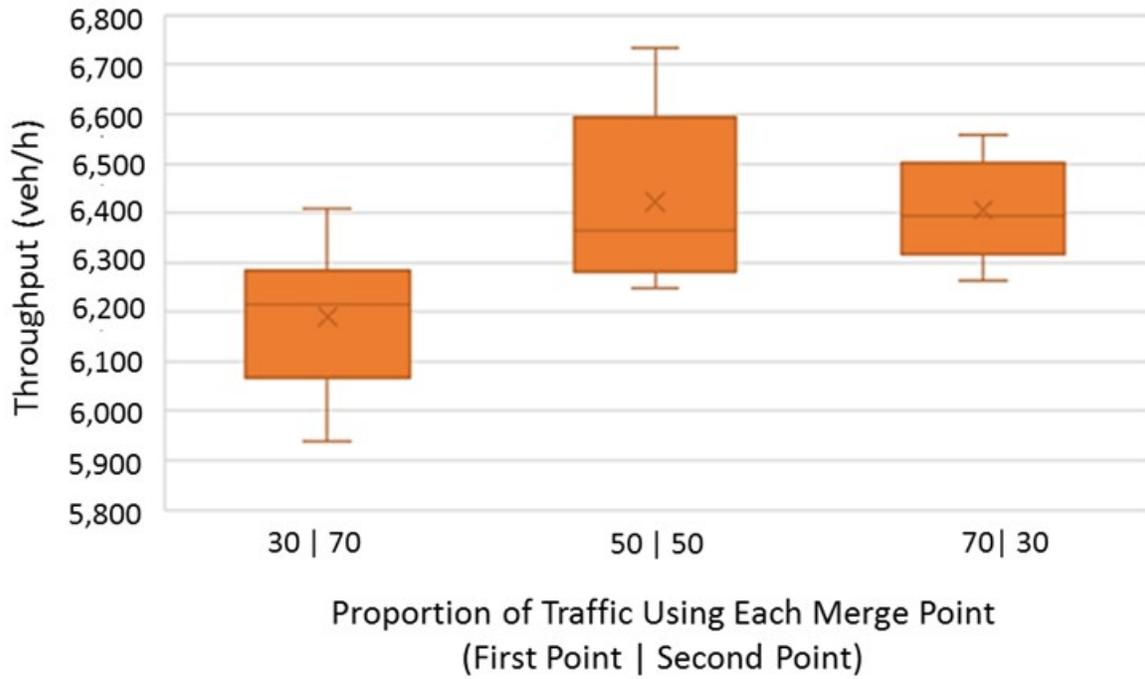
A. V/C ratio 1.2, merge volume 1,500 veh/h.
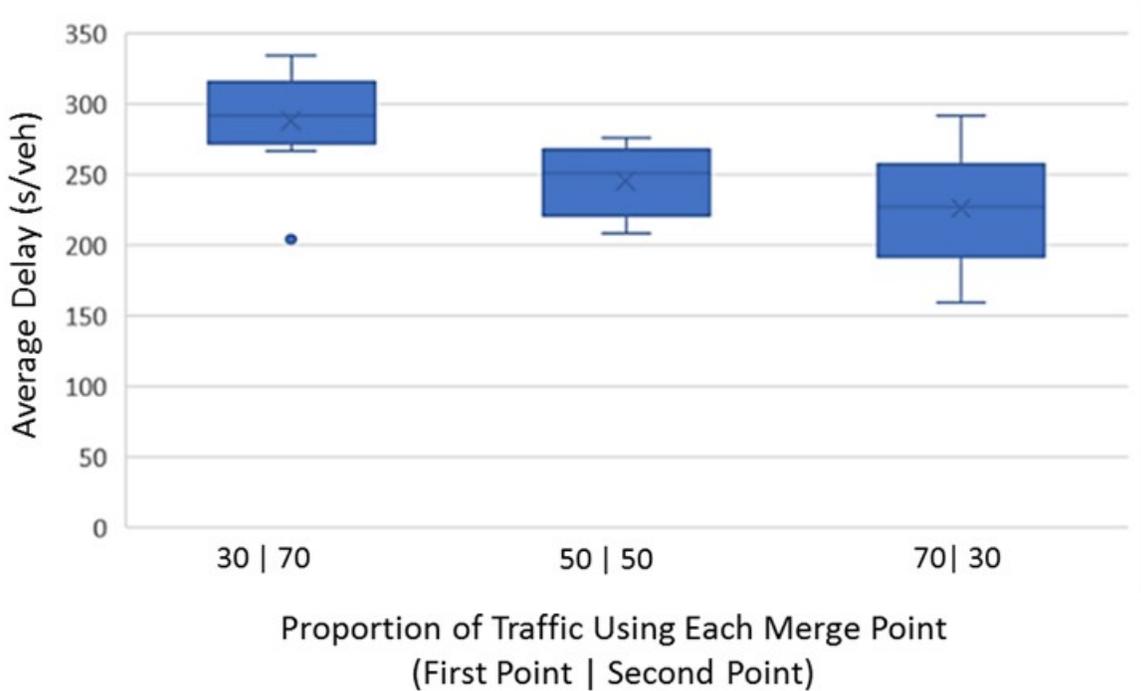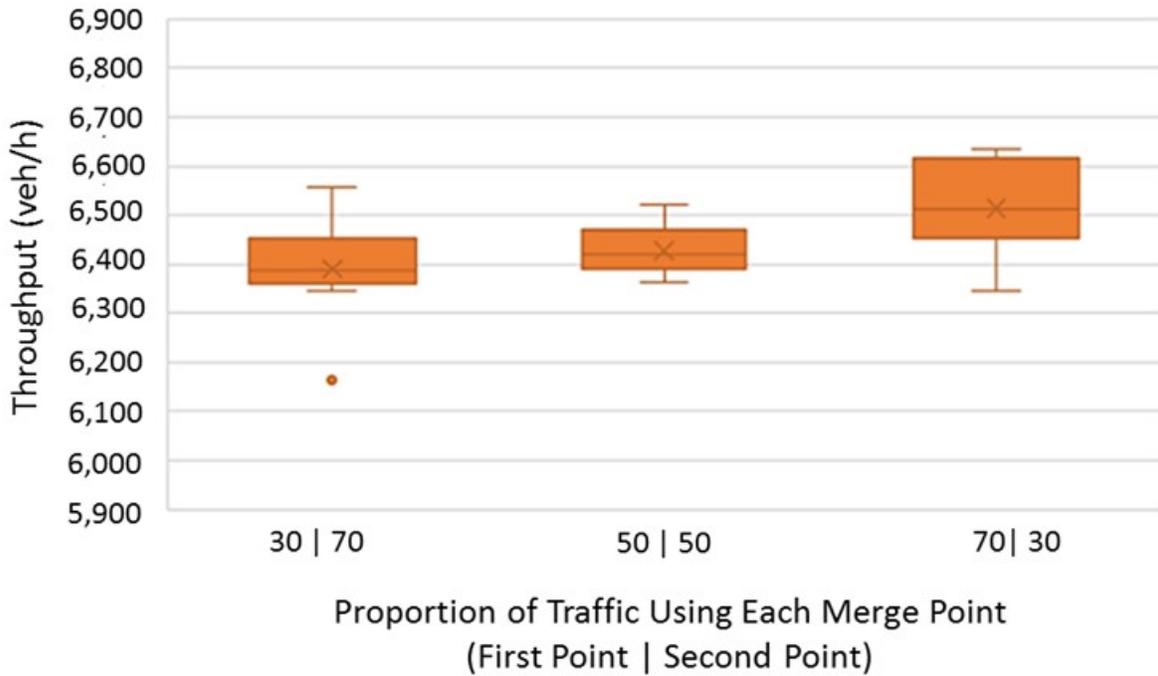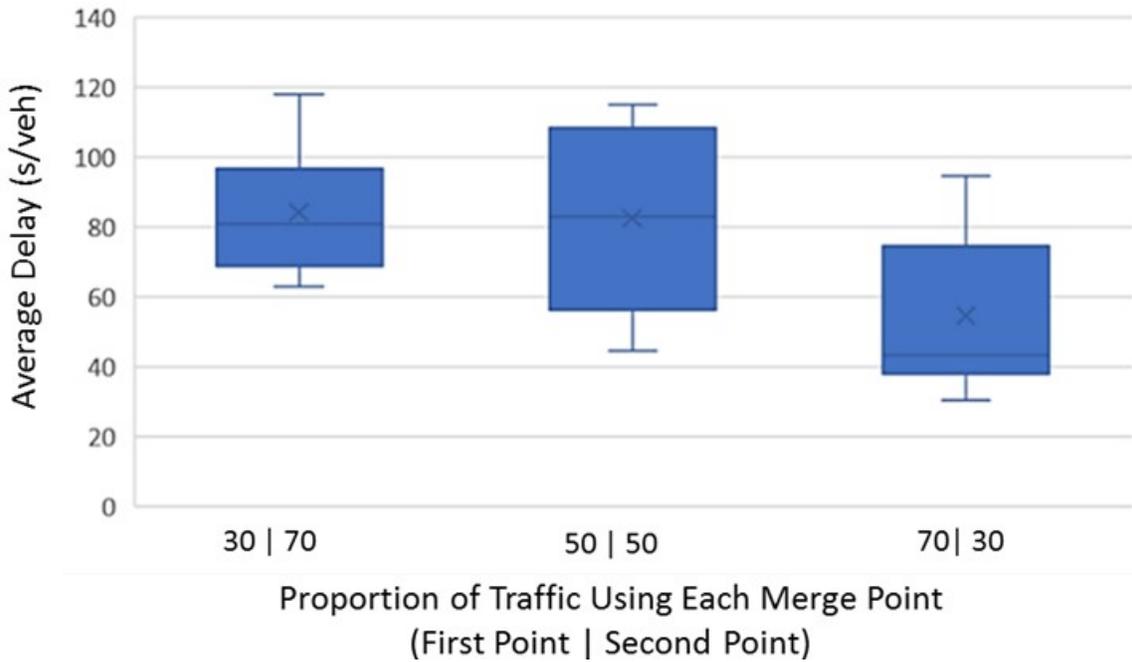
B. V/C ratio 1.2, merge volume 1,500 veh/h.

C. V/C ratio 1.2, merge volume 1,000 veh/h.
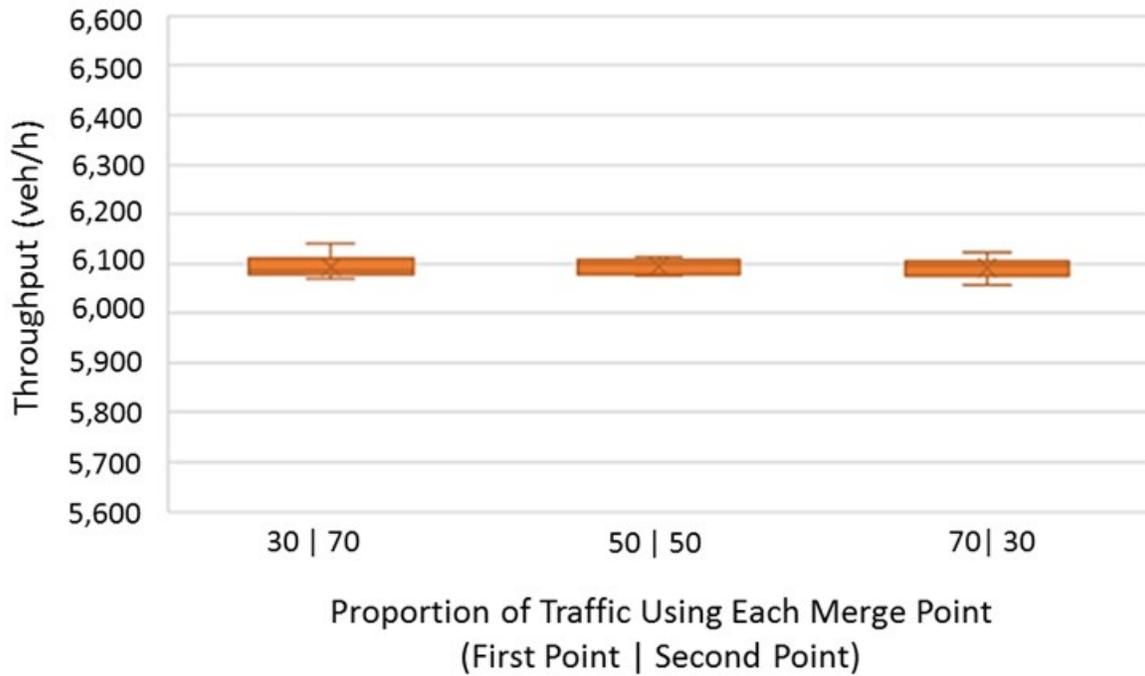
D. V/C ratio 1.2, merge volume 1,000 veh/h.
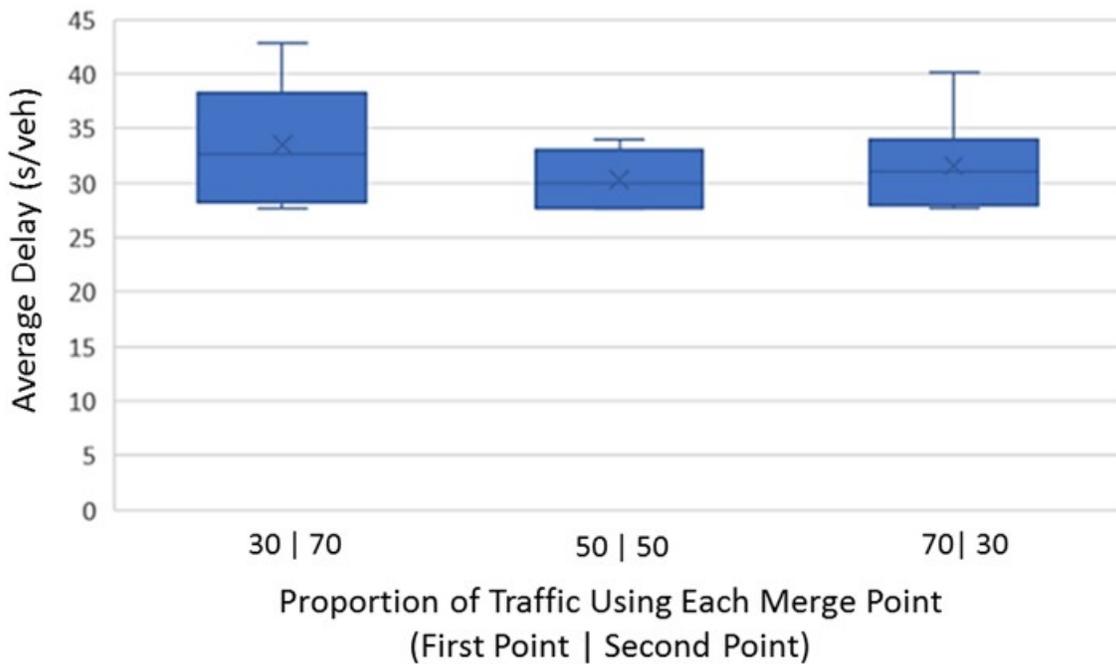
E. V/C ratio 1.2, merge volume 500 veh/h.

F. V/C ratio 1.2, merge volume 500 veh/h.
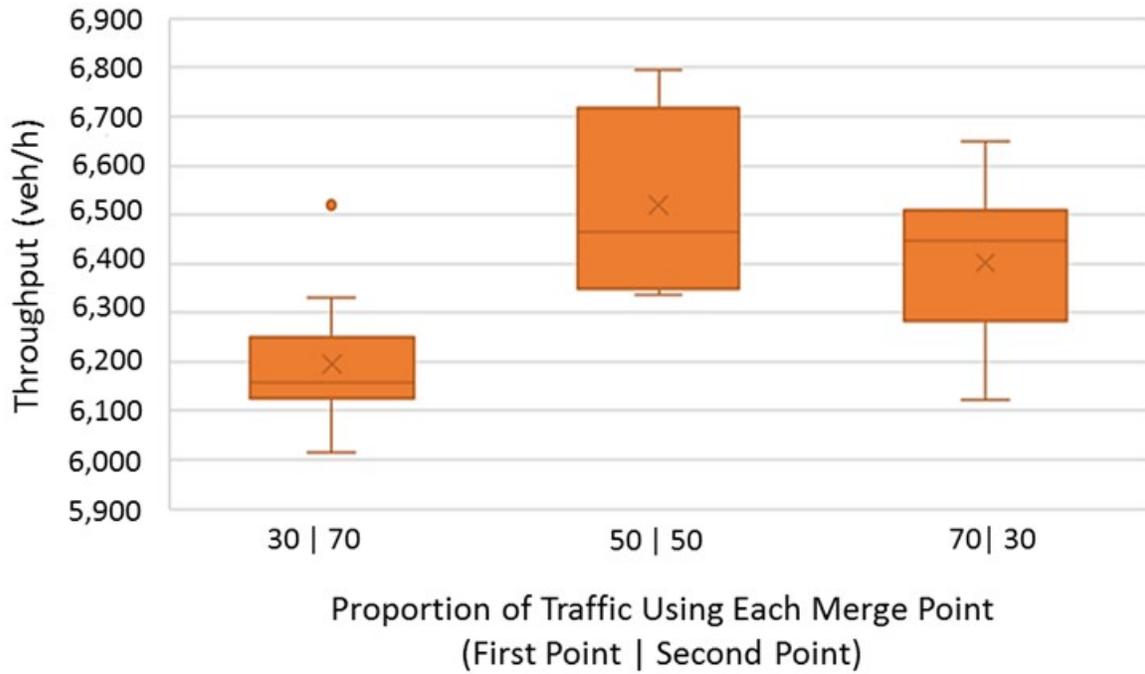
G. V/C ratio 0.9, merge volume 1,500 veh/h.

H. V/C ratio 0.9, merge volume 1,500 veh/h.

**Figure 36. Graphs. Bottleneck performance at 0.25-mi connection spacing.**

## Simulation Results in a Real-World Network

To test whether the alternative design would improve the performance under complex real-world traffic and geometric conditions, the team used a calibrated network of I–66 freeway segment in Vissim. The simulation network was I–66 westbound between interchange I–495 (MM 64) and US 29 (MM 51), six interchanges on this 13-mi-long section. RTMS trailers collected speed and volume data along major mainline segments and on- and off-ramp volume data collected by cameras (see figure 35 for a map and the locations of RTMS trailers, cameras, and interchanges). Initial calibration helped the team narrow down parameter set candidates by using the Latin hypercube sampling design (LHD) approach. Key car following and lane changing parameters were calibrated. Vissim evaluated 500 scenarios created by LHD, with 5 replications for each scenario to choose the best candidate scenario. The selected candidate was fine-tuned to obtain the final simulation model. Vissim used O-D matrices to specify travel demand. The I–66 freeway network has 10 zones. Zones 1 and 10 are the starting and ending points of the corridor. Zones 2–9 contain the intermediate interchanges. Two of the zones are only applicable to the existing HOV vehicles (i.e., exits for westbound, entrances for eastbound). The field-collected data in this study identified how many vehicles traveled between some, but not all, O-D pairs. To fill in the gaps, QueensOD software estimated the O-D matrices (Van Aerde 1993). Results indicated an excellent correlation between estimated and field-measured O-D trips. There is an HOV lane on the left-hand side of the base case calibrated network. For the HOV lane on the right-hand side, the team modified the network and specified the rightmost lane as the HOV lane. The team assigned the same HOV demand to the HOV lane on the right-hand side, and performed simulations 10 times to account for stochasticity.

Based on the base year data and simulation results of the calibrated benchmark network, congestion at interchanges 1, 2, 3, and 4 is relatively severe; therefore, the team made geometric conversions to create a split merge design at these locations. Figure 37-A shows the before and after designs for interchange 3. The connection spacing used here is approximately 0.25 mi based on the simulation results in the previous section. This design may not be the optimal location for the horizontal lines because many other real-world design factors, such as vertical grades, right-of-way, and construction costs, deserve consideration. This study only aims to study the potential traffic impact under one potential line location.



Original photo: © 2017 Google® (see acknowledgements).

A. Benchmark geometric design.

56

B. Split merge design.

**Figure 37. Photos. Interchange 3 before and after design.**

The simulation results show improvements in both throughput and average delay, and both improvements are statistically significant at the 95 percent confidence level, as illustrated in figure 38. On average, the throughput increases from 7,589 to 7,798 veh/h, representing a 2.75-percent improvement. The average delay decreases from 643 to 608 s, representing a reduction of 35 s of delay for each individual traveler on average, an improvement of 5.5 percent. Based on the results from the previous section and under the current demand scenarios, converting interchanges 1, 2, 3, and 4 mentioned above to the split merge design can generate significant improvements, which can be even greater when the demand becomes higher.
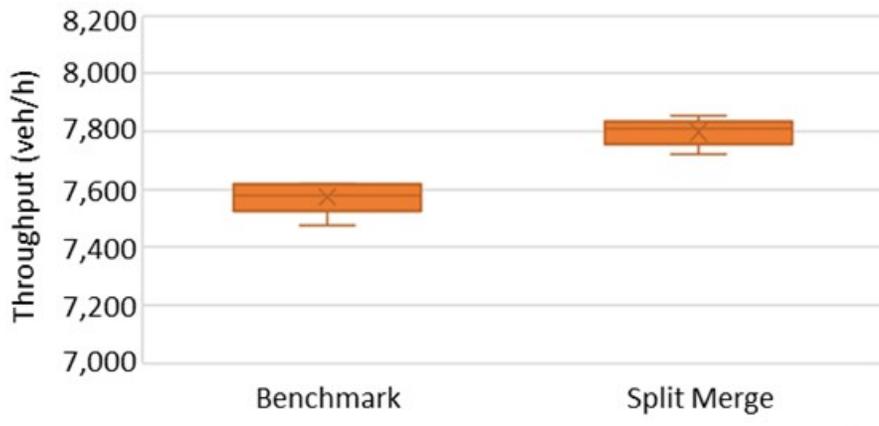
A. Throughput for the benchmark and split merge configurations.
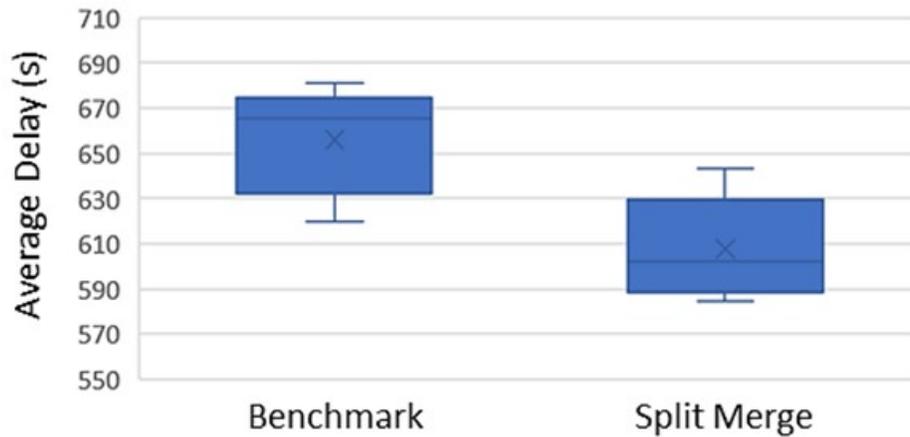
B. Average delay for the benchmark and split merge configurations.

**Figure 38. Charts. Throughput and average delay.**

**Summary**

In this study, the team conducted microscopic simulation to evaluate the effectiveness of the alternative geometric design of split merging, diverging, and weaving for reducing bottleneck congestion. The simulation also allowed the team to develop managerial insights for State DOTs to better design, enhance, and manage their freeway systems in the future.

The split merge design can effectively reduce the average delay and increase the traffic throughput under medium-to-high levels of traffic congestion. The split diverge is not effective under many traffic conditions and therefore not recommended for construction. Based on the results of the split merge and diverge designs, a partial split weaving design with the merge portion converted to the split merge design is recommended at congested weaving areas. Overall, this strategy can potentially increase throughput by 6 to 9 percent and reduce delay by 40 to 80 percent.

The team also analyzed scenarios having different percentages of merge volumes using the two merge locations. The team found that under most scenarios, a 50–50 split of the on-ramp volume generates the best bottleneck performance. This indicates that traffic managers only need to let the public know that both merge locations can be freely used and design the road sign such that a 50–50 split of ramp traffic volume can be achieved. The agencies can also use ITS equipment, such as dynamic message signs, to ensure a 50–50 split if a deviation is detected.

**SPEED OPTIMIZATION (E.G., VIA DYNAMIC TRAFFIC CALMING DEVICES)**

Speed harmonization and VSL studies imply that medium free-flow speeds (e.g., 30 mi/h) would be more effective than low speeds (e.g., 5 mi/h) or high speeds (e.g., 65 mi/h) at optimizing freeway traffic flow. In an age of high CAV market penetration, speed harmonization may be obtained directly by changing vehicle behavior. However, this project endeavors to focus on strategies not requiring CAV technologies, and the team believes that dynamic traffic calming

devices (e.g., overhead gantries, retractable rumble strips) may be capable of coercing drivers to obey medium speeds at higher rates of compliance. Figure 8 illustrates this concept.

Sensitivity analysis experiments for examining speed optimization effects were conducted in TSIS-CORSIM. Small generic datasets (also known as "toy networks") were generated for the initial experiments. The original expectation was to transition to the MnDOT I–394 TSIS-CORSIM datasets for further testing. Figure 39 shows the freeway geometry associated with the base dataset. For some experiments, the team eliminated the off-ramp to focus on merge maneuvers. For other experiments, the on-ramp is eliminated to focus on diverge maneuvers. Finally, a third set of experiments considered the full weaving section.



Source: FHWA.

**Figure 39. Illustration. Simple weaving section.**

## Experimental Design

Experimental design parameters were as follows:

- Base demands of 2,000 veh/h/l on the mainline and 1,800 veh/h on the single-lane ramp.
- Demand multipliers (both mainline and ramp) between 75–125 percent at 5 percent increments.
- Mainline free-flow speeds between 35–70 mi/h at 5 mi/h increments.
- Number of mainline lanes: two, three, and four.
- Car following aggressiveness: low, medium, and high.
- Various distances between on-ramp and off-ramp (only for weave section experiments).
- Key output measures: average segment speed and average network-wide speed.

## Results and Discussion

The most optimistic results saw average vehicle speeds more than doubling when imposing a lower free-flow speed. For example, in one weaving section experiment, average vehicle speeds upstream of the merge point jumped from 20.4 to 47.3 mi/h after reducing the free-flow speed from 65 to 50 mi/h. The impact on average vehicle speeds is generally less significant at higher numbers of mainline lanes and on other links downstream of the merge point (figure 40).



Benefits occur here, immediately upstream of the merge point

Source: FHWA.

**Figure 40. Illustration. Location of maximum benefits for speed optimization.**

In a second merge-only experiment (no off-ramp), average vehicle speeds upstream of the merge point jumped from 7.5 to 37.1 mi/h after reducing the free-flow speed from 65 to 45 mi/h. Table 5 shows these results. Many of the successful speed optimization experiments produced a similar "zipper" pattern of speeds with an asterisk, indicating the optimum combinations of demand versus posted limit. The red text indicates the location in the middle of the zipper, where the posted speed limit can produce the greatest benefits. The implication is that significant speed optimization benefits only occurred under a narrow range of demands (i.e., near capacity) and speed limit changes. The downside of this finding is that this narrow range of conditions producing maximum benefits, in terms of demand ranges and free-flow speed ranges, is often difficult to predict without first running a simulation.

**Table 5. Average speeds due to speed limit and demand.**

| Posted Speed Limit (mi/h) | Demand Multiplier (Percent) | | | | | | | | | | |
|---|---|---|---|---|---|---|---|---|---|---|---|
| | 75 | 80 | 85 | 90 | 95 | 100 | 105 | 110 | 115 | 120 | 125 |
| 70 | 68.6* | 67.7* | 66.8* | 62.8* | 9.6 | 7.3 | 7.6 | 7.6 | 6.6 | 6.5 | 6.5 |
| 65 | 63.3 | 63.7 | 62.6 | 62.1* | 9.4† | 7.5† | 7.2 | 6.4 | 6.9 | 6.9 | 6.4 |
| 60 | 58.8 | 58.0 | 57.8 | 57.1 | 35.9† | 9.6† | 7.0 | 7.2 | 6.6 | 6.9 | 6.4 |
| 55 | 53.4 | 53.7 | 52.4 | 53.0 | 52.6*† | 14.3† | 7.0 | 7.5 | 7.2 | 7.0 | 6.4 |
| 50 | 48.1 | 47.8 | 47.6 | 47.5 | 47.6† | 34.4† | 9.4 | 7.7 | 7.1 | 6.5 | 6.4 |
| 45 | 42.7 | 43.3 | 42.6 | 42.5 | 42.3† | 37.1*† | 11.0 | 7.7 | 7.0 | 6.8 | 6.2 |
| 40 | 38.1 | 37.6 | 37.9 | 37.8 | 37.2 | 17.0 | 12.5* | 8.0* | 7.0 | 6.8 | 6.3 |
| 35 | 33.2 | 33.1 | 32.9 | 31.8 | 30.1 | 9.0 | 7.4 | 6.9 | 6.0 | 5.9 | 5.4 |

*Optimum combinations of demand versus posted limit.
†Location in the middle of the zipper where the posted speed limit can produce the greatest benefits.

Procedures from the *HCM* can prescreen alternatives without running a simulation. However, a series of test runs conducted in the Highway Capacity Software (HCS) (merge module and weaving module) using similar input data did not predict any benefits of free-flow speed and/or speed limit optimization. The resulting hypothesis is that the *HCM* methods are perhaps not capable of recognizing or analyzing the same speed harmonization-type effects and benefits that are commonly observed in a microsimulation (and in the field). As such, using an offline or real-time microsimulation model might detect when the zipper conditions from table 5 are in effect for any local site or local conditions.

Although the significant speed optimization benefits were observed for some weaving and merge conditions as shown in table 5, the benefits were weaker (e.g., on the order of 2 to 6 percent) for diverge conditions.

Upon reaching the conclusion that speed optimization benefits can probably only be predicted by establishing an offline or real-time microsimulation model for local conditions, the need for additional experiments on a larger network (e.g., I–394 MN) diminished. As such, agencies willing to detect zipper conditions in real time can consider implementing countermeasures to reduce free-flow speeds (or speed limits) when such conditions are present. Such countermeasures could include dynamic traffic calming devices (e.g., retractable rumble strips),

dynamic VSL signs, or CAV speed controls. This approach also assumes that the offline or real-time microsimulation model is consistently and periodically recalibrated to reflect local field conditions accurately.

## MAINLINE METERING (I.E., DYNAMIC SIGNAL CONTROL)

A form of mainline metering to reduce demand and improve flow uses traffic metering upstream from a bottleneck, thereby regulating the number of vehicles moving through the bottleneck. At locations where capacity expansion is not feasible (i.e., at tunnels and bridges), implementation of this form of mainline metering can help. For example, metering for traffic arriving at the bridge or tunnel is used at the Bay Bridge in Oakland, CA; the Hampton Roads Bridge-Tunnel connecting Hampton, VA, and Norfolk, VA; and the Baltimore Harbor Tunnel in Baltimore, MD.

In situations where mainline and ramp vehicle speeds are both very low and fall below a defined threshold, such as 5 or 10 mi/h, traffic signal control applied to both upstream approaches could optimize the operation by eliminating merge friction. Figure 9 illustrates this concept. However, there is no known application of the treatment.

### Dynamic Signal Control Algorithm

For this strategy, the team developed a dynamic signal control algorithm to apply in an integrated ramp and mainline metering control strategy. The proposed dynamic signal control algorithm includes three main modules:

- In the first module, downstream traffic sensors update traffic flow and speed at every time point, and the proposed algorithm runs iteratively at the same discrete time points.
- The second module activates the dynamic signal controller when detecting a certain traffic speed drop at all lanes of the merge point. This module aims to stop the mainline traffic from entering the downstream queue until it is about to dissipate.
- The third module predicts the downstream traffic queue dissipation time based on the information provided by the traffic sensors. This process uses a reliable and efficient real-time algorithm, which the second module then uses to let the upstream traffic smoothly merge into the downstream queue (Ghiasi et al. 2017). For more detailed information about the developed algorithm, refer to Ghiasi et al. (2018).

### Test Environment

This project uses a merge section of I–35 in Kansas City, KS, to test the proposed algorithm. This section is approximately 1.4 mi long and is from the calibrated Vissim simulation network. The analysis is on the westbound side of the network and includes two merges. The team studied the second merge, located about 0.75 mi downstream of the input traffic. The dynamic signal control zone in the second merge area begins at the merge point. Figure 41 shows the control zone on the left-hand side. At the merge point, an on-ramp roadway merges the three-lane mainline freeway. Right after the merge point, an acceleration lane with the length of 922 ft begins. Therefore, a lane drop lies at the end of this acceleration lane, and traffic congestion may occur at this point of the freeway and can propagate backwards to the upstream sections.
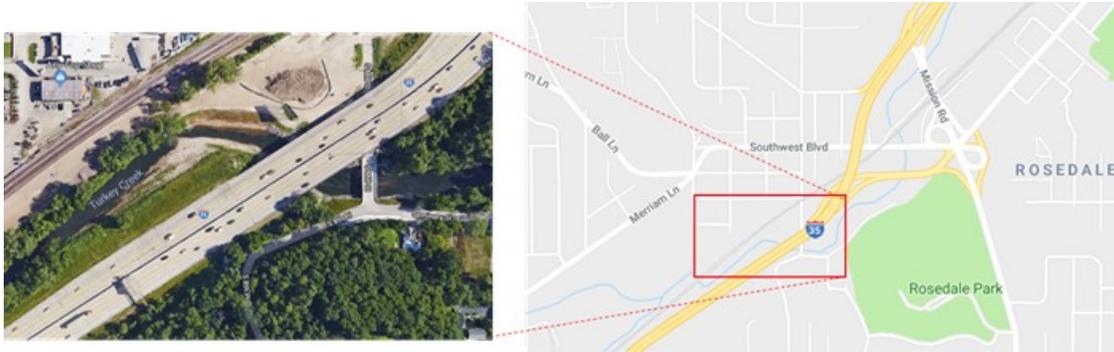
Original photo: © 2017 Google® (see acknowledgements).

**Figure 41. Map. Case study map for the dynamic signal control on I–35 Kansas City, KS.**

**Simulation Setup and Application**

The simulation model uses six sets of loop detectors in this area, where each set contains a number of loop detectors embedded next to one another to cover all lanes at a specific longitudinal location. Each loop detector set represents a traffic sensor in the analyses. These traffic sensors sit evenly along the merge section with the distance of 226 ft between sensors. Traffic includes 3.5 percent trucks, and the length of the regular vehicles and trucks are set as 23 and 80 ft, respectively. To evaluate the algorithm performance, four measures of effectiveness were chosen: throughput ($\Delta E^T$), average traffic speed ($\Delta E^S$), average traffic delay (per vehicle) ($\Delta E^D$), and total carbon monoxide emissions ($\Delta E^E$). Note that the throughput values are recorded at the end of the control zone (after the lane drop), but the other measures are network-wide average values.

Three time periods divide the simulation analysis. The first 900-s period is the warm-up period, with no traffic evaluation measurements conducted in this period. Traffic evaluation measurements start at the beginning of the second 900-s period. During this period (i.e., 900–1800 s), the team measured $\Delta E^T$, $\Delta E^S$, and $\Delta E^E$. To measure $\Delta E^D$, the team extended the simulation experiment to the third time period that includes no further mainline traffic input and the ramp traffic input of 970 veh/h that is the average of the field measured volumes. This period continues until the time when the last vehicle of the mainline approach exits the control zone. The reasoning for this is to let the existing traffic queue in the network discharge before obtaining the delay measurements. Although considering no further mainline traffic input in the third simulation period may look unrealistic, the simulation experiments end after the last vehicle of the mainline approach exits the control zone. Therefore, considering any further mainline traffic would not affect the simulation results. This zero-traffic-input assumption is only for the mainline approach because the mainline input traffic exits the control zone mostly after the merge input traffic.

For the simulation, the traffic demands of the mainline were denoted as $D^{main}$, the traffic demands of ramp approaches were denoted as $D^{ramp}$, the maximum red intervals for the mainline were denoted as $R^{main}$, and the maximum red intervals for ramp approaches were denoted as $R^{ramp}$. Further, the speed threshold at which the mainline signal control activates was denoted as $V^{threshold}$.

The team first presented the simulation results for a default parameter setting. In this setting, the team set $D^{main}$ = 8,000 veh/h; $D^{ramp}$ = 1,500 veh/h; $R^{main}$ = 60 s; $R^{ramp}$ = 20 s; and $V^{threshold}$ = 6 mi/h. Further, to ensure stability and efficiency of the signal timing plan, the team required that the red and green intervals at both approaches be no less than 10 s. Moreover, the algorithm update interval is set to 2 s. To consider the stochasticity effects of the simulation experiments, each simulation scenario runs 10 times with different random seeds. The obtained average mainline and ramp green intervals among all random seeds are 151 and 170 s, respectively, where on average 72 percent of the green intervals overlap. In this algorithm, the ramp red interval lasts until another mainline control activation happens or the red interval reaches $R^{ramp}$. In the default case scenario, the time between every consecutive mainline control activation is greater than 20 s, and the ramp red interval is always equal to $R^{ramp}$ = 20 s. Moreover, the average mainline red interval is 40 s. Figure 43 shows an example of a signal timing plan for the first two mainline and ramp cycles that resulted from the first simulation instance. Further, figure 42 compares the simulation results of the signal control algorithm with the benchmark case and without any control. The results indicate that the control algorithm does not significantly affect throughput. However, the other measures of effectiveness show significant improvements.
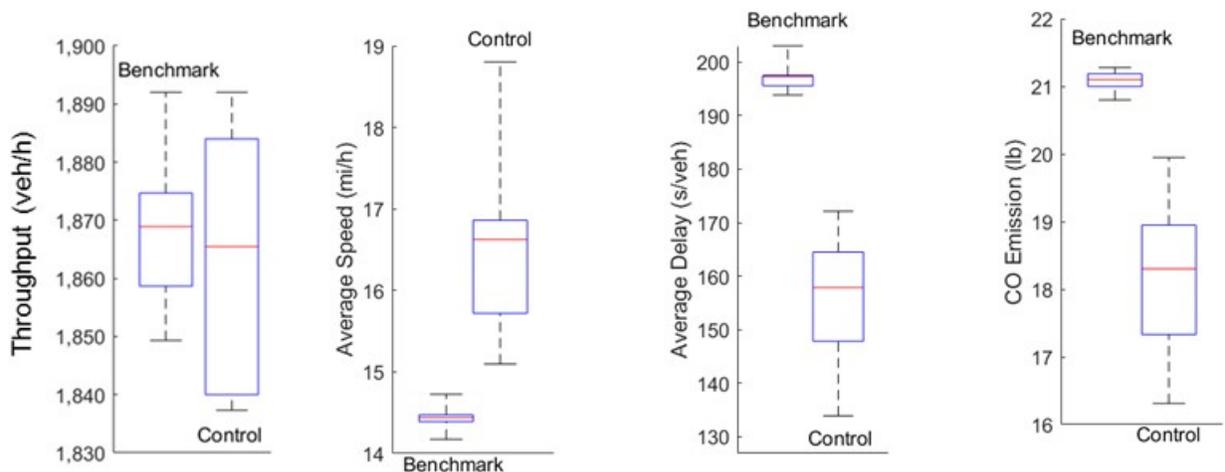


Source: FHWA.　　Source: FHWA.　　Source: FHWA.　　Source: FHWA.

A. Throughput.　　B. Average speed.　　C. Average delay.　　D. Carbon monoxide emissions.

**Figure 42. Charts. Simulation results for the default setting.**

## Mainline Signal Timing Plan

| Red phase length is 48 s. | Green phase length is 162 s. | Red phase length is 212 s. | Green phase length is 590 s. |

| Green phase length is 142 s. | Brief red phase (undefined). | Green phase length is 570 s. | Brief red phase (undefined). |

## Ramp Signal Timing Plan
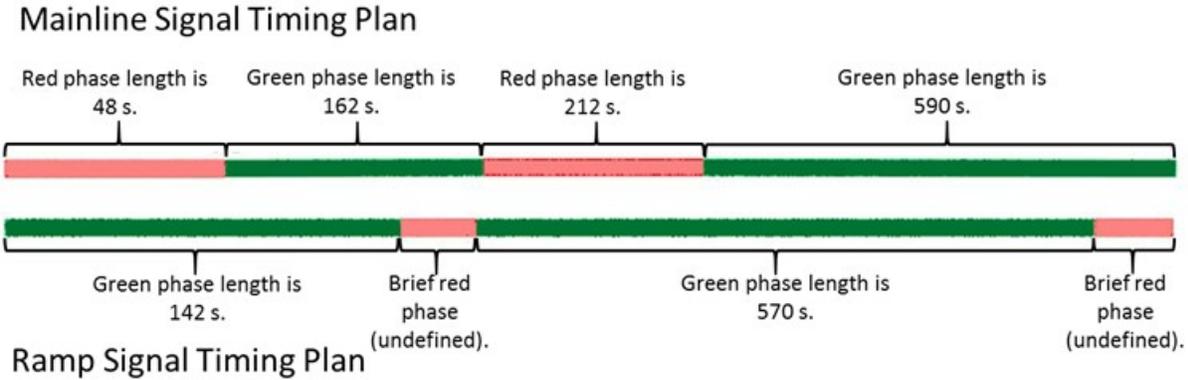
Source: FHWA.

**Figure 43. Illustration. Example signal timing plan.**

The team performed a sensitivity analysis on the $D^{main}$ and $D^{ramp}$ values. Then, the team looked at the effects of $R^{ramp}$ through simulation experiments. For these simulation analyses, different scenarios were considered for the $D^{main}$ and $D^{ramp}$ values, while other parameters were kept as their default values. Figure 44 shows the results of the sensitivity analysis on $D^{main}$ and $D^{ramp}$ values and shows the three-dimensional box-plots among all 10 random instances.
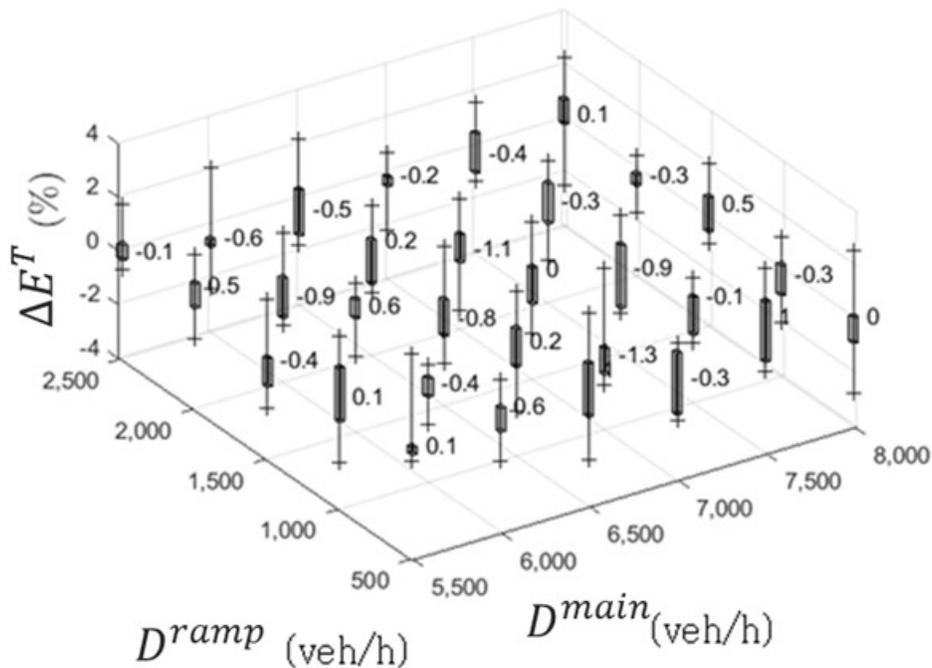


Source: FHWA.

A. Throughput impacts resulting from the changes in ramp and mainline demands.
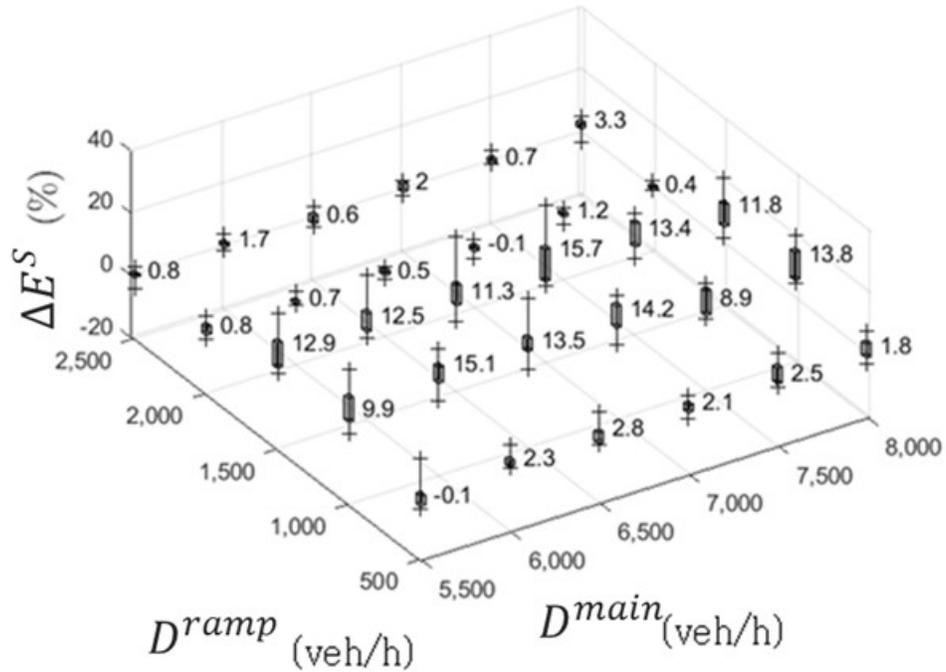
B. Average traffic speed impacts resulting from the changes in ramp and mainline demands.
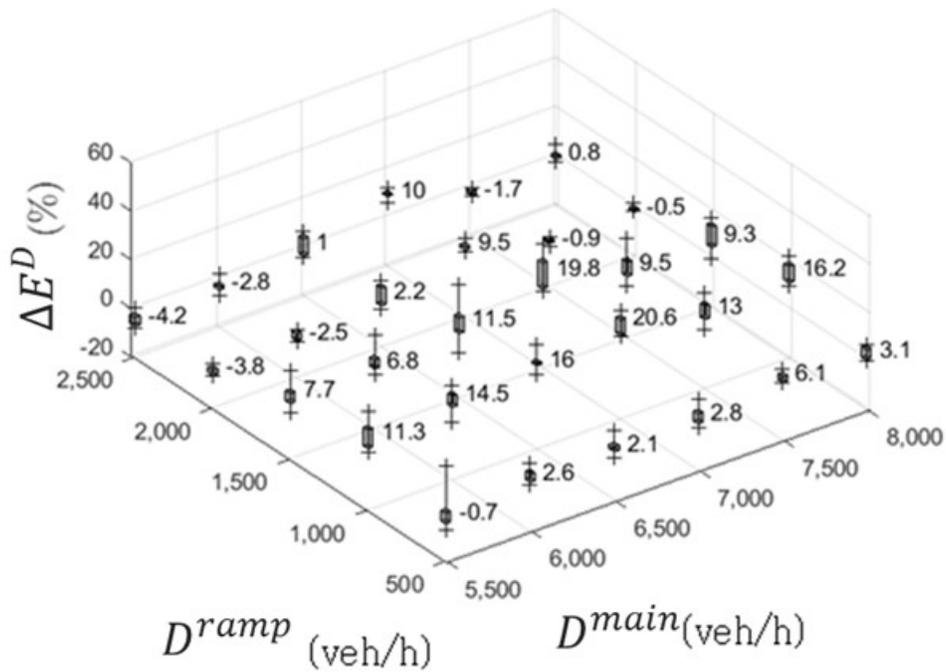
C. Average traffic delay impacts resulting from the changes in ramp and mainline demands.
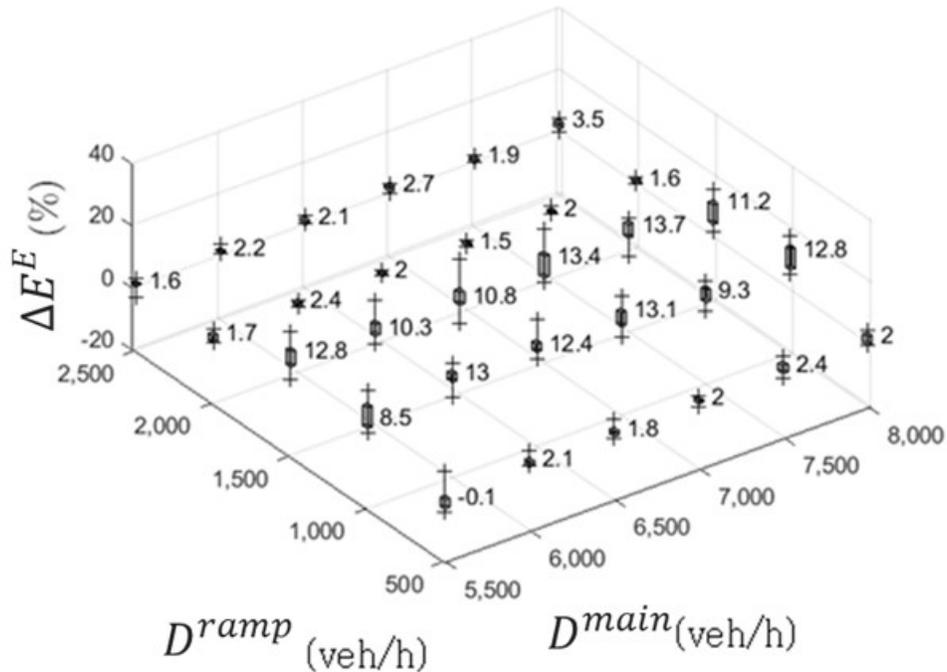
Source: FHWA.

D. Emissions impacts resulting from the changes in ramp and mainline demands.

**Figure 44. Graphs. Sensitivity analysis on $D^{main}$ and $D^{ramp}$.**

Again, the results indicate no significant effects on throughput; however, the other measures improve at various demand scenarios:

- Improvement of up to 15.7 percent in average speed.
- Reduction of 20.6 percent in average delay.
- Decrease of 13.7 percent in carbon monoxide emissions.

Achievement of the maximum benefits occurs at the mainline demand values of 7,000–7,500 veh/h (or 2,333–2,500 veh/h/l) and the ramp demand values of 1,000–1,500 veh/h. The minimum improvements result in relatively low demand values when traffic is undersaturated in such demand scenarios. Overall, this experiment reveals that the proposed algorithm can achieve significant improvements when high traffic saturation exists.

Next, the team performed a sensitivity analysis on the impacts of the $R^{ramp}$ parameter on the algorithm results, shown as box-plots in figure 45, in which the dotted-dashed green, solid yellow, and dashed red box-plots correspond to reasonably low, moderate, and high time intervals for $R^{ramp}$, respectively. The results indicate that throughput improves with $R^{ramp}$ because as $R^{ramp}$ increases the frictions between two approaches decrease and thus throughput increases. However, the other measures decrease with $R^{ramp}$. This is because greater $R^{ramp}$ values would worsen the ramp traffic performance that affects the network average speed, delay, and total emission. The maximum obtained benefits are a 3.1-percent increase in throughput at $R^{ramp} = 120$ s, a 15.7-percent improvement in average speed at $R^{ramp} = 20$ s, a 20.9-percent

reduction in average delay at $R^{ramp} = 10$ s, and a 13.4-percent decrease in carbon monoxide emissions at $R^{ramp} = 20$ s.
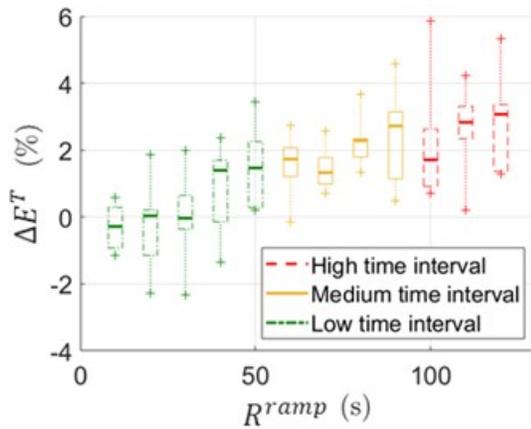
Source: FHWA.

A. The impact of maximum red intervals on throughput.
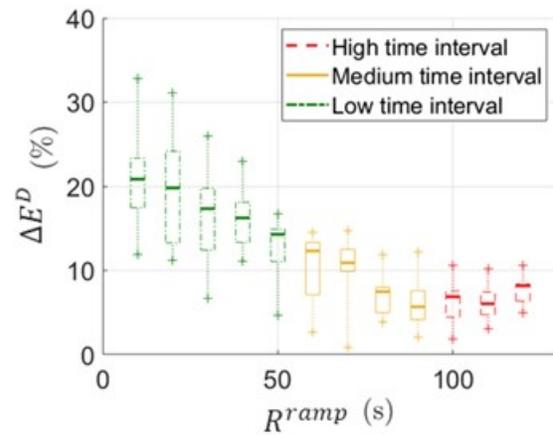
Source: FHWA.

C. The impact of maximum red intervals on average traffic delay.
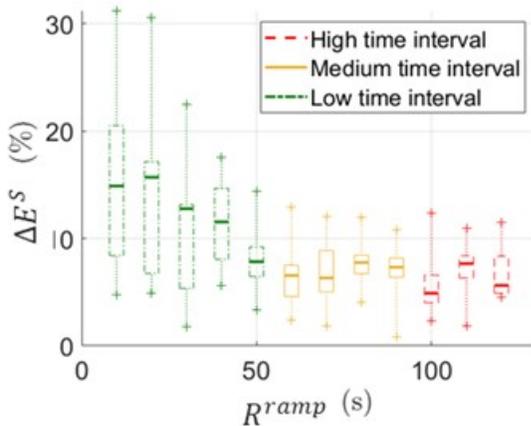
Source: FHWA.

B. The impact of maximum red intervals on average speed.
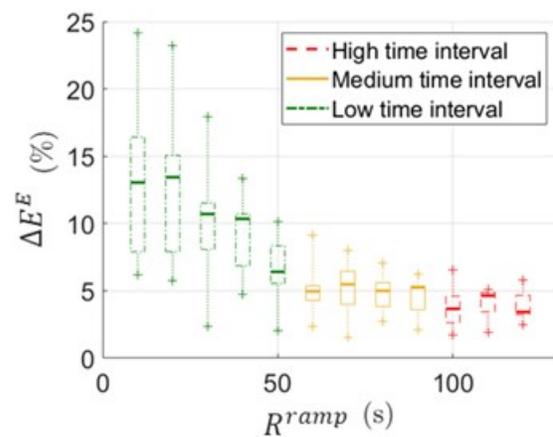
Source: FHWA.

D. The impact of maximum red intervals on emissions.

**Figure 45. Box-and-whisker plots. Sensitivity analysis on $R^{ramp}$.**

**Summary and Conclusions**

The team developed a dynamic signal control algorithm to apply as an integrated ramp and mainline metering strategy. When the traffic queue occurs due to a downstream lane drop or if a freeway merge spills all the way back to the merge point, the dynamic signal control algorithm is activated and turns the mainline signal to red to keep the mainline traffic from entering the downstream queue, which otherwise would exacerbate the traffic congestion. For safety reasons, the proposed algorithm does not activate the signal control unless the traffic speed at all mainline lanes drops below a safe speed threshold. This threshold is set to 6 mi/h in the experiments. After

activation, this algorithm predicts the future downstream queue status using the information provided by the deployed traffic sensors.

This prediction updates at every decision time point; as a result, the newly received information guides changes to the prediction. The mainline traffic signal turns to green a few seconds in advance of the predicted downstream queue dissipation time to let the mainline traffic smoothly join the downstream traffic. At the same time, the ramp signal turns to red to remove frictions between the merging and the mainline traffic. This red interval ends when detecting another speed drop at the mainline approach, and the mainline signal turns to red or reaches a maximum ramp red interval.

The team conducted simulation analyses using a calibrated Vissim network to evaluate algorithm performance under different traffic conditions and parameter settings. The implemented case study is a section of I–35 located in Kansas City, KS. This study considers four performance measures: traffic throughput, average network speed, average network delay, and total carbon monoxide emissions. Results of the simulation analyses show maximums of a 15.7-percent improvement in average speed, a 20.9-percent reduction in average delay, and a 13.7-percent decrease in carbon monoxide emissions. It is found that maximum improvements are obtained at relatively high traffic demands (i.e., the mainline demand values of 7,000–7,500 veh/h (or 2,333–2,500 veh/h/l) and the ramp demand values of 1,000–1,500 veh/h). Further, the improvements at low traffic demand values are comparatively limited. This implies that such treatments may not be needed when traffic demand is not sufficiently high. Results also indicate that no significant throughout improvement is achieved when $R^{ramp}$ is set to 30 s or less. That is because with low $R^{ramp}$, frictions between the mainline and on-ramp traffic increase. On the other hand, when $R^{ramp}$ is high, on-ramp traffic may greatly suffer, which impacts overall network-wide traffic performance. It should be noted that although throughput is not significantly improved when $R^{ramp}$ is set to a low value, as demonstrated in the network-wide average traffic speed, delay, and emission results, this control strategy does not simply shift the end of the queue to upstream sections without improving the overall traffic measures. Moreover, although these benefits are limited to a relatively small section of a network, like most other local control strategies, the proposed control approach can be implemented in other parts of the network. Therefore, achievement of further benefits for larger areas could justify system deployment costs.

Before implementing this control treatment, it is recommended that local transportation agencies perform more site-specific analyses. First, while the speed at which the control algorithm activates (i.e., $V^{threshold}$) is supposed to be set to a reasonably safe value, further safety analyses should be conducted to investigate the potential safety concerns of the proposed freeway signal control. The level of users' acceptance and compliance is another issue that needs to be comprehensively explored and addressed. Overall, this study can be represented as a baseline for highway mainline metering techniques. Thus, with some future improvements in the control algorithm, a superior and more cost-effective model, which relies on fewer traffic sensors, can be developed.

**COORDINATED ADAPTIVE RAMP METERING SYSTEM (E.G., HERO)**

Traditional ramp metering measures upstream freeway mainline volume to determine ramp flow, but rarely monitors downstream conditions. Downstream problems only show when congestion reaches the upstream ramp detector. Coordinated adaptive ramp metering (figure 12) uses feedback logic in a closed-loop control system. Traffic conditions measured at downstream bottlenecks determine critical occupancy and appropriate levels of traffic entering from upstream. The process assumes a historic or theoretical value of freeway capacity. Downstream flow conditions provide feedback to determine real-time ramp flow ($q_r$) and optimal occupancy ($q_{capN}$). When applied on a holistic, coordinated, system-wide basis, all ramps continuously communicate with each other to resolve complex traffic flow situations. One example of such a system is HERO, but the team identified several similar algorithms and systems during the task 2 effort. The team used the I–15 corridor model in San Diego, CA, to analyze the performance of the CRM algorithm HERO versus standalone algorithms (ALINEA and the San Diego ramp metering system (SDRMS)) and a base case without ramp metering. The team compared these scenarios to highlight the benefits provided by each ramp metering method for specific subsets of users in the corridor.

**Model Setup**

During an initial phase prior to the algorithm testing, the team added specific elements related to the ALINEA ramp meter implementation to the existing SDRMS along the I–15 corridor south of Lakes Hodges, CA, in a southbound direction. This area includes major congested areas of the corridor. The team coded the detection equipment for a total of 16 on-ramps and corresponding mainline sections. This setup allows the evaluation of the three different methods (SDRMS, ALINEA, and HERO) using the same Aimsun file, ensuring consistency among the different runs. Objects added to the network (figure 46) include:

- Queue (flush) detector.
- Middle (of the ramp) detector.
- Ramp meter.
- Exit detector.
- Mainline lane detectors.

© 2019 Aimsun.
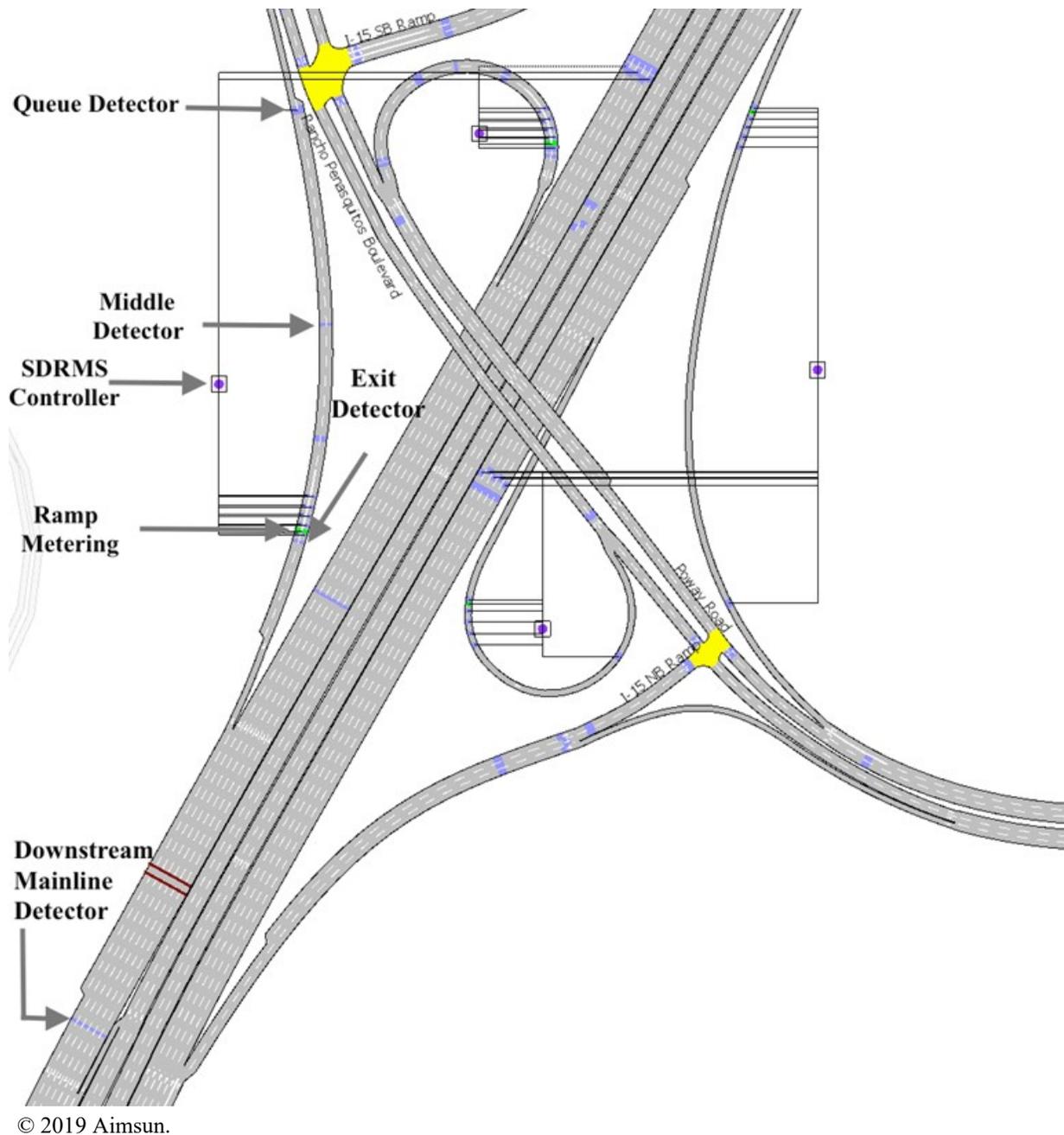
**Figure 46. Illustration. Selected area of the I–15 corridor and model setup for ALINEA and SDRMS ramp metering.**

## ALINEA Algorithm

As stated in chapter 2, ALINEA is a linear proportional-integral-derivative feedback process used locally to control the flow from the on-ramp to the mainline. The system is comprised of a ramp meter and mainline detectors. Expressed formally, the flow change from the on-ramp is proportional to the distance of the mainline occupancy from its target, as can be seen from the following equation. For a given on-ramp:

$$q_{k+1}^r = q_k^r + K_r(\rho_{target} - \rho_k)$$

<div align="right">(1)</div>

Where:

| | |
|---|---|
| $q_{k+1}^r$ and $q_k^r$ | = on-ramp flows at time step $k+1$ and $k$, respectively. |
| $k$ | = time step. |
| $k-1$ | = previous time step. |
| $K_r$ | = proportional-integral-derivative gain factor. |
| $\rho_{target}$ | = target occupancy on the mainline. |
| $\rho_k$ | = measured occupancy on the mainline at time step $k$. |

ALINEA has two principal parameters to calibrate and three secondary parameters:

- The gain factor.
- The target occupancy.
- The time step or calculation interval on which to apply the adjustment.
- The minimum and maximum values that can be used as flows for a given ramp meter.
- The distance of the mainline detectors to the on-ramp position.[1]

**HERO Algorithm**

As stated in chapter 2, HERO is based on ALINEA, coordinating the response from the ALINEA algorithm on a subset of upstream on-ramps (i.e., slaves). In addition to Aimsun's built-in ALINEA algorithm, queue control is added to limit the length of queues on the on-ramps. For a given on-ramp:

$$q_k^w = -T_c[w_{max} - w_k] + d_{k-1}$$

<div align="right">(2)</div>

Where:

| | |
|---|---|
| $q_k^w$ | = flow rate for the current queue at time step $k$. |
| $T_c$ | = calculation interval. |
| $w_{max}$ | = maximum possible queue at the on-ramp. |
| $w_k$ | = current queue at time step $k$. |
| $k$ | = time step. |
| $d_{k-1}$ | = on-ramp demand at time step $k-1$. |
| $k-1$ | = previous time step. |

---

[1]It should be noted that depending on the type of trigger and the underlying congestion environment, ALINEA can show sub-optimal results and exhibit an oscillating behavior, activating and deactivating frequently, or "flip-flopping." It is suggested by Wang and Papageorgiou (2006) to add a proportional term to the equation.

The following description of the HERO algorithm is taken from Papamichael (Papamichael 2008). To link the on-ramps together, changes to the previous local queue control formula include a coordination parameter on the minimum queue possible on a given on-ramp in the following linked control strategy. For a given on-ramp:

$$q_k^{LC} = -K_w * \left[w_k^{min} - w_k\right] + d_{k-1}$$

(3)

Where:

$q^{LC}_k$ = flow for local control at time step $k$.
$K_w$ = control parameter that is set to $1T_c$ like in the previous local queue control.
$1T_c$ = one calculation interval.
$w^{min}_k$ = minimum queue forced at time step $k$.
$w_k$ = current queue at time step $k$.
$d_{k-1}$ = previous on-ramp demand at time step $k-1$.

The flow from a given on-ramp is then chosen as the minimum from either ALINEA or the coordinated version of ALINEA with minimum queue, given that the storage space is available.

$$q_k = \max \left(\min\left(q_k^r, q_k^{LC}\right), q_k^w\right)$$

(4)

Where:

$q_k$ = on-ramp flow at time step $k$.
$q^r_k$ = flow for coordinated control at time step $k$.
$q^{LC}_k$ = flow for local control at time step $k$.
$q^w_k$ = flow rate for the current queue at time step $k$.

The minimum queue at time step $k$ ($w^{min}_k$) is calculated by coordinating all the queue information from the on-ramps, using all of the upstream on-ramps of a given on-ramp as a common storage space with local demand.

$$w_k^{i,min} = \frac{\sum w_k^j}{\sum_{j \neq i}^n w^{j,max}} w_k^{i,max}$$

(5)

Where:

$w^{i,min}_k$ = minimum queue for all time steps.
$\Sigma w^j_k$ = summation of queues at all time steps.
$\Sigma^n_{j \neq i} w^{j,max}$ = summation of maximum queues at all time steps.
$w^{i,max}_k$ = maximum queue for all time steps.

In effect, the relative queues at on-ramps (the ratio of the current queue to maximum queue) being equal for all ramps implies that the traffic conditions are being leveled across ramps by using the extra storage spaces of underused ramps. Furthermore, the HERO algorithm is not always in function; its authors intended it to trigger when the local ALINEA ramp metering response is failing for given traffic conditions. The triggering conditions are:

- The mainline occupancy is over a threshold of the target occupancy.
- The queue on the on-ramp (which will become the master ramp) is over a threshold of the maximum queue (corresponding to the ramp storage space available for vehicles).

In a similar fashion, deactivation is controlled by one of the following two conditions:

- The mainline occupancy drops below a threshold of the target occupancy.
- The queue on the master ramp is lower than a threshold of the maximum queue (corresponding to the ramp storage space available for vehicles).

When the activation threshold is met in one location, this embattled on-ramp becomes the master on-ramp of any upstream on-ramps who work as slaves to reduce the flow released to the mainline; this proceeds until one of the deactivation thresholds is met.

With the use of a "real" test case, the team added new features to the algorithm in this research to reflect certain specific issues that were not addressed in the literature, in particular:

- Minimum number of slaves.
- Maximum number of slaves.
- Concurrent triggering of independent activations.
- Merging behavior of overlapping activations.

The minimum number of slaves controls the possibility for an on-ramp to eventually become a master, should the conditions be satisfied. This parameter is useful to limit the trigger of HERO for an on-ramp as a master that is at the limit of a given network or study area or is just downstream from a major interchange. The maximum number of slaves controls the number of on-ramps used as extra storage space for a given master. This parameter is useful to limit the upstream impact of a bottleneck when the travel time of vehicles from an upstream on-ramp to the bottleneck is longer than the time it takes to reabsorb the congestion with the help of "closer" slaves.

Having the maximum number of slaves on a given network enables HERO to have multiple concurrent activations. This is useful to reabsorb multiple congestion hotspots occurring independently over the network (e.g., multiple interchanges of major highways). The behavior of HERO in those instances is the same. Finally, when HERO activations overlap (e.g. when a slave of a given master has itself a higher mainline occupancy and a high on-ramp queue), HERO activates this new master's slaves and transfers them to the original master, in effect using more slaves than the original maximum number. When deactivating the original master and not the "second," HERO will reactive for this on-ramp. When HERO deactivates, all the original slaves are reinitialized.

In summary, HERO uses ALINEA as a base and uses upstream on-ramps as extra storage space, using relative queues to level conditions across on-ramps. HERO uses the following 12 parameters:

From ALINEA:

- $K_r$.
- Target occupancy on the mainline.
- Calculation at the time step.
- Minimum and maximum values that can be used as flows for a given ramp meter.
- The distance of the mainline detectors to the on-ramp position.

Specific to HERO:

- Maximum queue.
- Mainline occupancy activation threshold.
- Mainline occupancy deactivation threshold.
- Ramp queue length activation threshold.
- Ramp queue length deactivation threshold.
- Minimum number of slaves.
- Maximum number of slaves.

HERO's time step calculation is set to be the same as ALINEA's.

The 12 parameters needed for HERO must be calibrated for the given traffic conditions. In favorable conditions, these parameters would be optimized using the Aimsun model as a cost function, using mathematical frameworks, such as the derivative free optimization project NOMAD, to determine the best parameter set that minimizes the objective function (e.g., global delay in a simulation) (Gerad Polytechnique Institute 2018). However, because of the relatively high dimensionality of the problem and the long computation time of the many ICM replications, an approximate sensitivity method is used to determine the best parameters, mostly based on a simplified version of the well-known "one at a time" (also known as "one factor at a time") and traffic engineering considerations. The team assumed that parameters have an independent impact on the overall cost—each parameter varying in a given simulation between two extremes, while all other values remain constant at a "reasonable" value. Observing the better result of these two extreme experiments, the team selected a new experiment by shifting the parameter value in the direction of the better extreme.

*Target Occupancy*

When the mainline is close to capacity, estimation of an algorithm to measure the proper target occupancy from downstream detector flow drop helps increment target occupancy on the calibrated network ramp meter until the capacity drops on the mainline. The target is just below this upper limit, without imposing strict constraints on the on-ramp itself. This way, ALINEA triggers before the occupancy on the mainline provokes an artificial flow drop due to reaching capacity. This parameter is set at around 23 percent for this corridor. A lower value would

penalize the on-ramps too much, while with a higher value the freeway would reach capacity too quickly, thus not preventing slowdowns on time.

### *Regulator Parameter (kr) and Calculation Interval*

The metered flow allowed through the on-ramp will vary depending on the difference between the target occupancy and the measured occupancy for each time interval. The *kr* and the time interval manage how fast the flow can vary and how often to take these measurements. Testing of different values of *kr* avoided a flip-flop behavior at the on-ramps and concluded with a value of 10. Moreover, using a smaller calculation interval produced better results. The best results were attained at a 1-min interval, while a 30-s interval showed no additional benefits.

### *Minimum and Maximum Flow*

A minimum and maximum flow can be set to ensure that the on-ramp performs at a certain level no matter what the occupancy. Placement of the detector is on the mainline to measure occupancy after the acceleration lane, in the merge portion of the mainline and the on-ramp. A wider range provides more flexibility for ALINEA and HERO to be more effective. A range of 200–2,500 veh/h is set to provide this flexibility. The ranges are explained as follows:

- 200 veh/h is very aggressive for the mainline. Depending on the geometrical considerations of the on-ramps and typical demand peak hour, this is the smallest flow that does not cause overflow to the arterial network.
- 2,500 veh/h is above the normal capacity for a typical on-ramp. By setting the maximum this way, the throughput is not limited by an artificial constraint given by the ramp meter when there is no traffic on the mainline. The typical throughput will be lower for all on-ramps, limited only by the characteristics of the on-ramps (e.g., geometry, speed limits) and the vehicle behavior itself.

### *Maximum Queue*

Estimation of the maximum queue used the length of the on-ramp divided by the average length of all the vehicles contained in the traffic demand of the experiment. Even weighted by the overall count of each vehicle class and given observations from the experiments, the team adjusted this number manually to represent an approximation.

### *Mainline Occupancy Activation and Deactivation Thresholds*

These thresholds, as applied to the target occupancy from ALINEA, represent the level of congestion in the mainline that would trigger HERO and deactivate it when the congestion is gone. Because the team calibrated the ALINEA target occupancy to trigger just before a capacity drop, the team used values between 75–125 percent. The team presented the results using values between 75–100 percent since higher values showed obvious degradation in the overall results.

### *Ramp Queue Length Activation and Deactivation Thresholds*

Ramp queue length activation and deactivation thresholds measure the ratio of the current queue length to the maximum queue needed for activation and deactivation. For activation, the team

used values ranging from 30–50 percent of maximum queue, while deactivation values ranging from 15–35 percent we used. Higher values for the activation threshold will not give enough time for HERO to prevent on-ramps from reaching capacity (maximum storage), while lower values of the deactivation threshold would have HERO activate without queues on the on-ramp.

*Minimum and Maximum Number of Slaves*

The minimum number of slaves is set to one to eliminate on-ramps at the edge of the network. The maximum number of slaves is set at three, and further experiments should show the impact of changing this number on the overall results.

*Tests and Measures of Performance (MOPs)*

As explained in the previous sections, a plausible range for the different values of the parameters required by both HERO and ALINEA were established after performing several tests. Table 8 presents the log of the activations and deactivations of the HERO algorithm that shows when, where, how long, and how many on-ramps were slaves during a given simulation. Table 6 and table 7 present a summary of six of the tests, showing the need to balance delay on the mainline, the on-ramps, and the arterial network for ALINEA and HERO algorithms, respectively. The following test performance measures describe the results qualitatively and quantitatively:

- Average speed on the mainline (mi/h).
- Speed contours on the mainline and on-ramps (descriptive).
- Weighted average harmonic speed on all on-ramps and mainlines (mi/h).
- Total travel time (h). This measure includes the travel time of the vehicles having exited the entire network (mainline, on-ramps, and arterials), the vehicles currently in the network, and the vehicles waiting to enter.
- Total distance traveled (mi). This measure includes the distance traveled by the vehicles having exited the network (mainline, on-ramps, and arterials) and the vehicles currently in the network.

Table 8 presents the log of the activations and deactivations of the HERO algorithm that shows when, where, how long, and how many on-ramps were slaves during a given simulation.

**Table 6. Parameters used for the six sensitivity analysis tests—ALINEA.**

| Test Number | Target Occupancy (Percent) | Minimum Flow (veh/h) | Maximum Flow (veh/h) | Calculation Interval(s) |
|---|---|---|---|---|
| One | 23 | 450 | 2,500 | 60 |
| Two | 23 | 200 | 2,500 | 60 |
| Three | 23 | 450 | 2,500 | 60 |
| Four | 23 | 450 | 2,500 | 30 |
| Five | 23 | 100 | 2,500 | 30 |
| Six | 23 | 300 | 2,500 | 30 |

**Table 7. Parameters used for the six sensitivity analysis tests—HERO.**

| Test Number | ML Activation (Percent) | ML Deactivation (Percent) | Queue Activation (Percent) | Queue Deactivation (Percent) |
|---|---|---|---|---|
| One | 100 | 75 | 30 | 15 |
| Two | 100 | 75 | 30 | 15 |
| Three | 100 | 75 | 50 | 30 |
| Four | 100 | 75 | 30 | 15 |
| Five | 100 | 75 | 50 | 30 |
| Six | 100 | 75 | 50 | 30 |

**Table 8. Summary of HERO activation and deactivation times for test six with the master ramp and its corresponding slaves.**

| Activation Time | Deactivation Time | Master Ramp | Slaves |
|---|---|---|---|
| 6:53:29 | 6:59:59 | 8 | 9, 10, 11 |
| 7:02:59 | 7:09:29* | 9 | 10, 11, 12 |
| 7:09:29 | 7:17:29 | 8 | 9, 10, 11, 12 |
| 7:21:59 | 7:23:29 | 9 | 10, 11, 12 |
| 7:29:59 | 7:42:29* | 9 | 10, 11, 12 |
| 7:42:29 | 7:46:29 | 8 | 9, 10, 11, 12 |
| 7:50:59 | 7:53:59 | 9 | 10, 11, 12 |
| 8:21:59 | 8:32:59 | 12 | 13, 14, 15 |

*When the current master merged with a downstream new master and became a slave.

## Results and Discussion

All experiments have similar traffic conditions (e.g., same replication seed, demand), but none have virtual queues at the end of the simulations, meaning that all the demand has been pushed through the network during the simulation time. Differences in results are due to differences in behavior of the ramp metering algorithms and the ensuing decisions taken by individual vehicles which cause (or do not cause) congestion.

When looking at the average travel times on the mainline in a series of heat maps, HERO exhibits faster overall times at 835 s for all experiments, representing a 19-s-per-vehicle (2-percent) gain over ALINEA and a 43-s-per-vehicle (5-percent) improvement over the no ramp metering alternatives (Belisle et al. 2019). Similarly, if the team includes the on-ramps with the mainline, the gain in total travel time is 282 h (3 percent) for HERO over ALINEA and 480 h (4 percent) over the no ramp metering scenario. While the focus of this study is the prevalence of the conditions on the mainline, the results do not focus solely on having the lowest possible travel times on the mainline. Other tests showing better mainline conditions at the expense of on-ramps and arterials were too severe.

The team generated speed contours showing overall traffic conditions for both the mainline and on-ramps for HERO, ALINEA, SDRMS, and no ramp metering. For example, starting at 7:15 a.m. near ramp 12, HERO limits the mainline bottleneck expansion both spatially (i.e., upstream) and temporally (i.e., to approximately 8:00 a.m.) relative to the other scenarios,

especially the no ramp metering scenario, and eases the merge, eliminating the upstream slowdown. On-ramp speeds were visibly slower in HERO than no ramp metering, with speeds ranging from 1–8 mi/h at 7:00 a.m. for HERO versus 5–30 mi/h for no ramp metering for on-ramps 13 to 16. The same is true for on-ramps 8–10.

By looking at the HERO logs, a correlation can be seen between the improvement of the speed contours graphs of the different methods and the activations (and deactivations) of HERO. For example, in the case of mainlines 8 and 9 between 7:00–8:00 a.m., a higher vehicular speed is the resultant of the activations of on-ramps 8 and 9 as masters with slaves 10, 11, and 12.

Comparing the speeds locally for two mainline sections just upstream of a given bottleneck highlights this behavior, as shown in figure 47. In all cases, the speed recovers faster with HERO than with the other algorithms. The fluctuation of the speed as the algorithm adapts to the current conditions is also noticeable on figure 47.

In summary, the main finding of this study is that for all three principal MOP (average speed on the mainline, weighted average harmonic speed on all on-ramps and mainlines, and global vehicle miles traveled (VMT)), HERO outperforms ALINEA by only a marginal amount, ALINEA outperforms SDRMS, and SDRMS outperforms the no ramp metering scenario. Ramp metering, and especially CRM, has the effect of transferring delay from the mainline to the on-ramps. Generally, this is a zero-sum game and no overall gain is expected; what the mainline gets is taken from the on-ramps. However, with the right set of parameters for test six, a "non-zero sum" result can be realized. By reducing the mainline friction and regulating flow, on-ramp merges are easier and travel times are shorter overall for the mainline, on-ramps, and arterials. This means that what the mainline gains is taken from the on-ramps but given back to the on-ramp vehicles on their mainline journey.

A. Merging area on-ramp 9.

B. Merging area on-ramp 8.

**Figure 47. Graphs. Mainline speed/time just upstream of on-ramp 9 and on-ramp 8.**

Table 9 through table 13 present a numerical comparison of the data shown in the speed contours, with the weighted average of the harmonic speed on all 16 on-ramps and the corresponding mainline sections. HERO had the fastest average harmonic speed in test six at 59.74 mi/h (decimals for differentiation, not significance), which is a 1-percent (0.7-mi/h) gain from ALINEA and a 2-percent (1.3-mi/h) gain from the no ramp metering alternative. Table 9 through table 13 also show that HERO is fastest on tests one, three, five, and six, while ALINEA is fastest on tests two and four by a small margin. These tables also present the overall total vehicle hours traveled (VHT) and total VMT, including the arterial network. The lowest total time traveled is for the no ramp metering scenario at 67,250 h; however, the total distance travelled MOP is a better indicator of the throughput of the network, with a higher number meaning a higher throughput. In this regard, HERO test six had the highest VMT at 2,781,946 mi, a very small improvement from both ALINEA and the no ramp metering base scenario. This small difference can be explained by the magnitude of the network and the large portions (both in time and space) when congestion is not present. A focus on the peak hour would show a larger relative improvement, but in all cases HERO still has the advantage, if only marginally, over all the other methods.

In summary, the main finding of this study is that for all three principal MOPs (average speed on the mainline, weighted average harmonic speed on all on-ramps and mainlines, and global VMTs), HERO outperforms ALINEA by only a marginal amount, ALINEA outperforms SDRMS, and SDRMS outperforms the no ramp metering scenario. Ramp metering, and especially CRM, has the effect of transferring delay from the mainline to the on-ramps. Generally, this is a zero-sum game and no overall gain is expected; what the mainline gets is taken from the on-ramps. However, with the right set of parameters for test six, a "non-zero sum" result can be realized. By reducing the mainline friction and regulating flow, on-ramp merges are easier and travel times are shorter overall for the mainline, on-ramps, and arterials. This means that what the mainline gains is taken from the on-ramps but given back to the on-ramp vehicles on their mainline journey.

**Table 9. Performance comparison among the different tests and for all four scenarios— mainline average travel time (s).**

| Test Number | HERO | ALINEA | SDRMS | No Ramp Metering |
|---|---|---|---|---|
| One | 836 | 854 | 858 | 878 |
| Two | 849 | 846 | 858 | 878 |
| Three | 838 | 843 | 858 | 878 |
| Four | 854 | 849 | 858 | 878 |
| Five | 838 | 848 | 858 | 878 |
| Six | 835 | 854 | 858 | 878 |

**Table 10. Performance comparison among the different tests and for all four scenarios—mainline and ramp total travel time (h).**

| Test Number | HERO | ALINEA | SDRMS | No Ramp Metering |
|---|---|---|---|---|
| One | 10,627 | 10,872 | 10,807 | 11,038 |
| Two | 10,852 | 10,684 | 10,807 | 11,038 |
| Three | 10,627 | 10,627 | 10,807 | 11,038 |
| Four | 10,851 | 10,762 | 10,807 | 11,038 |
| Five | 10,583 | 10,766 | 10,807 | 11,038 |
| Six | 10,558 | 10,840 | 10,807 | 11,038 |

**Table 11. Performance comparison among the different tests and for all four scenarios—mainline and on-ramp weighted average harmonic speeds (mi/h).**

| Test Number | HERO | ALINEA | SDRMS | No Ramp Metering |
|---|---|---|---|---|
| One | 59.2 | 59.2 | 59.1 | 58.4 |
| Two | 59.2 | 59.2 | 59.1 | 58.4 |
| Three | 59.6 | 59.4 | 59.1 | 58.4 |
| Four | 59.2 | 59.2 | 59.1 | 58.4 |
| Five | 59.6 | 59.1 | 59.1 | 58.4 |
| Six | 59.7 | 59.0 | 59.1 | 58.4 |

**Table 12. Performance comparison among the different tests and for all four scenarios—VHT (h).**

| Test Number | HERO | ALINEA | SDRMS | No Ramp Metering |
|---|---|---|---|---|
| One | 68,313 | 67,859 | 67,794 | 67,250 |
| Two | 68,065 | 68,168 | 67,794 | 67,250 |
| Three | 67,696 | 67,692 | 67,794 | 67,250 |
| Four | 67,554 | 67,717 | 67,794 | 67,250 |
| Five | 67,688 | 67,794 | 67,794 | 67,250 |
| Six | 68,157 | 67,890 | 67,794 | 67,250 |

**Table 13. Performance comparison among the different tests and for all four scenarios—VMT (mi).**

| Test Number | HERO | ALINEA | SDRMS | No Ramp Metering |
|---|---|---|---|---|
| One | 2,781,614 | 2,780,741 | 2,778,855 | 2,777,243 |
| Two | 2,781,273 | 2,779,039 | 2,778,855 | 2,777,243 |
| Three | 2,779,885 | 2,779,039 | 2,778,855 | 2,777,243 |
| Four | 2,779,701 | 2,778,783 | 2,778,855 | 2,777,243 |
| Five | 2,780,570 | 2,780,307 | 2,778,855 | 2,777,243 |
| Six | 2,781,946 | 2,780,461 | 2,778,855 | 2,777,243 |

Importantly, HERO must be adequately calibrated to attain good results (Amini 2015). Results will vary greatly depending on the underlying conditions and different networks, so while it is relatively easy to have better conditions on the mainline with HERO rather than any other

algorithm, it is just as easy to worsen the situation overall. Depending on the operators' objectives, finding the right balance can be a complicated task.

Furthermore, while the team proposed some basic enhancements to the "simple" version of the HERO algorithm, such as maximum number of slaves per master, other changes are possible. In particular, the mainline occupancy is an average of multiple lanes that exhibit different characteristics—this is especially true of a mainline with four or more lanes. The algorithm could be adapted to measure not the average occupancy but the maximum occupancy for a lane (or the average of a subset of lanes) at a given time when the bottleneck is slowly building up laterally downstream, which would help alleviate congestion by having a more precise indicator of when traffic is building up. Furthermore, an important issue is the concept of maximum queue. While sound in theory, this value does not correspond to a specific practical concept. This could be revised as a probability distribution, and the activation and deactivation thresholds could be translated as statistical concepts (i.e., distance from mean queue). While this would require more data and a small change in the basic algorithm, it would better indicate when a given queue is judged problematic and would limit the over triggering of HERO.

More generally, the question of whether ramp metering should be activated at all times needs studying. Indeed, having a ramp meter is analogous to a signalized intersection; delay of vehicles can happen even though no opposing traffic warrants a stop at a red light. However, it is easier to shutoff a ramp meter than it is a traffic signal. The question that remains is, "Which conditions should be met to start and stop the metering?"

In summary, when testing the HERO algorithm against the ALINEA, SDRMS, and no ramp metering scenarios using the ICM Aimsun network, a complete and wide-ranging network covers the San Diego, CA, I–15 mainline corridor, on/off-ramps, and arterial roads.

Different MOPs to assess the efficiency of each algorithm include:

- Average travel time on the entire mainline.
- Average weighted harmonic speed on the entire mainline and all ramps.
- The total distance and time traveled by a vehicle over the entire network (mainline, on-ramps, and arterials).

The team analyzed many tests to calibrate the different parameters needed by each method. In the best scenario, HERO outperformed all of the other algorithms, specifically:

- A 2-percent (19-s/vehicle (s/veh)) gain over ALINEA and a 5-percent (45-s/veh) gain over no ramp metering for mainline travel time.
- A 1-percent (0.7-mi/h) gain over ALINEA and a 2-percent (1.3-mi/h) gain over no ramp metering for the average weighted harmonic speed on the mainline and ramps.
- A higher vehicle distance traveled over the other methods, showing a higher throughput.

These results show that HERO is more efficient at reducing travel time on the mainline and on-ramps, regulating on-ramp merges to the mainline, and reducing the overall delay. This benefit is at no cost to the overall network, indicating that no delay transfers from the mainline travelers to other users of the network.

While these results favor HERO, this method requires careful calibration to obtain overall benefits. It is relatively simple to lower travel times on the mainline but still lead to overall worse results. Because of the need for more infrastructure (e.g., detectors, communications equipment) and the refinements needed by the HERO method, the ramp metering operator must carefully evaluate the cost-benefit ratio associated with its use. Even though ALINEA may show worse results, its simplicity and robustness is a factor in its favor. Finally, while the team examined only preliminary results, another method was being tested: optimized ramp coordination (based on California Partners for Advanced Transit and Highways' CRM algorithm). The objective of developing this new method is to use the strengths of HERO (the coordination of the behavior of multiple ramps) while limiting its weaknesses (the need to calibrate a several parameters).

## OPEN-ACCESS MLs ON THE RIGHT-HAND SIDE

Typically in the United States, managed HOV/HOT lanes provide an improved level of service to drivers and are at the far left-hand side, next to the median. Although locating the ML on the right-hand side would reduce its capacity, the overall impact on all lanes could be beneficial. The Alternative Freeway Designs at Merge and Diverge Segments project compared right-side ML designs to left-side designs (i.e., with continuous access or partial access). Reduction by 300 veh/h in the overall capacity of a four-lane freeway occurs if the right-side ML capacity is reduced from 2,000 to 1,700 veh/h and the other three lanes remain at 2,000 veh/h. However, MLs on the left-hand side can result in a much larger capacity loss since all lanes can experience the 300-veh/h capacity loss due to vehicles weaving from the right to the left. Even if only the middle two lanes were impacted by this weave friction and turbulence, there may be a capacity loss of 300 x 2 = 600 veh/h, or twice that of a right-side ML.

HOV lanes are usually for vehicles with a driver and one or more passengers, and are mostly on freeways with high demand and traffic congestion. HOV lanes have the potential to save travel time, increase throughput, and offer more reliable travel experiences. There is extensive literature investigating the effectiveness of HOV lanes, both in simulation and after field deployments. Many studies investigated different HOV lane designs, and most of them focused on the interaction between the HOV lane and the GP lane. Avelar et al. (2016) investigated the influence of GP lane traffic on ML speeds. The results from this study indicate that there is a significant positive relationship between the ML speed and the GP lane speed. Besides, the presence of pylons may help reduce the influence of GP lane speed on the ML. To better understand the relationship between GP and HOV lanes, Qi et al. (2015) conducted research on lane changing behavior along HOV facilities. The study used aerial photo data collected from the segment of SR 60 in Moreno Valley, CA, and compared traffic data of limited HOV lane access and continuous HOV lane access. Statistical tests compared the two HOV lane configuration types. The results suggest that two configuration types (i.e., limited and continuous) have no significant difference in the percentage of traffic volume of HOV lanes. The difference between the average speeds of HOV and mix-flow lanes is lower for the design with continuous HOV lane access.

Shan et al. (2016) investigated a partially limited access design of HOV lane to improve the performance of HOV facilities. To reduce the influence of cross-weave flow between the HOV and GP lanes, buffers were placed on selected segments of freeway between HOV and GP lanes. Simulation tests with three influential factors (cross-weave flow, number of GP lanes, and buffer

length) indicate that the HOV cross-weave flow has a negative effect on the capacity of GP lanes, while buffer-separated HOV facilities are better at regulating traffic flow. The length of the buffer does not affect the capacity of GP lanes. Furthermore, a simulation network of the same segment of eastbound SR 210 shows that the efficiency of the overall network with partially limited access design is 9 percent higher than that of the designs with limited access HOV facility and 4 percent higher than that of the designs with continuous access HOV facility. Fitzpatrick and Avelar (2016) investigated safety issues involving buffer-separated MLs. This study looked at the relationships between crashes and buffered ML features including buffer width, lane width, and shoulder width. Annual ADT data of freeways with three and four GP lanes in California and Texas used generalized data analysis of linear mixed models and showed that reductions in ML envelope widths (shoulder, lane, and buffer width) are associated with more crashes. In addition, reductions in freeway lane width or shoulder width are associated with more crashes.

Previous studies suggest that the traffic condition of GP lane has a significant association with the HOV lane, and many features of the freeway, such as lane width, shoulder width, and separation designs, affect the performance of the HOV lane. However, all of the previous studies looked at left-side HOV lanes. To investigate whether the location of the ML would influence its performance, the team conducted simulation evaluations for HOV lanes on the right-hand side.

## Methods

This section introduces modeling and analysis of the proposed new design (right-side HOV lanes) in a microsimulation environment to derive insights on the effectiveness. To evaluate the proposed strategy comprehensively under varying conditions, the team first built synthetic simulation networks for merging, diverging, and weaving segments and conducted a large number of sensitivity analyses to select best design parameters for different traffic conditions. Then, the team implemented the strategy with selected design parameters on a real-world simulation network to help the local agency understand the potential of this strategy to solve local congestion problems.

## Assumptions

The total length of the synthetic network mainline segment is around 3.7 mi for on-ramp simulations and 3.5 mi for off-ramp simulations, as shown in figure 48. Based on the *AASHTO Green Book*, the team assumed a traffic speed of 70 mi/h for the mainline and 30 mi/h as the lower speed range for the on-ramp and off-ramp in the simulations (AASHTO 2018). In the simulations, the team used recommended lengths for the acceleration and deceleration lanes of 1,300 and 560 ft, respectively (WSDOT 2017). The team conducted the simulations for the merge (on-ramp area) and diverge (off-ramp area) separately to assess how various parameters would affect operations of the network under different ML strategies.
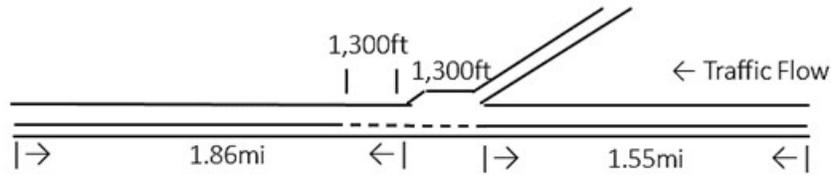
© 2019 Jiaqi Ma.

A. Merge benchmark design.
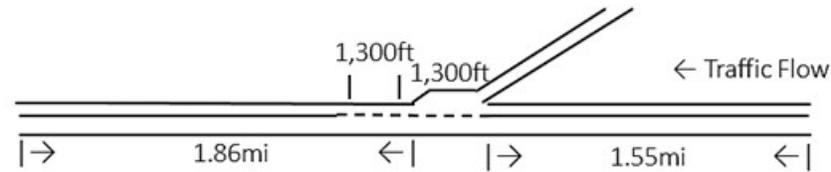


© 2019 Jiaqi Ma.

B. Merge alternative design.
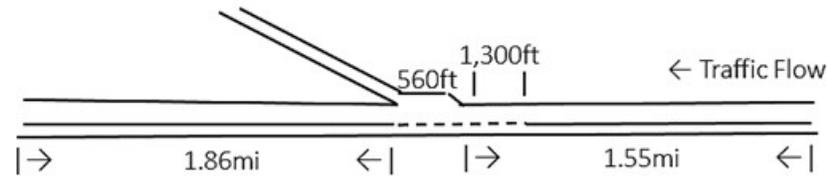


© 2019 Jiaqi Ma.

C. Diverge benchmark design.
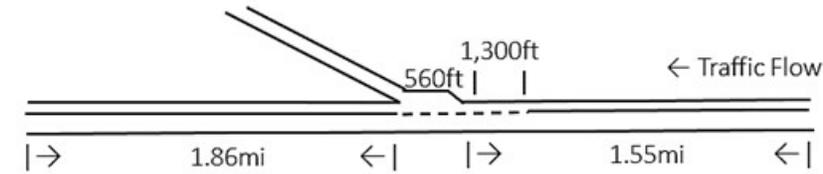


© 2019 Jiaqi Ma.

D. Diverge alternative design.

**Figure 48. Illustrations. Synthetic simulation network (merge and diverge).**

In addition to the merge and diverge segments, the team conducted simulation experiments on a weaving segment. The geometry of the weaving segment is shown in figure 49 and it is the basic design of a weaving segment as defined in the *HCM*, where both on-ramp and off-ramp vehicles are required to make at least one lane change to reach their destination. Also, the length between the ramps is usually less than a threshold, beyond which the merge and diverge area may not affect each other. The network reduces to the simple combination of the merge and diverge in figure 48.
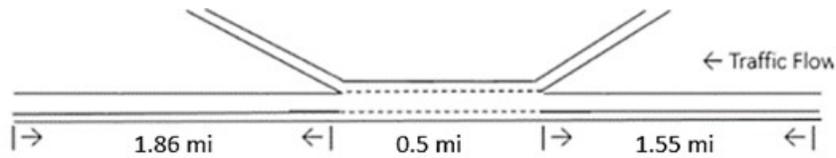
© 2019 Jiaqi Ma.

A. Weaving benchmark design, shared acceleration lane.
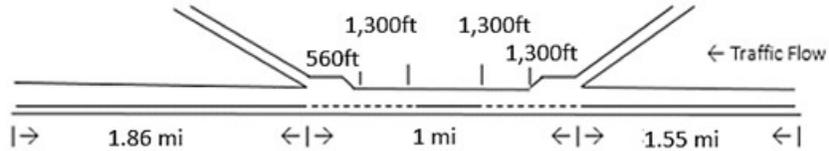


© 2019 Jiaqi Ma.

B. Weaving benchmark design, separate acceleration lanes.
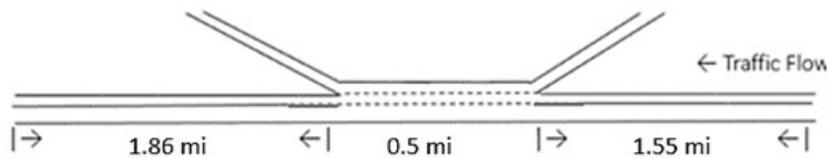


© 2019 Jiaqi Ma.

C. Weaving alternative design, shared acceleration lane.
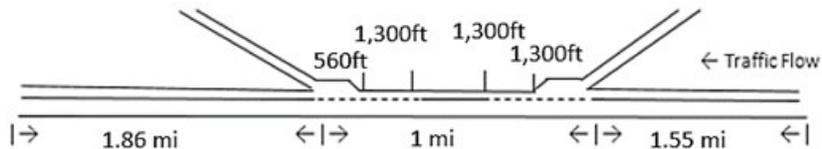


© 2019 Jiaqi Ma.

D. Weaving alternative design, separate acceleration lanes.

**Figure 49. Illustrations. Synthetic simulation network geometry (weaving).**

**Experimental Design**

As listed in table 14 below, five key factors that may affect the performance of the two designs are included in the simulation for sensitivity analysis: the mainline congestion (V/C ratio), ramp volume, number of lanes, ramp traffic HOV percentage, and merge/diverge buffer area length. The team also considered analysis of weaving area length. For each of the 72 total scenarios, the team conducted 10 simulations to account for stochasticity.

**Table 14. System parameters considered in study.**

| Parameters | Levels | Number of Levels |
|---|---|---|
| HOV position—HOV_POS | HOV lane on the left-hand side<br>HOV lane on the right-hand side | Two |
| Mainline input volume to capacity ratio—Volperlane | 55 percent, 80 percent, 110 percent | Three |
| On/off-ramp volume—VolRamp (veh/h/l) | 500; 1,000; 1,500 | Three |
| Number of lanes—NoLanes | 3, 4 | Two |
| Ramp traffic HOV percentage | 0.25, 0.5 | Two |
| Weaving area length (mi) | 0.5, 1 | Two |

The team found the capacity of the freeway network in Vissim is about 2,000 veh/h/l based on the initial data collection on the synthetic simulation network with specified driver parameters used in the previous studies and calibrated networks (TariVerdi and Miller-Hooks 2012). Therefore, the team set the three mainline input volumes to 1,100 veh/h/l (V/C = 0.55); 1,600 veh/h/l (V/C = 0.8); and 2,200 veh/h/l (V/C = 1.1) to test the alternative design under different congestion levels. Ramp traffic HOV percentage directly affects the number of lane changes, which indicates the intensity of disruptions to the mainline traffic. Generally, a merge area buffer of 0.25 mi is desirable for HOV lanes (Cothron et al. 2003). These openings should safely accommodate vehicles weaving to and from the HOV lane. Longer merge (or diverge) area buffers can have two distinct effects. Positively, they may give merging vehicles more chances to merge into the mainline smoothly. On the negative side, particularly for the alternative design, regular vehicles may have a higher impact on HOV lane operations.

The results analyzed two performance measures: average delay and throughput. GP vehicles and HOVs on both the mainline and on/off-ramp are measured separately. The sum of mainline and on/off-ramp throughputs determines total throughputs for both types of vehicles. The team calculated performance measures separately for all scenarios, including throughputs and delays of GP, HOV, and total vehicles on both the mainline and off-ramp. For merge scenarios, the team collected data on the HOV and GP lanes at the exit of the network. These variables are compared across different scenarios in the final statistical analysis.

**Simulation Approach**

The team used the PTV Vissim 10.0 microscopic traffic flow simulation tool to perform the experiments. The team modeled HOV lanes by setting the blocked vehicle type as a GP vehicle. To avoid additional confounding factors in the simulation, HOV vehicles only use HOV lanes and GP vehicles only use GP lanes on the freeway. The simulation on synthetic networks uses a set of calibrated Vissim behavior model parameters from an earlier study (TariVerdi and Miller-Hooks 2012). Table 15 lists the driver behavior parameters.

**Table 15. Driver behavior parameters.**

| Parameter | Definition | Default Value | Value for this Study |
|---|---|---|---|
| CC2 | Desired safety following distance | 13.12 ft | 39.37 ft |
| CC4 | Lower following threshold | 0.35 mi/h | 0.1 mi/h |
| CC5 | Upper following threshold | 0.35 mi/h | 0.1 mi/h |
| SDRF | Safety distance reduced factor: affects safety distance during lane changing | 0.6 | 0.1 |
| LBD | Look-back distance | 656 ft | 3,280 ft |

## Results and Analysis—Simulation Runs

Positioning HOV lanes on the right-hand side of the freeway may result in a deterioration in HOV lane performance, though the GP lanes and total system performance may improve. Therefore, the team first wanted to make sure the travel speed in the HOV lane is always faster than the GP lanes because the purpose the HOV lane is to provide better and more reliable services. Figure 50 shows that when the HOV percentage is 0.5, the HOV delay of the alternative design is higher than the GP delay in most cases. The plots show the differences between GP delay and HOV delay. The delay of HOV is smaller than the GP only in extremely congested conditions where the HOV percentage is 0.5. In reality, the HOV vehicles will not stay in the HOV lane if the HOV lane is slower than the GP lanes. Besides, the 50 percent HOV case is rare in the real world. Because of its rarity, the team did not present the results for the 50 percent HOV cases. When there is 25 percent HOV, there are a few cases where the delay of HOV is a little higher than GP for both traditional (i.e., HOV lane positioned on the left-hand side) and alternative (i.e., HOV lane positioned on the right-hand side) designs. These cases happen when the mainline traffic volume is relatively low for the four-lane alternative network in which the improvements to GP vehicles as a result of enhanced merging behavior is smaller compared to the adverse impacts on the HOV vehicles. In this study, the team was more interested in the performance under congested scenarios. Figure 50 indicates similar patterns of before and after delay differences between GP and HOV when there is 25 percent HOV.

Implementation of all levels of the six simulation parameters uses a factorial design of the simulation experiment. Plots of comparison between the two designs under different parameter combinations are presented. Next, the team conducted statistical analyses to investigate the significance of effectiveness for each parameter under a range of network scenarios. Considering that multiple scenarios provide similar insights, this report shows the following selected samples of plots and analysis: four-lane freeway, V/C = 0.8/1.1, HOV percentage = 0.25, on-ramp volume = 1,500. Note that the results presented in this example generally apply to all other scenarios unless the exceptions are specifically mentioned.

## Analysis of Merge Area

Results showed that when traffic density is low (e.g., when the input volume is 55 percent of capacity and on-ramp volume is 500 veh/h/l), both GP and HOV throughputs of the alternative design with the HOV lane on the right-hand side are the same as the normal design. The number of lanes show no significant impacts, thus only four lane cases are discussed here. When the

traffic density becomes higher, GP throughputs of the alternative design become higher than the normal design; however, HOV throughputs decline slightly in most of the scenarios. The team interpreted this to the fact that congestion caused by merging traffic blocks the HOV lane under the alternative design, while HOV vehicles in the normal design could travel with no disruption. In addition, the sensitivity analysis indicated that going from a certain degree of congestion (i.e., V/C ratio of 0.8) to severe congestion (i.e., V/C of 1.1) does not affect the HOV throughput performance, which can be observed by comparing the two plots in equation 6. In terms of total throughputs, the alternative design still performs significantly better than the normal design.

Next, the GP delay and total delay of the alternative design is remarkably lower than the delay of the normal design even though the HOV delay becomes higher. The GP vehicles have higher delays and the differences are between 0–700 s. To better understand how much improvement is gained by changing HOV lanes to the right-hand side, the percentage of change was calculated.

$$p = (MOE_{right} - MOE_{left})/MOE_{left}$$

(6)

Where:

$p$ = percentage of change.
$MOE_{right}$ = measure of effectiveness for HOV lanes on the right.
$MOE_{left}$ = measure of effectiveness for HOV lanes on the left.

Generally, the overall percent change in throughput is negligible. GP delay is lower, but mainline and HOV delay is much higher in the alternative design. However, since the number of GP vehicles greatly exceeds the number of HOV vehicles, the proposed right-side HOV design results in approximately a 20-percent delay reduction.

### ANOVA Tests

To further test and quantify the effects of each parameter on throughputs, ANOVA tests and paired T-tests were applied to GP throughputs and HOV throughputs separately. Then, a regression analysis was applied separately.

Table 16 shows the results of the ANOVA tests in throughputs and delays. Table 16 suggests that all factors significantly affect the throughput values, except for the number of GP lanes. Similar to the throughput findings, all factors significantly affect the delay, except that the number of lanes is insignificant to HOV delay.

**Table 16. Throughput and delay ANOVA table.**

| Measure | Response | GP p-Value | HOV p-Value | Total p-Value |
|---|---|---|---|---|
| Throughputs | HOV (right) | <2.2E−16 | 0.003615 | 1.434E−07 |
| Throughputs | Number of lanes | 0.1881 | 0.005253 | <2.2E−16 |
| Throughputs | V/C ratio | <2.2E−16 | <2.2E−16 | <2.2E−16 |
| Throughputs | On-ramp volume | 1.789E−09 | 1.092E−07 | 2.820E−10 |
| Throughputs | HOV percentage | 3.578E−05 | <2.2E−16 | <2.2E−16 |
| Average delay | HOV (right) | <2.2E−16 | <2.2E−16 | <2.2E−16 |
| Average delay | Number of lanes | <2.2E−16 | 0.1932 | <2.2E−16 |
| Average delay | V/C ratio | <2.2E−16 | <2.2E−16 | <2.2E−16 |
| Average delay | On-ramp volume | <2.2E−16 | <2.2E−16 | <2.2E−16 |
| Average delay | HOV percentage | 0.00837 | <2.2E−16 | 9.211E−07 |

$p$ = probability indicating the extent to which a factor is insignificant.

### *Paired T-tests*

Paired T-tests evaluate whether the two designs are different in each scenario. The null hypothesis is that the mean difference of the two designs is 0, while the alternative hypothesis is that the mean difference of the two designs is not 0. Estimations of mean difference and the probability indicating the extent to which a factor is insignificant ($p$) values are provided. Results of representative scenarios are listed. There is a significant difference between the throughputs of GP vehicles as shown in table 17 and table 19.

Contrarily, there is no significant difference between the HOV throughputs. The estimations of GP throughput differences between the design of the HOV lane on the right-hand side and the normal design HOV lane. Table 17 also indicates that in terms of GP delay, the two designs are different. For the GP delays, the column "estimated mean of right—left" are all negative, indicating the GP delay is lower in the alternative design compared to the normal design. In terms of HOV delays in table 18, the two designs are also significantly different. The column "estimated mean of right—left" are all positive, indicating the HOV delays are larger in the alternative design than the normal design. Table 19 shows the difference between the weighted total throughputs of the two designs for selected scenarios. Generally, when the V/C ratio is 0.55, the tests show there are no significant differences between the two. When the V/C ratio is higher, the test results are significantly different. The total throughputs of the alternative design are higher than the normal design where the improvements range from 140–170 veh/h/l. The total average vehicle delay shown in table 20 decreases in the alternative design, ranging from 70–150 s per vehicle. In total, the alternative design outperforms the normal design for the merge area for the synthetic simulation network and under the given system parameters.

**Table 17. T-test results—average delay and throughputs on the GP lanes.**

| Measure | Number of Lanes | HOV (Percent) | V/C Ratio | On-Ramp Volume (veh/h) | Estimated Mean of Right—Left | *p*-Value |
|---|---|---|---|---|---|---|
| Throughputs | Four | 0.25 | 0.8 | 1,000 | 152 | 4.02E−13 |
| Throughputs | Four | 0.25 | 0.8 | 1,500 | 130 | 2.56E−06 |
| Throughputs | Four | 0.25 | 1.1 | 1,000 | 147 | 2.18E−13 |
| Throughputs | Four | 0.25 | 1.1 | 1,500 | 124 | 7.73E−07 |
| Average delay | Four | 0.25 | 0.8 | 1,000 | −161 | 1.34E−14 |
| Average delay | Four | 0.25 | 0.8 | 1,500 | −131 | 7.93E−09 |
| Average delay | Four | 0.25 | 1.1 | 1,000 | −306 | 5.90E−14 |
| Average delay | Four | 0.25 | 1.1 | 1,500 | −223 | 6.21E−06 |

**Table 18. T-test results—average delay and throughputs on the HOV lanes.**

| Measure | Number of Lanes | HOV (Percent) | V/C Ratio | On-Ramp Volume (veh/h) | Estimated Mean of Right—Left | *p*-Value |
|---|---|---|---|---|---|---|
| Throughputs | Four | 0.25 | 0.8 | 1,000 | 0.1 | 0.88 |
| Throughputs | Four | 0.25 | 0.8 | 1,500 | 10.6 | 0.11 |
| Throughputs | Four | 0.25 | 1.1 | 1,000 | −0.9 | 0.49 |
| Throughputs | Four | 0.25 | 1.1 | 1,500 | 19.1 | 0.29 |
| Average delay | Four | 0.25 | 0.8 | 1,000 | 19 | 2.75E−07 |
| Average delay | Four | 0.25 | 0.8 | 1,500 | 41 | 2.41E−15 |
| Average delay | Four | 0.25 | 1.1 | 1,000 | 25 | 3.89E−10 |
| Average delay | Four | 0.25 | 1.1 | 1,500 | 50 | 5.20E−10 |

**Table 19. T-test results—total throughputs on the GP and HOV lanes.**

| HOV (Percent) | V/C Ratio | On-Ramp Volume (veh/h) | Estimated Mean of Right—Left | *p*-Value |
|---|---|---|---|---|
| 0.25 | 0.8 | 1,000 | 171 | 4.59E−11 |
| 0.25 | 0.8 | 1,500 | 149 | 7.29E−10 |
| 0.25 | 1.1 | 1,000 | 165 | 2.05E−11 |
| 0.25 | 1.1 | 1,500 | 144 | 5.60E−14 |

**Table 20. T-test results—total delay on the GP and HOV lanes.**

| HOV (Percent) | V/C Ratio | On-Ramp Volume (veh/h) | Estimated Mean of Right—Left | *p*-Value |
|---|---|---|---|---|
| 0.25 | 0.8 | 1,000 | −151 | 7.49E−11 |
| 0.25 | 0.8 | 1,500 | −101 | 3.67E−09 |
| 0.25 | 1.1 | 1,000 | −77 | 7.67E−13 |
| 0.25 | 1.1 | 1,500 | −102 | 1.19E−13 |

### Prediction Models

The team performed multivariate linear regression analyses to predict the total throughputs and total delays. The purpose of the model was to provide an analytical tool to estimate the potential benefits of positioning HOV lanes on the right-hand side. All statistical analyses were performed using the statistical software R (The R Foundation 2019). The level of significance is set at $p < 0.05$, and the confidence level is set at 95 percent. The following influencing factors are analyzed as numerical values: V/C ratio and on/off-ramp volume. Categorical variables are used for number of lanes, HOV location, and weaving length. The percent of HOV is not included since high-HOV-percent simulations are not realistic in real-world practices. Regression prediction models are generated based on simulation data. The $R$-squared value of the throughput model is 0.82. This value indicates that the model can explain and approximate about 82 percent of the throughput data. Similarly, the delay model with an $R$-squared value of 0.81 indicates that the model can explain and approximate about 81 percent of the delay data.

$$TotalTP = 1051.8 + 66.5 * I_{right} - 226.9 * Lanes + 361.2 * VCRatio + 0.67 * OnV$$
$$+ 267.8 * Lanes * VCRatio - 0.69 * VCRatio + OnV$$
$$R^2 = 0.82$$

(7)

$$AverageDelay = -218.79 - 57.52 * I_{right} * Lanes + 638.12 * VCRatio - 0.16 * OnV - 203.27$$
$$* Lanes * VCRatio + 0.42 * VCRatio * OnV$$
$$R^2 = 0.81$$

(8)

Where:

| | |
|---|---|
| *TotalTP* | = total throughput. |
| $I_{right}$ | = equal to 1 for right-side HOV lanes. |
| *Lanes* | = number of lanes. |
| *VCRatio* | = volume-to-capacity ratio. |
| *OnV* | = on-ramp volume. |
| $R^2$ | = coefficient of determination. |

### Analysis of Diverge Area

By checking the results of the GP and HOV throughputs on the mainline and off-ramp separately, the team found there is no difference between the two designs in terms of throughputs. When the off-ramp traffic volume is 1,500 veh/h/l and number of lanes is four, generally the alternative design performs better than the normal design in terms of delay. The GP delay is lower for both the mainline and off-ramp in the alternative design. The HOV delay is also lower in the alternative design for the off-ramp because the HOV lane is on the right-hand side and HOV vehicles do not need to wait for the GP vehicles to exit the freeway. The mainline delay of the alternative design is higher because the congestion at the diverge area blocks the HOV lane located on the right-hand side. In terms of total delay, the difference is small between the two, and the total delay is slightly lower in the alternative design than in the normal design. Generally, the GP vehicles have higher delays, but the differences are minor (less than 15 s).

Thus, the team concluded that the performance between the two designs in the diverge area is not significant as compared to the performance in the merge area. The differences in GP delay are less than 10 percent. The mainline HOV delay increases from 20 to 40 percent, and off-ramp HOV delay decreases from 30 to 40 percent. The total delay decreases about 10 percent.

To test and quantify the effects of parameters on throughputs and delays, ANOVA tests were applied to GP and HOV lanes separately. Table 21 through table 23 suggest that the two designs have no significant difference in throughputs since the *p*-values for HOV positions are larger than 0.05. They also suggest that the two designs are significantly different in terms of delay since the *p*-values are all smaller than 0.05. ANOVA tests of total measurements show that the two designs have no difference in total throughputs, while the differences in total delays are relatively significant.

**Table 21. ANOVA throughputs.**

| Response | Mainline GP *p*-Value | Mainline HOV *p*-Value | Off-Ramp GP *p*-Value | Off-Ramp HOV *p*-Value |
|---|---|---|---|---|
| HOV (right) | 0.7054 | 0.9783 | 0.78758 | 0.9888 |
| Number of lanes | <2.2E−16 | <2.2E−16 | 0.01002 | <2.2E−16 |
| V/C ratio | <2.2E−16 | <2.2E−16 | <2.2E−16 | 0.4532 |
| Off-ramp volume | <2.2E−16 | <2.2E−16 | <2.2E−16 | <2.2E−16 |
| HOV percentage | 0.9942 | <2.2E−16 | 0.82848 | <2.2E−16 |

**Table 22. ANOVA average delay.**

| Response | Mainline GP *p*-Value | Mainline HOV *p*-Value | Off-Ramp GP *p*-Value | Off-Ramp HOV *p*-Value |
|---|---|---|---|---|
| HOV (right) | 0.0146 | <2.2E−16 | 0.02479 | <2.2E−16 |
| Number of lanes | 0.45810 | <2.2E−16 | 0.01002 | 0.234211 |
| V/C ratio | <2.2E−16 | <2.2E−16 | <2.2E−16 | 0.003537 |
| Off-ramp volume | <2.2E−16 | 0.434557 | <2.2E−16 | <2.2E−16 |
| HOV percentage | 0.06190 | <2.2E−16 | 0.82848 | <2.2E−16 |

**Table 23. ANOVA total throughputs and delay.**

| Response | Throughputs | Delays |
|---|---|---|
| HOV (right) | 0.71170 | 0.05985 |
| Number of lanes | 0.01625 | 0.02167 |
| V/C ratio | <2.2E−16 | <2.2E−16 |
| Off-ramp volume | 0.92918 | <2.2E−16 |
| HOV percentage | <2.2E−16 | <2.2E−16 |

***Paired T-tests***

Paired T-tests were conducted for all scenarios. Table 24 and table 25 list the results of total throughputs and total delays, respectively. The throughputs show no differences, while the differences in delays are significant. The estimate means the difference between the designs where the HOV lane is on the left-hand side and where the HOV lane is on the right-hand side

are negative, but the values are small (nearly 0), indicating that the improvement in total delays is small.

**Table 24. Total throughput T-tests.**

| Number of Lanes | HOV (Percent) | V/C Ratio | On-ramp Volume (veh/h) | Estimated Mean of Right—Left | *p*-Value |
|---|---|---|---|---|---|
| Four | 0.25 | 0.9 | 1,000 | 0.1 | 0.56 |
| Four | 0.25 | 0.9 | 1,500 | −0.42 | 0.07 |
| Four | 0.25 | 1.2 | 1,000 | 22.72 | 0.1 |
| Four | 0.25 | 1.2 | 1,500 | 16.15 | 0.12 |

**Table 25. Total delay T-tests.**

| Number of Lanes | HOV (Percent) | V/C Ratio | On-ramp Volume (veh/h) | Estimated Mean of Right—Left | *p*-Value |
|---|---|---|---|---|---|
| Four | 0.25 | 0.9 | 1,000 | −0.48 | 5.34E−08 |
| Four | 0.25 | 0.9 | 1,500 | −0.38 | 0.005 |
| Four | 0.25 | 1.2 | 1,000 | −0.36 | 0.54 |
| Four | 0.25 | 1.2 | 1,500 | −1.74 | 0.018 |

*Prediction Model*

Since there is no substantial difference between the total throughputs of the two designs, and only the V/C ratio is significant in the test, the team only predicted total delays in this case. Regression prediction models were generated based on simulation data. The *R*-squared value of the model is 0.86. It indicates that the model can explain and approximate about 86 percent of the delay data.

$$AverageDelay = -7.16 - 0.4 * I_{right} - 1.51 * Lanes + 17.29 * VCRatio + 0.004 * OnV + 2.04 * Lanes * VCRatio - 0.003 * VCRatio * OnV$$
$$R^2 = 0.86$$

$$(9)$$

Where:

$I_{right}$ = equal to 1 for right-side HOV lanes.
$Lanes$ = number of lanes.
$VCRatio$ = volume-to-capacity ratio.
$OnV$ = on-ramp volume.
$R^2$ = coefficient of determination.

**Analysis of Weaving Area**

The results of the 0.5-mi and 1.0-mi weaving length area are presented separately. In this design, the team allowed 0.25 mi before or after the merge/diverge area for vehicles to make lane changes and enter the target lanes. When the diverge length is 0.5 mi, the acceleration lanes are connected as an additional lane. In this case, the on/off-ramp vehicles actually have a longer distance to change to their target lanes and potentially improve the system.

*Case 1: Weaving Length = 0.5 mi*

Generally, the GP throughputs are higher in the alternative design. The mainline HOV throughput is also higher in the alternative design, while the off-ramp HOV throughput shows no significant difference. The alternative design performs much better than the normal design in total throughputs. When the V/C ratio is 0.8, the alternative design provides higher HOV throughputs than GP. By checking the simulation, the team found that in this case, the on-ramp is congested in the normal design while there is no congestion in the alternative design. Thus, in the normal design case, a substantial number of vehicles were not able to enter the network, which causes lower HOV throughputs. When the V/C ratio is 1.1, congestion happens in both designs. There is no significant difference between the throughputs.

The GP delay was lower and the HOV delay was higher in the alternative design for both the mainline and off-ramp. However, the differences in HOV delays between the two were smaller (less than 50 s) than those of GP. In terms of total delays, the alternative designs were about 60 s lower than the normal delay. The delay of off-ramp HOV drops in the normal design as the V/C ratio increases. This was due to blocking of GP vehicles at the merge area, which leads to a decrease in the traffic volume at the weaving area. Thus, the HOV vehicles could exit the freeway more smoothly.

The total throughputs increased about 8 percent. The GP delays and total delays decreased about 60 percent when the V/C ratio is 0.8, and by 20 percent when the V/C ratio is 1.1. HOV delay increases about 100 percent when the V/C ratio is 0.8, and by 500 percent when the V/C ratio is 1.1. Thus, the team concluded that the alternative design performs better for the weaving area with 0.5-mi weaving length, and when the V/C ratio is 0.8, the improvement is most significant.

*Case 2: Weaving Length = 1 mi*

There is higher GP throughput in the alternative design, and the off-ramp shows no significant difference between the two designs. Total throughputs are higher in the alternative design. When the V/C ratio is 0.8, the alternative design also provides higher HOV throughputs than GP as the team mentioned in case 1. The reason is the same: congestion happens only in the design with the HOV lane on the left-hand side when V/C ratio is 0.8.

The GP delay is lower and HOV delay is higher for both the mainline and off-ramp in the alternative design. In terms of total delays, the alternative design with the HOV lane on the right-hand side performs better in general with lower total delays and higher total throughputs. Generally, the change in throughputs are insignificant. The amount of total GP delays decreases between 20–30 percent, while total HOV delays increase by 600 percent. Since the quantity of HOV delays is small, the total delays still decrease by about 20 percent.

*ANOVA Tests*

Table 26 and table 27 show the results of ANOVA tests in throughputs and delays, respectively. The results suggest that all of the parameters significantly affect throughputs and delays, except that the off-ramp volume does not affect the mainline GP delay. Table 28 provides the ANOVA tests of total measurements. The two designs show no difference in total throughputs, while there are significant differences in total delays.

**Table 26. ANOVA tests of total measurements—throughputs.**

| Response | Mainline GP *p*-Value | Mainline HOV *p*-Value | Off-Ramp GP *p*-Value | Off-Ramp HOV *p*-Value |
|---|---|---|---|---|
| HOV (right) | 8.049E−11 | <2.2E−16 | <2.2E−16 | <2.2E−16 |
| Number of lanes | <2.2E−16 | <2.2E−16 | <2.2E−16 | <2.2E−16 |
| V/C ratio | <2.2E−16 | <2.2E−16 | <2.2E−16 | 3.368E−06 |
| Off-ramp volume | <2.2E−16 | <2.2E−16 | <2.2E−16 | <2.2E−16 |
| HOV percentage | <2.2E−16 | <2.2E−16 | <2.2E−16 | <2.2E−16 |
| Weaving length | <2.2E−16 | <2.2E−16 | <2.2E−16 | <2.2E−16 |

**Table 27. ANOVA tests of total measurements—average delay.**

| Response | Mainline GP *p*-Value | Mainline HOV *p*-Value | Off-Ramp GP *p*-Value | Off-Ramp HOV *p*-Value |
|---|---|---|---|---|
| HOV (right) | <2.2E−16 | <2.2E−16 | <2.2E−16 | <2.2E−16 |
| Number of lanes | <2.2E−16 | 0.01179 | <2.2E−16 | 0.024792 |
| V/C ratio | <2.2E−16 | <2.2E−16 | <2.2E−16 | <2.2E−16 |
| Off-ramp volume | 0.2373 | <2.2E−16 | 0.00047 | 0.00208 |
| HOV percentage | <2.2E−16 | <2.2E−16 | <2.2E−16 | <2.2E−16 |
| Weaving length | <2.2E−16 | <2.2E−16 | <2.2E−16 | <2.2E−16 |

**Table 28. ANOVA total throughputs and delays.**

| Response: Total | Throughputs | Delays |
|---|---|---|
| HOV (right) | 0.3719 | <2.2E−16 |
| Number of lanes | <2.2E−16 | <2.2E−16 |
| V/C ratio | <2.2E−16 | <2.2E−16 |
| Off-ramp volume | 0.7192 | <2.2E−16 |
| HOV percentage | <2.2E−16 | <2.2E−16 |
| Weaving length | <2.2E−16 | <2.2E−16 |

*Paired T-tests*

Further paired T-tests quantify differences between the two designs. Table 29 shows that for both 0.5-mi and 1.0-mi cases, the alternative design performs better with higher throughputs and lower delays. When the weaving length is 1.0 mi, improvements in throughput are between 30–80 veh/h/l. This is more stable and greater on average compared with the 0.5-mi case. The delay decrease in the 1.0-mi case is between 40–90 s, which is better on average compared to the 0.5-mi case. Overall, the alternative design performs better at the weaving segments.

### Prediction Model

The team also performed multivariate linear regression analyses to predict the total throughputs and delays. The length of the weaving segment is a categorical variable since only two lengths were tested, and the network designs vary in separate ways based on real-world cases. The *R*-squared values of the two models are 0.85 and 0.75, respectively. It indicates that the throughput model can approximate about 85 percent of the throughput data, while the delay model can approximate about 75 percent of the delay data.

$$TotalTP = 1321.93 + 198.07 * I_{right} - 101.83 * Lanes + 497.83 * VCRatio + 0.13 * OnV \\ + 0.043 * OffV + 517 * I_{1-mile} - 41.7 * Lanes * I_{right} - 207 * Lanes \\ * I_{1-mile} - 0.13 * OnV * I_{1-mile}$$
$$R^2 = 0.85$$

$$(10)$$

$$TotalAverageDelay \\ = -52.7 - 56.16 * I_{right} - 98.1 * Lanes + 365.7 * VCRatio + 0.17 * OnV + 214 \\ * I_{1-mile}$$
$$R^2 = 0.75$$

$$(11)$$

Where:

| | |
|---|---|
| $TotalTP$ | = total throughput. |
| $I_{right}$ | = equal to 1 for right-side HOV lanes. |
| $Lanes$ | = number of lanes. |
| $VCRatio$ | = volume-to-capacity ratio. |
| $OnV$ | = on-ramp volume. |
| $OffV$ | = off-ramp volume. |
| $I_{1-mile}$ | = equal to 1 for 1-mile weaving lengths. |
| $R^2$ | = coefficient of determination. |

**Table 29. Total throughput and delay T-tests.**

| Number of Lanes | HOV Percent | Weaving Length (ft) | V/C Ratio | On-ramp Volume (veh/h) | Off-ramp Volume (veh/h) | Estimated Mean of Throughput (Right)—Throughput (Left) | Throughputs *p*-Value | Estimated Mean of Delay (Right)—Delay (Left) | Delay *p*-Value |
|---|---|---|---|---|---|---|---|---|---|
| Four | 0.25 | 2,625 | 0.8 | 1,000 | 1,000 | 8.3 | 0.01 | −20.51 | 0.007 |
| Four | 0.25 | 2,625 | 0.8 | 1,000 | 1,500 | 2.45 | 0.17 | −7.29 | 2.0E−06 |
| Four | 0.25 | 2,625 | 0.8 | 1,500 | 1,000 | 83.95 | 2.4E−07 | −72.59 | 7.3E−06 |
| Four | 0.25 | 2,625 | 0.8 | 1,500 | 1,500 | 106.72 | 3.8E−09 | −70.06 | 0.0002 |
| Four | 0.25 | 2,625 | 1.1 | 1,000 | 1,000 | 45.1 | 7.1E−08 | −9.80 | 0.002 |
| Four | 0.25 | 2,625 | 1.1 | 1,000 | 1,500 | 50 | 1.4E−05 | −34.33 | 7.47E−07 |
| Four | 0.25 | 2,625 | 1.1 | 1,500 | 1,000 | 41.37 | 0.001 | −1.78 | 0.061 |
| Four | 0.25 | 2,625 | 1.1 | 1,500 | 1,500 | 97.4 | 5.06E−09 | −38.48 | 6.16E−10 |
| Four | 0.25 | 5,250 | 0.8 | 1,000 | 1,000 | 65.6 | 4.1E−11 | −80.04 | 2.47E−06 |
| Four | 0.25 | 5,250 | 0.8 | 1,000 | 1,500 | 76.82 | 1.5E−10 | −91.59 | 6.98E−10 |
| Four | 0.25 | 5,250 | 0.8 | 1,500 | 1,000 | 53.35 | 1.9E−09 | −73.73 | 1.66E−07 |
| Four | 0.25 | 5,250 | 0.8 | 1,500 | 1,500 | 39.75 | 2.4E−06 | −42.88 | 5.92E−05 |
| Four | 0.25 | 5,250 | 1.1 | 1,000 | 1,000 | 59.85 | 4.1E−11 | −38.65 | 4.23E−10 |
| Four | 0.25 | 5,250 | 1.1 | 1,000 | 1,500 | 66.175 | 1.6E−13 | −42.04 | 9.56E−07 |
| Four | 0.25 | 5,250 | 1.1 | 1,500 | 1,000 | 61.87 | 9.4E−07 | −69.70 | 3.37E−10 |
| Four | 0.25 | 5,250 | 1.1 | 1,500 | 1,500 | 49.97 | 1.0E−08 | −57.70 | 3.51E−06 |

**I–66 Calibrated Network**

To test whether the alternative design would improve the performance on a real network since the previously presented results were from synthetic networks, a calibrated network of I–66's freeway segment in Vissim tested the design for real-world applications. The normal design and the alternative design were simulated in this network, and the total throughputs and delays were compared. The same calibrated network as shown in figure 28 was used. The section of split merging, diverging, and weaving design shows details of the model calibration. There is an HOV lane on the left-hand side of the base case calibrated network. For the HOV lane on the right-hand side, the team modified the network and specified the rightmost lane as the HOV lane, with the same HOV demand assigned to the HOV lane on the right-hand side. The team performed simulations 10 times to account for stochasticity.

Overall performance of the alternative design is consistent with the previous findings from simple networks. With the proposed HOV lane on the right-hand side, GP lane performance improves significantly, with a 4-percent throughput increase and a 19-percent delay reduction. Also, HOV lane performance degrades as expected. In terms of total performance, the alternative design has slightly higher throughput overall, but the difference is not significant. The average delay of the alternative design is much lower than the original case. The decrease in average delay is about 9 percent. Based on the I–66 calibrated network simulation, changing the HOV lane to the right-hand side would improve overall network performance in terms of vehicle delay, and total vehicle throughput would remain the same. In addition, GP lane delay was higher than HOV lane delay, as was assumed. This means the new design still ensures a higher level of service for HOV vehicles than GP vehicles, though the relative difference in performance is smaller. This verifies the feasibility of implementing HOV lanes on the right-hand side for this real-world freeway segment.

**Conclusions**

HOV lanes are in use worldwide. This study investigated an alternative design of freeways with the HOV lane on the right-hand side and how it can solve the congestion problem at merge/diverge and weaving areas. The objective was to find whether the alternative design would be helpful in reducing congestion, and to develop recommendations for the DOT and local agencies to manage HOV lanes and estimate traffic performance. Based on the simulations, several conclusions derived from the simulation tests and statistical analyses, including:

- Generally, the alternative design with the HOV lane on the right-hand side will help improve the performance of GP lane vehicles in most cases. However, the alternative design will degrade HOV lane performance, especially for HOV vehicles that do not exit at ramps. The system throughout improvements are significant for merge and weaving areas, ranging from 5–10 percent on average. The system delay enhancements are significant under all scenarios, ranging from 10–30 percent on average.

- The alternative design will reduce delay and increase throughput, though the improvements in throughput are sometimes not significant.

- Even though the HOV performance may be disturbed more in the case of HOV lanes on the right-hand side, HOV lane vehicles still experience a higher level of service than GP lane vehicles under the same background settings, though the difference in the level of service is smaller compared to HOV lanes on the left-hand side. This is dependent on the HOV traffic percentage. Lower HOV percentages lead to higher differences and better levels of service.

- The study also suggests that it is practical to implement the alternative design on freeway segments, especially for areas with low HOV traffic volume.

  - A case study on the calibrated I–66 network shows the alternative design contributes to a 10-percent decrease in total delays and a 20-percent decrease in GP vehicle delays, which indicates a significant improvement in the network performance.

For future research, more levels of HOV percentages and V/C ratios could be tried to provide more accurate results. Especially for the purpose of traffic performance estimation, more tests and simulations would be helpful to improve the accuracy of the analysis, particularly the regression models. Next, it might be valuable to add more system parameters, such as vehicle composition and more complex geometric designs. Furthermore, in terms of its influence on HOV vehicles, it is necessary to investigate the effects on people's willingness to drive in HOV lanes. People's willingness to drive in HOV lanes also concerns policy questions of implementing the new design.

# CHAPTER 5. CONCLUSIONS

Given the prevalence of the heavy friction problem that exists at freeway merge and diverge areas, any low-cost solution to reduce the friction associated with vehicle maneuvers, or facilitate smoother merging/diverging operations, could produce great savings. This project identified five candidate strategies to assess within microsimulation environments.

## ACCELERATION AND DECELERATION LANE DESIGNS

Restricting merging drivers to a specific new set of acceleration and deceleration lane locations may help to smooth traffic flow. Regarding acceleration lanes, figure 3 shows how drivers are prohibited from merging at the mid-section of acceleration lanes. By eliminating the uncertainty of merge maneuvers for both mainline and on-ramp drivers, both sets of drivers can prepare for and execute the merging maneuver efficiently. Regarding deceleration lanes, figure 4 shows how drivers merge at a mid-section of the off-ramp. Separating the turbulence associated with diverge maneuvers potentially mitigates mainline congestion.

The team conducted microscopic simulations to evaluate the effectiveness of the alternative geometric design of split merging, diverging, and weaving for reducing bottleneck congestion, and developed managerial insights for State DOTs to better design, enhance, and manage their freeway systems in the future. A partial split weaving design (with the merge portion converted to the split merge design) seems to work best at congested weaving areas and is the recommended method. These simulations only evaluated one-lane ramps, but the researchers believe two-lane ramps would exhibit similar impacts. Although the split merge design effectively reduced average delays (by up to 80 percent) and increased traffic throughputs, particularly under medium-to-high levels of traffic congestion, the results of this study show that the split diverge is not effective under many traffic conditions and therefore is not recommended. The team tested medium and high levels of traffic demand with the 0.25-mi connection spacing. Results from figure 36 clearly demonstrate that the 50–50 split results in the best performance under most scenarios, and performs almost as well for other scenarios. Statistical tests show that these minor differences are not statistically significant, indicating that the team did not find that the split diverge design enhances diverge area performance compared to the regular diverge. Therefore, the team recommend the use of the split merge design at congested merge or weaving areas.

## SPEED OPTIMIZATION (E.G., VIA DYNAMIC TRAFFIC CALMING DEVICES)

Speed harmonization and VSL studies for optimizing freeway traffic flow imply that medium free-flow speeds (e.g., 30 mi/h) would be more effective than low speeds (e.g., 5 mi/h) or high speeds (e.g., 65 mi/h). Although this project endeavors to focus on strategies not requiring CAV technologies, the team believes that dynamic traffic calming devices (e.g., retractable rumble strips) may someday be capable of coercing drivers to obey medium speeds at higher rates of compliance. Figure 8 illustrates this concept.

Many of the successful speed optimization experiments produced a "zipper" pattern as shown in table 5. The implication is that significant speed optimization benefits only occurred under a narrow range of demands (i.e., near capacity) and speed limit changes. The downside of this

finding is that this narrow range of conditions producing maximum benefits, in terms of demand ranges and free-flow speed ranges, is often difficult to predict without first running simulations.

*HCM* procedures are often used to prescreen alternatives without running simulations. However, a series of test runs conducted in the HCS (merge module and weaving module) using similar input data did not predict any benefits of free-flow speed and/or speed limit optimization. The resulting hypothesis is that the *HCM* methods are perhaps not capable of recognizing or analyzing the same speed harmonization-type effects and benefits that are commonly observed in microsimulation (and in the field). As such, an offline or real-time microsimulation model may be needed to detect when the zipper conditions from table 5 are in effect for any local site or local conditions.

In one merge area experiment, average vehicle speeds increased from 9 to 52 mi/h simply by reducing the posted speed limit from 65 to 55 mi/h. Although the significant speed optimization benefits were observed for some weaving and merge conditions as described in chapter 4, the benefits were weaker (e.g., on the order of 2 to 6 percent) for diverge conditions. As such, the researchers' recommendation is that agencies willing to detect zipper conditions in real time can consider implementing countermeasures to reduce free-flow speeds (or speed limits) when such conditions are present. Such countermeasures could include dynamic traffic calming devices (e.g., retractable rumble strips), dynamic VSL signs, or CAV speed controls. This approach also assumes that the offline or real-time microsimulation model is consistently and periodically recalibrated to reflect local field conditions accurately.

## MAINLINE METERING (I.E., DYNAMIC SIGNAL CONTROL)

A form of mainline metering to reduce demand and improve flow uses traffic metering upstream from a bottleneck, thereby regulating the number of vehicles moving through the bottleneck. At locations where capacity expansion is not feasible (i.e., at tunnels and bridges), implementation of this form of mainline metering can help. For example, metering for traffic arriving at the bridge or tunnel is used at the Bay Bridge in Oakland, CA; the Hampton Roads Bridge-Tunnel connecting Hampton, VA, and Norfolk, VA; and the Baltimore Harbor Tunnel in Baltimore, MD.

In situations where mainline and ramp vehicle speeds are both very low, and fall below a defined threshold, such as 5 or 10 mi/h, traffic signal control applied to both upstream approaches could optimize the operation by eliminating merge friction. Figure 9 illustrates this concept. However, there is no known application of the treatment.

Some mainline metering experiments produced approximately 20-percent delay reductions. Future research could investigate enhancing the benefits by deploying the strategy at several locations along a congested corridor. However, the improvements seen here used a refined algorithm. In addition, it is unclear whether drivers will comply with some sort of red signal on the mainline, even at low speeds. Finally, researchers noted that the left-most freeway lanes often did not show speeds below 10 mi/h, so it was often necessary to stop mainline vehicles traveling between 10 and 20 mi/h.

**COORDINATED ADAPTIVE RAMP METERING SYSTEM (E.G., HERO)**

Traditional ramp metering measures upstream freeway mainline volume to determine ramp flow, but rarely monitors downstream conditions. Downstream problems only show when congestion reaches the upstream ramp detector. Coordinated adaptive ramp metering uses feedback logic in a closed loop control system. Traffic conditions measured at downstream bottlenecks determine critical occupancy and appropriate levels of traffic entering from upstream. The process assumes an historic or theoretical value of freeway capacity. Downstream flow conditions provide feedback to determine real time ramp flow and optimal occupancy.

When applied on a holistic, coordinated, system-wide basis, all ramps continuously communicate with each other to resolve complex traffic-flow situations. One example of such a system is called HERO, but the team identified several similar algorithms and systems during the literature review effort. Simulation experiments conducted during this project found that HERO produced better traffic flow than ALINEA, and ALINEA outperformed SDRMS. Although the HERO method produced better traffic flow than using ALINEA or doing nothing, the improvements were minimal. However, it can be seen in test six that, with the right set of parameters, a "non-zero sum" game can be created; by reducing the mainline friction and regulating flow, on-ramp merges were made easier and travel times were shorter overall for the mainline, ramps and arterials. In addition, this study did not investigate city-wide CRM, which VicRoads has reported to be successful in Melbourne, Australia.

**OPEN-ACCESS MLs ON THE RIGHT-HAND SIDE**

Typically in the United States, managed HOV/HOT lanes provide an improved level of service to drivers and are at the far left, next to the median. Although locating the ML on the right side would reduce its capacity, the overall impact on all lanes could be beneficial. The Alternative Freeway Designs at Merge and Diverge Segments project compared right-side ML design to left-side designs (i.e., with continuous access or partial access). Reduction by 300 veh/h in the overall capacity of a four-lane freeway occurs if the right-side ML capacity is reduced from 2,000 to 1,700 veh/h and the other three lanes remain at 2,000 veh/h. However, MLs on the left-hand side can result in a much larger capacity loss since all lanes can experience the 300 veh/h capacity loss due to vehicles weaving from the right to the left. Even if only the middle two lanes were impacted by this weave friction and turbulence, there may be a capacity loss of 300 x 2 = 600 veh/h, or twice that of a right-side ML.

Simulation experiments conducted during this project found that the performance of GP lane vehicles improves in most cases when placing HOV lanes on the right-hand side. However, the alternative design degrades HOV lane performance, especially for HOV vehicles that do not exit at ramps. The system throughput improvement is significant for merge and weaving areas, ranging from 5 to 10 percent on average. The system delay enhancement is significant under all scenarios, ranging from 10 to 30 percent on average.

The alternative design will reduce delay and increase throughput, although the improvements are sometimes not significant. Even if HOV performance degrades more with HOV lanes on the right-hand side, HOV lane vehicles still experience a higher level of service than GP lane vehicles under the same background settings. However, the difference in the level of service is

smaller than with HOV lanes on the left. This is dependent on the HOV traffic percentage. Lower HOV percentages lead to higher differences and better levels of service. The simulation results also suggest that it is practical to implement the alternative design on freeway segments, especially for areas with low HOV traffic volume. Generally, the alternative design with the HOV lane on the right-hand side will help improve the performance of GP lane vehicles in most cases. However, the alternative design will degrade HOV lane performance, especially for HOV vehicles that do not exit at ramps.

# APPENDIX. DATA COLLECTION AND CALIBRATION

Following the down-selection of six candidate strategies and identification of nine candidate sites, the team then matched sites with strategies to begin the simulation experiments. For various reasons outlined in the next paragraph, some candidate sites were ultimately not used in the simulation experiments. This appendix describes a 3-mo data collection and simulation model calibration process, which took place prior to the main 6-mo period of simulation sensitivity analysis experiments.

To assess the readiness of the available datasets for project experiments, the team considered several factors. The first set of information pertains to throughput calibration. If throughput was already calibrated, when was this done (e.g., 2012), what was the methodology, and where is the documentation on this process or results? If throughput was not calibrated, what is the tentative plan for doing so? The second set of information pertains to the calibration of other performance measures (e.g., speed, travel time, density). Were any other performance measures calibrated? If tested, what was the methodology, and where is the documentation on this process or results? If other performance measures were not calibrated, what is the tentative plan for doing so? For each dataset, the team should try to calibrate at least one performance measure beyond throughput. Third, was there a "reasonableness" check on the animation? Did the team attempt to provide a few sentences to describe how the animation demonstrates how the simulation reasonably replicates real-world operations. If not, the team would develop a simple plan for how to use animation to verify the simulation. Last, is there sufficient documentation of the site for the project report(s) and journal publication(s)? At a minimum, this should include a Google® Maps™ screenshot or image. Preferably, it should further include a description of local bottlenecks, speed limits, number of mainline lanes, percent heavy vehicles, and average number of ramps per mile. During the 3-mo task 3 effort for data collection and model calibration (i.e., October 12, 2017–January 12, 2018), the team worked on assembling the data and information categories described above:

- Throughput calibration.
  - Date.
  - Methodology.
  - Documentation of results.
- Calibration of other performance measures (e.g., speed, travel time, density).
  - Selected measure(s).
  - Date.
  - Methodology.
  - Documentation of results.
- Reasonableness check on the animation.
  - Date.
  - Methodology.
  - Documentation of results.

- Documentation of site conditions.
  - Mandatory info.
    - Google® Maps™.
  - Optional info.
    - Number of mainline lanes.
    - Description of local bottlenecks.
    - Speed limits.
    - Percent heavy vehicles.
    - Average number of ramps per mile.

The subsequent sections give this site-specific information.

## I–66 VA VISSIM

### Background Information

This simulation network was obtained from a previous FHWA research project in which the network was used to evaluate the effectiveness of cooperative adaptive cruise control. It is worth mentioning that among the many scenarios analyzed in the study, one scenario converted the leftmost lane of I–66 to an ML and evaluated the effectiveness of the cooperative adaptive cruise control ML concept. This was helpful for analyzing HOV lanes on the left-hand side, and the scenario was then edited to test the impacts of HOV lanes on the right-hand side.

### Overview

Below is an overview of the network calibration:

- I–66 westbound between interchange I–495 (MM 64) and US 29 (MM 51), six interchanges on this 13-mi-long section.
- Data collection period: Wednesday, November 13, from 3:00–7:30 p.m.
- Data:
  - Speed and volume data collected by six RTMS trailers along major mainline segments.
  - On- and off-ramp volume data collected by portable action cameras.
- Calibration approach:
  - Initial calibration is performed to narrow down parameter set candidates by using the LHD approach and key car following and lane changing parameters were calibrated.
  - Vissim evaluated 500 scenarios created by the LHD approach with five replications for each scenario to choose the best candidate scenario.
  - The selected candidate is fine-tuned to obtain the final simulation model.
- Segment travel time data (INRIX 2018).

**Table 30. Westbound RTMS trailer locations.**

| Interchange ID | Nearest Exit | Nearest Crossing | Mile Marker | Latitude | Longitude |
|---|---|---|---|---|---|
| 1 | 62 | Rt 243/Nutley Street | 61.6 | 38.879646 | −77.250504 |
| 2 | 60 | Rt 123 | 60.0 | 38.8705306 | −77.3009333 |
| 3 | 57 | Rt 50 | 58.0 | 38.861246 | −77.352807 |
| 4 | 55 | Rt 286 | 55.5 | 38.856415 | −77.378025 |
| 5 | 53 | Rt 28/Sully Road | 53.0 | 38.847060 | −77.429654 |
| 6 | 52 | Rt 29 | 51.8 | 38.8386833 | −77.4462111 |

**Table 31. Westbound traffic management center (TMC) locations (INRIX 2018).**

| TMC Code | From (Latitude, Longitude) | From (Latitude, Longitude) | From (Latitude, Longitude) | To (Latitude, Longitude) | To (Latitude, Longitude) | To (Latitude, Longitude) | Mileage |
|---|---|---|---|---|---|---|---|
| 110+04176 | I–495/exit 64 | 38.88308 | −77.2295 | VA–243/ Nutley Street/ exit 62 | 38.87883 | −77.2628 | 1.8 |
| 110P04176 | I–495/exit 64 | 38.87883 | −77.2628 | VA–243/ Nutley Street/ exit 62 | 38.87824 | −77.2703 | 0.4 |
| 110+04177 | Vaden Drive/exit 62 | 38.87824 | −77.2703 | VA–123/ exit 60 | 38.87741 | −77.2748 | 0.3 |
| 110+04178 | VA–243/Nutely Street/exit 62 | 38.87741 | −77.2748 | VA–123/ exit 60 | 38.8704 | −77.3006 | 1.4 |
| 110P04178 | VA–123/exit 60 | 38.87041 | −77.30064 | US 50/ exit 57 | 38.8676 | −77.3162 | 0.9 |
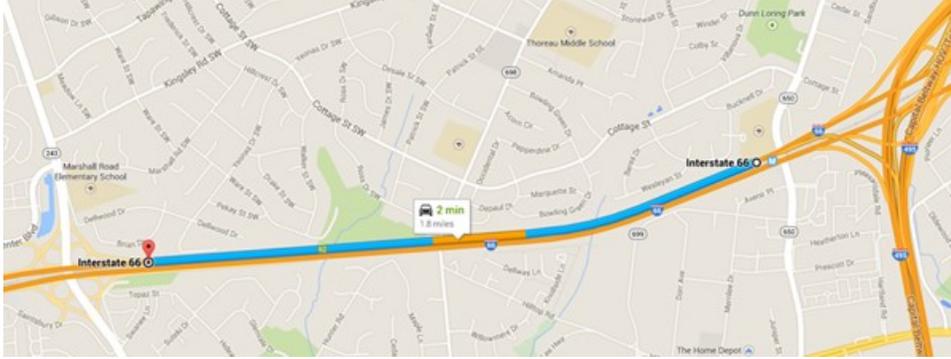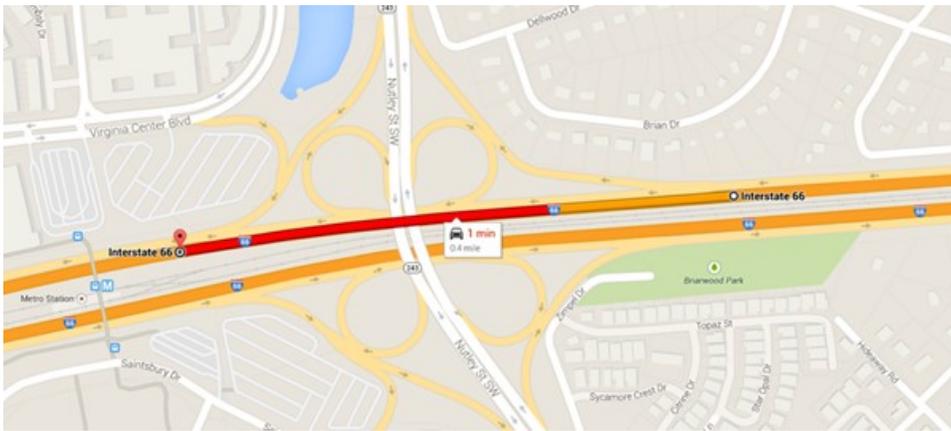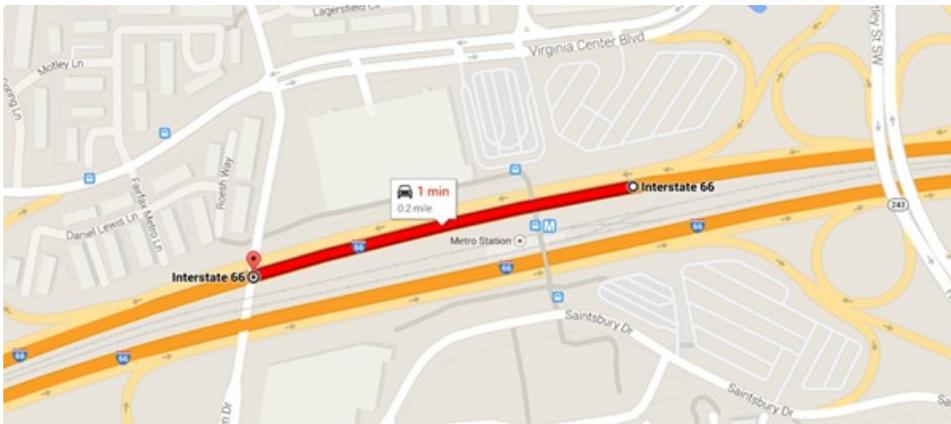
A. TMC 110+04176.

B. TMC 110P04176.

C. TMC 110P04177.
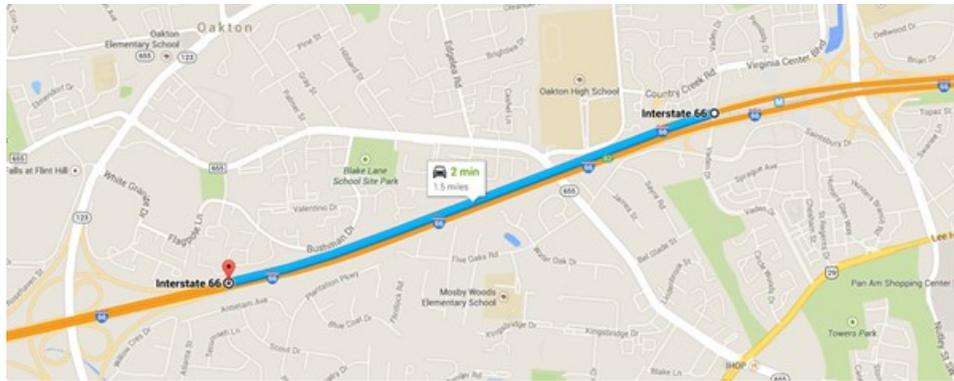
Original photo: © 2017 Google® (see acknowledgements).

D. TMC 110+04178.
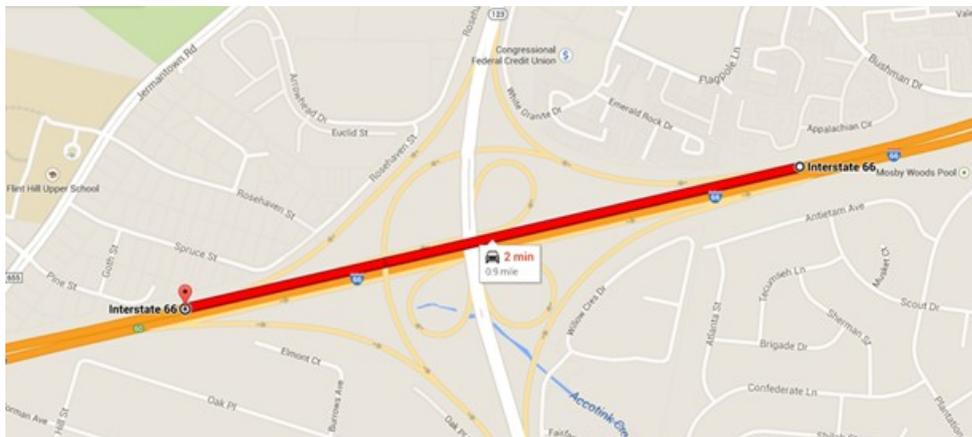


Original photo: © 2017 Google® (see acknowledgements).

E. TMC 11P04178.

**Figure 50. Maps. TMCs used in the calibration.**

## O-D Estimation

Vissim uses O-D matrices to specify travel demand. The I–66 freeway network has 10 zones, as shown in figure 51 and table 32. Zones 1 and 10 are the starting and ending points of the corridor. Zones 2–9 contain the intermediate interchanges. Note that zones 5 and 7 are only applicable to HOV vehicles (i.e., exits for westbound, entrances for eastbound).

The field-collected data in this study identified how many vehicles traveled between some, but not all, O-D pairs. To fill in the gaps, the QueensOD software estimated O-D matrices. For example, table 33 lists an estimated O-D matrix for the 3:00–3:15 p.m. time period. Figure 29 compares estimated flows with observed flows of the same period. Results indicate an excellent correlation between estimated and field-measured O-D trips.

**Table 32. Zone definitions**

| Zone ID | Zone Description |
|---|---|
| 1 | I–66 eastbound or I–495 |
| 2 | Exit 62 on/off-ramp |
| 3 | Exit 60 on/off-ramp to/from north |
| 4 | Exit 57 on/off-ramp to/from north |
| 5 | Exit to Monument Drive, destination only |
| 6 | Exit 55 on/off-ramp |
| 7 | Exit to Stringfellow Road, destination only |
| 8 | Exit 53 on/off-ramp to/from north |
| 9 | Exit 52 on/off-ramp to/from north |
| 10 | I–66 westbound |



Original photo: © 2017 Google® (see acknowledgements).

**Figure 51. Map. Zone locations.**

**Table 33. O-D example of 3:00–3:15 p.m. (veh/h).**

| Zone ID | 2 | 3 | 4 | 5 | 6 | 7 | 8 | 9 | 10 |
|---|---|---|---|---|---|---|---|---|---|
| 1 | 457 | 97.2 | 375.8 | 149 | 1.4 | 228.1 | 756.1 | 417.9 | 3599.7 |
| 2 | — | 287.2 | 414.8 | — | 14.2 | — | 31.3 | — | — |
| 3 | — | — | 861.4 | — | 72.2 | — | 0.1 | — | — |
| 4 | — | — | — | — | 242 | — | 71.7 | 39.1 | 41.7 |
| 6 | — | — | — | — | — | — | 1164.5 | 8.9 | 401.8 |
| 8 | — | — | — | — | — | — | — | 64.2 | 1223.8 |
| 9 | — | — | — | — | — | — | — | — | 925.6 |

—No data.

## Throughput Calibration

Throughput calibration was performed from 3:30–7:00 p.m. at all six interchanges. The plotted and graphed throughputs were deemed reasonably consistent between the simulated and field-measured results.

## Calibration of Speed Flow Curves

Speed flow curves were plotted from 3:30–7:00 p.m. at all six interchanges. The plotted and graphed throughputs were deemed consistent with traffic engineering principles (and consistent with each other) for both simulated and field-measured results.

## Calibration of Travel Time

Travel time calibration was performed from 3:30–7:00 p.m. at all six interchanges. The plotted and graphed throughputs were deemed reasonably consistent between the simulated and field-measured results. Peak travel time occurred at approximately 5:45 p.m.

## Reasonableness of Animation

The simulation network is all of the freeway networks with connecting ramps and local roads where traffic demands are generated. The simulation calibration and validation have confirmed the reasonableness of simulation volumes at key areas (selected locations before and after merging areas) and travel time of key segments (especially those the merging segments). This section focuses on checking the reasonableness of simulation behavior at key locations of the network, including car following behavior at basic segments, merging behavior at on-ramps, and merging behavior at lane drops. Figure 52 through figure 54 demonstrate simulation behavior of the above-mentioned three key areas. Animation checks at multiple key locations do not reveal abnormal behavior, and thus confirm the reasonableness of the simulation.
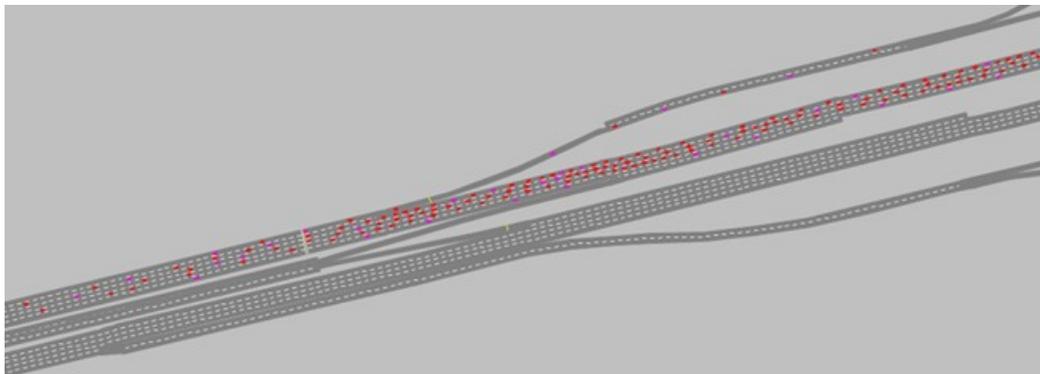


Source: FHWA.

**Figure 52. Screenshot. Merging area simulation example one (bird's eye view).**
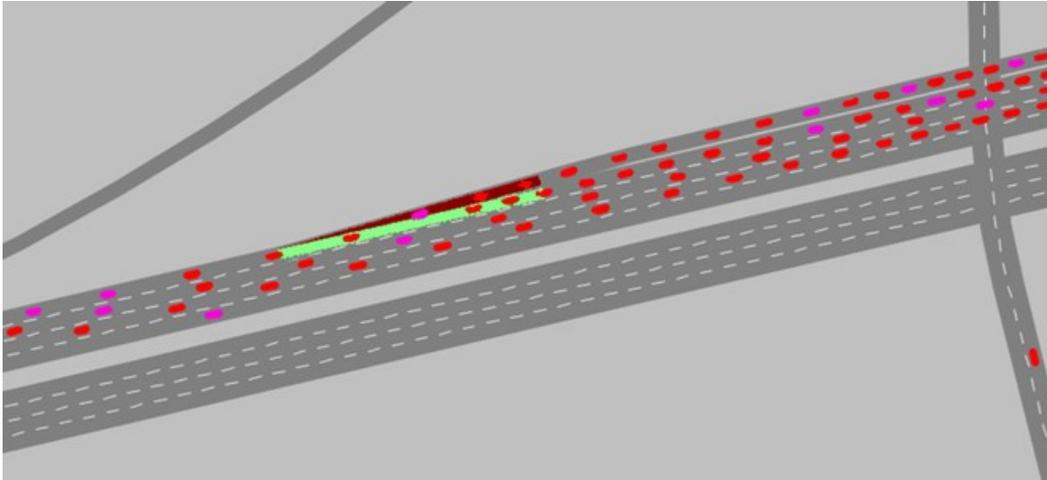
Source: FHWA.

**Figure 53. Screenshot. Merging area simulation example two (zoomed-in view).**
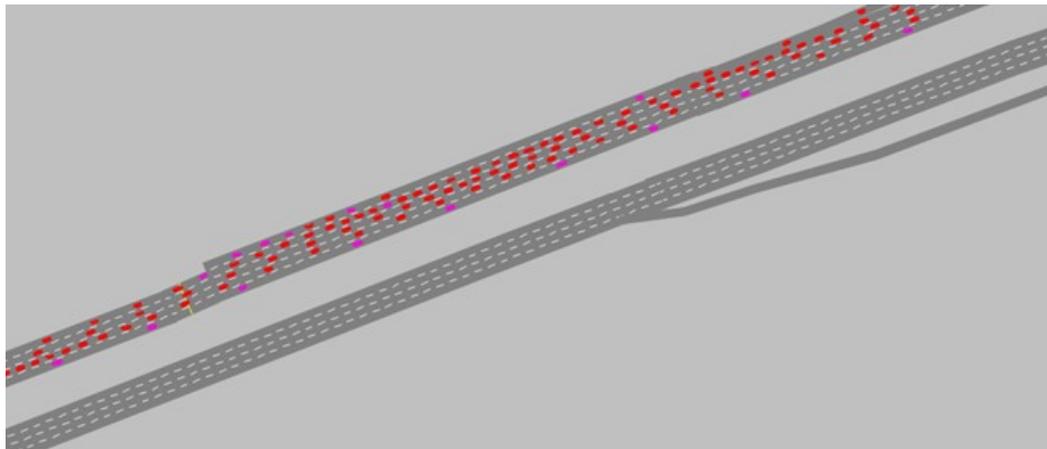


Source: FHWA.

**Figure 54. Screenshot. Lane drop simulation (zoomed-in view).**

## I–270 MD VISSIM

### Background Information

The network contains the following characteristics:

- Hourly volume: 12,300 veh/h.
- 10 percent trucks in the traffic stream.
- Speed limit: 55 mi/h.
- Number of mainline lanes: four.
- Shoulder width: approximately 12 ft on both sides.
- Number of ramps: 1.1 per mile.

## Overview

The section of roadway selected for analysis is located in Montgomery County, MD, and spans approximately 5.5 mi in the freeway's southbound direction between Shady Grove Road and the I–270 west spur to I–495. The facility spans two collector-distributor (C-D) lanes separated out from the four GP lanes by a Jersey barrier and has shoulder widths varying anywhere from 2 to 10 ft. The GP lane closest to the median operates as an HOV lane during the morning rush, from 6:30–9:30 am Monday–Friday, and the whole cross section (C-D and GP lanes) carries over 125,000 vehicles per day in the I–270 southbound direction alone. The C-D lane ends at the southern end of this section of the I–270 corridor, just south of Montrose Parkway. In this 5.5-mi section, there are three slip ramps from the C-D lanes to the GP lanes, and two slip ramps from the GP lanes to the C-D lanes. Within the C-D lanes, there are five merge locations, two diverge locations, and one weaving condition, excluding those generated by the slip ramps. The posted speed limit for both the C-D and GP lanes is 55 mi/h.
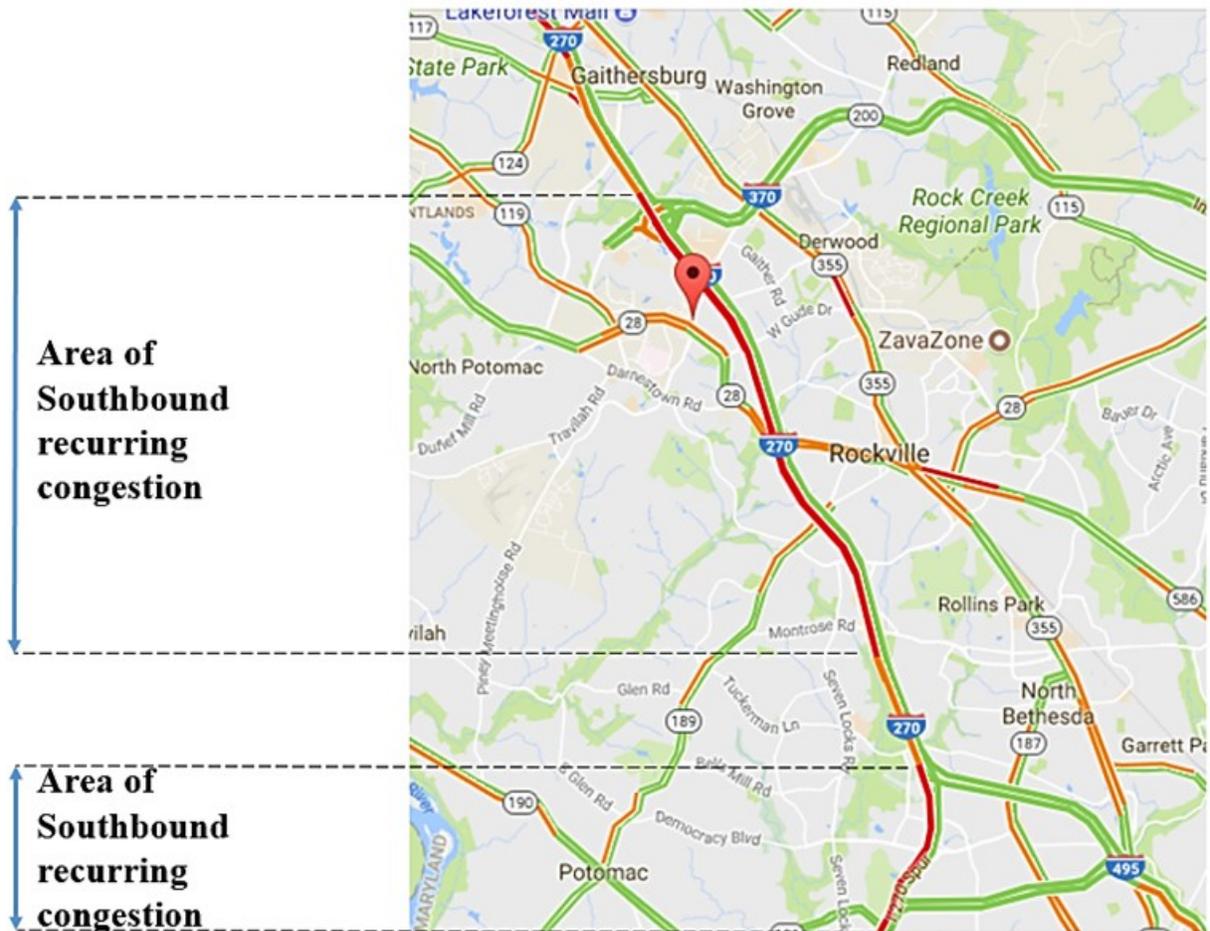


© 2017 Google®.

**Figure 55. Map. I–270 southbound starting at Shady Grove (a.m. peak).**

114

Noteworthy for the I–270 corridor in this section of roadway is the lack of ITS. There are no overhead gantries with lane assignment, VSL signs, and only one dynamic message sign located at the southern end of the corridor. Bridge structures along the entire stretch of I–270 are a significant constraint to potential widening, as bridge piers interfere with the potential of shifting lanes or widening without significant structural costs. Additionally, this section of the I–270 corridor experiences significant delays due to capacity constraints just south of this corridor along the I–270 spur and further at the American Legion Bridge along I–495 going into Virginia. The I–270 corridor ranks in the top locations around the State for recurring and non-recurring congestion, with a travel time index ranging anywhere between 1.87 and 2.49 between Shady Grove Road and Montrose Parkway during the morning rush. Subsequent data and information were obtained in a memo from the Maryland Department of Transportation State Highway Administration (Whitman, Requardt & Associates 2015). Because the calibration outcomes were relatively recent and favorable, the team did not perform additional calibration of this network.

**Throughput Calibration**

The Maryland Department of Transportation State Highway Administration's Data Services Engineering Division developed 2015 peak hour traffic volumes for the study area. They found the a.m. and p.m. peak hours were 7:00–8:00 a.m. and 5:00–6:00 p.m., respectively, as shown in table 34 and table 35. The traffic demand is balanced throughout the entire network for both a.m. and p.m. peaks.

**Table 34. 2015 a.m. peak hour traffic volumes for I–270.**

| I–270 Southbound | GP Count Volume (veh/h) | GP Vissim Volume (veh/h) | GP Difference (Percent) | HOV Lane Count Volume (veh/h) | HOV Lane Vissim Volume (veh/h) | HOV Lane Difference (Percent) | C-D Lanes Count Volume (veh/h) | C-D Lanes Vissim Volume (veh/h) | C-D Lanes Difference (Percent) |
|---|---|---|---|---|---|---|---|---|---|
| North of Shady Grove | 4,506 | 4,111 | −9 | 1,187 | 1,265 | 7 | 2,409 | 2,942 | −14 |
| South of MD 124 | 6,864 | 6,930 | 1 | — | — | — | — | — | — |
| South of Middlebrook Road | 6,917 | 6,737 | −3 | — | — | — | — | — | — |
| North of MD 118 | 3,944 | 4,665 | 18 | — | — | — | — | — | — |
| North of MD 121 | 3,408 | 3,800 | 12 | — | — | — | — | — | — |

—No data.

115

**Table 35. 2015 p.m. peak hour traffic volume for I–270.**

| I–270 Southbound | GP Count Volume (veh/h) | GP Vissim Volume (veh/h) | GP Difference (Percent) | HOV Lane Count Volume (veh/h) | HOV Lane Vissim Volume (veh/h) | HOV Lane Difference (Percent) | C-D Lanes Count Volume (veh/h) | C-D Lanes Vissim Volume (veh/h) | C-D Lanes Difference (Percent) |
|---|---|---|---|---|---|---|---|---|---|
| North of Shady Grove | 4,392 | 4,789 | 9 | 1,075 | 1,026 | −5 | 4,029 | 4,148 | 3 |
| South of MD 124 | 4,078 | 4,713 | 16 | 1,195 | 1,280 | 7 | 2,577 | 2,448 | −5 |
| South of Middlebrook Road | 5,330 | 6,115 | 15 | 1,281 | 1,190 | −7 | — | — | — |
| North of MD 118 | 4,343 | 4,409 | 2 | — | — | — | — | — | — |
| North of MD 121 | 3,603 | 3,787 | 5 | — | — | — | — | — | — |

—No data.

## Calibration of Additional Measures

Signal timing data are provided by the Maryland Department of Transportation State Highway Administration's Data Services Engineering Division for signalized intersections within the corridor to ensure that the Vissim models include accurate existing signal timings. The Vissim model ring barrier controller files were verified and/or modified to match the signal data. Travel time and RITIS data are provided by the Maryland Department of Transportation State Highway Administration's Data Services Engineering Division for segments along the I–270 GP, HOV, and C-D lanes. The data are shown in table 36 through table 39.

**Table 36. 2015 a.m. travel time calibration results for I–270: I–270 northbound from the I–495 interchange.**

| I–270 Northbound | Segment Length (mi) | Field(s) | Vissim(s) | Difference(s) (Percent) |
|---|---|---|---|---|
| To MD 187 | 1.8 | 109.7 | 109.0 | −0.7 |
| To I–270 split | 0.6 | 35.8 | 37.5 | 1.8 |
| To Montrose Road | 1.8 | 97.9 | 100.1 | 2.2 |
| To MD 189 | 1.0 | 55.3 | 57.6 | 2.3 |
| To MD 28 | 1.0 | 52.6 | 55.1 | 2.5 |
| To Shady Grove Road | 1.9 | 104.7 | 108.4 | 3.7 |
| To I–370 | 0.9 | 51.1 | 53.0 | 1.9 |
| To MD 117 | 1.5 | 81.6 | 85.5 | 3.9 |
| To MD 124 | 0.6 | 33.4 | 34.5 | 1.1 |
| To Middlebrook Road | 2.5 | 137.9 | 140.9 | 3.0 |
| To MD 118 | 1.1 | 62.2 | 64.8 | 2.6 |
| To MD 27 | 0.9 | 50.9 | 51.8 | 1.0 |
| To MD 121 | 2.4 | 132.4 | 135.3 | 2.8 |
| To MD 109 | 4.1 | 216.1 | 234.5 | 18.3 |
| To MD 80 | 3.7 | 198.7 | 213.8 | 15.2 |
| To MD 85 | 5.3 | 283.2 | 309.0 | 25.7 |
| To I–70 | 1.4 | 80.0 | 79.9 | −0.1 |
| I–270 total (min) | 32.5 | 29.7 | 31.2 | 1.5 |
| I–270 total percent difference | — | — | — | 4.9 |

—No data.

**Table 37. 2015 a.m. travel time calibration results for I–270: I–270 southbound from I–70.**

| I–270 Southbound | Segment Length (mi) | Field(s) | Vissim(s) | Difference(s) (Percent) |
|---|---|---|---|---|
| To MD 85 | 1.7 | 97.4 | 97.0 | −0.4 |
| To MD 80 | 5.4 | 484.0 | 414.5 | −69.5 |
| To MD 109 | 3.7 | 397.7 | 390.6 | −7.1 |
| To MD 121 | 3.6 | 281.4 | 273.2 | −8.2 |
| To MD 27 | 2.5 | 356.5 | 296.2 | −60.3 |
| To MD 118 | 1.1 | 172.0 | 223.8 | 51.8 |
| To Middlebrook Road | 1.1 | 120.5 | 132.6 | 12.1 |
| To MD 124 | 2.2 | 495.5 | 535.2 | 39.7 |
| To MD 117 | 0.9 | 67.0 | 77.0 | 10.0 |
| To I–370 | 1.0 | 240.0 | 160.7 | −79.3 |
| To Shady Grove Road | 1.5 | 277.5 | 133.7 | −143.8 |
| To MD 28 | 1.9 | 541.5 | 492.8 | −48.7 |
| To MD 189 | 1.0 | 129.5 | 260.0 | 130.5 |
| To Montrose Road | 1.0 | 185.0 | 394.5 | 209.5 |
| To I–270 split | 1.9 | 142.0 | 217.0 | 75.0 |
| To MD 187 | 0.4 | 29.3 | 30.0 | 0.7 |
| To I–495 interchange | 1.9 | 122.4 | 131.8 | 9.4 |
| I–270 total (min) | 32.8 | 69.0 | 71.0 | 2.0 |
| I–270 total percent difference | — | — | — | 2.9 |

—No data.

**Table 38. 2015 a.m. travel time calibration results for I–270: I–270 spur northbound from Cabin John Parkway.**

| I–270 Spur Northbound | Segment Length (mi) | Field(s) | Vissim(s) | Difference(s) (Percent) |
|---|---|---|---|---|
| To MD 190 | 0.5 | 25.6 | 32.2 | 6.6 |
| To I–495 | 1.1 | 64.1 | 66.7 | 2.6 |
| To Democracy Boulevard | 1.4 | 81.6 | 91.2 | 9.6 |
| To I–270 split | 0.9 | 49.9 | 51.0 | 1.2 |
| To I–70 | 30.0 | 1,638.1 | 1,724.3 | 86.2 |
| I–270 spur total (min) | 33.9 | 31.0 | 32.8 | 1.8 |
| I–270 spur total percent difference | — | — | — | 5.7 |

—No data.

**Table 39. 2015 a.m. travel time calibration results for I–270: I–270 spur southbound from I–70.**

| I–270 Spur Southbound | Segment Length (mi) | Field(s) | Vissim(s) | Difference(s) (Percent) |
|---|---|---|---|---|
| To I–270 split | 30.3 | 3,987.5 | 4,098.7 | 111.2 |
| To Democracy Boulevard | 0.7 | 86.4 | 88.4 | 2.0 |
| To I–495 | 1.3 | 132.1 | 183.1 | 51.0 |
| To MD 190 | 1.3 | 77.4 | 92.2 | 14.9 |
| To Cabin John Parkway | 0.6 | 33.9 | 35.0 | 1.1 |
| I–270 spur total (min) | 34.2 | 72.0 | 75.0 | 3.0 |
| I–270 spur total percent difference | — | — | — | 4.2 |

—No data.

## Reasonableness of Animation

To check the reasonableness of the simulation animation and consistency with the field measurements, the animation results are compared with the field-measured speed data downloaded from the RITIS database (RITIS 2018). The time period between October 1, 2017–November 15, 2017, was selected for the speed data because traffic is not much affected by occasional trips and bad weather conditions in this period. Moreover, only Tuesdays, Wednesdays, and Thursdays are selected for the data collection since traffic volumes are less likely to be affected by leisurely trips on these days. Figure 56 and figure 57 show the average speed heat map from 6:00–10:00 a.m. and from 4:00–8:00 p.m. for the selected days, respectively. In these heat maps, the horizontal and vertical axes represent the location and time, respectively. As shown in the figures, three locations are already linked to the heat maps. With this, the team can measure the scale of the location axes and thus link any other locations along the simulated corridor to the heat maps. The team focuses on the peak hours that are bordered by the green block in the figures (i.e., from 7:00–8:00 a.m. in figure 56 and from 5:00–6:00 p.m. in figure 57).

The team split the peak hour period into six 10-min time intervals and then compared the simulation animation results with the field-measured speed heat maps. In this report, the team selected four locations for each a.m. and p.m. peak hours as benchmarks. Figure 58 and figure 59 zoom in to the freeway geometry associated with the base dataset to the peak hour periods and tag the four selected benchmark locations. For comparison purposes, the team classified vehicle colors in the simulation based on their speeds.

Figure 60 through figure 66 are examples of the comparison results. The comparison results indicate that the simulation animations match the field-measured speed heat map for most of the space-time points. The team found a few inconsistencies between the animation and the field-measured speeds (e.g., figure 67). However, most of these inconsistencies are related to microscopic traffic oscillations and do not necessarily indicate serious inconsistencies with the macroscopic field-measured speeds. In addition to these comparisons, the team checked the simulation animation carefully to identify the existence of any stuck vehicles. There were no stuck vehicles on the I–270 freeway; however, the team found one minor problem on an

on-ramp, as shown in figure 67. Since this issue was located on an on-ramp and not on the mainline, it was not expected to significantly impact the simulation validity and results.
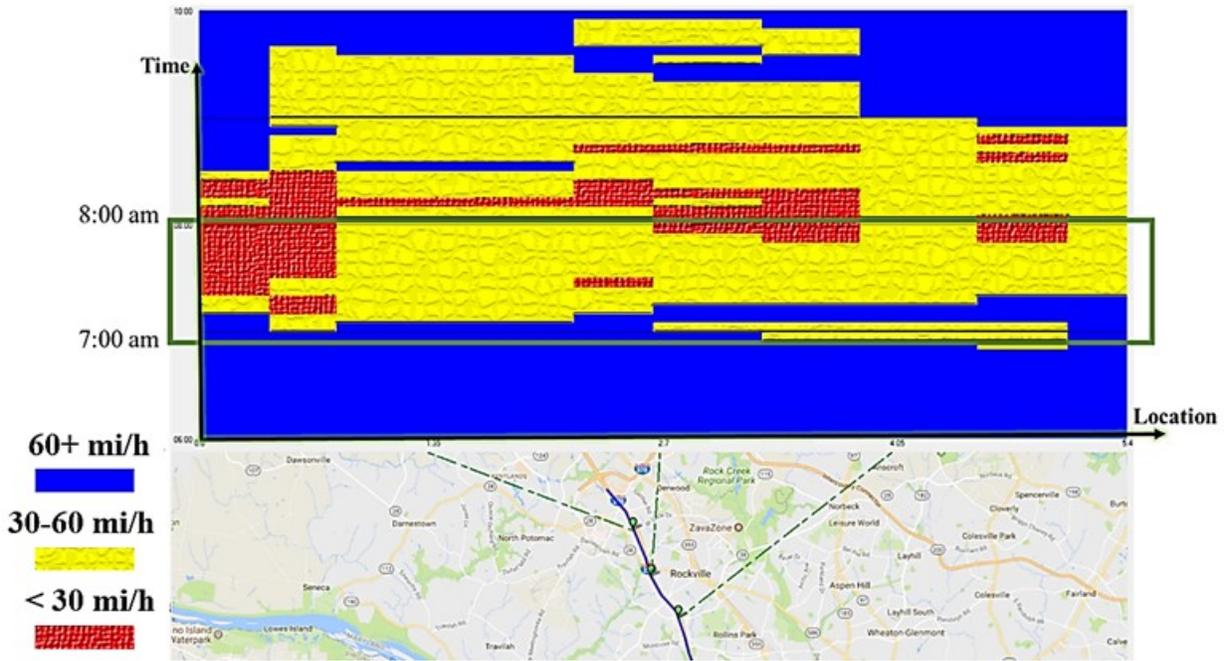


Original map: © 2017 Google® (see acknowledgements).

**Figure 56. Illustration. Field-measured speed heat map from 7:00–8:00 a.m.**



Original map: © 2017 Google® (see acknowledgements).

**Figure 57. Illustration. Field-measured speed heat map from 5:00–6:00 p.m.**

Original map: © 2017 Google® (see acknowledgements).

**Figure 58. Illustration. Field-measured speed heat map for p.m. peak hour.**



Original map: © 2017 Google® (see acknowledgements).

**Figure 59. Illustration. Field-measured speed heat map for a.m. peak hour.**
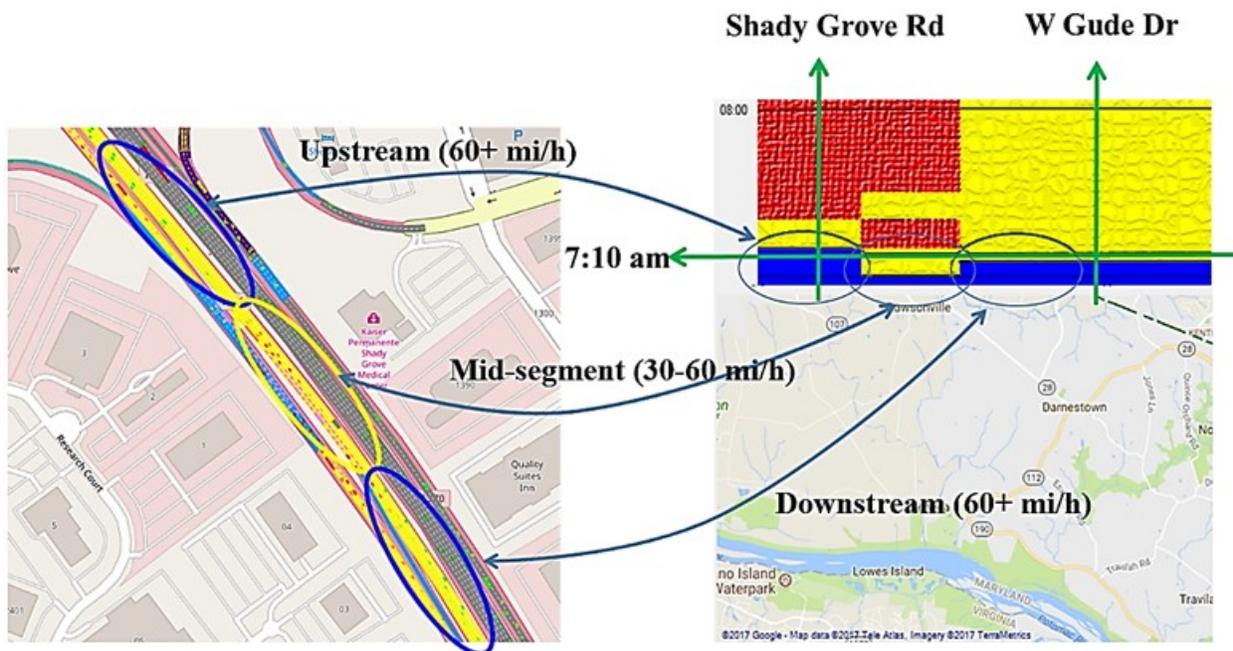
Original map: © 2017 Google® (see acknowledgements).

**Figure 60. Diagram. Animation check at 7:10 a.m.**
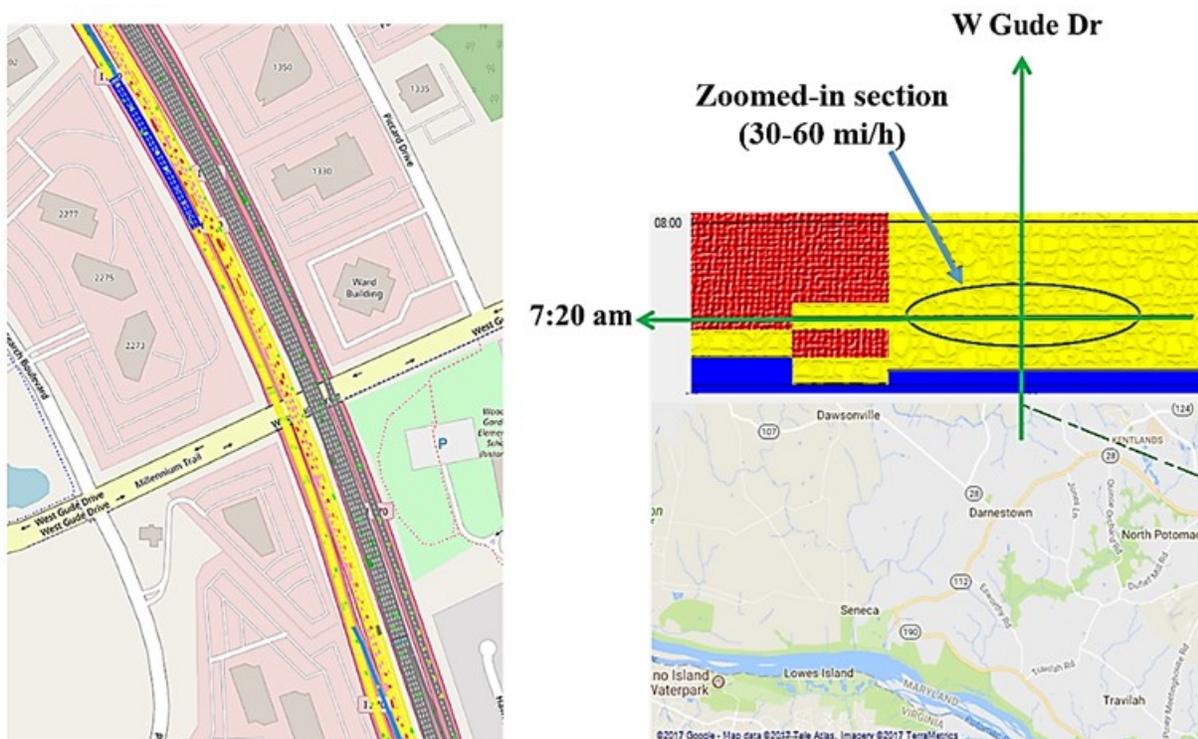


Original map: © 2017 Google® (see acknowledgements).

**Figure 61. Diagram. Animation check at 7:20 a.m.**
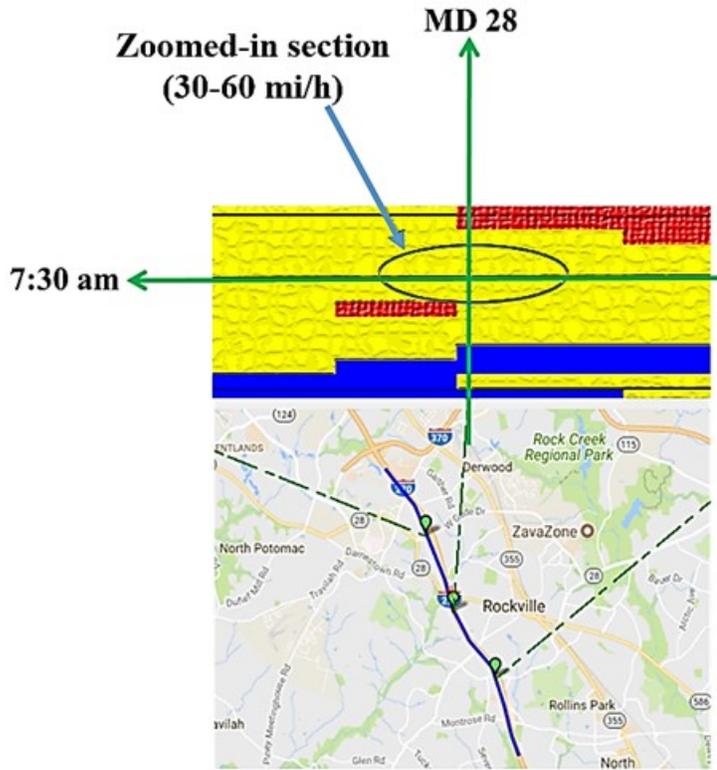
**Figure 62. Diagram. Animation check at 7:30 a.m.**
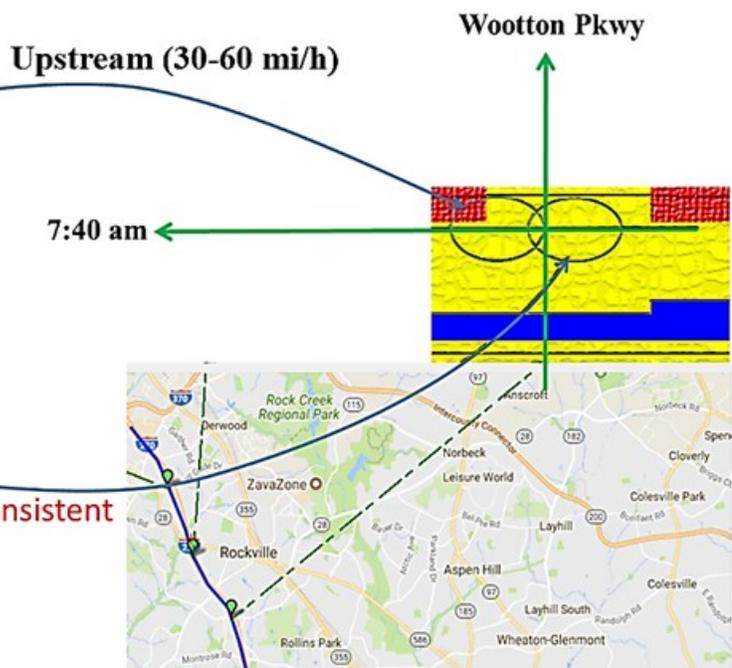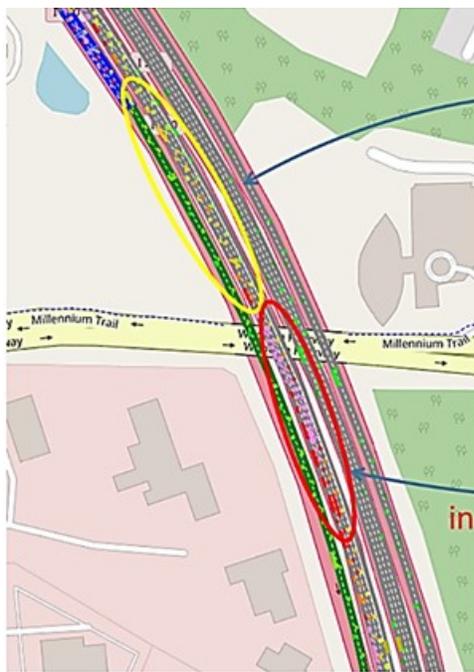
**Figure 63. Diagram. Animation check at 7:40 a.m.**

123
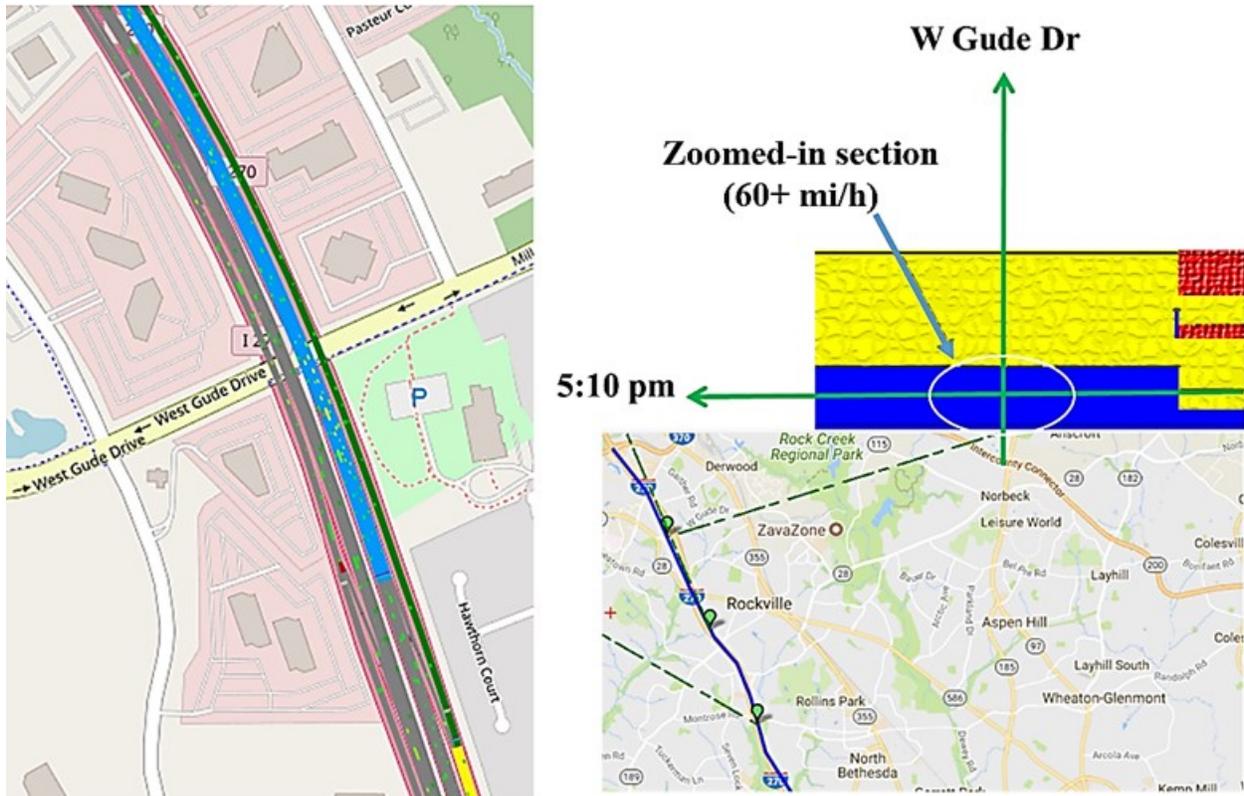
**Figure 64. Diagram. Animation check at 5:10 p.m.**
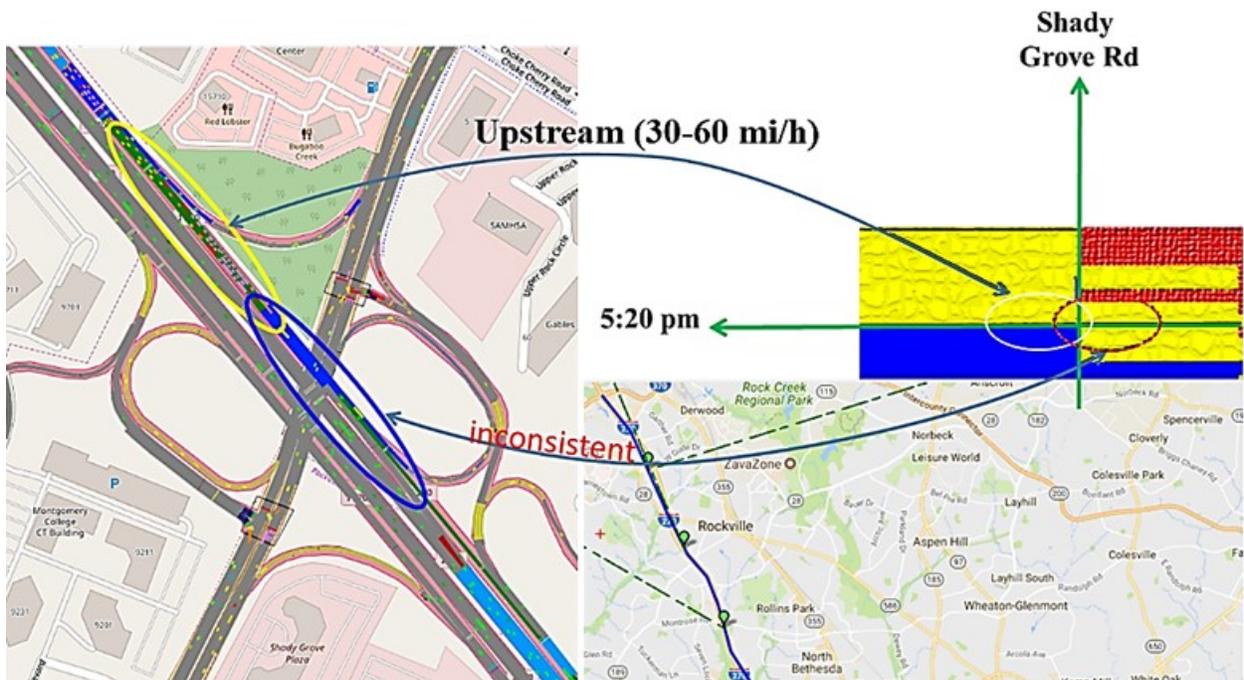
**Figure 65. Diagram. Animation check at 5:20 p.m.**
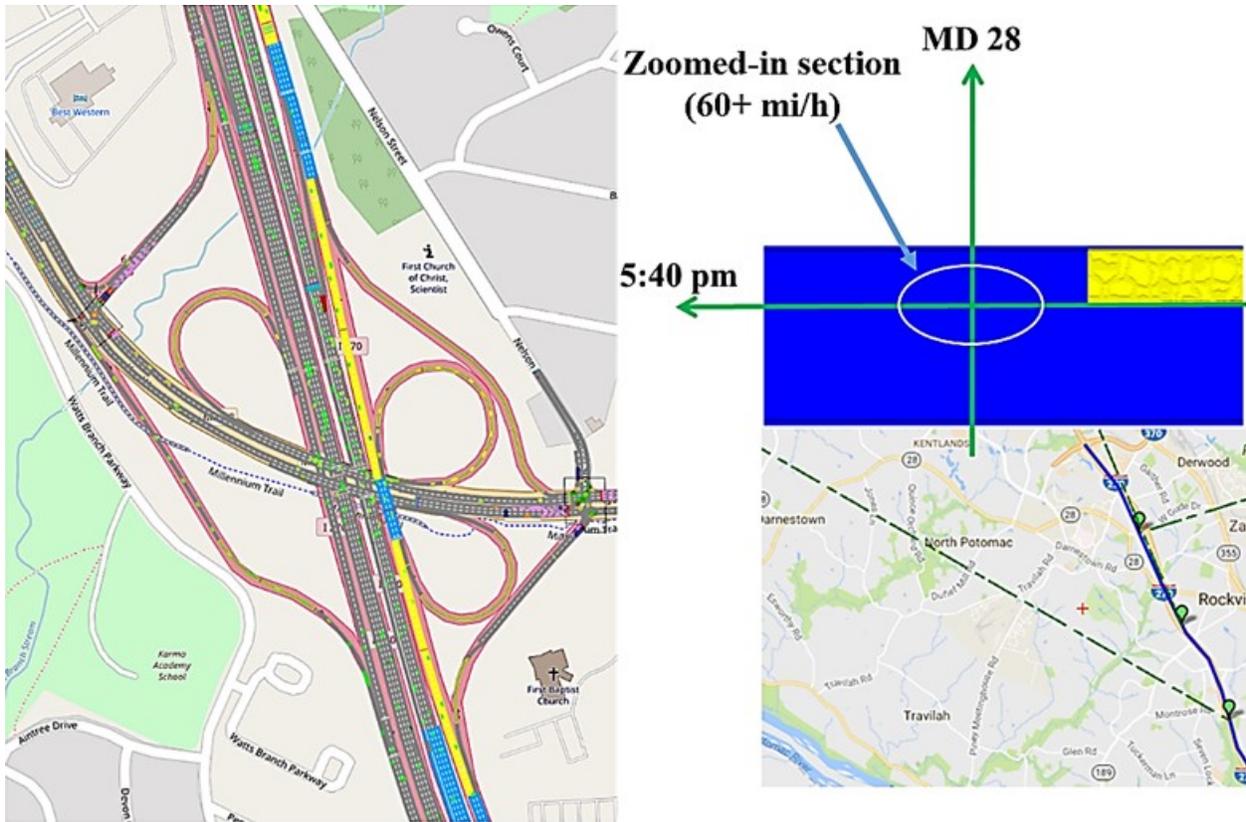
Original map: © 2017 Google® (see acknowledgements).

**Figure 66. Diagram. Animation check at 5:40 p.m.**
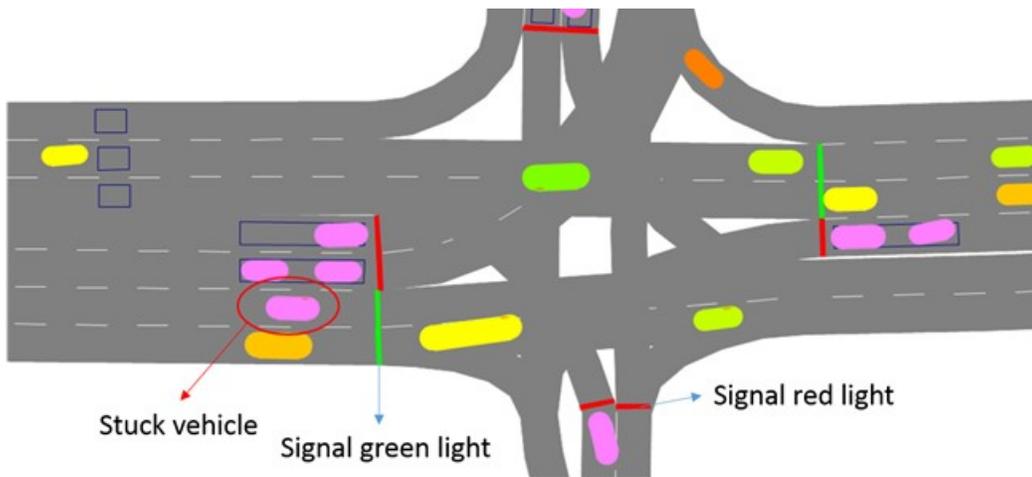


Source: FHWA.

**Figure 67. Illustration. A stuck vehicle on an on-ramp.**

**I–95 PA VISSIM**

**Background Information**

There are presently a number of transportation improvement projects in progress along I–95 in Pennsylvania. While there are five active projects that will reconstruct, widen, and improve I–95 in Pennsylvania, these projects do not include sector C, which covers the study corridor. PennDOT's website gives detailed information regarding each of these projects (Pennsylvania Department of Transportation 2018).

**Overview**

This section provides an overview of I–95 in Pennsylvania, including traffic information, and describes ongoing projects and plans for the I–95 corridor. The I–95 corridor is a vital north-south transportation corridor in Pennsylvania serving the airport, the stadiums, and Philadelphia, PA. The corridor carries an average of 102,000 vehicles, including 13,000 trucks every day (Pennsylvania Department of Transportation 2018). The corridor is divided into four sectors by PennDOT, including sector A, B, C, and D. The study corridor selected as part of this simulation effort covers sector C, from the Delaware State line to the Schuylkill River (figure 68). Figure 69 shows ADT volumes on the I–95 corridor on a typical (non-event) day in Pennsylvania. While the ADT ranges from 60,000 to 160,000 vehicles, sector C, the focus of this study, has approximately 120,000 vehicles. Figure 70 indicates average weekday speed profiles from 5:00 a.m.–8 p.m. on a typical (non-event) day along the corridor and highlights some of the existing bottlenecks. For this study corridor, the US 322 interchange and north appears to be the main bottleneck, especially during the p.m. peak where average speeds can drop below 30 mi/h.
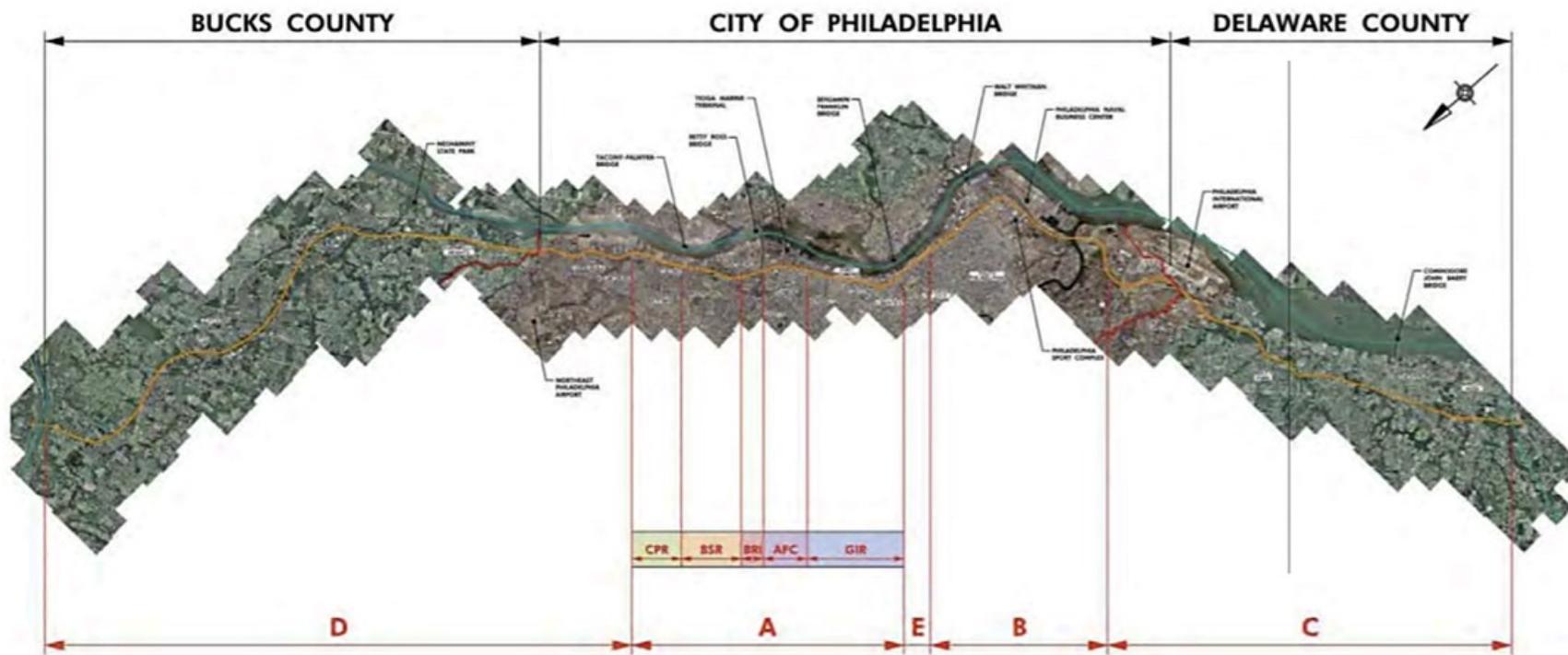
Figure 68. Map. I–95 corridor in Pennsylvania.
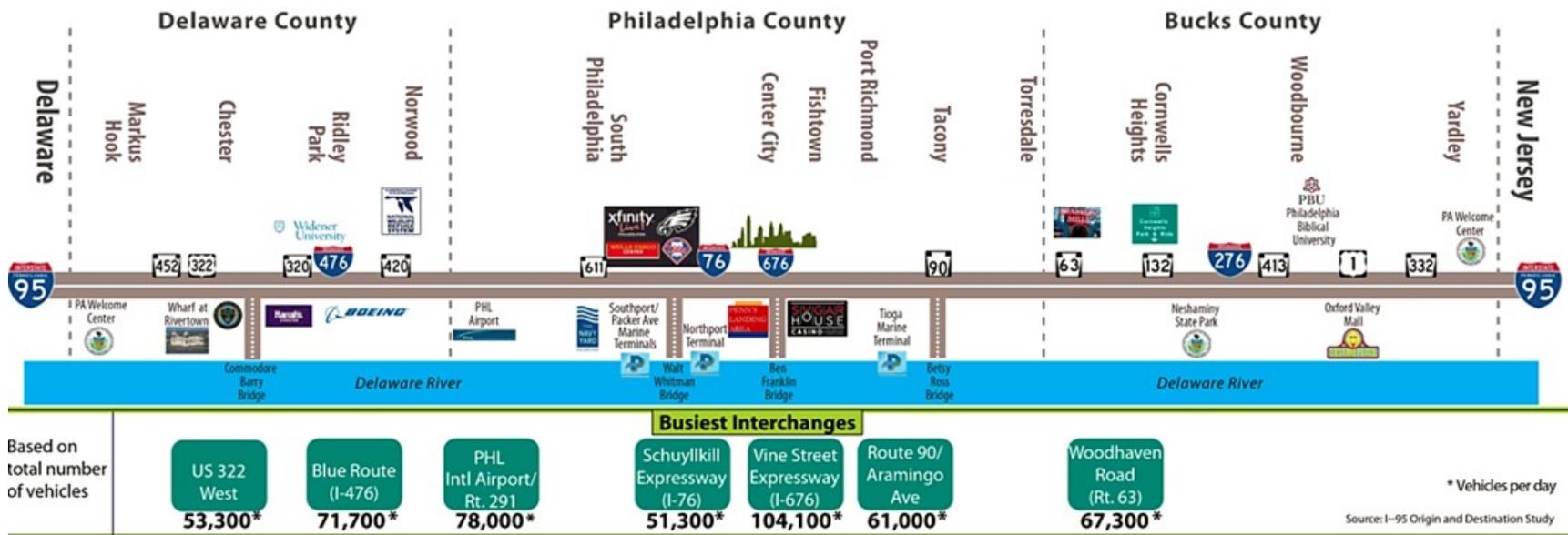
© 2019 Kittleson & Associates, Inc.

A. Busiest interchanges on I–95 in Pennsylvania during a typical, non-event day.
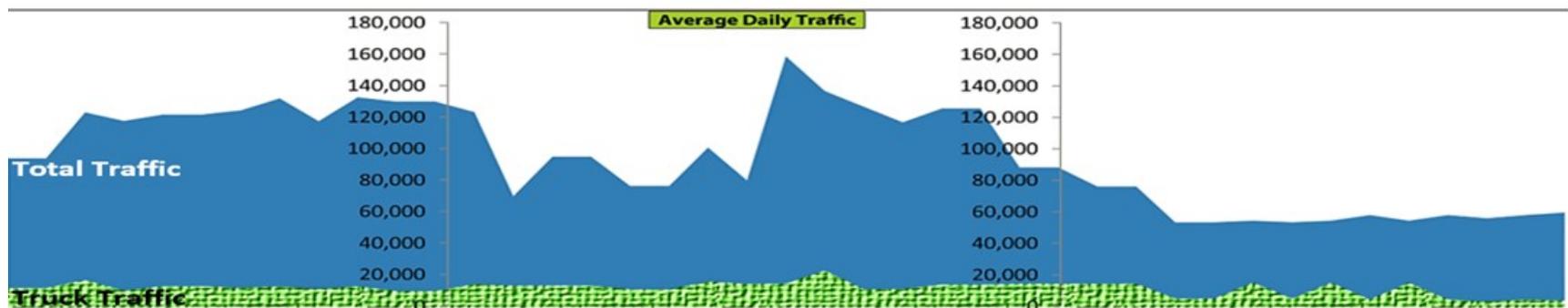


© 2019 Kittleson & Associates, Inc.

B. ADT on the I–95 corridor in Pennsylvania.

**Figure 69. Illustrations. How traffic flows on the I–95 corridor in Pennsylvania.**

© 2019 Kittleson & Associates, Inc.

A. I–95 layout of counties.
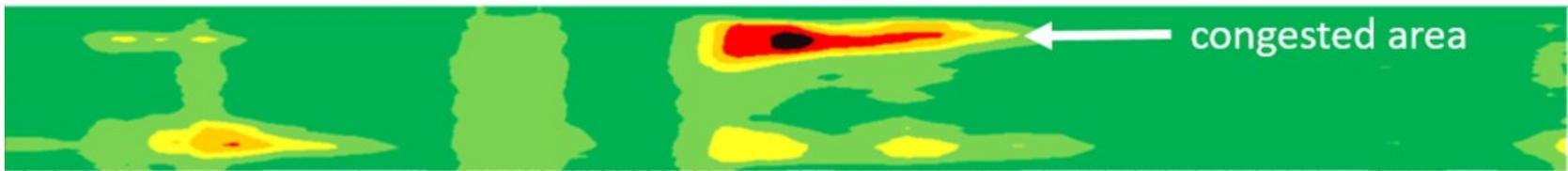


© 2019 Kittleson & Associates, Inc.

B. I–95 southbound (right-to-left) congestion profile, 5:00 a.m.–8 p.m. (top-to-bottom).



© 2019 Kittleson & Associates, Inc.

C. I–95 northbound (left-to-right) congestion profile, 5:00 a.m.–8 p.m. (top-to-bottom).

**Figure 70. Illustrations. I–95 weekday congested locations.**

**Throughput Calibration**

Since the volumes are from 2011, an update is needed for the volumes based on the growth rate along I–95 within the study area. Table 40 and table 41 show the 2009 and 2015 ADT results on the corridor (the latest ADT results are from 2015). Based on the results shown below, applying a global growth rate to bring the 2011 volumes to 2017 is needed to maintain the O-D routing structure in the Vissim model.

**Table 40. I–95 PA throughput calibration plan—Philadelphia County, PA.**

| Location | 2009 ADT | 2015 ADT | 6-Year Growth Factor |
|---|---|---|---|
| I–95 just northeast of Delaware State line | 124,000 | 134,000 | 1.081 |
| I–95 by Philadelphia Airport | 71,000 | 72,000 | 1.014 |
| I–95 west of Schuylkill River | 96,000 | 102,000 | 1.063 |
| I–95 east of Schuyklill River (right after the study area) | 77,000 | 107,000 | 1.390 |

**Table 41. I–95 PA throughput calibration plan—Delaware County, PA.**

| Location | 2009 ADT | 2015 ADT | 6-Year Growth Factor |
|---|---|---|---|
| I–95 west of Chichester Avenue | 95,000 | 97,000 | 1.021 |
| I–95 east of Chichester Avenue | 124,000 | 100,000 | 0.806 |
| I–95 west of Conchester Highway (US 322) | 119,000 | 135,000 | 1.134 |
| I–95 west of Edgmont Avenue (PA Rt 352) | 125,000 | 127,000 | 1.016 |
| I–95 east of Darby Creek | 134,000 | 121,000 | 0.903 |
| I–95 east of PA Rt 420 | 131,000 | 127,000 | 0.969 |
| I–95 west of Philadelphia Airport | 131,000 | 134,000 | 1.023 |

In order to obtain throughput in the simulation model, permanent oversaturation is required at the bottleneck locations for the analysis period. The visual inspection of the base model indicated that these bottleneck locations already experience very long queues and capacity breakdowns under the base volume scenario. To ensure permanent oversaturated conditions for the analysis period, base traffic volumes were increased artificially by 5 percent. It should be noted that 5 percent was arbitrarily selected by the team.

In order to estimate throughput, data collection points were placed just downstream of the bottleneck locations (figure 71 shows screenshots from the model). Ten simulation runs were performed to collect results. The results were obtained from the peak hour following a 1-h warmup period. Since field data are not available to compare simulation throughput values against field results, theoretical recommended capacity along with previous studies found in the literature were used for comparison. Table 42 shows the locations where throughput data were collected and provides throughput results.

**Table 42. I–95 PA throughput calibration summary.**

| Bottleneck Location | Vissim Screenshot | Number of Lanes | Vehicle Throughput (veh/h) | HV Proportion (Percent) | PCPHPL |
|---|---|---|---|---|---|
| Downstream of I–476 southbound on-ramp (right merge) | Figure 71-A. Downstream of I–476 southbound on-ramp (right merge). | Three | 5,084 | 6.3 | 1,817 |
| Downstream of I–476 southbound off-ramp (right exit) | Figure 71-B. Downstream of I–476 southbound off-ramp (right exit). | Two | 3,368 | 5.9 | 1,799 |
| Downstream of US 322 northbound on-ramp (left merge) | Figure 71-C. Downstream of US 322 northbound on-ramp (left merge). | Three | 5,057 | 6.8 | 1,817 |

HV = heavy vehicles; PCPHPL = passenger cars per hour per lane.



Source: FHWA

A. Downstream of I–476 southbound on-ramp (right merge).
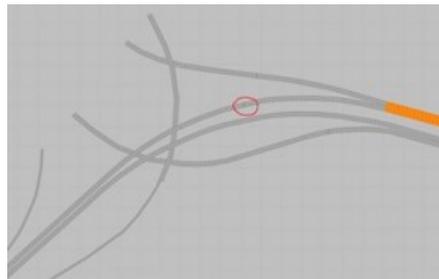


Source: FHWA

B. Downstream of I–476 southbound off-ramp (right exit).
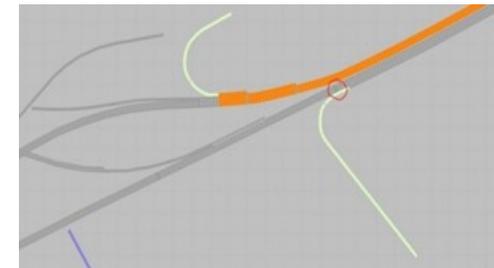


Source: FHWA

C. Downstream of US 322 northbound on-ramp (left merge).

**Figure 71. Screenshots. Vissim screenshots of I–95 PA.**

Results indicated throughput values that were slightly above 1,800 passenger cars per hour per lane and were consistent for each bottleneck location. While 1,800 passenger cars per hour per lane is lower than what is recommended in the *HCM* as theoretical capacity, several field studies found in the literature showed that *HCM* values tend to be higher, in particular at locations where there is heavy weaving with short merge/diverge sections.

**Calibration of Additional Measures**

Field speeds are based on March 2017 and October 2017 HERE archived historical probe data (Here 2019) from every Tuesday, Wednesday, and Thursday. Vissim results are based on the peak hour following a 1-h warmup time (so the team ran the models for 2 h). Vehicle inputs (volumes) were kept the same for the warmup time and the analysis time. A total of 10 simulation runs were performed in Vissim. Driving behavior was adjusted at certain locations to more accurately model merge/diverge behavior, in particular at the bottleneck locations. The adjusted calibration parameters at key segments are described below:

- At Conchester Highway (US 322) and I–95, due to the short left-hand on-ramp that includes heavy merging, the default parameters did not properly reflect field conditions in which ramp vehicles were "zippering" into the left lane, causing major congestion to mainline I–95. To more accurately model this behavior, the safety distance reduction factor within the lane change parameters in the Wiedemann 99 car following model (PTV Group 2019) was reduced from 0.60 to 0.30. In addition, the overall capacity within the segment was reduced (due to heavy weaving and an unusual left entrance) by increasing headway time and from 0.9 to 1.45 s and the following variation from 13.12 to 25.00.

- The southbound I–476 on-ramp is a right-hand add-lane ramp that is upstream of an off-ramp. This area experiences significant weaving due to the add lane being at capacity. As such, vehicles wishing to exit need to merge into shorter gaps, while vehicles in the add lane attempt to move to the left lanes and a more free-flow condition. This causes significant friction to mainline I–95. In order to replicate this condition in the model, the safety distance reduction factor was reduced from 0.60 to 0.10. Furthermore, to reduce overall capacity within the segment, the headway time was increased from 0.9 to 1.50 s and the following variation was increased from 13.12 to 25.00.

Overall, simulation speeds are generally consistent with the field data. Major bottlenecks observed in the field are reflected in the simulation, as can be seen in the speed comparison in table 43 and table 44.

**Table 43. 2017 calibration of speeds and travel times on I–95 PA—northbound direction.**

| Segment (Northbound) | Field TT (min) | Vissim TT (min) | Field Speed (mi/h) | Vissim Speed (mi/h) | Speed Difference (Percent) |
|---|---|---|---|---|---|
| Delaware State line (TMC 103+04114) to Rt 452 off-ramp; TMC 103P04115 | 3.1 | 3.0 | 30.2 | 30.8 | −1.7 |
| Rt 452 off-ramp to exit 3 (Highland Avenue); TMC 103P04116 | 2.4 | 3.2 | 27.4 | 21.3 | 22.4 |
| Exit 3 (Highland Avenue) to Barry Bridge on-ramp; TMC 103+04118 | 2.3 | 2.6 | 40.7 | 37.2 | 8.6 |
| Barry Bridge on-ramp to Edgmont Avenue off-ramp; TMC 103P04119 | 1.1 | 1.0 | 53.2 | 52.7 | 0.8 |
| Edgmont Avenue off-ramp to I–476 off-ramp; TMC 103P04121 | 1.3 | 1.4 | 52.9 | 51.9 | 1.8 |
| I–476 off-ramp to Stewart Avenue off-ramp; TMC 103P04122 | 1.4 | 1.4 | 54.3 | 55.3 | −1.9 |
| Stewart Avenue off-ramp to Wanamaker Ave off-ramp; TMC 103P04123 | 1.1 | 1.1 | 60.6 | 55.7 | 8.1 |
| Wanamaker Avenue to PA 291 off-ramp; TMC 10304124 | 1.5 | 1.7 | 62.5 | 55.7 | 11.0 |
| PA 291 off-ramp to I–95 at Bartram Avenue; TMC 103P04125 | 1.0 | 1.1 | 63.9 | 56.1 | 12.2 |
| Total northbound | 15.1 | 16.4 | 44.6 | 41.0 | 8.0 |

TT = travel time.

**Table 44. 2017 calibration of speeds and travel times on I–95 PA—southbound direction.**

| Segment (Southbound) | Field TT (min) | Vissim TT (min) | Field Speed (mi/h) | Vissim Speed (mi/h) | Speed Difference (Percent) |
|---|---|---|---|---|---|
| I–476 on-ramp to Edgmont Avenue on-ramp (TMC 103N04119 end) | 2.0 | 1.3 | 33.4 | 52.0 | −55.6 |
| Edgmont Avenue on-ramp to US 322 on-ramp (103-04116 start) | 2.5 | 1.8 | 39.0 | 53.8 | −38.1 |
| US 322 on-ramp to Highland Avenue on-ramp (TMC 103-04115 start) | 1.3 | 1.1 | 43.4 | 51.1 | −17.7 |
| Highland Ave on-ramp to Chichester Avenue on-ramp (TMC 103-04113 start) | 1.7 | 1.70 | 58.7 | 58.0 | 1.3 |
| TMC 103-4125 to I–95 at Bartram Avenue (TMC 103N04125) | 1.5 | 1.3 | 43.2 | 50.7 | −17.2 |
| I–95 at Bartram Avenue to I–95 (TMC 103N04124 End) | 1.5 | 1.3 | 41.0 | 46.6 | −13.7 |

| Segment (Southbound) | Field TT (min) | Vissim TT (min) | Field Speed (mi/h) | Vissim Speed (mi/h) | Speed Difference (Percent) |
|---|---|---|---|---|---|
| From TMC 103N04124 end to Wanamaker Avenue on-ramp (103-04122 start) | 2.2 | 2.0 | 40.0 | 44.7 | −11.8 |
| Wanamaker Avenue on-ramp to Stewart Avenue on-ramp (TMC 103-04121 start) | 2.5 | 3.2 | 29.7 | 22.8 | 23.4 |
| Stewart Avenue on-ramp to I–476 on-ramp (TMC103-04120 start) | 3.0 | 2.8 | 25.0 | 26.8 | 23.4 |
| Total southbound | 18.1 | 16.4 | 37.5 | 41.4 | −10.3 |

TT = travel time.

The initial I–95 model was from 2011 and was calibrated to GEH volume (which the team did not follow for this project) and corridor travel times. Table 45 through table 48 give the travel time calibration results from the 2011 study.

**Table 45. Morning travel time calibration measurements—northbound.**

| Measurement | Delaware State Line to US 322 Left Entry (Exit 3) | US 322 Left Entry (Exit 3) to Barry Bridge On-Ramp (Exit 4) | Barry Bridge On-Ramp (Exit 4) to I–476 Off-Ramp (Exit 7) | I–476 Off-Ramp (Exit 7) to Bartram Avenue On-Ramp (Exit 14) | Total—Delaware State Line to Bartram Avenue On-Ramp (Exit 14) |
|---|---|---|---|---|---|
| Field (min) | 3.24 | 2.45 | 1.81 | 7.54 | 15.03 |
| Model (min) | 3.10 | 2.37 | 2.20 | 8.78 | 16.45 |
| Difference (percent) | 4.3 | 3.2 | 22.0 | 16.5 | 9.5 |

**Table 46. Morning travel time calibration measurements—southbound.**

| Measurement | Enterprise Avenue Off-Ramp (Exit 15) to Past Airport Frontage Exit (Exit 13) | Airport Frontage Exit (Exit 13) to I–476 On-Ramp (Exit 7) | I–476 On-Ramp (Exit 7) to Delaware State Line | Total—Enterprise Avenue Off-Ramp (Exit 15) to Delaware State Line |
|---|---|---|---|---|
| Field (min) | 1.75 | 6.28 | 6.01 | 14.04 |
| Model (min) | 2.05 | 6.96 | 6.58 | 15.58 |
| Difference (percent) | 17.3 | 10.7 | 9.4 | 11.0 |

**Table 47. Evening travel time calibration measurements—northbound.**

| Measurement | Delaware State Line to US 322 Left Entry (Exit 3) | US 322 Left Entry (Exit 3) to Barry Bridge On-Ramp (Exit 4) | Barry Bridge On-Ramp (Exit 4) to I–476 Off-Ramp (Exit 7) | I–476 Off-Ramp (Exit 7) to Bartram Avenue On-Ramp (Exit 14) | Total—Delaware State Line to Bartram Avenue On-Ramp (Exit 14) |
|---|---|---|---|---|---|
| Field (min) | 4.85 | 3.07 | 2.45 | 7.66 | 18.04 |
| Model (min) | 4.23 | 2.73 | 1.93 | 8.49 | 17.38 |
| Difference (percent) | 12.8 | 11.3 | 21.2 | 10.8 | 3.7 |

**Table 48. Evening travel time calibration measurements—southbound.**

| Measurement | Enterprise Avenue Off-Ramp (Exit 15) to Past Airport Frontage Exit (Exit 13) | Airport Frontage Exit (Exit 13) to I–476 On-Ramp (Exit 7) | I–476 On-Ramp (Exit 7) to Delaware State Line | Total—Enterprise Avenue Off-Ramp (Exit 15) to Delaware State Line |
|---|---|---|---|---|
| Field (min) | 2.10 | 10.79 | 6.23 | 19.12 |
| Model (min) | 2.14 | 12.11 | 6.61 | 20.86 |
| Difference (percent) | 1.4 | 12.3 | 6.2 | 9.1 |

**Reasonableness of Animation**

Check 1: during the p.m. peak hour, both probe data and Google® Maps™ typical traffic data indicated heavy southbound congestion originating from the I–476 interchange. This was consistent in the Vissim model where queues extending beyond the Stewart Avenue interchange as shown in figure 72. Vehicles in Vissim were color-coded by their speed to easily identify congested segments, and figure 73 displays defined speed intervals for each color.

Check 2: in the northbound direction, the main bottleneck along the study corridor during the p.m. peak is the US 322 interchange where queues originating from this location extend beyond Chichester Avenue. Similar queuing and bottleneck conditions also occurred in the simulation model, as demonstrated in figure 74 and figure 75.
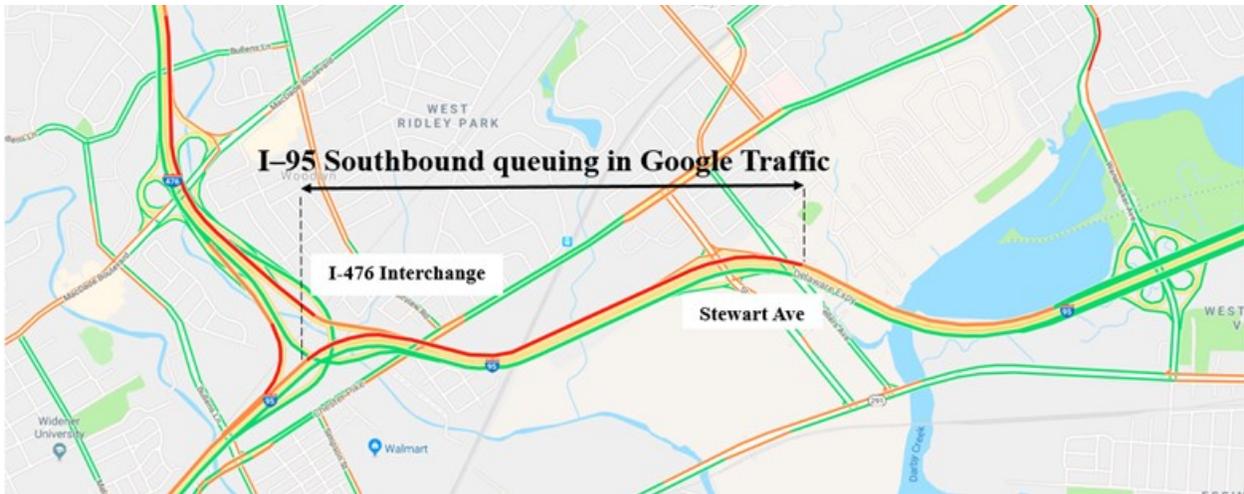
Original map: © 2017 Google® (see acknowledgements).

**Figure 72. Map. Typical Tuesday traffic at 5:00 p.m. for I–95 southbound.**
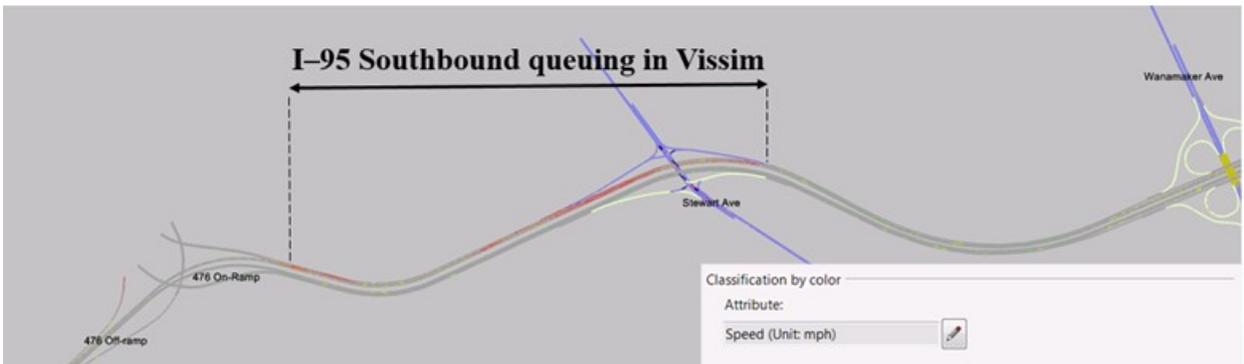


© 2019 Kittleson & Associates, Inc.

**Figure 73. Screenshot. Vissim screenshot during the p.m. peak hour for I–95 southbound.**
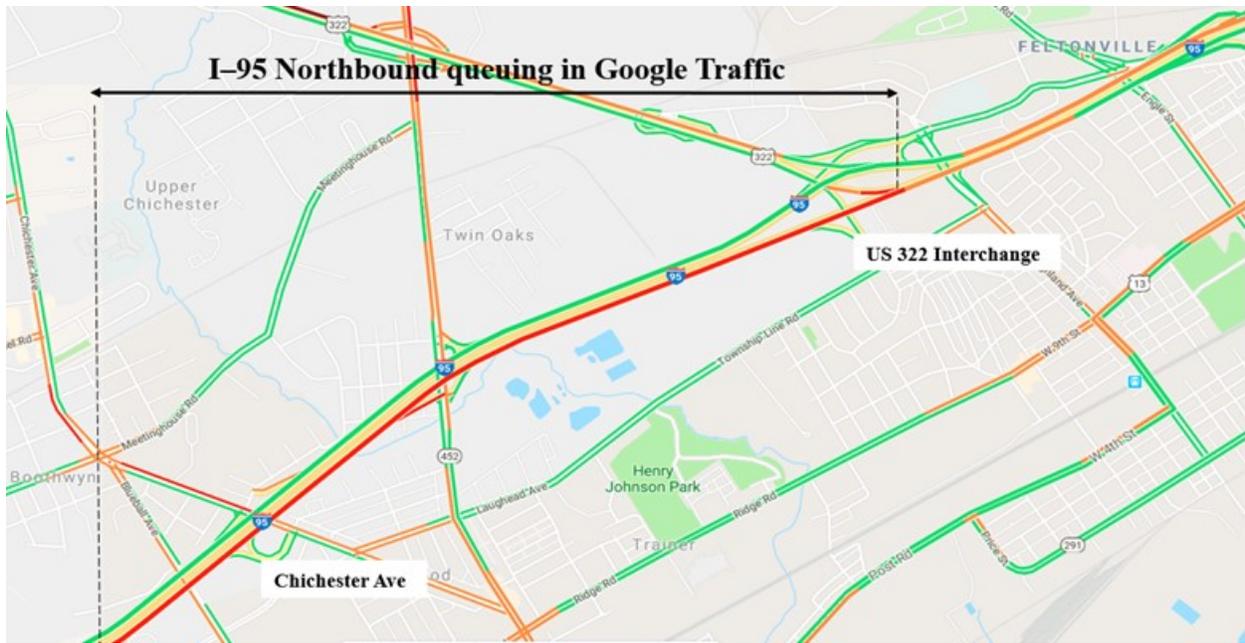
Original map: © 2017 Google® (see acknowledgements).

**Figure 74. Map. Typical Tuesday traffic at 5:00 p.m. for I–95 northbound.**
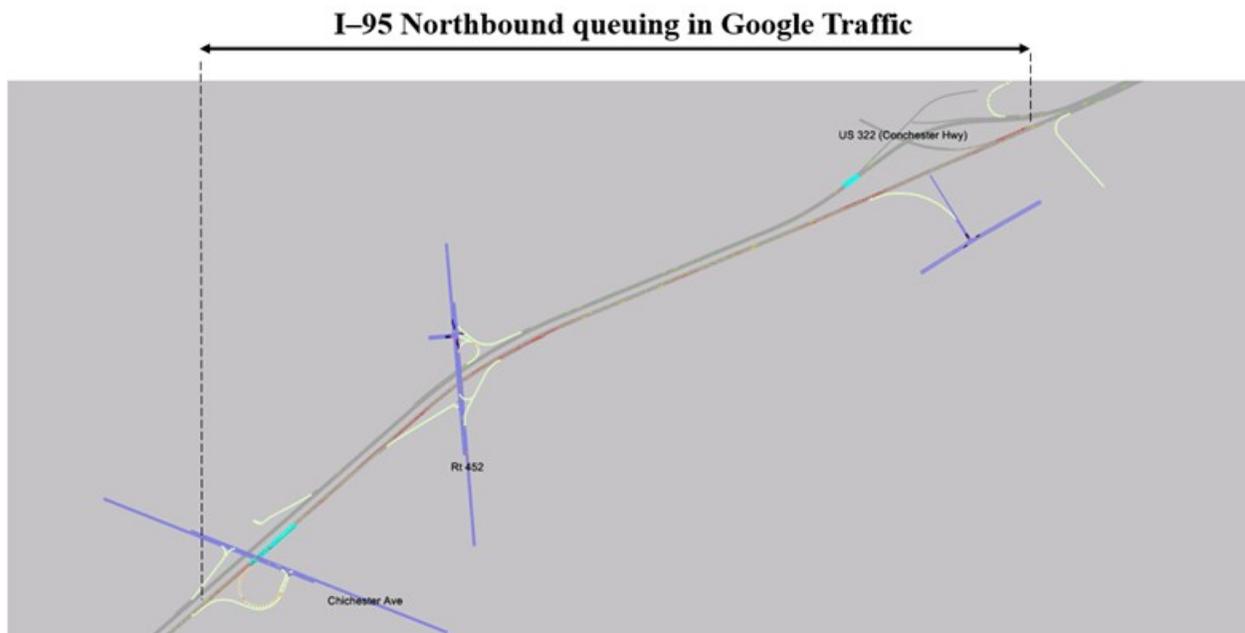


© 2019 Kittleson & Associates, Inc.

**Figure 75. Screenshot. Vissim screenshot during the p.m. peak hour for I–95 northbound.**

## I–35 KS VISSIM

### Background Information

This facility is approximately 10 mi long and it consists of several interchanges. The bottlenecks at the southbound direction are located at Southwest Boulevard (merge), Shawnee Mission Parkway (weave), and 67th Street (merge). The last two bottlenecks interact with each other, and it appears that queue from 67th Street propagates upstream to Shawnee Mission Parkway and even further upstream (spillback reaches the Metcalf Avenue interchange). At the southbound direction, KDOT is operating ramp metering at 7th Street, Southwest Boulevard, 18th Street, and 67th Street.

In the northbound direction, the facility is experiencing recurrent congestion at the 87th Street interchange (merge). In that direction, ramp meters operate at the 7th Street on-ramp and at Johnson Drive. Figure 26 is a map of the facility showing the congestion areas and the locations of the ramp meters. Only two of the six ramp meters were installed at bottleneck locations. Ramp metering was installed in the summer of 2017, and the algorithm that is currently used is the CARMA algorithm, which is a system-wide algorithm based on speeds. KDOT has decided to switch to another system-wide algorithm that uses occupancies as thresholds for metering rate determination. However, given that the metered ramps are not consecutive, it is impossible to leverage the full capabilities of a system-wide ramp metering algorithm.

### Overview

The team obtained permission from KDOT to use their I–35 Vissim model. KDOT provided the University of Kansas with the Vissim simulation network of the I–35 corridor, and the University of Kansas team performed the calibration task. The facility is equipped with radar sensors. Field data at those sensor locations along the freeway and the on-ramps are available to the researchers through Kansas City Scout (Kansas DOT and Missouri DOT 2018).

### Modeling the Facility

The geometric modeling of the facility in Vissim consists of creating links and connectors. All links in the Vissim model are modeled to have a 12-ft width and a number of lanes that correspond to the field. A background map was used to draw the links of I–35 southbound from Cambridge Drive to 75th Street, including on-ramps and off-ramps. Traffic signals on the adjacent arterial streets were removed from the simulation model because the signal timing and the volume distribution on the arterial was not known. Figure 76 is a schematic of the Vissim model.
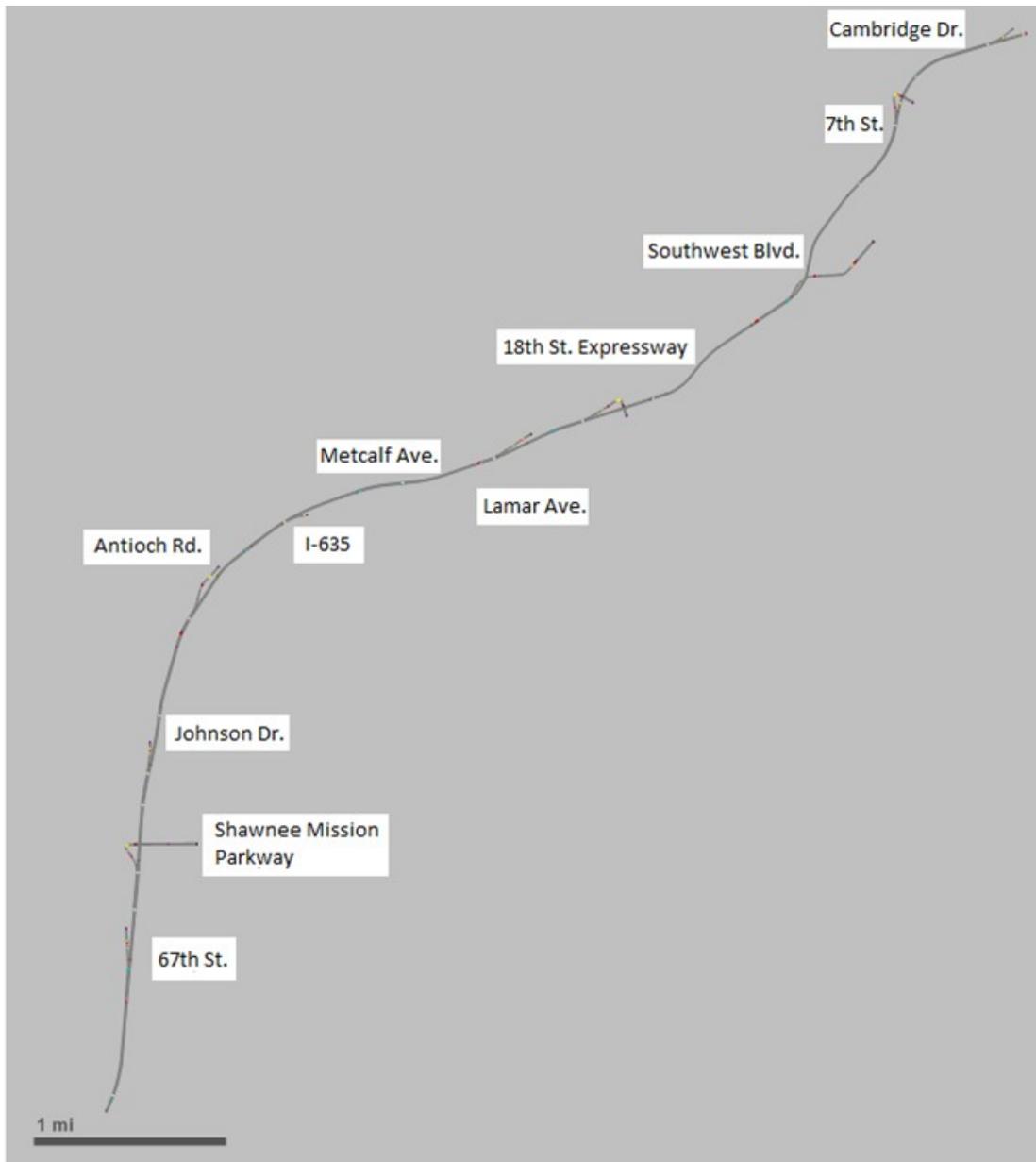
© 2018 Alexandra Kondyli.

**Figure 76. Screenshot. Vissim model of the I–35 KS corridor.**

## Data Inputs

Traffic volume and speed data at the mainline, on-ramp, and off-ramp were obtained from the Kansas City Scout Portal. The team selected a day without incidents or adverse weather throughout the corridor for the model calibration. The selected calibration day was April 22, 2016. The simulation period is the afternoon peak period from 3:15–6:15 p.m., and 25 min were added in the beginning of the simulation period for initialization. The Vissim model provided by KDOT was used to obtain the percentage of passenger cars, heavy goods vehicles, and large goods vehicles. For the desired speed, the mainline detectors' speed readings obtained from

Kansas City Scout Portal were reviewed and a mean speed of 64 mi/h was identified. The desired speed distribution follows an S-shaped curve.

**Model Calibration**

The speed distribution from the simulation has to match roughly the speed distribution of real-life data with an admissible error of 10 percent. The Vissim model is calibrated by changing the driver behavior parameters in the links and connectors.

The calibration was conducted by changing the values of multiple car following and lane changing parameters throughout the software. The calibration was done manually, by changing all relevant parameters on a one-at-a-time basis. The calibration day needs to start in uncongested conditions and end in uncongested conditions to verify that the calibrated model is functioning properly and that the modelling includes vehicle route decisions. To compare the simulation model to the calibration day, detectors were established in the Vissim model in the same locations that they exist in real life. After that, an initial simulation running using one random seed was conducted to compare the calibration day speed profile to the simulation model speed profile. Through the simulation animation, unrealistic driver behaviors were identified and were resolved with the help of the calibration. To achieve a speed profile similar to the calibration day, different sets of driver behavior parameters in links were developed and tested. This process was done on a trial and error basis depending on how well the simulation model represents the real world on each link. The process of running one seed and adjusting the parameters was executed until a similar speed profile was achieved. Then, the simulation model ran multiple times with different seeds. The average speed profile of those runs was compared to the calibration day speed profile.

The team adapted the connectors' lane change distance from Leyn and Vortisch (2015) for the simulation trials. According to Leyn and Vortisch (2015), lane distance for an off-ramp diverge should be at least 2,100 ft. The suggested value was used in the initial runs, and then it was adjusted for the next test runs so that the vehicle maneuverability looked realistic and the speed profile of the simulation roughly matched the calibration day speed profile.

The car following and lane changing parameters were adjusted to produce similar speed profiles to those of the calibration day. Table 49 and table 50 show the selected calibration values of the parameters. The Vissim model is calibrated by matching the speed profile obtained from Kansas City Scout to the calibrated model profile shown in figure 77 and figure 78. Based on the data, there are two active bottlenecks along the corridor. The first one is located at the interchange with 67th Street, and the second one is located at Southwest Boulevard. The simulation results also suggest that the calibration was able to replicate the active bottlenecks; however, the extent of congestion at the most downstream bottleneck is not replicated accurately. At the locations where the calibration was successful, the speed difference between field and simulated data was within 10 percent.

The team constructed speed-flow graphs of the calibrated and field-measured network to evaluate the fit of the calibration process. Figure 79 shows the speed-flow graph at selected locations.

**Table 49. Calibrated Wiedemann 99 model parameters.**

| Parameter | Default | Freeway | Diverge | Merge | Weave |
|-----------|---------|---------|---------|-------|-------|
| CC0 | 4.92 | 5.60 | 7.50 | 7.80 | 9.00 |
| CC1 | 0.90 | 1.05 | 1.15 | 1.30 | 1.45 |
| CC2 | 13.12 | 13.10 | 12.00 | 12.00 | 12.60 |
| CC3 | −8.00 | −8.00 | −8.00 | −8.00 | −8.00 |
| CC4 | −0.35 | −0.30 | −0.35 | −0.35 | −0.35 |
| CC5 | 0.35 | 0.30 | 0.35 | 0.35 | 0.35 |
| CC6 | 11.44 | 11.44 | 11.44 | 11.44 | 11.44 |
| CC7 | 0.82 | 0.82 | 0.82 | 0.82 | 0.82 |
| CC8 | 11.48 | 10.48 | 10.48 | 12.48 | 12.48 |
| CC9 | 4.92 | 4.92 | 4.92 | 4.92 | 4.92 |

CC0 = standstill distance; CC1 = spacing time; CC2 = following variation, maximum drift; CC3 = threshold for entering following; CC4 = negative following threshold; CC5 = positive following threshold; CC6 = speed dependency of oscillation; CC7 = oscillation acceleration; CC8 = standstill acceleration; CC9 = acceleration at 50 mph.

**Table 50. Calibrated lane changing parameters.**

| General Behavior | Default Free Lane Selection | Freeway Free Lane Selection | Diverge Free Lane Selection | Merge Free Lane Selection | Weave Free Lane Selection |
|---|---|---|---|---|---|
| Maximum deceleration – subject vehicle (ft/s$^2$) | −13.12 | −13.12 | −13.12 | −13.12 | −13.12 |
| Maximum deceleration – trailing vehicle (ft/s$^2$) | −9.84 | −9.84 | −9.84 | −9.84 | −12.00 |
| −1 ft/s$^2$ per distance – own (ft) | 100 | 300 | 200 | 300 | 400 |
| −1 ft/s$^2$ per distance – trailing vehicle (ft) | 100 | 200 | 200 | 200 | 400 |
| Accepted deceleration – own (ft/s$^2$) | −3.28 | −3.00 | −3.00 | −4.50 | −4.50 |
| Accepted deceleration – trailing vehicle (ft/s$^2$) | −3.28 | −2.25 | −3.00 | −3.00 | −4.50 |
| Waiting before diffusion(s) | 60 | 60 | 60 | 60 | 60 |
| Minimum headway (front/rear) | 1.64 | 1.64 | 1.64 | 1.64 | 1.64 |
| Safety distance reduction factor | 0.60 | 0.60 | 0.7 | 0.45 | 0.4 |
| Maximum deceleration for cooperative braking (ft/s$^2$) | −9.84 | −9.84 | −16.00 | −18.00 | −18.00 |
| Advanced merging | Activated | Activated | Activated | Activated | Activated |
| Cooperative lane change | Activated | Activated | Activated | Activated | Activated |
| Maximum speed difference | 1.84 | 16.00 | 16.00 | 16.00 | 16.00 |
| Maximum collision time | 10.00 | 10.00 | 10.00 | 10.00 | 10.00 |

**Figure 77. Map. Kansas City Scout speed profile.**

**Figure 78. Map. Calibrated Vissim model speed profile.**

A. Main 7th Street

D. Main 18th Street.

B. Main Southwest Boulevard upstream.
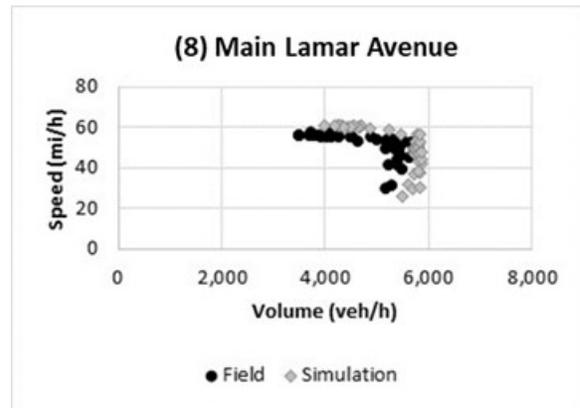
E. Main Lamar Avenue.
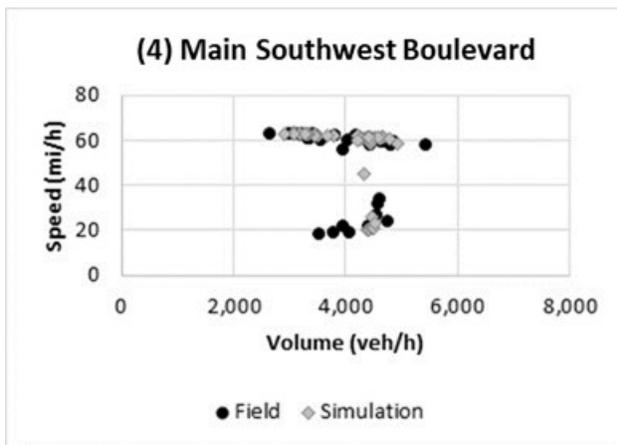
C. Main Southwest Boulevard.
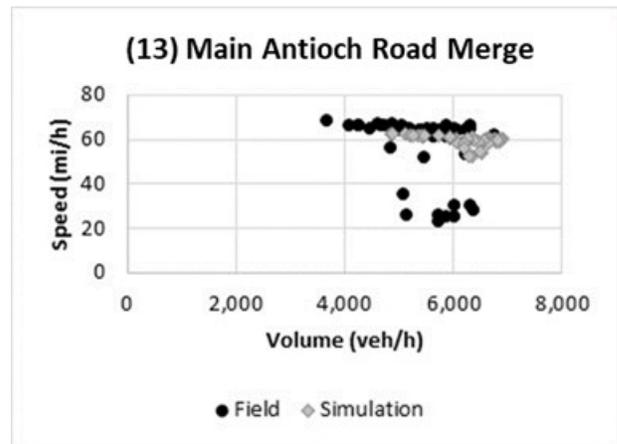
F. Main Antioch Road merge.
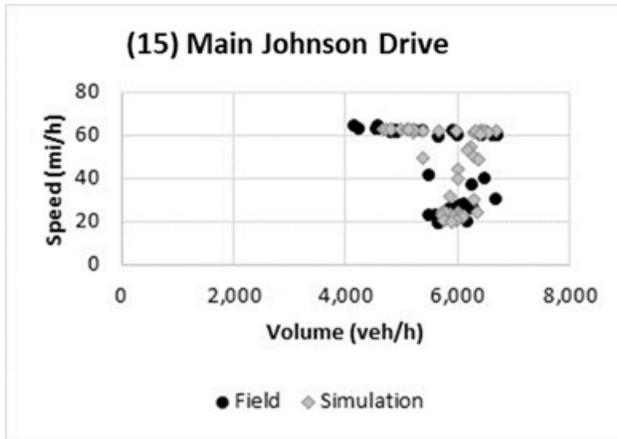
© 2019 Alexandra Kondyli.

G. Main Johnson Drive.
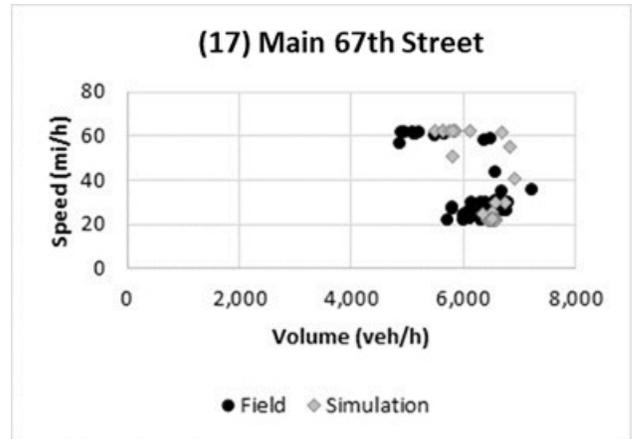


© 2019 Alexandra Kondyli.

I. Main 67th Street.
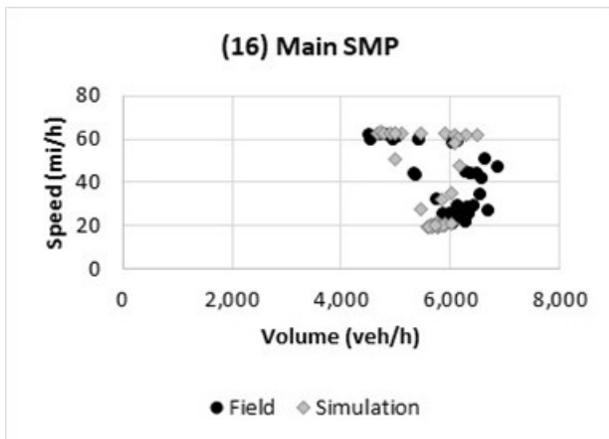


© 2019 Alexandra Kondyli.

H. Main SMP.
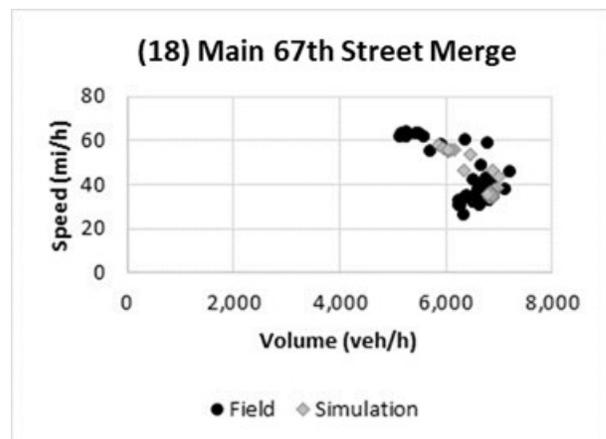


© 2019 Alexandra Kondyli.

J. Main 67th Street merge.

**Figure 79. Charts. Speed-flow graphs along the I–35 southbound corridor.**

## I–15 CA AIMSUN

### Background Information

The network contains the following characteristics:

- Total length: 20 mi.
- Starting and ending points: SR 52 at its southern end to SR 78 at its northern end.
- Number of lanes: 8–10.
- Speed limit: 65 mi/h.

## Overview

The calibration approach applied to the San Diego, CA, I–15 ICM Aimsun online model is based off of the approaches laid out by FHWA within the Traffic Analysis Toolbox Volume III and Volume IV: Guidelines for Applying CORSIM Microsimulation Modeling Software (Dowling et al. 2004; Holm et al. 2007).
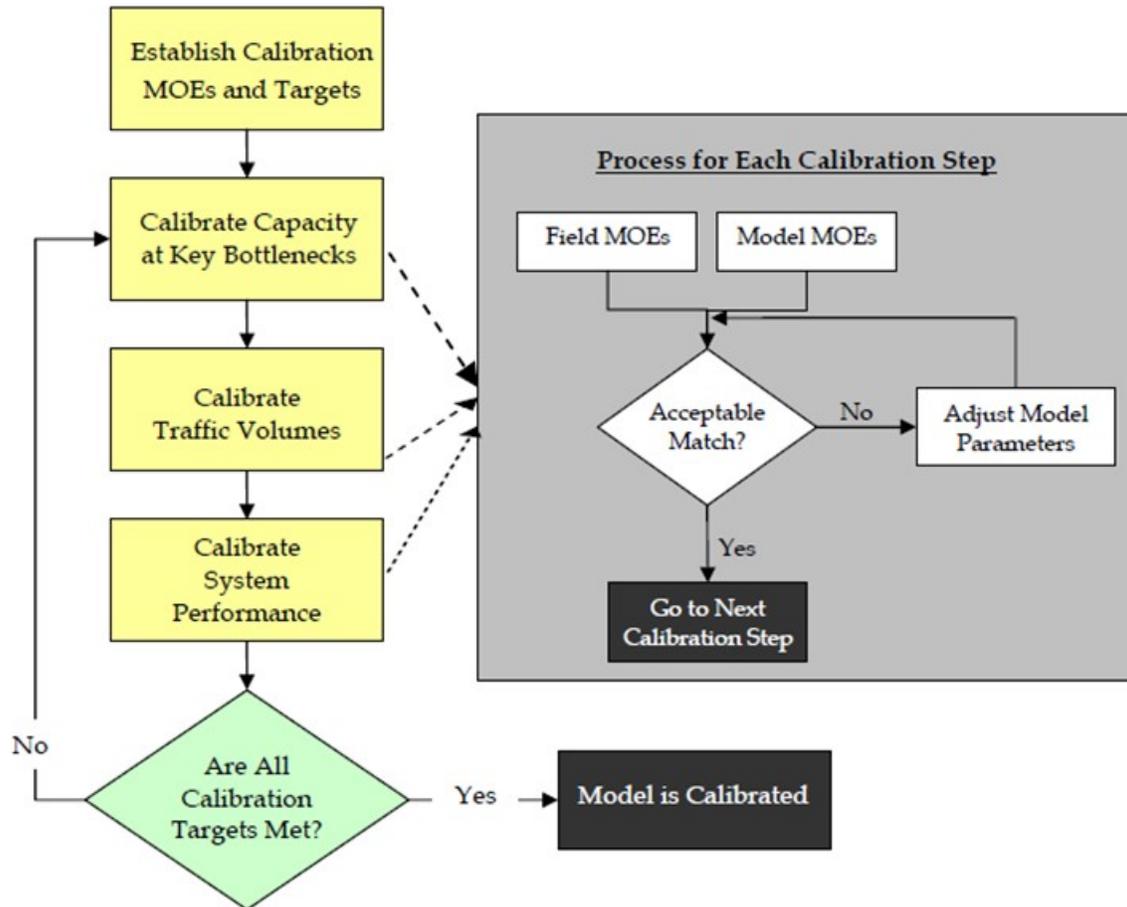


Source: FHWA.

**Figure 80. Diagram. Flowchart describing the calibration approach (Dowling, Skabardonis, and Alexiadis 2004).**

The data collection plan and its appendices detail the data points to be collected and the sources for each data point. The team used these data to calibrate and validate the base 24-h model. To replicate the various ITS that are currently part of the corridor, the model team created application programming interfaces (APIs) to emulate the functionality of the systems, including ramp metering. To ensure the system was properly calibrated for this purpose, tests on a single on-ramp at Carmel Mountain Road were performed by making sure the correct number of vehicles per green light were entering and that the system was properly activating and deactivating as well as stepping through the rate table. The prescribed check is as follows:

1. Warm up the network by running a relatively low demand for several hours to ensure network stabilization at a value other than 0.
2. Gradually increasing the mainline flow showed that the ramp metering follows the trend of the traffic volume and the rate is increased, thus reducing the input volume rate.
3. Decreasing the mainline flow showed the opposite trend of the previous step. The rate decreased until meeting the shutoff threshold, after which the ramp metering turned off.
4. Finally, traffic increased once more to show that the meter turned back on.

Throughout the process, the ramp meter functioned properly. The ramp meter turned on when reaching the threshold value (8,250 veh/h) for the associated mainline flow detector. Once the minimum release rate was reached, the flows were decreased and the on-ramp again responded accordingly by increasing the rate of discharge. Finally, when the mainline flow reached the threshold value for the shutdown (6,625 veh/h), the on-ramp turned off metering as expected.

After this, the team needed to verify the entire system, which was more of a general check by means of visually inspecting the network and did not involve stepping through all the rates for every location. The verification was as follows:

1. It is necessary to see the on-ramps moving through the rates as traffic increases in the peak periods of demand on the network.
2. The team checked the previous step for both a.m. and p.m., as different rate tables were used. It was important to verify that the system works in both peak periods. As the demand increased over the peak period, it was necessary that the systems adjusted the rates accordingly.

**Driver Behavior Calibration**

Calibration is the adjustment of the various local and global parameters available within a software package to ensure that the model is able to reproduce the local driver behavior, traffic conditions, and performance. Aimsun comes with default parameters, but those parameters provide a starting point and will rarely replicate the local behavior. Therefore, comparing against field-observed data, the analyst can go step by step through a calibration process to achieve this goal. While preparing to undertake the calibration, it is important that the analyst identify within Aimsun which parameters require no further adjustment and which should be reviewed in order to match local conditions. The adjustable set of parameters can then be divided into two classes: those that affect capacity and those that affect route choice.

*Calibration for Capacity*

For each vehicle type, the length and other characteristics were adjusted to meet North American standards (especially vehicle length to represent larger cars, as the defaults were closer to European values).

For the freeway capacity calibration, the main driver behavior parameter that influences capacity is the reaction time. By using an iterative process of comparing the calculated real-world capacities to the estimated model capacities as well as the flow/speed relation diagram, this global parameter was adjusted to 0.85 s. By comparing the correlation between speed drops and the development of congestion and queues, the team adjusted the speed acceptance and the

sensitivity factor to better represent real-world conditions and establish a reasonable representation of the correct capacity.

For surface street capacity calibration, the local and global parameters associated with intersection approaches and intersection movements were adjusted using an iterative process. By adjusting the reaction time at a stop (the time it takes a vehicle to react from a stopped position) and the reaction time at a signal (the time it takes a vehicle to react at a signal), the real-world and model intersection capacities were matched. Based on the analysis, the average approach capacity or saturation flow rate for signalized locations was approximately 1,495 veh/h/l. Prior to changing the parameters, the simulated saturation flows were significantly higher than those observed.

### *Calibration for Traffic Volumes and Route Choice*

Traffic volumes and flows were the principal measures of effectiveness (MOEs) used for the calibration of traffic volumes and route choice in the model. For the freeway sections, the volumes were compared at on-ramps, off-ramps, GP sections, and express lane sections. For the arterial sections, the volumes were compared at intersection approaches, turn movements, and mid-block sections.

The C-logit route choice model was chosen to calculate costs and paths for each O-D pair, as it takes into account the degree of overlapping among the different routes to reduce the tendency of the logit model to produce route oscillations resulting in a flip-flop process. A route choice recalculation cycle of 5 min was set to dynamically update the cost of alternative paths, and a scale factor of 2.5 ensured the correct distribution of trips along freeways and arterials. The attractiveness weight was set to 1.5 to favor freeways and wider roads instead of local roads when experiencing the same cost.

### Throughput Calibration

- Type: 24-h mainline freeway counts; source: Caltrans Performance Measurement System (PeMS) online database (California Department of Transportation 2019).
- Type: 24-h ramp counts; source: PeMS and ramp metering information system (RMIS) (San Diego Association of Governments 2008).
- Type: 24-h express lane counts; source: PeMS (limited) and congestion pricing system (CPS) (San Diego Association of Governments 2008).
- Type: 24-h arterial link counts; source: Sensys arterial travel time system (Wang et al. 2010).
- Type: 13-h turning movement counts; source: video counts.

Calibration targets were introduced to provide more granularity and visibility to the model and to help better understand the volumes and speeds. This enhanced granularity and detail helps show how the model has been able to replicate the real-world conditions. The team defined new criteria to draw a reference between the modeled and observed locations where the hourly volume was less than 2,000 veh/h. This volume was raised due to concerns of the levels of traffic observed on the local arterials. Showing the validation at all levels results in more confidence in the model.

To perform this analysis and provide more insight to the model, the various counts below 2,000 veh/h are summarized using two sets of guidelines. The first criterion shows counts within 15 percent of the observed count, in comparison to the following targets:

- 75 percent of flows between 750–20,00 veh/h with differences under 15 percent.
- 70 percent of flows between 0–750 veh/h with differences under 20 percent or under 150 veh/h.

The second criterion is the GEH.[1] GEH is a statistic often used in transportation modeling to show the representation between the modeled and observed counts/flows and to avoid some of the problems when only using absolute difference. The formula for the GEH is as follows:

$$GEH = \sqrt{\frac{2(M - C)^2}{M + C}}$$

(12)

Where:

$M$ = modeled volume in veh/h.
$C$ = observed volume in veh/h.

From documentation on GEH provided by the UK's Highway Agency and by Wisconsin Department of Transportation, GEHs with a value of 5.0 or lower are a representation of a very good fit. A GEH between 5.0 and 10.0 is a satisfactory fit and requires further investigation. A GEH greater than 10.0 is indicative of a potential error or a bad fit. Values greater than 10 are usually unavoidable in complex models but should be limited as much as possible. The following lists the criteria guidelines that Aimsun used to show the validation of the model, as previously agreed to with the San Diego Association of Governments:

- 85 percent GEH less than 5.0 for flows greater than 2,000 veh/h.
- 95 percent GEH less than 10.0 for flows greater than 2,000 veh/h.
- 70 percent GEH less than 5.0 for flows less than 2,000 veh/h.
- 95 percent GEH less than 10.0 for flows less than 2,000 veh/h.

Volumes and flows were able to meet the requirements and fell within the GEH < 10 criteria. For some outlying periods or shoulder hours, the count validation fell short of meeting the criteria (e.g., 9–10 a.m. flows between 750–2,000 veh/h within 15 percent was at 43 percent). This is because:

- 750–2,000 veh/h flow count samples were a much smaller range when compared to flow counts less than 750 veh/h.
- In a shoulder hour, it can be very tricky to always meet the calibration targets when the full period is as long as 4 or 5 h. In the live system, there are no shoulder hours in the

---

[1]The GEH formula gets its name from Geoffrey E. Havers, who invented it in the 1970s while working as a transportation planner in London, England.

model, as the model only runs for the next hour regardless if it is peak, off-peak, or in between. For 2016, the following criteria shown in table 51 were set.

**Table 51. Calibration criterial and acceptance targets for 2016.**

| Calibration Criteria and Measures | Calibration Acceptance Targets |
|---|---|
| Traffic flows within 15 percent of observed volumes for links with peak-period volumes greater than 2,000 veh/h | For 85 percent of cases for links with peak-period volumes greater than 2,000 veh/h |
| Sum of all link flows | Within 5 percent of sum of all link counts |
| Visual audits individual link speeds: visually acceptable speed-flow relationship | To analyst's satisfaction |
| Visual audits bottlenecks: visually acceptable queuing | To analyst's satisfaction |

The summary of link count reasonableness assessment results for a typical, no-incident day include:

- 91 of the 93 links (97 percent) met the 15 percent comparison criterion for the a.m. peak period—criterion one is met for the a.m. peak.
- 91 of the 96 links (94 percent) meet the 15 percent comparison criterion for the p.m. peak period—criterion one is met for the p.m. peak.
- 69 of the 70 links (98 percent) meet the 15 percent comparison criterion for the midday peak period—criterion one is met for the midday peak.
- The sum of all model link flows across all periods is 6,881,464, while the sum of observed link counts is 6,879,777. These volume sums are within 5 percent and thus criterion two is met for the three combined periods.
- The sum of all model link flows in the a.m. peak period is 2,407,128, while the sum of observed link counts is 2,407,567. These volume sums are within 5 percent and thus criterion two is met for the a.m. peak period.
- The sum of all model link flows in the p.m. peak period is 2,625,769, while the sum of observed link counts is 2,613,164. These volume sums are within 5 percent and thus criterion two is met for the p.m. peak period.
- The sum of all model link flows in the midday peak period is 1,848,567, while the sum of observed link counts is 1,859,046. These volume sums are within 5 percent and thus criterion two is met for the midday peak period.
- For all the peak periods, none of the arterial counts meet the required 2,000 veh/h, thus there is no criterion to meet. Although there are differences between observed and modeled arterial volumes, these counts are all included with the model sums for each period and thus the general flow of traffic along freeways and arterials meets criterion two.

**Calibration of Additional Measures**

Ramp metering:

- The team utilized the ITS API calibration.
- The team utilized 30-s data provided from the RMIS system and used it for the calibration of the ramp metering API within the Aimsun model.

Travel times:

- If not from the Sensys database, the team manually collected travel times for the major corridors throughout the model.
- Validation of the transit operations used and available transit vehicle travel times. The source of these data was the automatic vehicle location system and the RTMS.

Field measurements for the travel times included a combination of field-collected travel times and travel times available through the Sensys database. The model was adjusted to meet the target of modeled travel times within 15 percent of observed travel times in more than 85 percent of cases. Table 52 summarizes these results.

**Table 52. Number of travel times run and percentage by period.**

| Period | Number of Travel Times Runs | Percentage |
|---|---|---|
| Morning peak period 5:00–10:00 a.m. | {41 (62)} {pass travel times (total)} | 66 |
| Midday peak period 10:00 a.m.–2:00 p.m. | {34 (42)} {pass travel times (total)} | 81 |
| Evening peak period 2:00–7:00 p.m. | {39 (51)} {pass travel times (total)} | 76 |

*Queue Data*

Queue data were collected and used from a few sources. As queue data were not readily available, it is recognized that these data may not be fully accurate but were used as a base for the congestion in order to conduct the visual audit.

*Bottlenecks and Speed Contours*

For each section of the I–15 corridor, the PeMS database provided 5-min aggregated speed data (California Department of Transportation 2019). Although some stations were not providing observed data, aggregate PeMS data were used. To show the calibration of the I–15 mainline, speed contour diagrams were created from the PeMS data and the modeled data (average of 10 seeds, although any future comparisons based on non-typical day simulations would be produced only for one random seed).
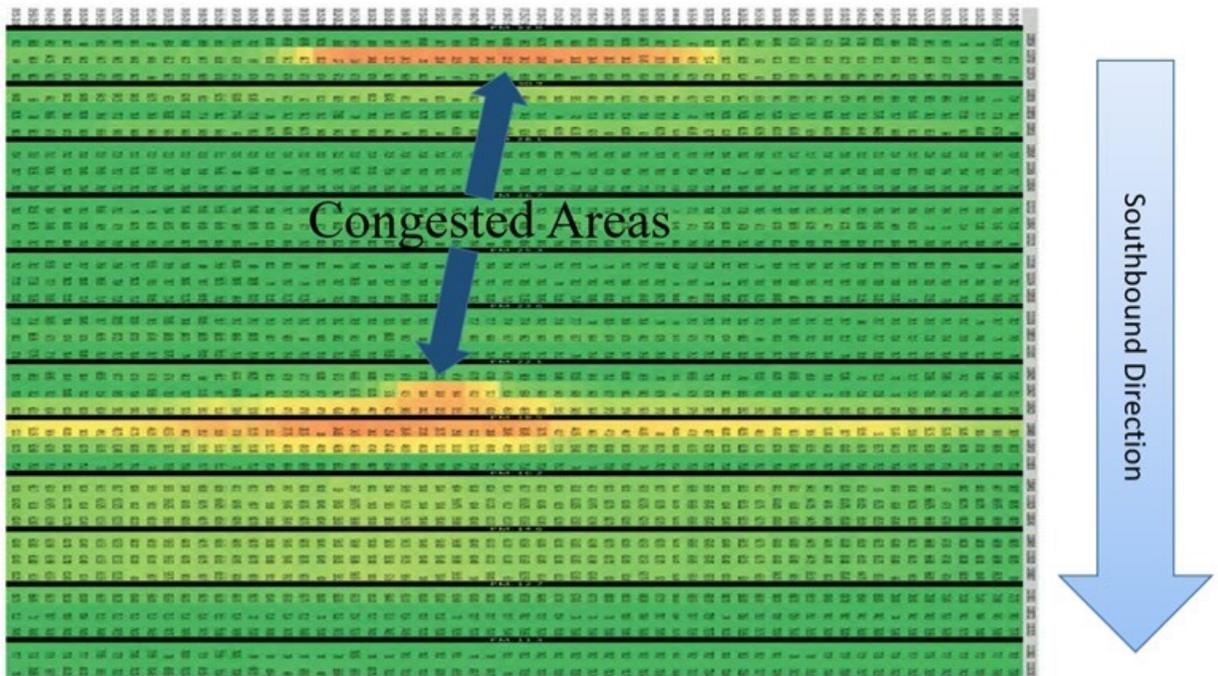
**Figure 81. Illustration. Updated PeMS I–15 a.m. southbound speed contour.**
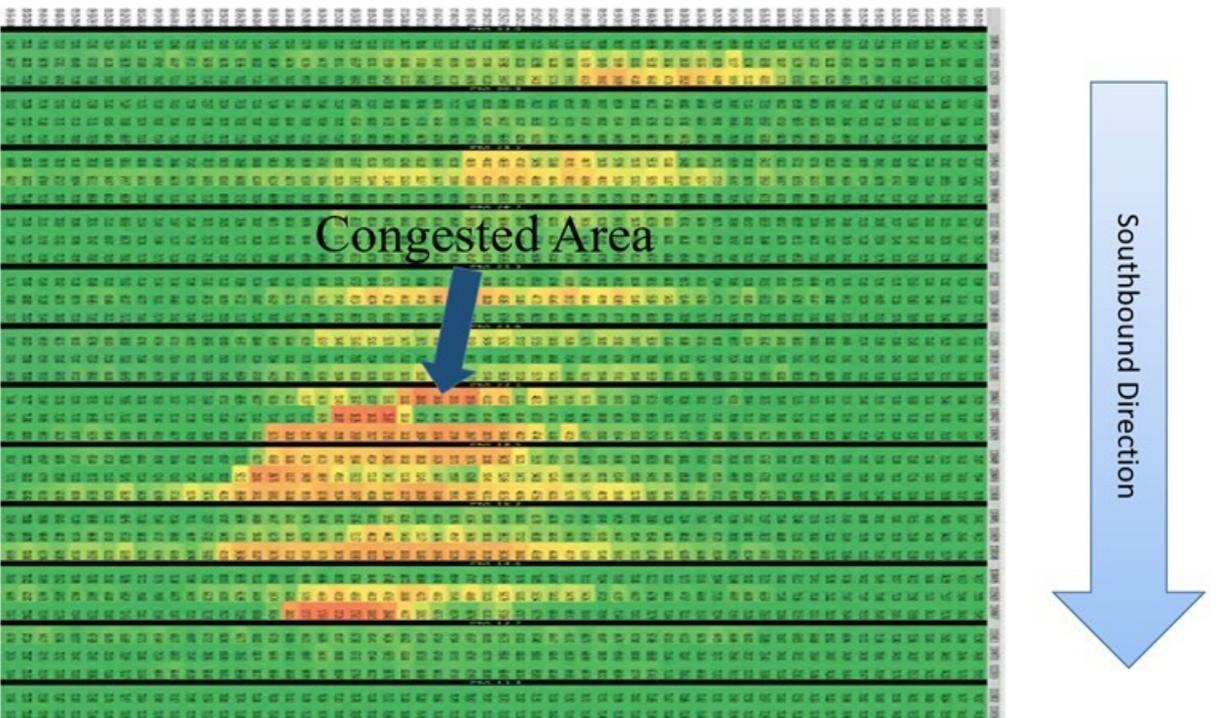
**Figure 82. Illustration. Updated Aimsun modeled I–15 a.m. southbound speed contour.**

The speed contours as well as the work done to match queues and bottlenecks served as the basis for the approval of the visual audit. Comparison of the real-world data and the modeled data showed a small contradiction because the data reported by the PeMS system were reduced significantly for the data collection period between February 1, 2012–May 1, 2012. It is the understanding of the group that the reduction was due to the construction within the express lanes and the upgrades to the advance traffic management system. Accordingly, the team worked with PeMS to better understand the process used to calculate speeds within PeMS and complete the comparison where higher levels of confidence were available.

**Reasonableness of Animation**

Following the latest visual audits, the team showed that the congestion levels within the model improved greatly. In particular, the mainline and CPS appeared to have much more reasonable levels of traffic for the a.m. and p.m. peaks. Due to the lack of recent PeMS data, further improvements to the bottlenecks and queuing could be required. Following the comments from the second San Diego Association of Governments' visual audit of bottlenecks and the review of the model conducted by the San Diego Association of Governments, a few questions were asked to the Freeway Service Patrol (FSP) drivers since they have the best knowledge of the network. The following are the a.m. questions asked, followed by the FSP response and the updated model solution or response:

- Between approximately 7:30–9:00 a.m., does the southbound mainline experience congestion between Bernardo Center Drive to Mercy Road?
  - FSP response: queue exists from Mercy Road to Sabre Springs Defense Access Road.
    - Model shows heavy traffic between Mercy Road to Carmel Mountain Road, with low speeds under 15 mi/h.
- Between approximately 7:45–8:30 a.m., does the southbound mainline experience congestion at Carroll Canyon Road?
  - FSP response: yes, slows to 10–15 mi/h due to Miramar Road congestion downstream.
    - Model represents this congestion at this time due to the merging movements at Carroll Canyon Road.
- Between approximately 7:30–9:00 a.m., does the southbound mainline experience congestion at Miramar Way?
  - FSP response: no.
    - In the model, this is generated by weaving movements before the I–15 mainline merge to SR 163. Some intermittent slow traffic is generated, but it is only minor and short-lived congestion.
- Between approximately 7:00–9:00 a.m., does the southbound mainline experience congestion north of SR 78?
  - FSP response: no.
    - In the model, this area is not congested during this time either.

The following are the responses to the p.m. FSP questions:

- Between approximately 4:00–6:00 p.m., does the northbound mainline experience congestion around Carroll Canyon Road?
  - FSP response: yes, bumper-to-bumper.
    - The model does show congestion, but not exactly "bumper-to-bumper." See the speed contour maps (figure 81 and figure 82).
- Between approximately 4:30–6:00 p.m., does the northbound mainline experience congestion between Bernardo Center Drive and Lake Hodges? (this is from PeMS but not in the simulation)
  - FSP response: yes, very heavy traffic.
    - The model does have congestion, but it is not too heavy. The model shows congestion is between the Via Rancho Parkway exit to Pomerado Road. Once the model is online and the PeMS detection is providing current not-pre-Thanksgiving data, the model will be fine-tuned.
- Between approximately 4:30–6:00 p.m., does the northbound mainline experience congestion between Lake Hodges and SR 78?
  - FSP response: yes, from Valley Parkway to the SR 78 ramps.
- If so, is it related to the northbound-to-westbound connection between I–15 and SR 78? If not, can other choke points be identified?
  - FSP response: yes, related to the northbound-to-westbound connector ramp.
    - The updated model does have congestion along all connector ramps from I–15 to SR 78.
- Between approximately 4:00–6:00 p.m., does the eastbound-to-southbound connector ramp between SR 78 and I–15 experience congestion?
  - FSP response: yes, traffic on the connector is heavy but still flowing.
- If so, how far back on SR 78 is the queue?
  - FSP response: the queue goes back to the beginning of the off-ramp on SR 78.
    - The model has some traffic at this location, but is not currently able to represent the true level of congestion. As better live data become available, the model will be improved. It should be noted that the model at SR 78 is only calibrated for I–15 and not to the same level for SR 78.
- Between approximately 4:00–6:00 p.m., does eastbound SR 56 experience congestion and a queue from the Ted Williams interchange?
  - FSP response: yes, the queue goes back to the Rancho Peñasquitos interchange.
    - The model has some traffic, but it does not go back to the Rancho Peñasquitos interchange (approximately halfway). As better real-time data become available, this congestion will be improved.
- Between approximately 4:00–6:00 p.m., does the northbound mainline experience congestion north of SR 78?
  - FSP response: no.
    - The model also shows no congestion north of SR 78 in northbound mainline I–15.
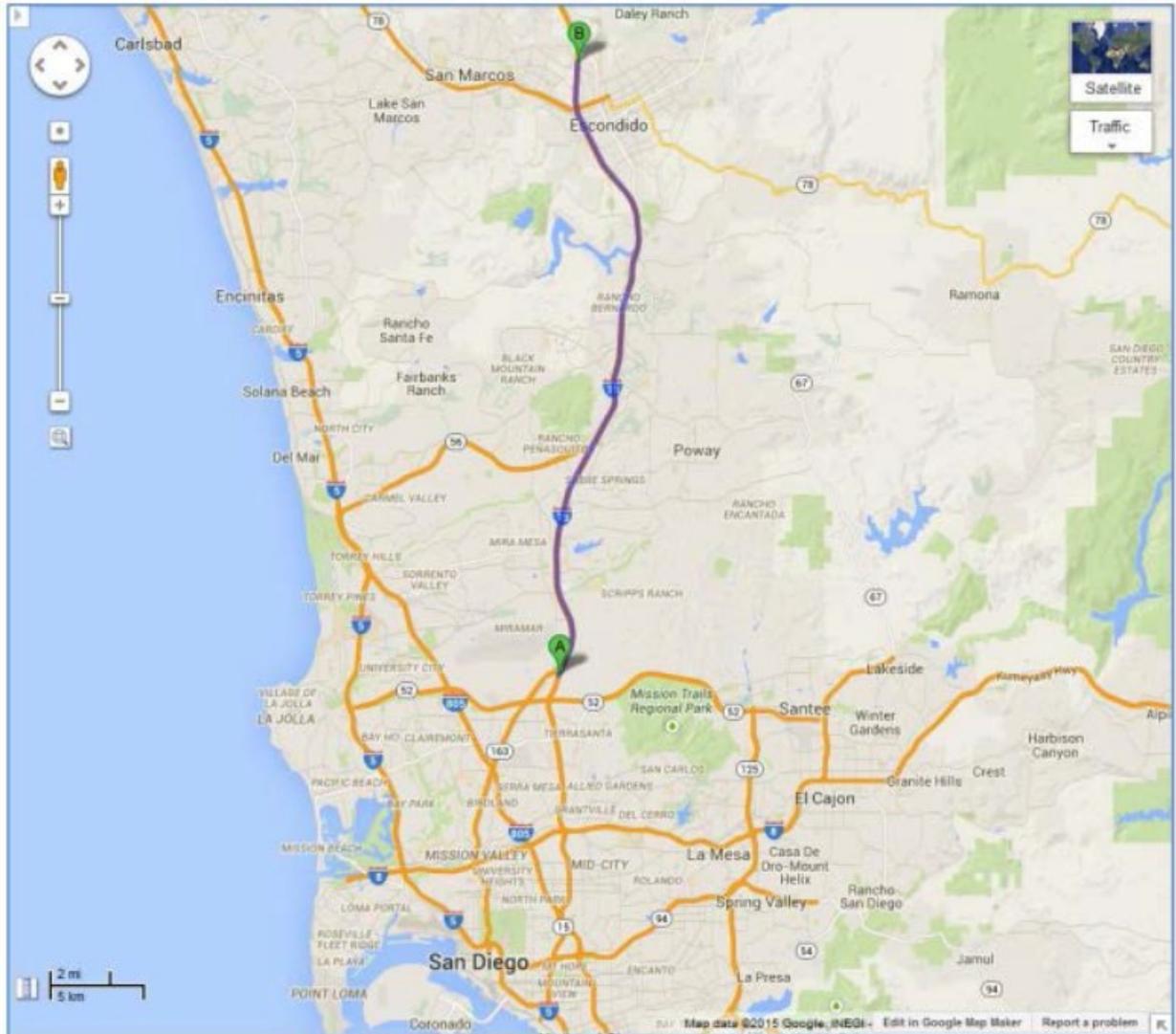
Original photo: © 2017 Google® (see acknowledgements).

**Figure 83. Map. Location and geographic boundaries of the I–15 corridor (Dion and Skabardonis 2015).**

## I–394 MN TSIS-CORSIM

### Background Information

The I–394 TSIS-CORSIM model is for the length of I–394 in Minnesota between I–494 and I–94, as illustrated in figure 84 and figure 85. The I–394 network was calibrated by MnDOT. Because the calibration outcomes were relatively recent and reasonable, no additional calibration was performed by the researchers.

Original map: © 2017 Google® (see acknowledgements).

**Figure 84. Map. Calibrated 8-mi stretch of I–394 eastbound between I–494 and I–94.**



© 2019 Minnesota Department of Transportation.

**Figure 85. Map. Speed limits near Minneapolis.**

## Overview

Volume data is from September 30, 2014. This was a Tuesday. The a.m. model was calibrated according to volumes and speeds along the parameters set out in chapter 6 of the Advanced TSIS-CORSIM Manual found on the MnDOT website in early 2017 (Minnesota Department of Transportation 2017). To enhance the calibration, other checks have been added that are not listed in the manual. Proportions of inequality are used to check the fit of the simulated data to the real data for both volumes and speed. Volumes are also checked using the GEH statistic with a target of under 5 percent (less than 3 percent preferred) for the peak hour and under 3 percent for the 3-h simulation. Results are also compared to the 2017 Congestion Report to verify that congestion is occurring in the correct areas and for the same time (by use of animation files) (Minnesota Department of Transportation 2017).

157

The team obtained spreadsheets[2] from MnDOT listing the balanced 2014 volumes, a calibration worksheet that checks the percentages (volumes of 10 percent, speed of 20 percent), and a graphical representation of the I–394 corridor. The graphical representation is complete with peak hour modeling results at both the segment and by lane level. MnDOT also provided speed limits for I–394 between TH 169 and I–94, and the 2014 Congestion Report (Minnesota Department of Transportation 2014). Proportions of inequality can be found in the CalibVolume or CalibSpeed tabs of the spreadsheet. GEH values can be found in the FREReport tab. Other information related to developing the TSIS-CORSIM input file is also in this Excel document.

**Throughput Calibration**

The throughput calibration sheet provides simulated volumes, which are transferred to the main calibration spreadsheet. Figure 86 and figure 87 illustrate the user interface of the calibration spread sheet. Although the throughput numbers in figure 86 are not legible in the context of this report, the team reviewed these numbers and plots to determine that throughputs from the microsimulation model were reasonably accurate. The same is true for the calibration of speeds and densities, as shown in figure 87 and figure 88.
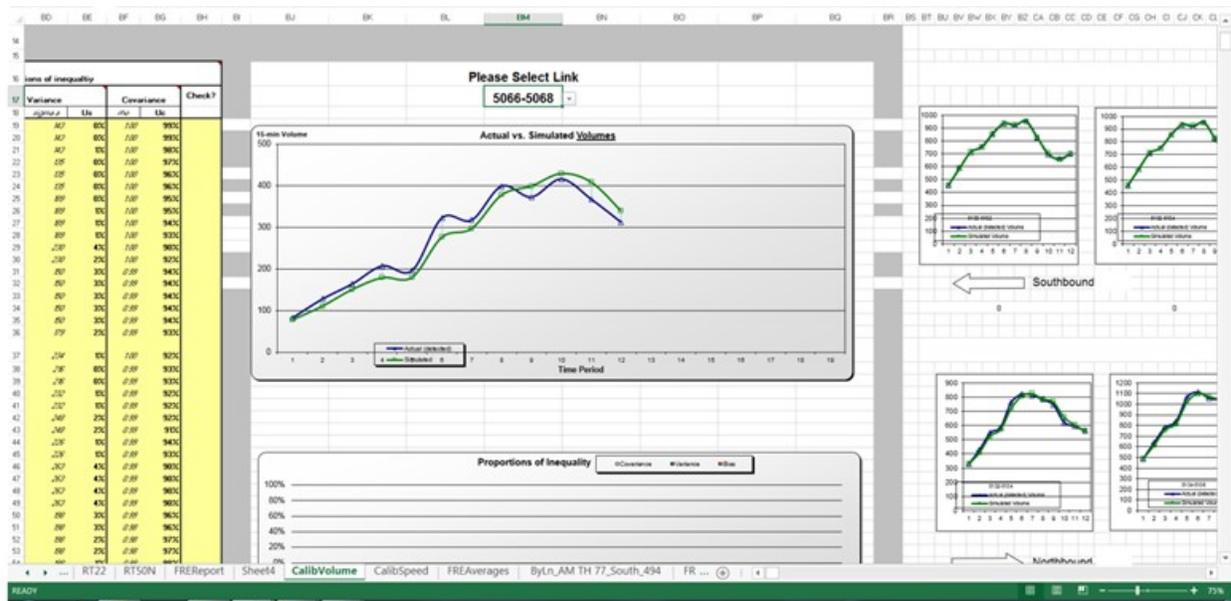


© 2019 Minnesota Department of Transportation

**Figure 86. Screenshot. Calibration of I–394 MN volumes.**

**Calibration of Additional Measures**

The team further reviewed the calibration of speed data and density data, as shown in figure 87 and figure 88.

---

[2]The spreadsheet documents are unpublished.
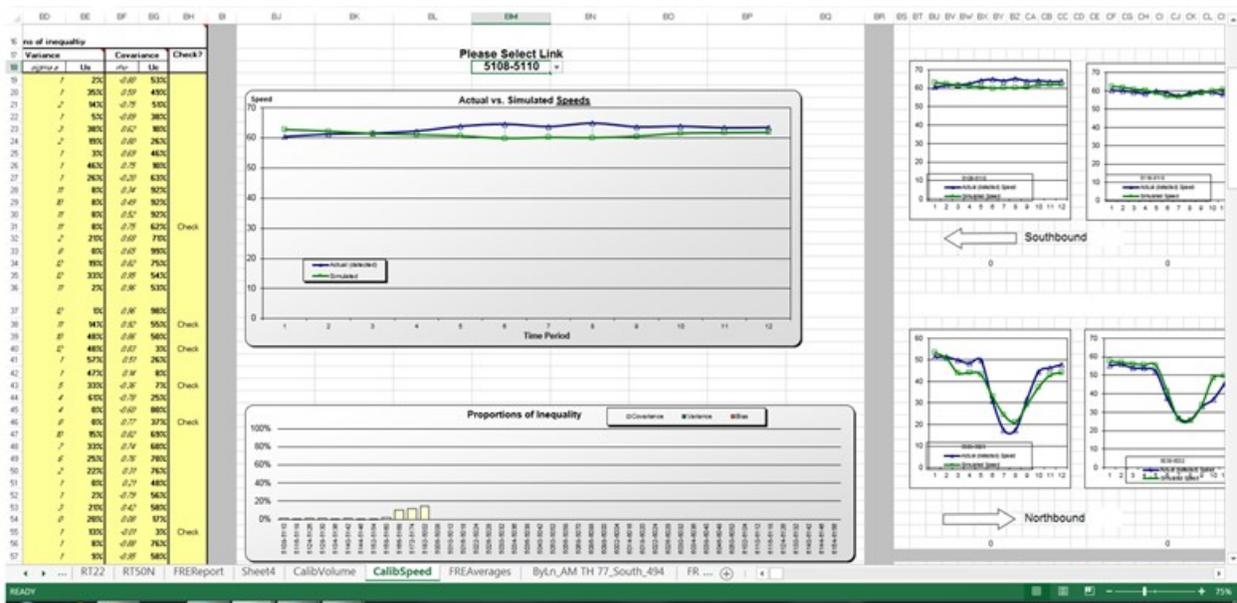
© 2019 Minnesota Department of Transportation.

**Figure 87. Screenshot. Calibration of I–394 MN speeds.**
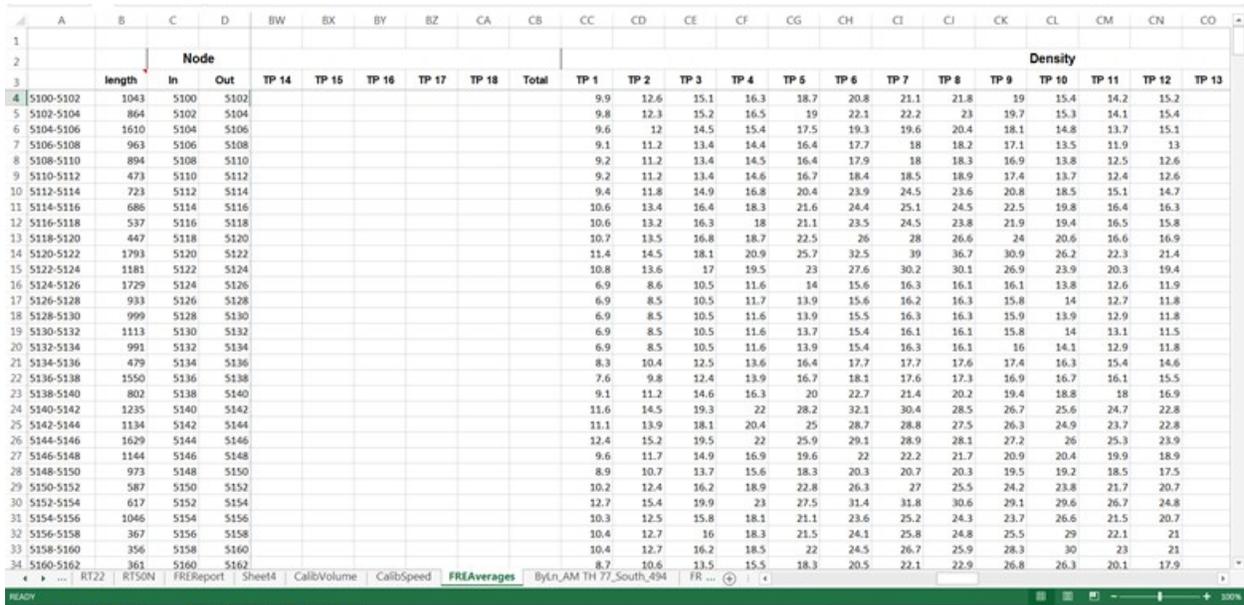


© 2019 Minnesota Department of Transportation.

**Figure 88. Screenshot. Calibration of I–394 MN densities.**

## Reasonableness of Animation

The review of animation will consider the consistency of animated and field-measured results (regarding congested segments and time periods) and the existence of any "stuck" vehicles.

Check 1: the MnDOT calibration spreadsheet showed level of service (LOS) F (forced or breakdown flow) during the "MOE hour" (i.e., 7:00–8:00 a.m., or time periods 5 through 8 out

of 12) between upstream node 5172 and downstream node 5008. This was mostly consistent with the animation shown in figure 89. Segment 5006–5008 seemed like it might be slightly better than LOS F, but the density (43 vehicles per mile per lane) was right on the LOS F threshold. Queuing began to form in time period 5 near downstream node 5006. The furthest upstream node (5172) did not experience congestion until time period 8 (i.e., the queue gradually became longer and stretched further upstream between time period 5 and time period 8).



Source: FHWA.

**Figure 89. Screenshot. Formation of queue spillback on I–394 MN.**

Check 2: a similar situation occurred between upstream node 5022 and downstream node 5048, except this time the queue seemed to extend well upstream of node 5022. This is shown in figure 90.



Source: FHWA.

**Figure 90. Screenshot. Queue spillback extent on I–394 MN.**

The original hypothesis was that a different version of TSIS-CORSIM may have been used to generate the performance measures used for calibration, but this was not the case. Instead, the reason for link 5020–5022 not showing up as LOS F has to do with the 500-ft lane drop. When the toolset calculates the link MOEs, it includes the lane drop as part of the number of lanes. As this lane drop is a little over half the length of the link, this is causing the link speed and density numbers to be better than anticipated. This also happens on links with lane additions, acceleration lanes, and deceleration lanes. This discovery gave more confidence that the model was calibrated well.

# ACKNOWLEDGEMENTS

The original map depicted in figure 26 is the copyright property of Google® Maps™ and can be accessed from https://www.google.com/maps. The map shows the congested areas and ramp locations of I–35 northbound and southbound.

The original map depicted in figure 27 is the copyright property of Google® Maps™ and can be accessed from https://www.google.com/maps. The map indicates the I–66 study corridor for this research project.

The original map depicted in figure 28 is the copyright property of Google® Maps™ and can be accessed from https://www.google.com/maps. The map overlay indicates the locations of six interchanges on the I–66 study corridor and the data collection instruments near each intersection. The overlay was developed as a result of this research project.

The original map depicted in figure 41 is the copyright property of Google® Maps™ and can be accessed from https://www.google.com/maps. A map overlay serves to indicate the segment of I–35 in Kansas City, KS, that is being called out in a satellite image. The overlay was developed as a result of this research project.

The original maps depicted in figure 50 are the copyright property of Google® Maps™ and can be accessed from https://www.google.com/maps. The overlay for each map uses red or blue lines to indicate the locations of INRIX traffic management centers on I–66. The overlay was developed as a result of this research project.

The original map depicted in figure 51 is the copyright property of Google® Maps™ and can be accessed from https://www.google.com/maps. The map overlay indicates the locations of zones 1 through 10. The overlay was developed as a result of this research project.

The original map depicted in figure 55 is the copyright property of Google® Maps™ and can be accessed from https://www.google.com/maps. A map overlay serves to indicate the recurring congestion segments of I–270 in Maryland. The overlay was developed as a result of this research project.

The original map depicted in figure 56 is the copyright property of Google® Maps™ and can be accessed from https://www.google.com/maps. The map overlay includes a field-measured heat map illustrating speeds on the study section shown in the map during the 4-h morning period of 6–10 am. The overlay was developed as a result of this research project.

The original map depicted in figure 57 is the copyright property of Google® Maps™ and can be accessed from https://www.google.com/maps. The map overlay includes a field-measured heat map illustrating speeds on the study section shown in the map during the 4-h evening period of 4–8 p.m. The overlay was developed as a result of this research project.

The original map depicted in figure 58 is the copyright property of Google® Maps™ and can be accessed from https://www.google.com/maps. The map overlay includes a field-measured heat map illustrating speeds on the study section shown in the map during the evening peak hour with location benchmarks. The overlay was developed as a result of this research project.

The original map depicted in figure 59 is the copyright property of Google® Maps™ and can be accessed from https://www.google.com/maps. The map overlay includes a field-measured heat map illustrating speeds on the study section shown in the map during the morning peak hour with location benchmarks. The overlay was developed as a result of this research project.

The original map depicted in figure 60 is the copyright property of Google® Maps™ and can be accessed from https://www.google.com/maps. The map overlay includes a field-measured heat map illustrating speeds on the study section shown in the map during the afternoon peak period with location benchmarks. The map overlay includes simulation animations that match the field-measured speed heat map for most space-time points measured at 7:10 a.m. The overlay was developed as a result of this research project.

The original map depicted in figure 61 is the copyright property of Google® Maps™ and can be accessed from https://www.google.com/maps. The map overlay includes simulation animations that match the field-measured speed heat map for most space-time points measured at 7:20 a.m. The overlay was developed as a result of this research project.

The original map depicted in figure 62 is the copyright property of Google® Maps™ and can be accessed from https://www.google.com/maps. The map overlay includes simulation animations that match the field-measured speed heat map for most space-time points measured at 7:30 a.m. The overlay was developed as a result of this research project.

The original map depicted in figure 63 is the copyright property of Google® Maps™ and can be accessed from https://www.google.com/maps. The map overlay includes simulation animations that match the field-measured speed heat map for most space-time points measured at 7:40 a.m. The overlay was developed as a result of this research project.

The original map depicted in figure 64 is the copyright property of Google® Maps™ and can be accessed from https://www.google.com/maps. The map overlay includes simulation animations that match the field-measured speed heat map for most space-time points measured at 5:10 p.m. The overlay was developed as a result of this research project.

The original map depicted in figure 65 is the copyright property of Google® Maps™ and can be accessed from https://www.google.com/maps. The map overlay includes simulation animations that match the field-measured speed heat map for most space-time points measured at 5:20 p.m. The overlay was developed as a result of this research project.

The original map depicted in figure 66 is the copyright property of Google® Maps™ and can be accessed from https://www.google.com/maps. The map overlay includes simulation animations that match the field-measured speed heat map for most space-time points measured at 5:40 p.m. The overlay was developed as a result of this research project.

The original map depicted in figure 72 is the copyright property of Google® Maps™ and can be accessed from https://www.google.com/maps. The map shows heavy southbound congestion originating from the I–476 interchange.

The original map depicted in figure 74 is the copyright property of Google® Maps™ and can be accessed from https://www.google.com/maps. The map shows queues originating at the US 322 interchange and extending beyond Chichester Avenue.

The original map depicted in figure 83 is the copyright property of Google® Maps™ and can be accessed from https://www.google.com/maps. This map shows the upstream and downstream endpoints of the I–15 corridor.

The original map depicted in figure 84 is the copyright property of Google® Maps™ and can be accessed from https://www.google.com/maps. The map shows the calibrated 8-mi stretch of I–394 eastbound between I–494 and I–94.

# REFERENCES

Cothron, A. Scott, Stephen E. Ranft, Carol H. Walters, David W. Fenno, and Dominique Lord. 2003. *Guidance for Future Design of Freeways with High-Occupancy Vehicle (HOV) Lanes Based on an Analysis of Crash Data from Dallas, Texas*. Washington, DC: Federal Highway Administration. https://static.tti.tamu.edu/tti.tamu.edu/documents/0-4434-P1.pdf.

AASHTO. 2018. *A Policy on Geometric Design of Highways and Streets, 7th Edition*. Washington, DC: American Association of State Highway and Transportation Officials.

Ahn, S., Robert L. Bertini, Benjamin Auffray, June H. Ross, and Oren Eshel. "Evaluating Benefits of Systemwide Adaptive Ramp-Metering Strategy in Portland, Oregon." *Transportation Research Record* 2012, (December 2007): 47–56. https://doi.org/10.3141/2012-06.

Aimsun. 2019. Aimsun (website). Accessed October 7, 2019. https://www.aimsun.com.

Amini, Nima, Hanna Grzybowska, Kasun Wijayaratna, and S. Travis Waller. 2015. "Aimsun HERO Implementation." Presented at *The 2015 IEEE 18th International Conference on Intelligent Transportation Systems*, Las Palmas, Gran Canaria, Spain, September 15–18, 2015. Washington, DC, IEEE Computer Society.

Avelar, R., Kay Fitzpatrick, Karen Dixon, and Tomas Lindheimer. 2016. "The Influence of General Purpose Lane Traffic on Managed Lane Speeds: An Operational Study in Houston, Texas." *Transportation Research Procedia* 15, (June) 548–560. https://doi.org/10.1016/j.trpro.2016.06.046.

Bared, J. and Wei Zhang. 2016. *Synthesis of the Median U-Turn Intersection Treatment, Safety and Operational Benefits*. Washington, DC: Federal Highway Administration. https://www.fhwa.dot.gov/publications/research/safety/07033.

Belisle, F., Laura Torres, Pascal Volet, David K. Hale, and Anjana Avr. 2019. "Evaluating the HERO Ramp-Metering Algorithm with San Diego's Integrated Corridor Management System Model." *Transportation Research Record*, (July 2019). https://doi.org/10.1177/0361198119858078.

Caltrans PeMS. 2019. California Department of Transportation (website). Accessed June 14, 2019. http://pems.dot.ca.gov.

California Department of Transportation. 2011. *Updated Managed Lane Design: Traffic Operations Policy Directive 11-02*. Sacramento, CA: Caltrans.

Cambridge Systematics, Inc. 2018. *WestConnect Planning and Environmental Linkages (PEL) Study*. Denver, CO: Colorado Department of Transportation. https://drive.google.com/file/d/1gskECp_eva-8zIgNFL_HqEcaJa3WUPgO/view.

Dowling, R., Alexander Skarbardonis, and Vassili Alexiadis. 2004. *Traffic Analysis Toolbox Volume III: Guidelines for Applying Traffic Microsimulation Software*. Washington, DC: Federal Highway Administration. https://ops.fhwa.dot.gov/trafficanalysistools/tat_vol3/vol3_guidelines.pdf.

Dowling, R., Paul Ryus, Bastian Schroeder, Michael Kyte, F. Thomas Creasey, Nagui Rouphail, Ali Hajbabaie, and Danica Rhoades. 2016. *Planning and Preliminary Engineering Applications Guide to the Highway Capacity Manual*. Washington, DC: The National Academies Press. https://doi.org/10.17226/23632.

Dowling, R., Rich Margiotta, and Leslie Jacobsen. 2011. *Evaluation of Operational and Safety Characteristics of Shoulders Used for Part-time Travel Lanes*. Washington, DC: Federal Highway Administration.

Faulkner, L., Frans Dekker, David G. Gyles, Ioannis. Papamichail, and Markos Papageorgiou. 2014. "Evaluation of HERO-Coordinated Ramp Metering Installation at M1 and M3 Freeways in Queensland, Australia." *Transportation Research Record* 2470, no 1 (January): 13–23. https://doi.org/10.3141/2470-02.

Fitzpatrick, K. and Raul Avelar. 2016. *Safety Implications of Managed Lane Cross Sectional Elements*. Washington, DC: Federal Highway Administration. https://ops.fhwa.dot.gov/publications/fhwahop16076/fhwahop16076.pdf.

Fitzpatrick, K., Marcus A. Brewer, and Steven Venglar. 2003. *Managed Lane Ramp and Roadway Design Issues*. Washington, DC: Federal Highway Administration. http://tti.tamu.edu/documents/4160-10.pdf.

Ghiasi, A., David K. Hale, Joe Bared, Alexandra Kondyli, and Jiaqi Ma. 2018. "A Dynamic Signal Control Approach for Integrated Ramp and Mainline Metering." Presented at the *21st IEEE International Conference on Intelligent Transportation Systems, Maui, HI, November 4–7, 2018*. https://ieeexplore.ieee.org/document/8569567.

Ghiasi, A., Jiaqi Ma, Fang Zhou, and Li Xiaopeng. 2017. "Speed Harmonization Algorithm Using Connected Autonomous Vehicles." Presented at the *Transportation Research Board 96th Annual Meeting, Washington, DC, January 8–12, 2017*. http://amonline.trb.org/63532-trb-1.3393340/t024-1.3404251/798-1.3404376/17-02565-1.3404418/17-02565-1.3404419?qr=1.

Hale, D., Thomas Phillips, Kelli Raboy, Jiaqi Ma, Patrick Su, Xiao-Yun Lu, Hesham Rakha, and Daniel J. Dailey. 2016. *Introduction of Cooperative Vehicle-to-Infrastructure Systems to Improve Speed Harmonization*. Washington, DC: Federal Highway Administration. https://www.fhwa.dot.gov/publications/research/operations/16023/16023.pdf.

HERE Traffic. 2019. Here (website). Accessed October 7, 2019. https://www.here.com/products/traffic-solutions.

Holm, P., Daniel Tomich, Jaimie Sloboden, and Cheryl Lowrance. 2007. *Traffic Analysis Toolbox Volume IV: Guidelines for Applying CORSIM Microsimulation Modeling Software*. Washington, DC: Federal Highway Administration. https://ops.fhwa.dot.gov/trafficanalysistools/tat_vol4/vol4_guidelines.pdf.

INRIX. 2018. INRIX (website). Accessed September 18, 2019. http://inrix.com.

ITE Community. 2017. ITE Community (website). Accessed June 13, 2019. https://community.ite.org/communities/community-home/viewthread?GroupId=133&MessageKey=cb2315cb-6d4e-41f5-bc98-578f36b406cc&CommunityKey=d04ead71-64dc-4b03-98fc-120353eef4d9&tab=digestviewer.

Jenior, P., R. Dowling, B. Nevers, and L. Neudorff. 2016. *Use of Freeway Shoulders for Travel – Guide for Planning, Evaluating, and Designing Part-Time Shoulder Use as a Traffic Management Strategy*. Washington DC: Federal Highway Administration. https://ops.fhwa.dot.gov/publications/fhwahop15023/fhwahop15023.pdf.

Jiang, X., Joe Bared, Michael Maness, and David Hale. 2015. "Traffic Performance Analysis of Dynamic Merge Control Using Microsimulation." *Transportation Research Record* 2484, no. 1 (January): 23–30. https://doi.org/10.3141/2484-03.

Kansas City Scout. Kansas DOT and Missouri DOT (website). Accessed September 18, 2019. http://www.kcscout.com.

Katz, B., Jiaqi Ma, Heather Rigdon, Kayla Sykes, Zhitong Huang, and Kelli Raboy. 2017. *Synthesis of Variable Speed Limit Signs*. Washington, DC: Federal Highway Administration. https://ops.fhwa.dot.gov/publications/fhwahop17003/fhwahop17003.pdf.

Kondyli, A., Bryan St. George, Lily Elefteriadou, and Gina Bonyani. 2017. "Defining, Measuring, and Modeling Capacity for the Highway Capacity Manual." *ASCE Journal of Transportation Engineering, Part A: Systems* 143, no. 3 (March). https://doi.org/10.1061/JTEPBS.0000017.

Kuhn, B., Ginger Goodin, Andrew Ballard, Marcus. Brewer, Robert Brydia, Jodi Carson, Susan Chrysler, et al. 2005. *Managed Lanes Handbook*. Washington, DC: Federal Highway Administration. https://static.tti.tamu.edu/tti.tamu.edu/documents/0-4160-24.pdf.

Kuhn, B., Kay Fitzpatrick, Marcus Brewer, Ginger Goodin, Melisa Finley, and Bastain Schroeder. 2013. *Design and Operations Elements of Dynamic Shoulder Use*. Washington, DC: Federal Highway Administration.

Ma, J., Jia Hu, David K. Hale, and Joe Bared. 2016. "Dynamic Hard Shoulder Running for Traffic Incident Management." *Transportation Research Record* 2554, no. 1 (February): 120–128. https://doi.org/10.3141/2554-13.

Martin, P., Herbert S. Levinson, and Texas Transportation Institute. 2012. *TCRP Report 151: A Guide for Implementing Bus on Shoulder (BOS) Systems*. Washington DC: The National Academies Press. https://doi.org/10.17226/22809.

Minnesota Department of Transportation. 2014. *Metropolitan Freeway System 2014 Congestion Report*. https://www.dot.state.mn.us/rtmc/reports/congestionreport2014.pdf.

Minnesota Department of Transportation. 2017. *Metropolitan Freeway System 2017 Congestion Report*. https://www.dot.state.mn.us/rtmc/reports/congestionreport2017.pdf.

National Academies of Sciences, Engineering, and Medicine. 2012. *Analysis of Managed Lanes on Freeway Facilities*. Washington, DC: The National Academies Press. https://doi.org/10.17226/22677.

Papamichail, I, Markos Papageorgiou, Vincent Vong, and John Gaffney. 2010. "HERO Coordinated Ramp Metering Implemented at the Monash Freeway." Presented at the *Transportation Research Board 89th Annual Meeting, Washington, DC, January 10–14, 2010*. https://trid.trb.org/view/1149987.

Papamichail, I., Markos Papageorgiou, Vincent Vong, and John Gaffney. 2010. "Heuristic Ramp-Metering Coordination Strategy Implemented at Monash Freeway, Australia." *Transportation Research Record* 2178, no. 1 (January): 10–20. https://doi.org/10.3141/2178-02.

PTV Vissim. 2019. PTV Group (website). Accessed October 7, 2019. https://vision-traffic.ptvgroup.com/en-us/products/ptv-vissim.

Regional Integrated Transportation Information System. 2018. RITIS (website). Accessed September 18, 2019. https://www.ritis.org.

Regional Transportation Management Center (RTMC) – Traffic Operations – MnDOT. 2019. Minnesota Department of Transportation (website). Accessed September 18, 2019. https://www.dot.state.mn.us/rtmc/trafficoperations.html.

San Diego Association of Governments. 2008. *Final I-15 ICM System Requirements*. San Diego: San Diego Association of Governments. https://www.sandag.org/uploads/publicationid/publicationid_4472_23297.pdf.

Schneider Electric and RK&K. 2015. *Bryan Park Interchange Dynamic Lane Merge Assessment*. Richmond, VA: Virginia Department of Transportation.

Sieminski, B. 2017. "Diverging Diamond Interchanges Gain Traction." *The Municipal*, January 23, 2017, http://www.themunicipal.com/2017/01/diverging-diamond-interchanges-gain-traction.

Spiller, N., Katherine Blizzard, and Rich Margiotta. 2017. *Recurring Traffic Bottlenecks: A Primer, Focus on Low-Cost Operational Improvements, Fourth Edition*. Washington DC: Federal Highway Administration. https://ops.fhwa.dot.gov/publications/fhwahop18013/fhwahop18013.pdf.

Stanitsas, P., John Hourdos, and Stephen Zitzow. 2014. *Evaluation of the Effect of MnPASS Lane Design on Mobility and Safety*. Minneapolis, MN: University of Minnesota. http://www.its.umn.edu/Publications/ResearchReports/reportdetail.html?id=2578.

TariVerdi, M. and Elise Miller-Hooks. 2012. "Standardizing and Simplifying Safety Service Patrol Benefit–Cost Ratio Estimation." M.S. thesis, University of Maryland at College Park. http://hdl.handle.net/1903/13806.

Taylor, C. and Deirdre Meldrum. 2000. *Evaluation of a Fuzzy Logic Ramp Metering Algorithm: A Comparative Study Among Three Ramp Metering Algorithms Used in the Greater Seattle Area*. Olympia, WA: Washington State Department of Transportation. https://www.wsdot.wa.gov/research/reports/fullreports/481.2.pdf.

Taylor, C., Deirdre Meldrum, and Les Jacobson. 1998. "Fuzzy Ramp Metering: Design Overview and Simulation Results." *Transportation Research Record* 1634, no. 1 (January): 10–18. http://dx.doi.org/10.3141/1634-02.

The R Project for Statistical Computing. 2019. The R Foundation (website). Accessed October 7, 2019. https://www.r-project.org.

Transportation Research Board. 2016. *Highway Capacity Manual, Sixth Edition: A Guide for Multimodal Mobility Analysis*. Washington, DC: The National Academies of Sciences, Engineering, and Medicine.

Van Aerde, M. et al. (1993). "QUEENSOD: A Method for Estimating Time Varying Origin-Destination Demands for Freeway Corridors/Networks." Presented at the *Transportation Research Board 72nd Annual Conference, Washington, DC, January 10–14, 1993*.

Wang, J., Ben Robinson, Steven G. Shelby, Kenneth B. Cox, and Walt Townsend. 2010. "Evaluation of ACS Lite Adaptive Control Using Sensys Arterial Travel Time Data." Presented at *ITS America 20th Annual Meeting & Exposition, Houston, TX, May 3–5, 2010*. https://pdfs.semanticscholar.org/5f8d/719dc47873d2291a1352611e87370526fed9.pdf.

Wang, Y. and Markos Papageorgiou. 2006. "Local ramp metering in the case of distant downstream bottlenecks." Presented at the *2006 IEEE Intelligent Transportation Systems Conference, Toronto, ON, Canada, September 17–20, 2006*. https://doi.org/10.1109/ITSC.2006.1706778.

Washington State Department of Transportation. 2017. *Design Manual M 22-01.12*. Olympia, WA: Washington State Department of Transportation. https://www.wsdot.wa.gov/publications/manuals/fulltext/M22-01/M22-01.12Revision.pdf.

Whitman, Requardt & Associates. 2015. *I–270 Model Calibration Methodologies*. Baltimore, MD: Whitman, Requardt & Associates.

Xiao, H., Kevin Sommers, David K. Hale, and Dimitra Michalaka. 2015. "Enhanced Calibration Method for Micro-Simulation Analysis of Tolled Managed Lanes." Presented at the *2015 Road Safety & Simulation International Conference, Orlando, FL, October 6–8, 2015*. https://doi.org/10.13140/RG.2.1.2641.9609.

Xiaonian S., Peng Hao, Kanok Boriboonsomsin, Guoyuan Wu, Matthew Barth, Xiaohong Chen. 2016. "Partially Limited Access Design Methodology for Freeway High Occupancy Vehicle Lanes." Presented at the *Transportation Research Board 96th Annual Meeting, Washington, DC, January 8–12, 2017*. https://trid.trb.org/view/1438879.

Xuewei Q., Guoyuan Wu, Kanok Boriboonsomsin, Matthew. J. Barth. 2015. "Comparative Study of Lane Changing Characteristics on Different Types of HOV Facilities Using Smoothed Aerial Photo Data." *Journal of Transportation Engineering* 142, no. 1 (January). https://doi.org/10.1061/(ASCE)TE.1943-5436.0000803.

Yelchuru, B., Paolo Rinelli, Laura Torres, and Raj Kamalanathsharma. 2017. *Analysis, Modeling, and Simulation (AMS) Testbed Development and Evaluation to Support Dynamic Mobility Applications (DMA) and Active Transportation and Demand Management (ATDM) Programs – Evaluation Summary for the San Diego Testbed*. Washington, DC: Federal Highway Administration. https://rosap.ntl.bts.gov/view/dot/32673.

Yuan, Y., Winnie Daaman, Serge Hoogendoorn, and Jos Vrancken. 2009. "Coordination Concepts for Ramp Metering Control in a Freeway Network." Presented at the *12th IFAC Symposium on Transportation Systems, Redondo Beach, CA, September 2–4 2009*. https://pdfs.semanticscholar.org/f3d7/aaf39ef1c6a8634a626da98f16e605fd73ce.pdf.

Zhang, L., Lei Zhang, David K. Hale, Jia Hu, and Zhitong Huang. 2017. "Cycle-Based Variable Speed Limit Methodology for Improved Freeway Merging." *IET Intelligent Transport Systems* 11, no. 10 (November): 632–640. https://doi.org/10.1049/iet-its.2017.0017.

Zhang, L., Zhitong Huang, Yi Wen, and Lei Zhang. 2014. *I-55 Integrated Diversion Traffic Management Benefit Study*. Washington, DC: Federal Highway Administration. https://rosap.ntl.bts.gov/view/dot/28529.

Zitzow, S., Gordon Parikh, and John Hourdos. 2018. *A Tool for Designing MnPASS Access Spacing*. Saint Paul, MN: Minnesota Department of Transportation. http://www.dot.state.mn.us/research/reports/2018/201811.pdf.